"THE USE OF MULTIPLE CAMERAS AND GEOMETRIC CONSTRAINTS FOR 3-D MEASUREMENT"

By

JIN CHEN

A thesis submitted for the award of the degree of Doctor of Philosophy

THE CITY UNIVERSITY

DEPARTMENT OF ELECTRICAL, ELECTRONIC, AND INFORMATION ENGINEERING

February, 1995

Table of Contents

Title **1**

Table of Contents **2**

List of Figures **7**

List of Tables **12**

Acknowledgements **13**

Abstract **14**

Declaration **15**

Chapter 1 Introduction **16**

1.1. Statement of the problem and research objectives 16

1.2. Goal for the research project 17

1.3. Overview and organisation of the thesis 17

Chapter 2 A survey and theory of digital photogrammetry and machine vision **20**

2.1. Introduction 20

2.2. Review of the history of photogrammetry and machine vision 20

2.2.1. History of photogrammetry 20

2.2.2. History of machine vision 24

2.2.3. The current state of the art of photogrammetry using machine vision techniques 29

2.3. Theory of digital photogrammetry 33

2.3.1. Collinear equation 34

2.3.2. Geometric lens distortion 35

2.3.3. Camera calibration 38

2.3.4. The self calibration bundle adjustment. 43

2.3.5. Statistical analysis of the result of bundle adjustment 50

2.3.6. Blunder detection 51

2.4. Theory of machine vision related to digital photogrammetry 53

2.4.1. Low-level: image acquisition and processing 53

2.4.2. Middle-level: target image recognition, location and matching: 55

2.4.3. High-level: the use of expert systems 62
2.5. Current trends in photogrammetry based on machine vision 63
2.6. Summary 63

Chapter 3 Analysis of fundamental hardware characteristics of a digital photogrammetric system 65
3.1. Introduction 65
3.2. The characteristics of photogrammetric error sources 66
3.2.1. Illumination 66
3.2.2. Characteristics of targets 66
3.2.2.1. Naturally reflective targets 67
3.2.2.2. Retro-reflective targets 67
3.2.2.3. Laser targets 69
3.2.2.4. Projected targets 70
3.2.2.5. Comparison of target characteristics 71
3.2.3. Characteristics of sensor 71
3.2.3.1. Electron beam image sensors (Vidicon) 72
3.2.3.2. Solid-state image sensors 73
3.2.4. Lens characteristics 78
3.2.5. Characteristics of framegrabber 81
3.3. Test and calibration of hardware components 83
3.3.1. Temperature effects 83
3.3.1.1. Temperature effects on camera performance 84
3.3.1.2. Temperature effects of framegrabber 86
3.3.1.3. Temperature effects of combined with both components 87
3.3.1.4. Conclusion 88
3.3.2. Analysis and calibration of geometric distortion 89
3.3.2.1. Principal point 89
3.3.2.2. Lens distortion 90
3.3.2.3. Line-jitter 105
3.4. Photogrammetric evaluation of complete photogrammetric system 107
3.5. Summary 109

Chapter 4 Automatic 3-D object measurement 111
4.1. Introduction 111
4.2. Automatic estimation of camera orientation 112
4.2.1. Overview of methods for estimation of camera orientation 112
4.2.1.1. Perspective transformation method 113
4.2.1.2. A non-linear optimisation method 114
4.2.1.3. Geometric vector method 117

4.2.1.4. Comparison of the methods 119
4.2.2. Implementation by an automatic three sided rectangle method 120
4.2.2.1. The building of the test frame 121
4.2.2.2. Segmentation and extraction of line segments 121
4.2.2.3. Recognition, merge, and fit of line segments 124
4.2.2.4. Determination of the co-ordinates of the intersection and termination points 124
4.2.2.5. Evaluation of the method 126
4.2.3. Camera orientation by an automatic laser spot extraction method 127
4.2.3.1. The laser spot projection system 127
4.2.3.2. Extraction of the laser target images 127
4.2.3.3. Evaluation of the method 129
4.3. A 2-D epipolar line matching method 130
4.3.1. Introduction to the epipolar line matching method 130
4.3.2. Discussion 133
4.4. The 3-D space intersection matching method 133
4.4.1. The 3-D space intersection matching principle 134
4.4.2. Discussion 139
4.5. Summary 140
Chapter 5 Optimisation of the multiple camera 3-D matching method 141
5.1. Introduction 141
5.2. Iterative 3-D target matching with network and constraints 142
5.2.1. Global uniqueness constraints 143
5.2.2. Local uniqueness constraints 145
5.3. Matching as a space search process 148
5.3.1. Local point pair matching as a tree search problem 148
5.3.2. Searching in the correspondence space 150
5.4. Global consistency search, hypothesis-testing, and heuristic methods 153
5.4.1. Global consistency searches 153
5.4.1.1. Depth first search 153
5.4.1.2. Width first search 154
5.4.2. The introduction of pseudo targets images to deal with occlusion 155
5.4.3. Sub-global uniqueness constraints 157
5.4.4. Hypothesis-testing and heuristic methods 160
5.4.5. Optimised 3-D target matching algorithm 162
5.4.5.1. Initialisation algorithm 163
5.4.5.2. Search and hypothesis 166
5.4.5.3. 3-D target position estimation 166
5.4.5.4. Validation verification 166

5.5. Evaluation of the method by simulation and experiment 166
5.5.1. Evaluation by simulation 166
5.5.1.1. The simulation package 166
5.5.1.2. Test one: The ideal case 168
5.5.1.3. Test two: The introduction of random errors 170
5.5.1.4. Test three: The influence of target density 173
5.5.2. Evaluation by experiment 175
5.5.2.1. Experimental test using targeted brick 175
5.5.2.2. Experimental test using car gear box 176
5.5.2.3. Experiment test using a plaster cast of a foot 178
5.6 Summary 180

Chapter 6 The design of an automated 3-D measuring system 182
6.1. Introduction 182
6.2. System Hardware 184
6.2.1. Support frame 185
6.2.2. Test field 186
6.2.3. Targeting 187
6.2.4. Translation and rotation mechanisms 187
6.2.5. Cameras and lens 189
6.2.6. Frame grabber 190
6.2.7. Interface box 190
6.2.8. Computer 191
6.3. Software system design. 192
6.3.1. The image acquisition module 195
6.3.2. The image processing and analysis module 196
6.3.2.1. The image segmentation module 197
6.3.2.2. The target recognition module 197
6.3.2.3. The subpixel target location module 198
6.3.3. The camera orientation module 199
6.3.3.1. The automatic three sided rectangle extraction module 199
6.3.3.2. The automatic laser target extraction module 200
6.3.4. The target correspondence module 200
6.3.5. Bundle adjustment module 201
6.3.6. Object reconstruction module 202
6.3.6.1. An AutoCAD interface module 202
6.3.6.2. The DTM module 203
6.4. Summary 205

Chapter 7 Some system application examples 206

7.1 Introduction 206
7.2. Example applications 206
7.2.1. Object measurement under laboratory conditions 206
7.2.1.1. Test one: Propeller 206
7.2.1.2. Test two: Test field 210
7.2.1.3. Test three: Mirror 212
7.2.2. The application of this system to deformation analysis of wood panels 213
7.2.2.1. System configuration 214
7.2.2.2. System Calibration 215
7.2.2.3. Data acquisition 219
7.2.2.4. Data process and analysis 223
7.3. Summary 226

Chapter 8 Conclusions and suggestions for further work 227
8.1 Contributions of investigations and researches 227
8.2 Suggestions for further work 230

References 232

List of Figures

Figure 2.1 Stages in the development of photogrammetry 20
Figure 2.2 Flow chart of photogrammetric information construction 24
Figure 2.3 Automatic inspection flow chart 26
Figure 2.4 A cross-section at a tunnel profile 30
Figure 2.5 Construction of photogrammetry and machine vision system 32
Figure 2.6 The connection between photogrammetry and machine vision 32
Figure 2.7 The central perspective projection of a camera 34
Figure 2.8 Effect of radial distortion 36
Figure 2.9 Effect of decentering 36
Figure 2.10 A test object with control targets 40
Figure 2.11 Straight line on image plane 41
Figure 2.12 The basic configuration for the bundle adjustment 44
Figure 2.13 a). An original image b) A part of the turbine blade 54
Figure 2.14 Inverted intensity profile of marked section 54
Figure 2.15 Results of local image normalisation 55
Figure 2.16 Section of target image shown in Figure 2.13b 59
Figure 2.17 Epipolar line matching method 61
Figure 3.1 A 3-D intensity profile of naturally reflective targets 67
Figure 3.2 Structure of retro-reflective material 68
Figure 3.3 Working principal of retro-reflective material 68
Figure 3.4 A 3-D intensity profile of retro-reflective targets 69
Figure 3.5 A 3-D intensity profile of projected targets 70
Figure 3.6 A 3-D intensity profile of laser targets without speckle 70
Figure 3.7 A 3-D intensity profile of laser targets with speckle 70
Figure 3.8 Construction of a vidicon camera 72
Figure 3.9 a) Interline transfer b) Frame transfer 73
Figure 3.10 The Pulnix TM-6CN camera with a Fujinon 25 mm lens 74
Figure 3.11 Grey level response at two gamma settings 76
Figure 3.12 Spectral sensitivity of the sensor in TM-6CN camera 76
Figure 3.13 Sensor output without lens 77
Figure 3.14 RMS grey level for three camera/lens combinations 79
Figure 3.15 RMS grey level and lens aperture for two lenses 79
Figure 3.16 An image of a lens test resolution chart 80
Figure 3.17 Intensity profiles through three sets of line pairs 80

Figure 3.18 a) Using a 5m cable b) Using a 2m cable 82
Figure 3.19 The warm-up test setup 83
Figure 3.20 The test field used for the warm-up tests 84
Figure 3.21 x, y co-ordinate warm-up shift for target image (camera 1) 85
Figure 3.22 x,y co-ordinate warm-up shift for target image (camera 2) 85
Figure 3.23 x, y co-ordinate warm-up shift for target image (camera 3) 85
Figure 3.24 Vectors of the warm-up characteristics of the three cameras 86
Figure 3.25 Vectors of the warm-up characteristics of the framegrabber 87
Figure 3.26 x, y co-ordinates warm-up shift for framegrabber 87
Figure 3.27 Vectors of warm-up of the camera and framegrabber 88
Figure 3.28 x, y co-ordinates warm-up shift for camera and framegrabber 88
Figure 3.29 Test of principal point setting up 89
Figure 3.30 Setting up the plumb lines and camera 91
Figure3.31 The configuration of the plumb lines (plan view) 91
Figure 3.32 Close up view of the string at 0.5 meters 94
Figure 3.33 Radial distortion for three cameras and three lenses 97
Figure 3.34 Decentering distortion for three camera and three lenses 98
Figure 3.35 Radial distortion graph of mean results 99
Figure 3.36 Decentering distortion graph of mean results 99
Figure 3.37 Radial distortion for three cameras and three lenses by K_1 101
Figure 3.38 Two lines method for calculating K_1 102
Figure 3.39 View of target test field and frame 103
Figure 3.40 Image used to compute K_1 and bundle 103
Figure 3.41 Synchronisation with composite video and PLL 105
Figure 3.42 a) Subpixel errors in x direction b) Subpixel errors in y direction 106
Figure 3.43 The configuration of the bundle adjustment 108
Figure 4.1 Perspective transformation 113
Figure 4.2 The geometry of camera location 117
Figure 4.3 The physical meaning of a, b, c 118
Figure 4.4 The three side rectangle for orientation 121
Figure 4.5 The result of segmenting the frame in test field 122
Figure 4.6 a) Pattern one b) Pattern two 122
Figure 4.7 The result of thinning the image in Figure 4.5 124
Figure 4.8 Determination of the four points 125
Figure 4.9 Results of different viewpoints for three cameras 126
Figure 4.10 Configuration of the laser diode system 127

Figure 4.11 a) Laser spots in space plane b) Laser spot images in image plane 128
Figure 4.12 Geometric relation of target images between two viewpoints 131
Figure 4.13 Epipolar line in image plane 2 for a target image in image plane 1..... 132
Figure 4.14 Space intersection of two viewpoints..... 135
Figure 4.15 Space intersection of **nth** viewpoint 139
Figure 5.1 Epipolar plane. 144
Figure 5.2 Two targets on the epipolar plane in viewpoints V_1, and V_2..... 147
Figure 5.3 Two targets on the same epipolar planes in viewpoints V_1, V_2 and V_2, V_3.147
Figure 5.4 An object target occluded in viewpoint V_1..... 147
Figure 5.5 Principle of 3-D space matching..... 149
Figure 5.6 Matching combinations..... 150
Figure 5.7 Tree search for matching. 150
Figure 5.8 Matching space. 151
Figure 5.9 Matching points. 151
Figure 5.10 Part of unmatching subspace. 152
Figure 5.11 Matching subspace..... 153
Figure 5.12 Depth first search. 154
Figure 5.13 Width first search..... 155
Figure 5.14 Pseudo target expression..... 156
Figure 5.15 Search through pseudo target..... 156
Figure 5.16 Unsolvable case one..... 158
Figure 5.17 Unsolvable case two. 158
Figure 5.18 Unsolvable case three. 158
Figure 5.19 Incorrect matching. 160
Figure 5.20 The perspective transformation in spherical co-ordinate system 167
Figure 5.21 The simulation system under Microsoft Windows^{TM} environment 167
Figure 5.22 Eight views obtained from the simulation system. 169
Figure 5.23 The result of random camera position parameter shifts. 171
Figure 5.24 Result of camera rotation parameter shift. 171
Figure 5.25 Result of target image co-ordinates x, y shifts..... 172
Figure 5.26 Result of camera orientation parameters shift..... 173
Figure 5.27 Results of matching with different target image densities 174
Figure 5.28 Matching errors in ten cubes..... 174
Figure 5.29 Matching errors in one cube 174
Figure 5.30 a) Image from view 1 b) Image from view 8 175
Figure 5.31 Car gearbox..... 176

Figure 5.32 One view of the gearbox 177
Figure 5.33 CAD reconstruction of the gearbox 177
Figure 5.34 View of foot model 178
Figure 5.35 Image grabbed for target location 179
Figure 5.36 Position of the 25 camera views 179
Figure 5.37 CAD reconstruction of the foot (looking up from bottom) 180
Figure 6.1 Overview of the prototype system. 184
Figure 6.2 Structure of the 3-D measuring system. 185
Figure 6.3 The camera support frame. 186
Figure 6.4 Test field for camera calibration and orientation. 186
Figure 6.5 Laser target projection system. 187
Figure 6.6 The object rotate mechanism. 188
Figure 6.7 The camera pan and tilt mechanism. 189
Figure 6.8 Structure of the EPIX frame grabber. 190
Figure 6.9 Overview of computer interface box. 191
Figure 6.10 DOS version system menu. 193
Figure 6.11 Windows version system menu 194
Figure 6.12 Diagram of the system software 194
Figure 6.13 Four image views of an object grabbed by one camera and lens. 196
Figure 6.14 a) The testfield b) Reconstruction of the test field 202
Figure 6.15 Bilinear interpolation for DTM. 203
Figure 6.16 Reconstruction of a gearbox through the DTM module 204
Figure 7.1 Original propeller with some targets 207
Figure 7.2 Propeller image grabbed for location 207
Figure 7.3 Position of the nineteen camera views 208
Figure 7.4 A view of the 3-D model of the marine propeller 209
Figure 7.5 Test field 210
Figure 7.6 Image of targeted mirror 212
Figure 7.7 Test field 215
Figure 7.8 Radial distortion of the five cameras 217
Figure 7.9 Decentering distortion of the five cameras 217
Figure 7.10 Plumb line image grabbed by the 6.5 mm lens 218
Figure 7.11 The system setting up 219
Figure 7.12 Targets were placed on each panel 220
Figure 7.13 a) Image grabbing menu b) Image save menu 221
Figure 7.14 Target location menu 221

Figure 7.15 a) Previous epoch b) Current epoch 225
Figure 7.16 Visualisation of deformation of the panel 3O8 225
Figure 7.17 Edges for panel 3O8 rapid test (10x exaggeration).....226

List of Tables

Table 3.1 Comparison of four types of targets....71
Table 3.2 Characteristics of Pulnix TM-6CN camera....75
Table 3.3 Specification of the EPIX framegrabber....81
Table 3.4 Principal point measurement....90
Table 3.5 Variation of lens focal point....90
Table 3.6 Environment parameters for the plumb line method experiments....93
Table 3.7 Radial and decentering lens distortion in micrometers....95
Table 3.8 Mean values of lens distortion in micrometers....95
Table 3.9 Convergence value of K_1, K_2, K_3, P_1 and P2....96
Table 3.10 Radial lens distortion in micrometers using K_1....100
Table 3.11 Mean values of lens distortion in micrometers using K_1....100
Table 3.12 Radial lens distortion in micrometers using only two lines....103
Table 3.13 Mean values of lens distortion in micrometers using only two lines....103
Table 3.14 RMS image co-ordinate residual standard deviation for all images....107
Table 3.15 Results of camera self calibration....109
Table 3.16 System precision by using self calibration bundle adjustment....109
Table 4.1 Relative merits of the three methods....120
Table 5.1 Definition of viewpoint orientation.....170
Table 5.2 Number of target images visible in each view.....170
Table 5.3 Table of the distribution of target visibility.....170
Table 5.4 Number of correct matches per viewpoint.....176
Table 5.5 Successful matches from the gearbox application....178
Table 5.6 Target matches by iteration....179
Table 6.1 A summary of some of the 3-D measuring system....183
Table 7.1 Result of bundle adjustment....209
Table 7.2 Comparison of RMS error in camera orientation parameters....211
Table 7.3 Results of self calibration....211
Table 7.4 Precision of image co-ordinates....213
Table 7.5 Precision of object co-ordinates....213
Table 7.6 Results of principal point of symmetry....216
Table 7.7 Convergence value of K_1, K_2, K_3, P_1, and P_2....216
Table 7.8 Focal length calibration....218
Table 7.9 Camera orientation calibration....219

Acknowledgements

I would like to thank Professor K.T.V. Grattan, my supervisor, for his guidance through my studies in the University. I acknowledge his care and encouragement whenever I have been to see him; his support for the numerous letters especially for the annual visa extension applications; his arrangement of financial funding to secure my studies; and his organisational and management skill which were invaluable in the practical promotion of the production of this thesis.

I cannot express how I should credit the thesis to the support of Dr T.A. Clarke. Without his guidance and help, this thesis would not be in its current form, or even exist. I want to thank him for the provision of the initial idea to set-up an automated photogrammetric 3-D measuring system and numerous advice during my studies; the patience when listening to my original Chinese English; the torture when he went through my earlier writings; the time spent on trains, at home, and on holidays to read and correct the thesis; his enthusiasm to improve my English, both oral and written; his suggestions and discussions and criticisms; and the excellent financial support of the last two years for both my living expenses and attending several international conferences.

I wish to thank Dr S. Robson for his considerable contribution during the last three years. He provided a detailed introduction when I first stepped into the world of photogrammetry. I would like to thank him for not only always providing a satisfactory answer whenever I needed his help, but also for reviewing and correcting every single chapter of my thesis many times. I would like at this point to make especial thanks to him for contributing his advice and help through the research of this thesis.

I would also like to thank Professor M.A.R. Cooper, who helped me on numerous occasions especially in implementing a self calibration bundle adjustment and in understanding the theory of photogrammetry. I express my great thanks to him for employing me in a post doctoral level research assistant position, which provided an excellent application example for my thesis research work.

I thank Professor S.L. Huang, in Chongqing University, China, who gave me the chance to come and study here and who also gave me much advice. I thank the Education Commission of China who gave me one and a half years financial support for my PhD study.

Many thanks I want to give to Professor J. Fryer, who gave me great help in using plumb line methods for camera calibration and supplying the source code and technique of this method. I thank Dr T.J. Ellis, who helped me in many ways: from advising me about the machine vision techniques; to using any equipment in his laboratory. I would also like to thank my friends who have provided great support over many years.

Last but by no means least, I acknowledge my family for their understanding and so much encouragement and support from outside of the "ivory towers".

Abstract

This thesis addresses some of the problems involved in the automation of 3-D photogrammetric measurement using multiple camera viewpoints. The primary research discussed in this thesis concerns the automatic solution of the correspondence problem. This and associated research has led to the development of an automated photogrammetric measuring system which combines the techniques from both machine vision and photogrammetry. Such a system is likely to contribute greatly to the accessibility of 3-D measurement to non-photogrammetrists who will generally have little knowledge and expertise of photogrammetry.

A matching method, which is called the 3-D matching method, is developed in the thesis. This method is based on a 3-D intersection and "epipolar plane", as opposed to the 2-D intersection of the epipolar line method. The method is shown to provide a robust and flexible procedure, especially where camera orientation parameters are not well known. The theory of the method is derived and discussed. It is further developed by combination with a bundle adjustment process to iteratively improve the estimated camera orientations and to gradually introduce legitimate matched target images from multiple cameras. The 3-D target matching method is also optimised using a 3-D space constrained search technique. A globally consistent search is developed in which pseudo target images are defined to overcome problems due to occlusion. Hypothesis based heuristic algorithms are developed to optimise the matching process. This method of solving target correspondences is thoroughly tested and evaluated by simulation and by its use in practical applications.

The characteristics of the components necessary for a photogrammetric measuring system are investigated. These include sources of illumination, targets, sensors, lenses, and framegrabbers. Methods are introduced for analysis of their characteristics. CCD cameras are calibrated using both plumb line and self calibration methods. These methods provide an estimation of some of the sources of error, which influence the performance of the system as a whole.

The design of an automated photogrammetric measuring system with a number of novel features is discussed and a prototype system is developed for use in a constrained environment. The precision, accuracy, reliability, speed, and flexibility of the developed system are explored in a number of laboratory and experimental applications. Trials show that with further development the system could have commercial value and be used to provide a solution suitable for photogrammetrists and trained operators in a wide range of applications.

Declaration

I grant powers of discretion to the University Librarian to allow this thesis to be copied in whole or in part without further reference to me. This permission covers only single copies made for study purposes, subject to normal conditions of acknowledgement.

Chapter 1 Introduction

1.1. Statement of the problem and research objectives

The availability of tools to perform 3-D engineering measurement using digital photogrammetry have undergone significant advances in recent years. The invention of imaging systems, such as vidicon tubes and solid-state sensors have contributed to this. The charge-coupled device (CCD), invented only twenty years ago, has proven to be an excellent image sensor. The CCD is high geometric uniformity and stability make it ideally suited for digital photogrammetry. Framegrabbers, which integrate a fast analogue-digital converter with high speed memory and processing elements, have become standard commodities. The ongoing rapid increase in the performance of computers and other processing systems have enabled photogrammetrists to employ ever more demanding algorithms. Highly accurate methods have been derived from various ways: for target location, such as least squares matching(LSM) are a prerequisite for attaining high precision 2-D target location and subsequent 3-D target measurements; Multiple cameras have been used to construct stronger measurement networks and to produce statistical high precision results. Existing methods and algorithms such as self-calibration and the free bundle adjustment provide important tools for data processing. Software, such as Microsoft Windows^{TM} based graphical user interface, has enabled the development of powerful and user-friendly tools for data processing and analysis with semi-automated and fully-automated methods.

However, only a few of the measurement systems in industrial application are currently based on photogrammetric techniques. The main reason why the application of photogrammetry in industry is relatively rare is the degree of expertise required is normally only found in trained photogrammetrists. The design and use of a photogrammetric system is a complex task. It involves, for example, planning the distribution of targets which will be measured, deciding what image processing steps are necessary to extract the target location, estimating the initial camera orientation parameters and the starting values of each target's 3-D co-ordinates, using appropriate algorithms to get the unique target image labelling, and many other considerations. These numerous considerations and constraints are difficult for non-photogrammetrists.

1.2. Goal for the research project

The aim of this work was to consider the tasks required to develop a high precision real-time and automated photogrammetric 3-D measuring system which could be used with greater flexibility and simplicity than those currently available. Flexibility means that the system should be able to deal with a wide range of industrial tasks without modifying both the system hardware components and software structure. Simplicity means that the system can be easily operated by any non-photogrammetrist. The tasks entailed in this work are thus:

- Develop an automated photogrammetric system with advanced capabilities based on targeting techniques;
- Investigate the characteristics of all system components in order to get an overview of the numerous problems and assess the importance of each effect;
- Combine photogrammetry with machine vision techniques to develop an automatic target location method which can deal with various environmental conditions;
- Develop a method to automatically estimate the camera orientation parameters and the starting values of target 3-D co-ordinates;
- Investigate the problems, such as ambiguities and occlusion, in target images correspondence and develop a method, which is 3-D based space intersection of target image, to automatically match target images between any number of views and targets;
- Optimise the automatic 3-D matching method by efficiency and performance; and
- Demonstrate the easy operation of the system in a practical application.

High accuracy is not the aim of the project. The level of accuracy is determined by the tasks of industry and it is a trade off with the speed, automation, and operation. The relative accuracy obtained using such systems is between 1:5,000 to 1:50,000 of the object space depending on the application requirements.

1.3. Overview and organisation of the thesis

Chapter two gives a comprehensive review of digital photogrammetry and machine vision. Both these techniques have been developed over a number of years. However, in recent years much more progress has been made in both areas. In this chapter, the theories of digital photogrammetry and machine vision are discussed. It seems likely that the combination of digital photogrammetry and machine vision technique will be increasingly important.

Chapter three is concerned with the analysis of the fundamental hardware characteristics of digital photogrammetric systems. The components, which are used to build a digital photogrammetric engineering measurement system, include: sources of illumination; targets;

and consider sources of error. Some calibration methods for CCD cameras are investigated. Techniques used to improve the statistical reliability of measurement are discussed, analysed, evaluated, and summarised.

Chapter four describes two methods of which are necessary and normally difficult for an automated system. There are two key requirements for a target based automated digital photogrammetric system: (i) the estimation of starting values of camera orientation and the 3-D target co-ordinates; and (ii) the automatic matching of corresponding target images from multiple camera views. In this chapter methods for estimation of camera orientation are discussed. Two implementations are presented for an automatic estimation of camera orientation and target 3-D co-ordinates. They are: i) an automatic three sided rectangle method; and ii) an automatic laser spot extraction method. With respect to solving the correspondence problem the 2-D epipolar line method for automatic target image correspondence is discussed. An alternative target matching technique, which is based on a 3-D intersection and an epipolar plane, as opposed to the 2-D intersection of the epipolar line method, is developed to automatically match the target images from multiple camera views. The theory of the approach is described and discussed.

In chapter five, the 3-D target matching method is developed to iteratively improve the estimated camera orientation by combining the matching procedure with the bundle adjustment method. Several methods are discussed to improve the reliability of correspondence. The 3-D target matching method is optimised using a 3-D space constrained search technique. Various search methods are discussed for the matching of target images in multiple viewpoints. A globally consistent constraint search is developed, in which pseudo target images are defined to overcome search problems in occluded viewpoints and hypothesis based heuristic algorithms are used to optimise the matching process. A theoretical analysis of the methods used is given. A general algorithm is designed with consideration of likely practical situations. The resulting general algorithm is shown to match target images, such as circular retro-reflective targets, using any number of viewpoints. Both simulation and practical tests are carried out to verify the algorithm.

Chapter six discusses the design of an automated measuring system. The aim for the design of an automated 3-D measuring system using photogrammetric and machine vision techniques is for the process to be automatic, real-time, accurate, robust and economic. It has been assumed that initially this system will be used in a constrained environment. At a later stage it is anticipated that further developments will allow the system to be used in an unconstrained environment. To achieve the objective described in section 1.2 there are some specific problems in both hardware and software which will influence the overall measuring processes

such as: lighting, targeting, camera orientation estimation, target matching, bundle adjustment implementation, blunder detection, and representation of the final result. In this chapter, the hardware components and software modules are integrated and the performances of these as a system are analysed.

In chapter seven, several examples of using the automated measuring system are presented. The flexibility of the developed system is evaluated by a number of example applications under both laboratory and experimental conditions. A successful application of the system to deformation analysis of wood panels as part of an academic research project is presented. The precision, accuracy, reliability, and speed are analysed.

The conclusions in chapter eight provide an evaluation of the photogrammetric 3-D measuring system using the methods presented in this thesis. This chapter also describes problems met in the research and contains suggestions for future research.

Chapter 2 A survey and theory of digital photogrammetry and machine vision

2.1. Introduction

Both photogrammetry and machine vision are well established disciplines. Machine vision has been a rapidly developing area since the 1970s. Close range digital photogrammetry which also began in 1970s is now one of the most rapidly developing branches of photogrammetry. This survey investigates the historical development and the state of the art in both photogrammetry and machine vision. A historical perspective of both areas is given followed by the basic theory. The review will emphasise the complementary nature of machine vision and photogrammetry.

2.2. Review of the history of photogrammetry and machine vision

2.2.1. History of photogrammetry

Photogrammetry has a history of about one and half centuries. It can be divided into four stages (Figure 2.1): the initial photogrammetric stage; the analogue photogrammetric stage; the analytical photogrammetric stage and the digital photogrammetric stage.

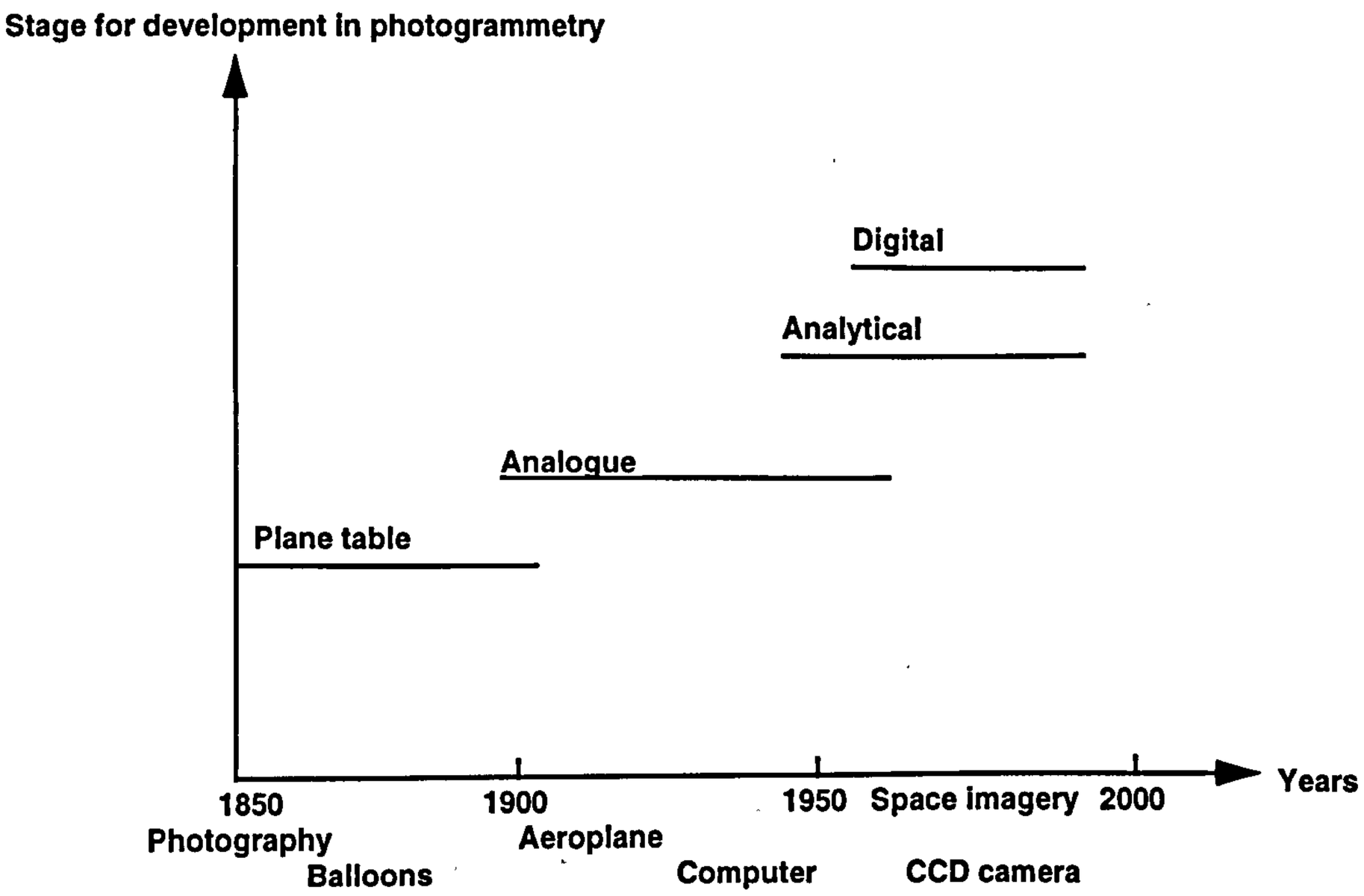

Figure 2.1 Stages in the development of photogrammetry

(i). The plane table photogrammetric stage:1840-1900

Photogrammetry originated in Europe. In 1839, Arago in France invented the photograph and at the same time, Niepoe and Daguerre, also in France, used this technique and invented plane table photogrammetry. The science of photogrammetry began to be developed from this time. In 1851, the French scientist Laussedat began to use terrestrial photographs to develop photogrammetric methods. In 1859, he constructed the first photographic apparatus, which was used to construct a map of a city, and for which he was later recognised as the "The Father of photogrammetry". Meanwhile, these photogrammetric methods were transmitted into Germany and in 1855, Kersten devised the term "photogrammetry", which originally signified "measuring graphically by means of light" derived from the roots of the Greek words "photos" and "gramma" (American, 1989). Koppe used the term in the first German textbook on photogrammetry in 1856. In 1858, an architect Meydenbauer used the photogrammetric method to survey churches and historical monuments. Between 1830 and 1832, the stereoscope was invented and was used as a measurement tool for stereophotogrammetry in 1892. In 1895, Deville, in Canada, developed the first instrument for stereo-observation of overlapping photographs. In 1901, Pulfrich at Zeiss in Germany, built the first stereocomparator for the measurement of image co-ordinates using a floating mark. All of these developments defined the basic equipment and principles of photogrammetry.

(ii). The analogue photogrammetric stage: 1900-1960

In the beginning of twentieth century, aerial (or topographic) photogrammetry was developed after the Wright brothers in American invented the motor-driven aeroplane. At this time a number of photogrammetric instruments were invented, such as the stereo-plotter (1908), stereo-photograph (1908), stereo-autograph (1911), stereo-projector (1915). These instruments provided the basis for analogue photogrammetry. In several European countries, numerous and successive refinements of these instruments took place by: Zeiss and Hugershoff in Germany (1919); Nistri and Santani in Italy (1921); Poivilliers in France (1923); and Wild in Switzerland (1916). These instruments were mainly used in aerial photogrammetry.

Since the 1920's, non-topographic photogrammetry, as opposed to aerial photogrammetry, began to be developed. The term non-topographic photogrammetry has now largely been replaced by the phrase "close range photogrammetry". The use of photogrammetric techniques spread into: architecture; archaeology; biostereometrics; engineering and industrial fields; forensic science; and numerous other areas of application during the period 1920-1960.

(iii). The analytical photogrammetric stage: 1960-present

The invention of the electronic computer started a new era in the development of photogrammetry. Early in 1899, Finsterwalder of Germany proposed the analytical photogrammetric idea. Church repeated the proposal in 1945. The first system was designed by E.H. Thompson in 1936 based on existing theory and practice. In 1953, H. Schmid and D. Brown in American invented the modern multi-station analytical photogrammetric approach. Soon afterwards a digital computer was used in the system so that these instruments were called "computer-assisted systems", such instruments included stereo-comparators (Zeiss PEK and Wild STK), and stereo plotters (produced by O.M.I. in collaboration with Bendix). Advances in the computer processing of numerical data have revolutionised photogrammetric procedures and products. Whereas previously the end product of the photogrammetric process was usually a map, a chart, a measurement datum or a photographic image, the modern product is often an array of 3-D co-ordinates, which can be used to reconstruct a structure, check for deformation, build a numerical model and so on. Since the 1970's, a large number of analytical photogrammetric instruments have been commercially developed, such as AC1, BC1, AC2, BC2 series (Switzerland), C100, C110, C120, C130 series (Germany), US-1, US-2 series (America), and DSR1, DSR11 series (Switzerland). More recently, analytical photogrammetric instruments based on data base methods have been put into use, such as P1, P2, P3 (Germany) and System 9, DSR-15, BC-3 (Switzerland). The further development of analytical photogrammetric instruments has led to the era of digital photogrammetric systems.

(iv). The digital photogrammetric stage: 1970's-present

The main developments of this period have occurred in both branches of photogrammetry: topographic photogrammetry and non-topographic photogrammetry.

(1). Topographic photogrammetry: In 1957, the first satellite was invented by U.S.S.R. From this time scientists have been able to obtain the photographs from space. However true digital photogrammetry did not began until the 1970's when the first Earth source satellite Landsat was sent into the space in 1972 by America. Digital tools for image acquisition have been developed from visible light to multi-spectrum image obtained by remote sensing systems. The resolution of remote sensing systems has been improved from 80 metres to 5 metres on the ground. Konecny, in 1985, indicated that the development of digital photogrammetry had been progressing in parallel with the development of remote sensing. Digital systems have been built to process the information coming from photogrammetry and remote sensing. Such systems benefit from real-time and automation techniques which can be implemented in both hardware and software, transputers, parallel computer arrays, pipe processors etc. As these

developments have been used in digital photogrammetry and remote sensing, photogrammetric scientists have added to the systems, such as Geographical Information System (GIS), Land Information System (LIS), Digital Elevation Model (DEM), Digital Object Model (DOM), and Digital Terrain Model (DTM). In the International photogrammetric societies, such as ISPRS Commission III and IV, the working groups concerned with the theory of GIS and photogrammetric databases have been formed to specialise the study of these areas.

(2). Non-topographic photogrammetry: Digital non-topographic photogrammetry started with the invention of the CCD camera in 1972. In close-range measurement, the CCD camera is used to acquire object images which then can be measured by mean of automatic computer processing techniques. Real time digital photogrammetric system have been built for industrial control and robots vision applications using advanced hardware. The main characteristics of digital non-topographic photogrammetry are: (a). the small image size (less than 4000x4000 pixel resolution, typically 512X512); (b). the large number of images (more images in sequential systems); (c). real time or near real time processing; and (4). varying levels of automation.

Currently, the emphasis of the research in this area is in: system integration; calibration of the CCD camera (inner and outer parameters); optimisation of the design of close-range multi-photo networks; on line triangulation measurement (image sequence Kalman filter and recursive estimation); multi-image matching; moving object 3-D tracking; industrial measurement; computer assisted architectural photogrammetric measurement, and automatic deformation measurement. It can be said that digital photogrammetry provides the means of applying close-range photogrammetry to many industrial applications. There are a very large number of current and future applications and the goal of an automated photogrammetric measurement is likely to be achieved in the near future, first in constrained applications and later in general.

A summary of the previous discussion, the composition and interactions of photogrammetry are illustrated in Figure 2.2.

Figure 2.2 summarises the whole process of photogrammetric information gathering, processing, assembling and expressing of results, and the generic connection between them. It includes: analogue, analytical and digital photogrammetry, and remote sensing, as well as industrial applications.

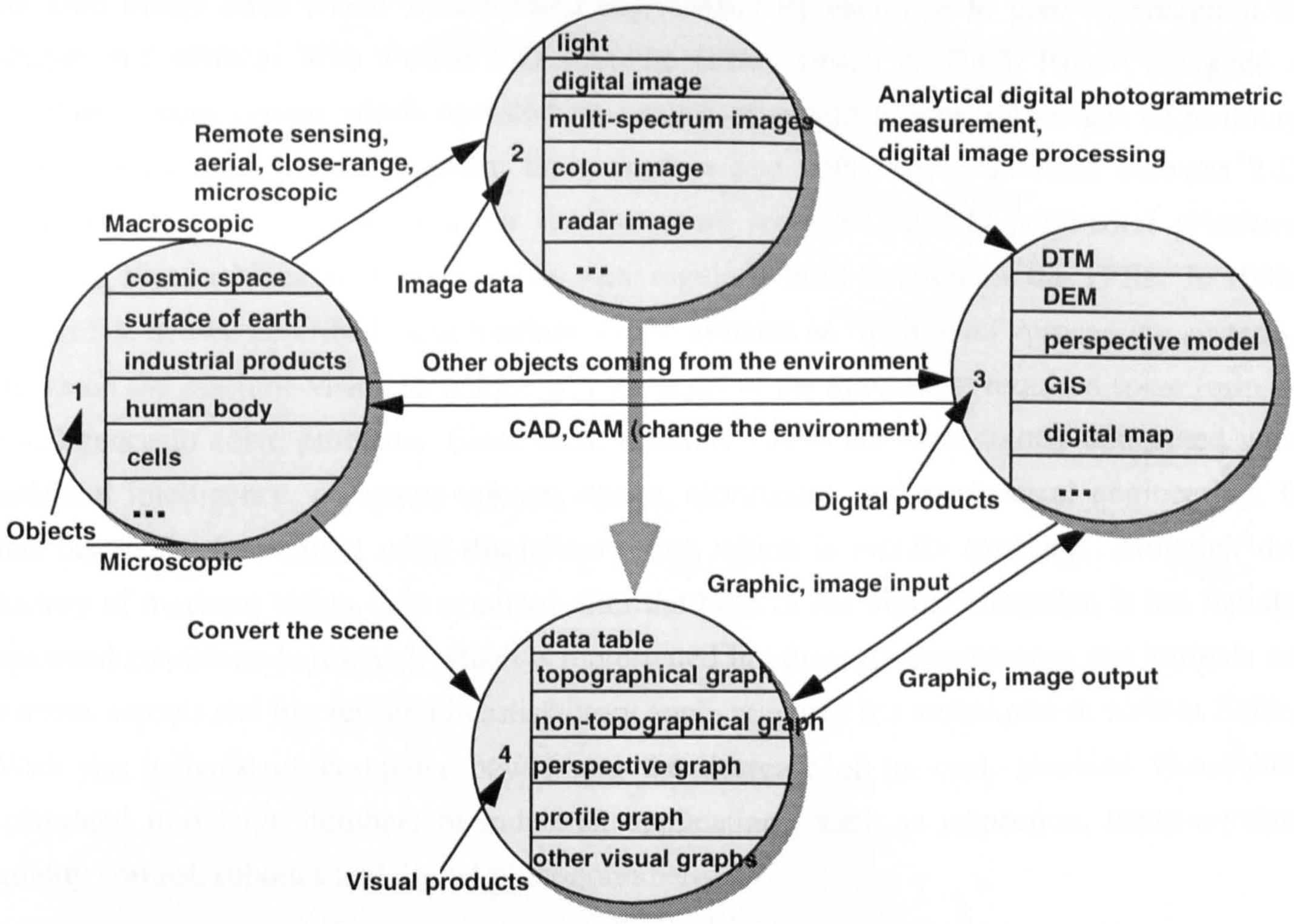

Figure 2.2 Flow chart of photogrammetric information construction

2.2.2. History of machine vision

Machine vision is the study of how to build intelligent machines using vision. Machine vision has it's origins in visual perception, by which the human looks and sees the world and comes to know the world. An understanding of visual perception can be dated from Greek writing. However, there was no significant progress in this area until the eighteenth century when the industrial revolution was fully under way. In 1704, one of the great scientists, Newton, laid the foundations for modern work on colour vision by defining physical optics. With the development of industry, new inspection tools and new optical methods were required to speed the production of products and automatically monitor the quality of the products. However, the true beginning of the machine vision occurred in the mid 1960s as the digital electronic computer was invented and this is why machine vision is often called "computer vision". Some researchers also call machine vision "robot vision" or "image understanding" and use these terms with slightly different meanings and emphasis. Wong, 1992b, gave a

detailed definition of these terminology. In 1960, Bela devised robot stereo-vision, in which he used image pairs which were viewed individually by each eye to give a perception of shapes and surfaces with a clear 3-D structure (Low, 1991). In 1965, Robert designed a machine vision system which operated on images of planar polyhedral shapes of building blocks. This system could segment lines, vertices and polygons, and match between 2-D images. The result was a computer data structure representing 3-D polyhedral primitive building blocks. Machine vision systems were regularly built through out the 1970s. In 1982, Ballard & Brown described these machine vision systems as "high-level" processing systems, in which the machine vision technique was the heart of the system but required some form of intelligence to solve problems. Since then, machine vision has been tightly connected with artificial intelligence, computer science, optics, electronics, and mechanical engineering. It has become a fascinating multi-disciplinary area which is rapidly evolving. Although the history of machine vision only occurred after the birth of the digital computer, it has rapidly spawned considerable research which is represented in numerous conferences and journals on various aspects and has resulted in satisfactory applications of it's techniques in various fields. With the increase of computer power and the decrease of its cost, machine vision has infiltrated into large numbers of industrial applications, such as inspection, measurement, quality control, robotics and digital photogrammetry.

(i). Measurement, inspection and quality control

The application of machine vision in measurement, inspection and quality control is concerned with performing the quantitative or qualitative measurement of the dimensional characteristics of objects and object verification, i.e. establishing whether there are any extraneous parts or sections of objects which should not be present. Machine vision is very important in the area of automatic measurement, inspection and quality control and most of the potential applications of vision in industry are in this area. There are two main requirements for industrial automatic measurement, inspection or quality control: **(1).** assembly tasks, and **(2).** automatically inspecting products by measurement. The former is mainly used for robots and the latter is mainly used for quality control. In the manufacturing assembly process, components must be located and oriented so that a robot can pick them up and assemble them. For example, the varying parts of a car in manufacture need to be taken in turn and put into the correct positions. In inspection, objects may pass the inspection station on a moving conveyer very quickly and the task is to ascertain whether there are any defects. If defects are detected the object will usually have to be rejected. An important feature of most industrial tasks is that they take place in real time. Hence, machine vision systems must be able to keep up with the manufacturing process. It follows that inspection systems will often use computer hardware such as a parallel processors or digital signal processors to

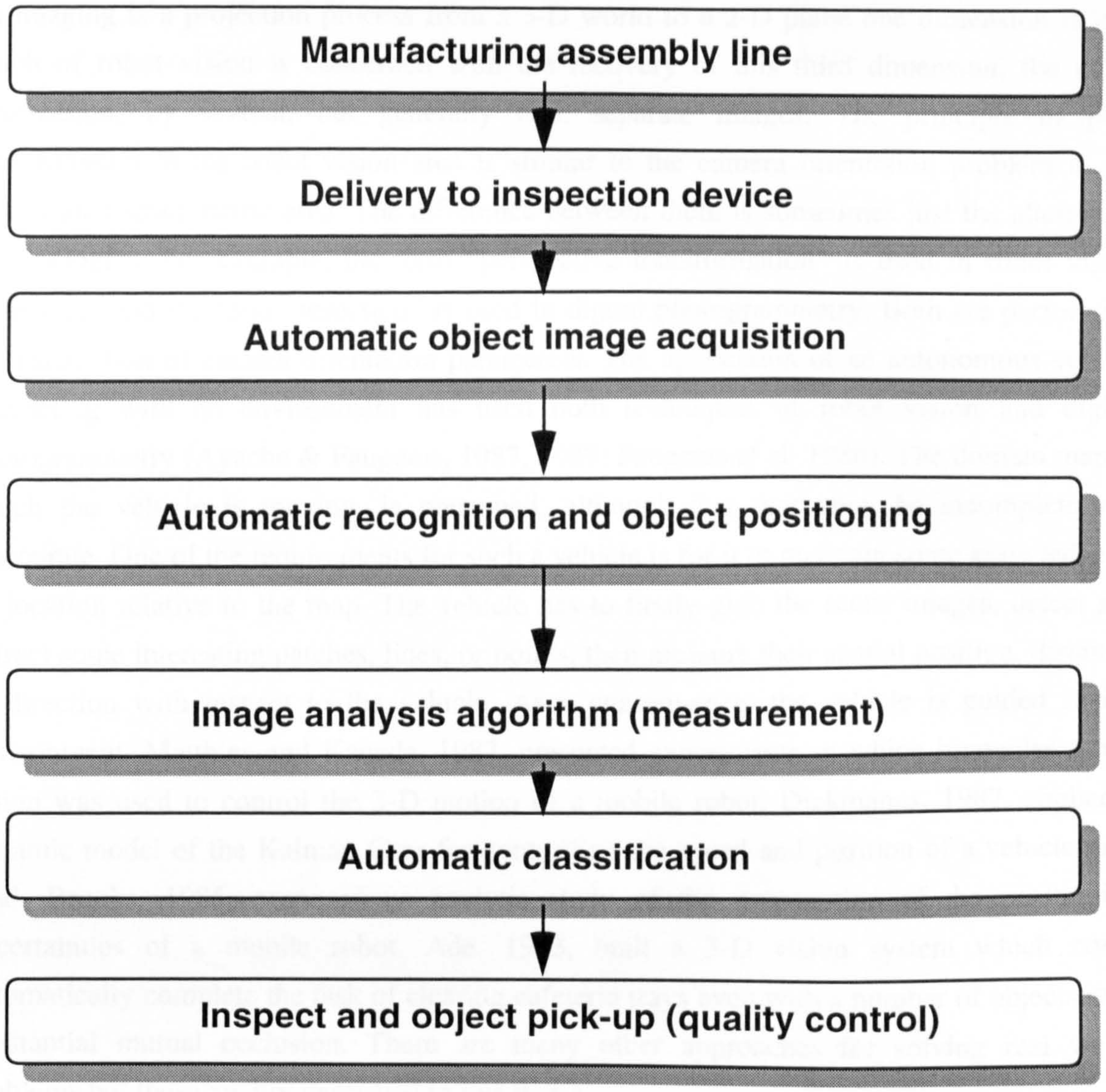

Figure 2.3 Automatic inspection flow chart

operate quickly enough. Figure 2.3 shows an inspection flow chart.

There are a number of comprehensive books on these topics by: Brown (1982); Davis (1990); Vernon (1992); and Haralick (1993).

(ii). Robotics

The application of machine vision techniques in robotics is concerned with determining the 3-D position and orientation of objects in the real world, i.e. how to obtain their image position and orientation and derive their 3-D pose, followed by effecting the robot's manipulation of the objects recognised location and orientation.

As imaging is a projection process from a 3-D world to a 2-D plane one dimension is lost. Much of robot vision is concerned with the recovery of this third dimension, the depth information, by several, but generally two, separate images. The principle of pose determination in the robot vision area is similar to the camera orientation problem in the digital photogrammetric area. The difference between them is sometimes just the alternative terminologies. For example, the term "perspective transformation" is used in robot vision techniques and the term "resection" is used in digital photogrammetry. Both are performing the calculation of camera orientation parameters. The application of an autonomous vehicle interacting with an environment has used both techniques of robot vision and digital photogrammetry (Ayache & Faugeras, 1987, 1989; Faugeras et al. 1986). The domain map in which the vehicle is moving, is presumed, although that map may be incomplete and inaccurate. One of the requirements for such a vehicle is for it to maintain some knowledge of its location relative to the map. The vehicle has to firstly grab the scene images, detect and extract some interesting patches, lines, or points, then measure their spatial position, distance, or direction with respect to the vehicle. As a consequence, the vehicle is guided in it's environment. Matthies and Kanade, 1987, presented experiments in which binocular stereo vision was used to control the 3-D motion of a mobile robot. Dickmanns, 1987, applied a dynamic model of the Kalman filter for controlling the speed and position of a vehicle on a road. Brooks, 1985, proposed an analytic study of the propagation of the positioning uncertainties of a mobile robot. Ade, 1993, built a 3-D vision system which could automatically complete the task of clearing cafeteria trays even with a number of objects with substantial mutual occlusion. There are many other approaches for solving real world problems but these are not described in this thesis.

(iii). Digital photogrammetry

Digital photogrammetry, using in some cases machine vision techniques, has opened the way to new applications for static and kinematic 3-D measurement techniques, leading to a new era in photogrammetry. There is a trend to move from photographically recording (analytical photogrammetry) to electronic image acquisition (digital photogrammetry) by means of CCD cameras. Many digital photogrammetric systems for automated 3-D co-ordinate measurement in a production environment have been developed. In recent years, the scientists in both the machine vision community and photogrammetric community have closer connections and more and more interesting topics. Evidence for this can be found in the conferences held by each group, where there are usually scientists in attendance from both societies. Hence, image processing based digital photogrammetric systems have been rapidly developed (Case, 1982; Alkertz, 1984; Gruen, 1989; and Dowman et al, 1992). Two main hardware architectures are available: a workstation based system and a PC based system.

(1). Workstation based system.

During 1980's. digital photogrammetric workstations (DPWS) have been rapidly developed. A DPWS consists of hardware and software to carry out photogrammetric tasks in an interactive and automated way using image data as input and image processing techniques as a tool.

A typical workstation configuration is the following:

- a central processing unit consisting of a RISC chip processor;
- 16 or more Mbytes RAM;
- a hard disk of 600 or more Mbytes;
- a high resolution graphic board that provides a memory image of 1024X1280 pixels of 8 bits in depth and a 24 bits look-up table to allow 256 colours from a palette of 16.7 (2^{24}) millions.
- back-up devices (tape streamer or floppy disk).

Haggren, 1987, developed a DWPS for industrial quality control applications. Muller, 1988, produced a SUN station photogrammetric system for stereo image display and point measurement using split screen viewing. Riechmann, 1990, introduced a modular approach to DPWS to meet the requirements of a DPWS for off-line close-range applications. Gruen, 1989, gave a detailed descriptions of the current status and prospects of DPWS in 1980's. Dowman et al, 1992, surveyed the development of digital photogrammetric workstations in Europe.

(2). IBM PC based system

The arrival on the market in 1990's of the IBM PC based photogrammetric systems has revolutionised the formerly inaccessible world of photogrammetry by their cheap price and has begun to open this formerly confined field of activities to a wide number of new users (land surveyors; industrial inspectors; public utility users and development researchers etc.). As a consequence, these new users will not need to be expert operators because the system will be easier to operate and the use of such systems can be more independent of the expert operator traditionally required.

A typical PC based configuration is likely to consists of the following:

- a central processing unit consisting of a 80386 or better chip with a 32 bit data path and an integrated math coprocessor;
- a high resolution graphic board which can provides a memory image not less than 1024x768 pixel of 8 bits in depth and a 24 bit look-up table;
- a hard disk with a sufficient storage (not less than 250 Mbytes);

- one or more back-up devices (floppy disks, tape streamer).

Turner, 1988, developed a PC based real time photogrammetric system for underwater robot operation and measurement. Sun, 1992, designed a PC based electron microscope digital image 3D processing system (EM3DPS), which integrates the image processing, image analysis, 3-D measurement and display into one package. Clarke & Robson, 1993, built a PC based digital close range three dimensional measurement system for less than 5000 pounds for the automated measurement of small industrial objects.

2.2.3. The current state of the art of photogrammetry using machine vision techniques

Photogrammetry has been developed for automatic or semi-automatic, real time or near real time and on-line or off-line applications. Such system are suited to industrial inspection, 3-D measurement, quality control and robotics based on machine vision. It is impossible deal adequately in one small section of this thesis all the applications of photogrammetry. Therefore only a few examples, which are closely related to the research in this thesis, are reviewed to illustrate the flexibility of the technique.

(i). Survey of industrial applications of photogrammetry using machine vision techniques

(1) Shipbuilding and aircraft-building

Kenefick, 1977, described how results of photogrammetric surveys can be applied in shipbuilding. He concentrated his discussion on predicting the fit of complicated double-hull sections of a ship built in halves. The co-ordinates of the the photogrammetric solution were transformed on the computer to put the as-built data into the ship's co-ordinate system, resulting in co-ordinates of 3-D surface, offsets, elevations and deviations from the transverse plane. Final manoeuvring, trimming and fitting took only 4.5 hours whereupon welding of the master butt commenced. Powell, 1984, used the same techniques to the measurement for a F-15 trim tool at McDonnell aircraft company. Recently, Fraser, 1992, established the degree of structural correspondence between the as-built development fixtures for a large C-17 military transport aircraft and its design, which was embedded in a computer-aided design (CAD) database. The measurement task involved the photogrammetric positioning to 0.2mm accuracy of more than 1400 points on interior loft surfaces.

(2) Antenna

Examples of the application of photogrammetry for antenna measurements can be found in Brown, 1982; El-Hakim, 1985b, 1986a; and Oldfield, 1986. Fraser 1984, designed a optimised network, which considered accuracy, economy and reliability in the measurement operation, to measure a parabolic antenna and to an accuracy of about one part of a quarter million. Fraser, 1992, also concluded that recent technological advances in industrial photogrammetry had great potential to improve on the accuracy and economy of antenna mensuration. He also indicated that industrial photogrammetric measurement to an accuracy of 1 part in 1,000,000 of the size of the object was obtainable.

(3) Tunnel (mining)

The surveying and monitoring of tunnels is often required to measure the shape of a tunnel's surface of tunnel since deformation caused by pressure in the tunnel linings can lead to collapse. Photogrammetry has proved to be a quick an reliable means for rapid data collection, cross-section profiling and determination of shape and structure. Figure 2.4 illustrates a tunnel cross-section profile collected by City University (Cooper & Clark, 1984) using photogrammetric techniques. Similar reports on the use of photogrammetry in measurement of tunnels can be found in Anderson and Stevens, 1984; and Wong, 1986.

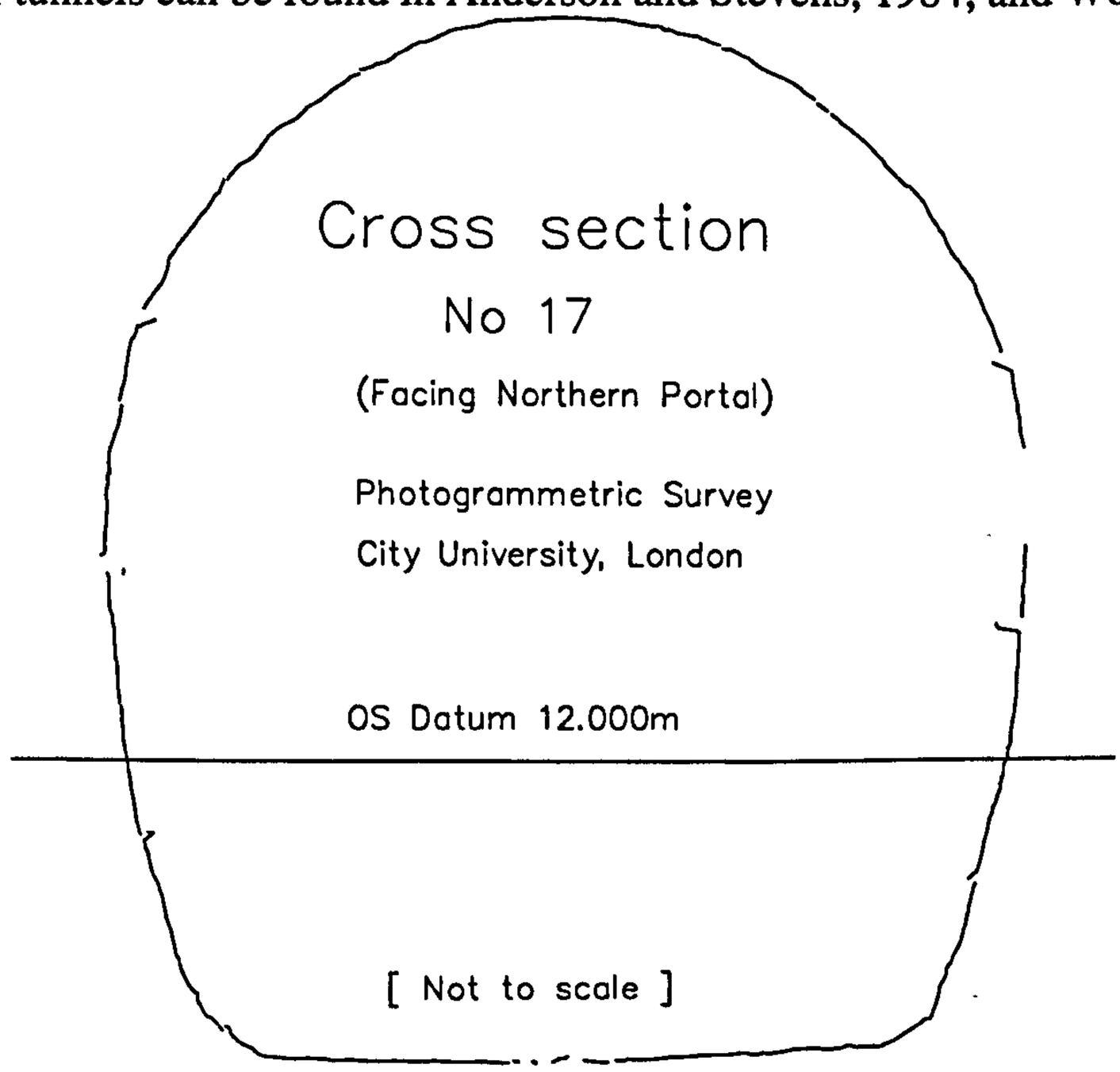

Figure 2.4 A cross-section at a tunnel profile

(4) Automobile

The application of photogrammetry in the automobile industrial has been one of the most successful applications of photogrammetry. As early as 1979, Cooper gave three feasibility studies of photogrammetry in automobile engineering. Godding & Luhmann, 1992, presented a machine vision based photogrammetric system which was suitable for measurement of dynamic processes and analysis of deformation in car crash tests with reasonable accuracy.

(ii). The connection between digital photogrammetry and machine vision

Although conventional analytical photogrammetric techniques can obtain 3-D measurement data at high accuracy, it is still difficult to use as an on-site inspection instrument. This is because there is a time interval between taking the photographs and obtaining the results. The image on film need to be processed, dried and then measured. These facilities are difficult to provide on-site so that conventional photogrammetry is usually often not rapid enough for many required measurement tasks. Digital photogrammetric systems have been developed based on the methodology of analytical photogrammetry implemented with the use of solid state image sensors. The development of the CCD camera and associated frame grabber technology has led researchers in the photogrammetric community into the area of digital image processing and machine vision. Many digital photogrammetric systems with industrially useful features have been proposed. El-Hakim, 1986a, 1989; Wong, 1986; Gruen, 1989; Dowman et al, 1992, have provided detailed overviews about these systems.

Figure 2.5 illustrates an IBM PC based digital photogrammetric system. It is similar to systems used to machine vision in terms of its hardware construction. The components used are typical of many digital photogrammetric systems. However, more powerful systems with higher resolution, more functions, and higher speed are now becoming available. The software may be divided into two sections: image processing elements and photogrammetric elements. Figure 2.6 illustrates a general software construction for a digital photogrammetric system.

The tasks for the machine vision section in the digital photogrammetric system are:

- acquire geometrically controlled images of the object scene directly in digital data form;
- preprocess the images to reduce noise of the digital image and extract target information from a noisy background;
- recognise targets with prior knowledge of the object target characteristics and produce a list of targets; and
- locate targets to obtain the 2-D co-ordinates of the target images to subpixel

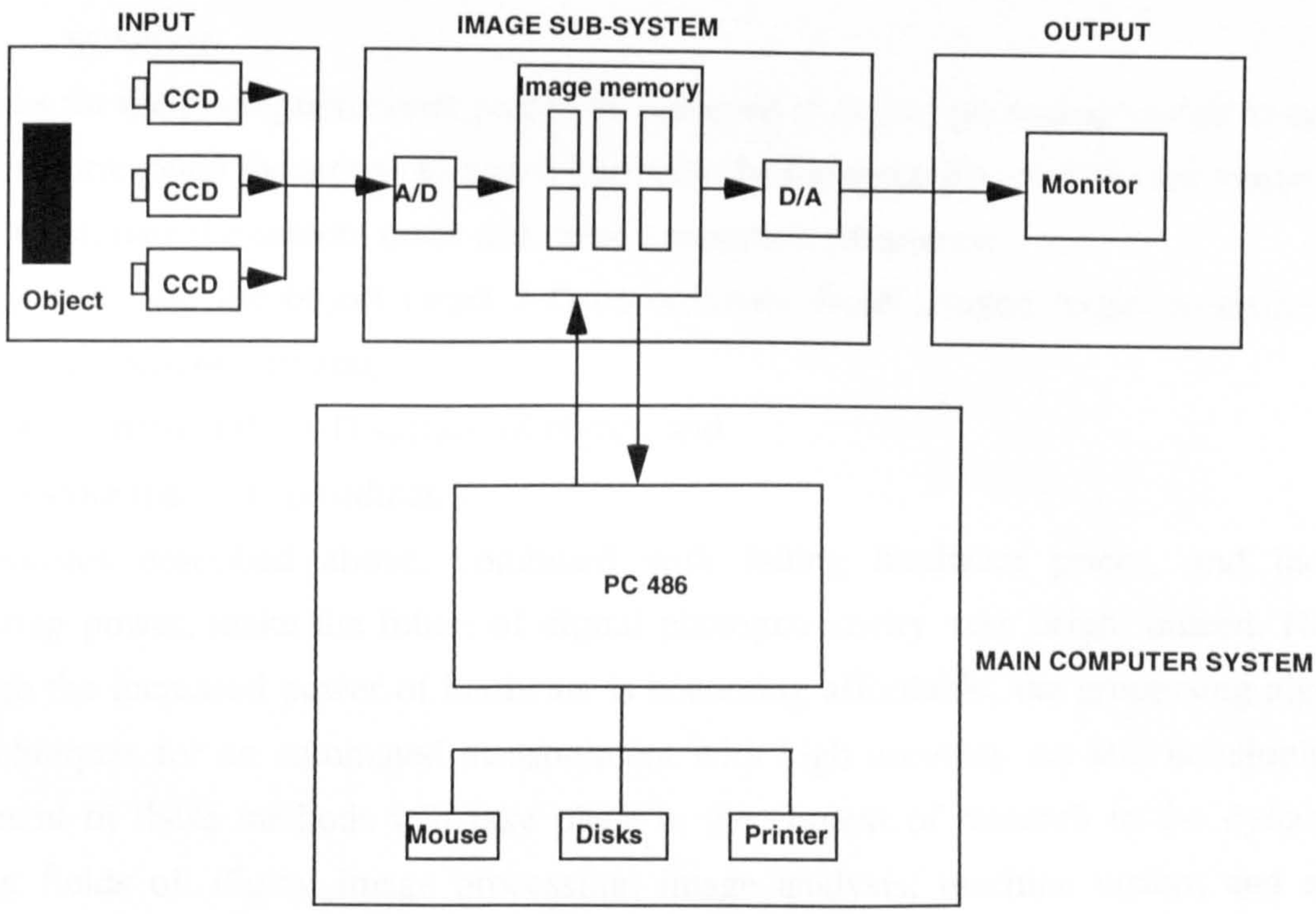

Figure 2.5 Construction of photogrammetry and machine vision system

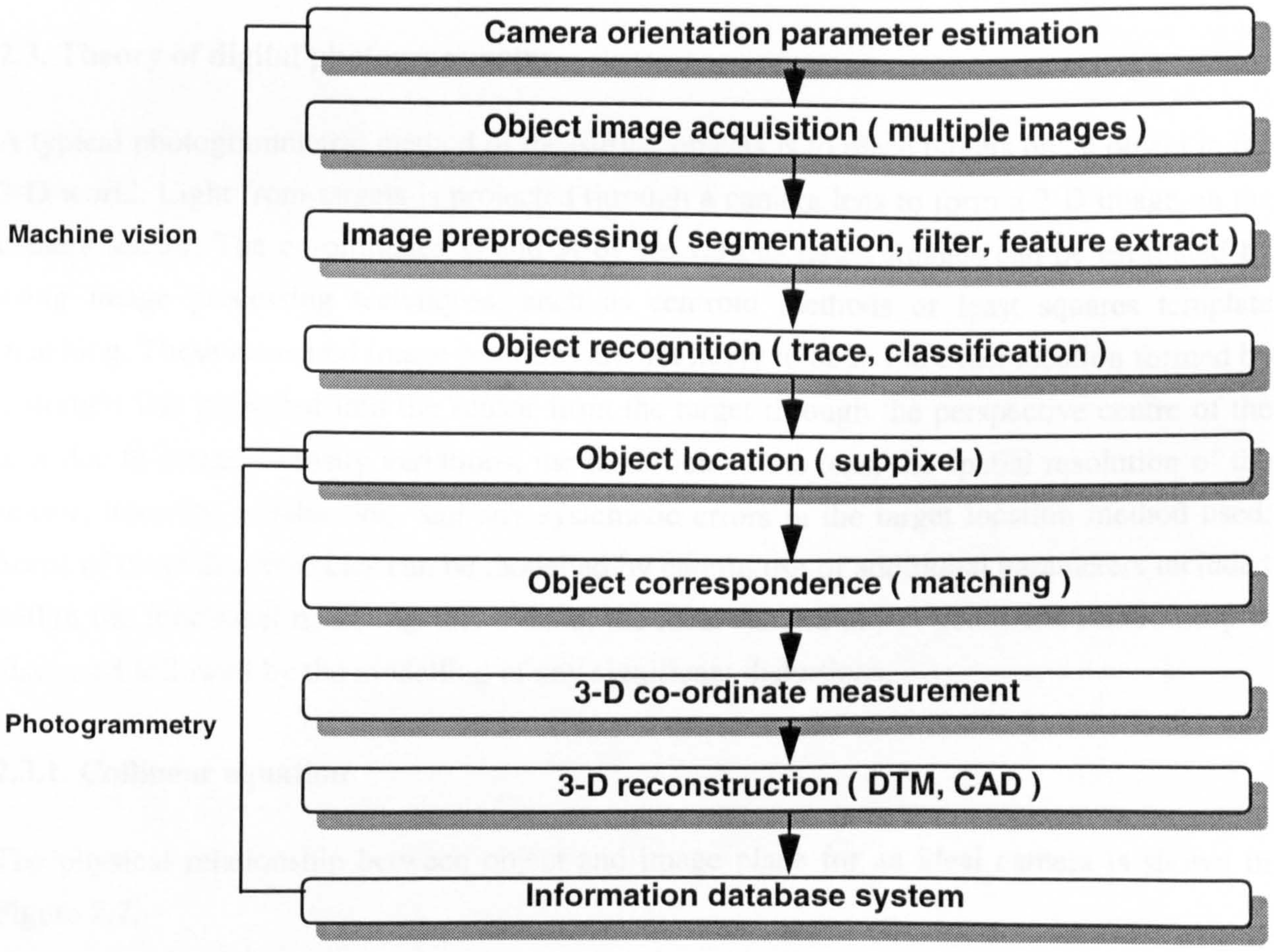

Figure 2.6 The connection between photogrammetry and machine vision

accuracy.

The tasks for the photogrammetric part to be achieved in digital photogrammetric system are:

- correspond the targets to match correctly the image targets in different images;
- estimate the camera outer and inner orientation parameters;
- calculate the object target 3-D co-ordinates from imaged target co-ordinates and camera orientation;
- reconstruct the 3-D surface of object; and
- store the 3-D co-ordinates.

The features described above, combined with falling hardware prices, and increasing computing power, make the future of digital photogrammetry very bright indeed. However, although the increased power of hardware is becoming affordable, the processing algorithms and techniques for an automated measurement with high accuracy are still developing. The refinement of these methods will take place in the context of research in the dynamic and exciting fields of: digital image processing; image analysis; machine vision; and artificial intelligence. Researchers in the area of digital photogrammetric systems must develop algorithms for an automatic object measurement with sub-pixel accuracy. These algorithms must be robust, efficient, practical, fast, and adaptable to different industrial applications.

2.3. Theory of digital photogrammetry

A typical photogrammetric method of measuring objects is to place targets on an object in the 3-D world. Light from targets is projected through a camera lens to form a 2-D image on the camera sensor. The co-ordinates x_i and y_i of the various target images can be estimated by using image processing techniques, such as centroid methods or least squares template matching. These measured image positions are not likely to be in the exact location formed by a straight line projected into the sensor from the target through the perspective centre of the lens due to image intensity variations, the distortion of the lens, the spatial resolution of the sensor, intensity equalisation, and any systematic errors in the target location method used. Some of these discrepancies can be modelled by careful use of additional parameters included within the functional model. In this section, the ideal camera-object geometric relationship is discussed followed by the modelling of any significant distortions.

2.3.1. Collinear equation

The physical relationship between object and image plane for an ideal camera is shown in Figure 2.7.

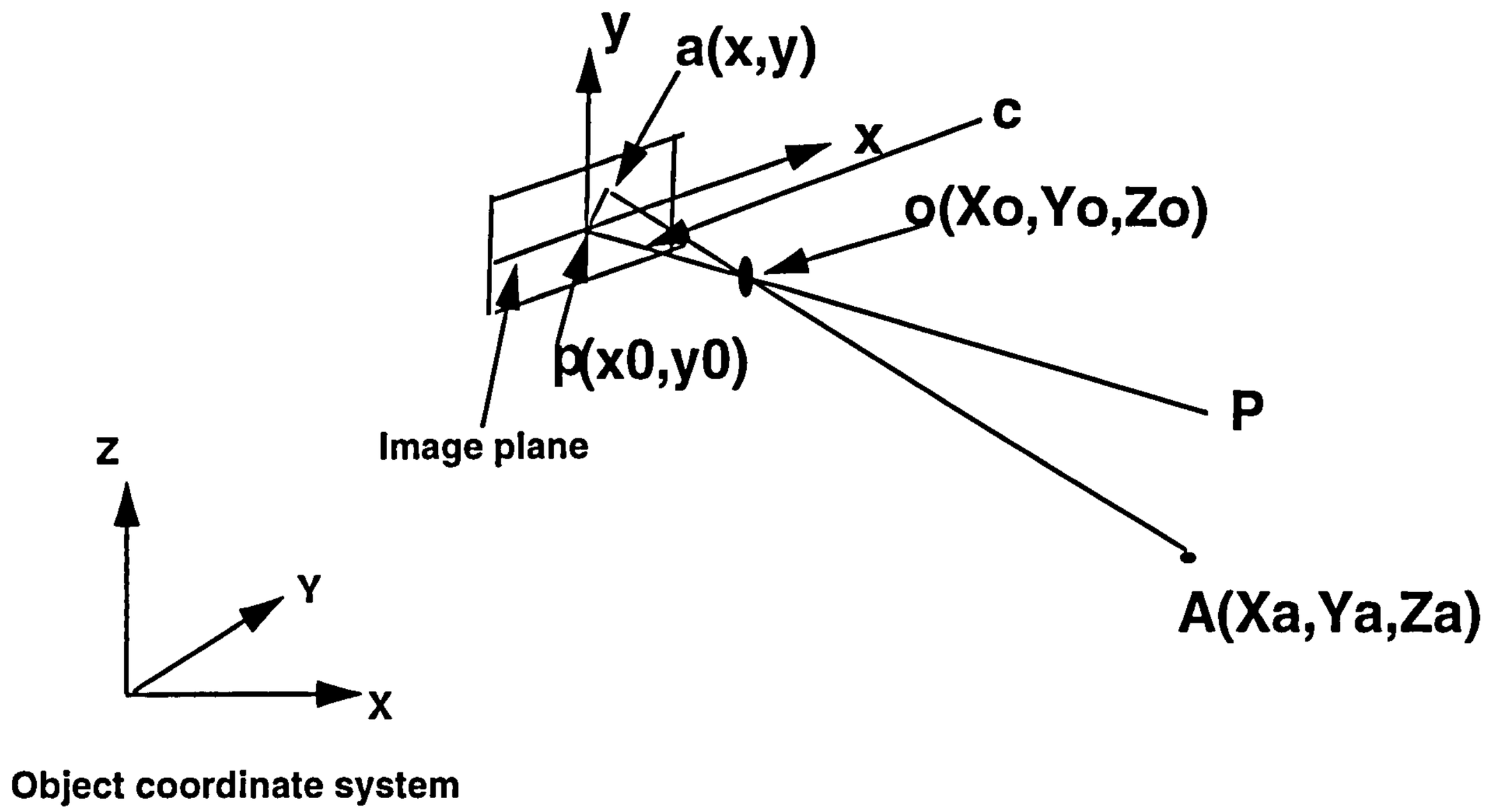

Figure 2.7 The central perspective projection of a camera

This figure shows the central perspective projection of an ideal camera. The principal point (p) is defined as the origin of the image plane; the perspective centre (**o**) of the lens is positioned at a point mutually perpendicular to the x, y axes. The principal distance (**c**) is the perpendicular distance from the origin of the image plane to the perspective centre of the lens. **Pop** is the optical axis. A(Xa,Ya,Za) and a(x,y) are object point co-ordinates and image co-ordinate point co-ordinates respectively.

From the central perspective projection it can be seen that a ray of light from the object point **A** passes through the perspective centre **o** and projects onto position **a** in the image plane. These three points are defined to lie on a straight line so that the fundamental collinearity equations are formed as follows (Methley, 1986):

$$-c\frac{m_{11}(Xa-Xo)+m_{12}(Ya-Yo)+m_{13}(Za-Zo)}{m_{31}(Xa-Xo)+m_{32}(Ya-Yo)+m_{33}(Za-Zo)}=(x-x_o) \qquad (2.1a)$$

$$-c\frac{m_{21}(Xa-Xo)+m_{22}(Ya-Yo)+m_{23}(Za-Zo)}{m_{31}(Xa-Xo)+m_{32}(Ya-Yo)+m_{33}(Za-Zo)}=(y-y_o) \qquad (2.1b)$$

where

m_{11} - m_{33}: · is a 3 x 3 orthonormal rotation matrix,

$m_{11} = \cos\varphi \cos\kappa$

$m_{12} = \sin\omega \sin\varphi \cos\kappa + \cos\omega \sin\kappa$

$m_{13} = -\cos\omega \sin\varphi \cos\kappa + \sin\omega \sin\kappa$

$m_{21} = -\cos\varphi \sin\kappa$

$m_{22} = -\sin\omega \sin\varphi \sin\kappa + \cos\omega \cos\kappa$

$m_{23} = \cos\omega \sin\varphi \sin\kappa + \sin\omega \cos\kappa$

$m_{31} = \sin\varphi$

$m_{32} = -\sin\omega \cos\varphi$

$m_{33} = \cos\omega \cos\varphi$

Xa,Ya,Za defines the object space co-ordinates of the point of interest,

$\mathbf{X_o, Y_o, Z_o}$ defines the projection centre position,

ω, φ, and κ are three angles rotating around X, Y, and Z axes respectively,

x,y are the co-ordinates of any point in the image plane,

$\mathbf{x_0}$, $\mathbf{y_0}$ defines the origin of the image plane, and,

c is the principal distance.

Two equations can be formed for each point of intersection on an object. Sets of equations can be obtained from additional cameras, which are able to view the same object points. For each of these equations there will be a number of known and unknown parameters. Some of the parameters will be the same for each camera, such as location of each corresponding point on the object. In general there will be more observations than unknowns, and so a least squares estimation of all the unknown parameters, including the 3-D location of the object targets which can be iteratively refined. This procedure is usually called a bundle adjustment (Grashaw, 1980).

A real lens will exhibit some deviations from this ideal collinear model. The object point, the perspective centre, and the projected point on the image plane, may not be collinear, therefore, additional parameter are added to the collinear equations to model these discrepancies.

2.3.2. Geometric lens distortion

Lens distortion can be thought of as the deviation of the image ray from ideal collinearity with the object ray. An ideal lens has collinear imaging geometry over its entire field of view and range of focus. However, no real lens has this perfect behaviour and will always suffer from several types of aberration, which will reduce both image quality and image geometric

fidelity.

Lens distortion is usually divided into two types, radial and decentering. As its name implies, radial distortion affects the position of image points on a straight line radially out from the principal point of the camera. It is also known as a symmetric distortion, since it is a function only of radial distance and is the same at any angle around the principal point. Decentering distortion, often caused by the improper manufacture of the lens, has both a tangential and a radial asymmetric component. Tangential distortion occurs in a parallel orientation at each point across the image and varies as a function of the radial distance and the orientation of the line from the point to the principal point with respect to a reference direction. The radial

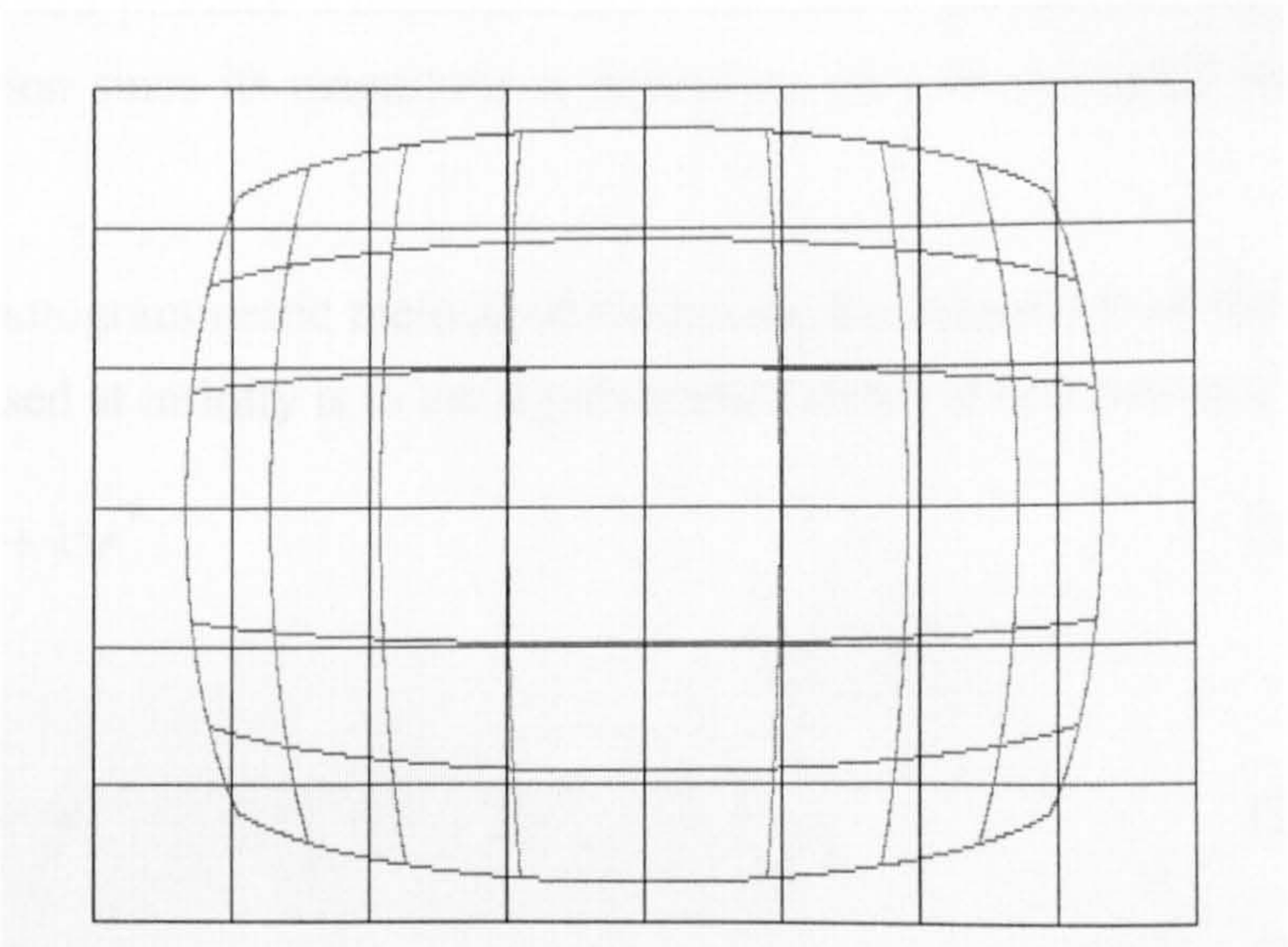

Figure 2.8 Effect of radial distortion

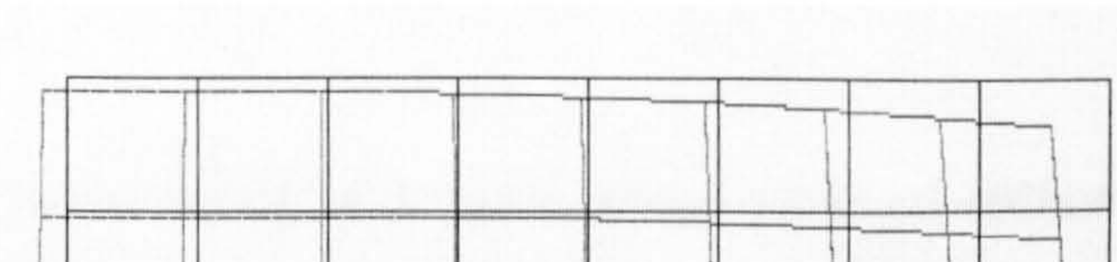

Figure 2.9 Effect of decentering

asymmetric component is added to the radial component. Figure 2.8 and Figure 2.9 illustrate the effects of radial distortion and decentering distortion by showing a 8 x 6 square grid with the distorted grid overlaid on top.

(i). Radial lens distortion

An ideal lens would produce an image with c constant over the whole field of view. That is the image produced by the lens will be geometrically the same as that produced by a central projection, this condition is known as orthoscopic. For practical lenses focused at infinity, the perspective centre must be split into front and rear nodes which may not coincide with the optical axis. This will produce a departure from the central perspective projection, known as radial lens distortion since its magnitude is dependent only on the radial distance **r** from the optical axis.

The traditional photogrammetric method of modelling the magnitude of lens radial distortion Δr for a lens focused at infinity is to use a polynomial series of odd powered terms:

$$\Delta r = k_1 r^3 + k_2 r^5 + k_3 r^7 \qquad (2.2)$$

and,

$$x_r = (x_{ij} - x_0) * \Delta r / r \qquad (2.3a)$$

$$y_r = (y_{ij} - y_0) * \Delta r / r \qquad (2.3b)$$

where k_1, k_2, k_3 are known as the coefficients of radial distortion and,

$$r^2 = (x - x_0)^2 + (y - y_0)^2$$

where **r, x, x_0, y** and **y_0** are the radial distance, image plane co-ordinates and the origin of the image plane respectively.

(ii). Decentering distortion

Each element of a lens has its own unique axis which is defined as the line joining the centres of curvature of the front and back surfaces. In an ideal lens system, the centres of curvature of all the spherical surface will be collinear to the optical axis. However, in a practical lens there can be a slight misalignment of components that will produce a displacement of the image from its ideal position. This misalignment of the unique axes to the optical axis of the compound lens, known as decentering distortion, is caused by manufacturing errors and is a highly individual property. Decentering distortion is complicated because it involves both a

radial and a tangential component.

The magnitude of lens decentering distortion r_d can also be approximately expressed by a polynomial function.

$$x_d = [p_1(r^2 + 2(x-x_0)^2) + 2p_2(x-x_0)(y-y_0)] \qquad (2.4_a)$$

$$y_d = [p_2(r^2 + 2(y-y_0)^2) + 2p_1(x-x_0)(y-y_0)] \qquad (2.4_b)$$

where:

p_1 and p_2 are the parameters of decentering distortion.

x_d and y_d are the components of decentering distortion at an image point x, y.

It can be seen that the first term of the equation (2.4) represents the radial component of decentering distortion and the remaining terms represent the tangential component of decentering distortion. The corrections for radial distortion and decentering distortion are independent of each other so that both corrections can be simply added together.

$$x_{lens} = x_r + x_d \qquad (2.5_a)$$

$$y_{lens} = y_r + y_d \qquad (2.5_b)$$

where: x_{lens} and y_{lens} are the total corrections for both the radial and decentering distortion corrections.

The influence of both radial distortion and decentering distortion can be taken into account by adding these geometric distortion parameters to the image measurements as additional parameters. Therefore, equations 2.1_a and 2.1_b may be rewritten as:

$$-c\frac{m_{11}(Xa-Xo)+m_{12}(Ya-Yo)+m_{13}(Za-Zo)}{m_{31}(Xa-Xo)+m_{32}(Ya-Yo)+m_{33}(Za-Zo)} = (x-x_o)+x_{lens} \qquad (2.6_a)$$

$$-c\frac{m_{21}(Xa-Xo)+m_{22}(Ya-Yo)+m_{23}(Za-Zo)}{m_{31}(Xa-Xo)+m_{32}(Ya-Yo)+m_{33}(Za-Zo)} = (y-y_o)+y_{lens} \qquad (2.6_b)$$

This may be regarded as the general equation for 3-D photogrammetric measurement.

2.3.3. Camera calibration

Geometric calibration of a CCD camera is an important aspect in a digital photogrammetric system whenever accurate measurement results are expected. A number of algorithms for CCD camera calibration have been presented and have been used in industrial fields for many

years (Tsai, 1987; Beyer, 1989; Fryer and Mason, 1989 Burner at el, 1990; and Dold, 1994) . The calibration of a CCD camera is usually classified into three forms: laboratory, on-the-job, and self-calibration. Laboratory calibration is typically performed with instruments such as goniometers and collimators, or with specially designed test arrangements. On-the-job calibration is performed together with the measurement task, but uses object space information in order to derive the required calibration parameters. Self-calibration is also performed with the measurement task, but extends the mathematical definitions in equation (2.6) to include calibration parameters in the bundle adjustment as variables. Camera calibration includes two groups of parameters: (1) interior orientation parameters calibration, which comprise the geometric parameters of the camera itself **c**, $\mathbf{x_0}$, $\mathbf{y_0}$, and geometric distortion parameters $\mathbf{k_1}$, $\mathbf{k_2}$, $\mathbf{k_3}$, $\mathbf{p_1}$, and $\mathbf{p_2}$; (2) exterior orientation parameters calibration, which defines the position of the camera perspective centre and optical axis to the object space X_0, Y_0, Z_0, ω, φ, κ. Calibration of both inner and outer parameters can be either separated or combined. These methods of calibration are now discussed in detail.

(i). Laboratory calibration

A camera can be calibrated in an optical laboratory environment. However such methods and equipments are expensive and so these complex calibration techniques are usually only used for calibration of precise aerial metric cameras. The laboratory method is based on a precise knowledge of the position and direction of light beams that are transmitted through the lens to or from an array of fixed collimators. In such calibration methods, the intersection of projected light beams with the image plane are subsequently measured. The accuracy of this calibration technique depends on the known geometry of the target collimator and on the accurate measurement of the images (Slama, 1980).

In the calibration method based on the goniometer technique, the emerging direction of the images from a precise grid held at the image plane are observed on the object side of the lens by a movable goniometer. The accuracy of the calibration depends on the known geometry of the grid plate and on the positioning accuracy of the goniometer (Fryer, 1989).

Fryer, 1989, gave some examples of laboratory calibration methods. Burner, 1990, presented a laboratory calibration method in which the principal point of a sensor was found by first aligning the sensor so that it was perpendicular to the sensor surface using an unexpanded HeNe laser beam, and then replacing the lens to find the principal point which is defined as the center of the sensor image. The disadvantage of a laboratory calibration method, compared with on-the-job calibration or self calibration, is that the calibration is not simultaneous with the use of the cameras so that errors may be introduced by changes in the

camera after calibration. The advantages of the method are the time for calibration can be saved and ***a priori*** knowledge is introduced which may be of use in reducing the number of unknown, so strengthening the least squares solution of unknown parameters in real-time applications.

(ii). On-the-job calibration

In on-the-job calibration methods, a test field is usually built. At least one control target for every two unknown parameters is required to build the equations for least squares calculation. Using control targets for which co-ordinates are accurately known, the camera distortion parameters and orientation parameters can be calculated followed by photogrammetric measurement of the object to be investigated. Calibration accuracy is usually dependent on the number of control targets and their distribution. Figure 2.10 shows a simple 2-D

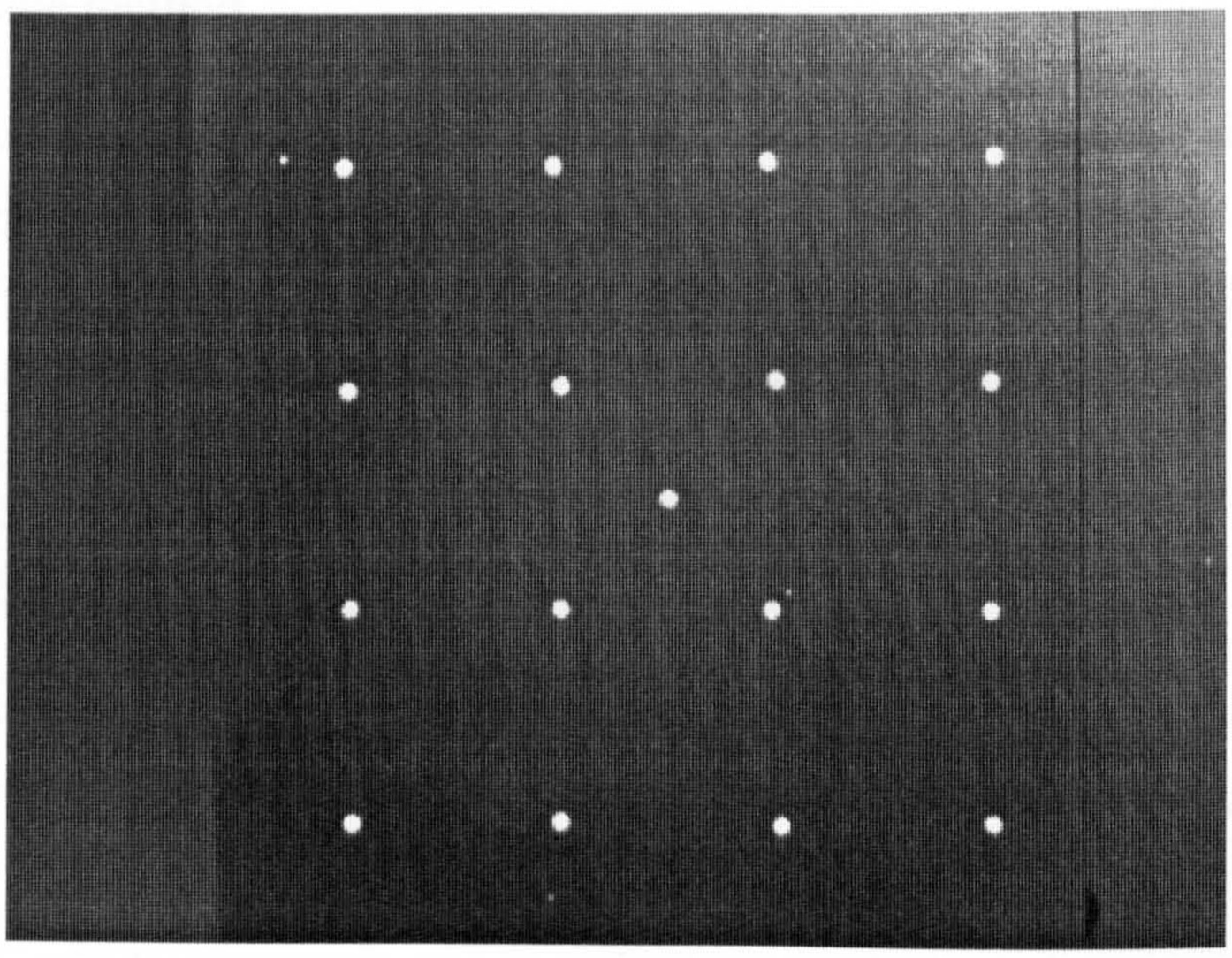

Figure 2.10 A test object with control targets

measurement calibration test field used in some of the experiments conducted for this thesis. The disadvantage of this method is that control targets are required. The advantage of on-the-job calibration is that the test field can be built so that automatic calibration can take place by choosing some easily identified control targets.

(iii). Self-calibration

The principle of self-calibration involves the extension of the mathematical model (Equation 2.1) that includes the camera distortion parameters (Equation 2.6). Equation 2.6 expresses the relationship between the image co-ordinates and object co-ordinates of targets as a function of inner orientation, outer orientation and camera geometric distortion parameters.

Self-calibration, as its name suggests, attempts to solve equation 2.6 without requiring any additional observation to estimate the camera distortion parameters. The self calibration is completed during the least squares procedure as an integrated part of computing the 3-D object co-ordinates by including these unknown parameters in the adjustment. Hence, self-calibration means that the camera distortion parameters are estimated "on-line". Self-calibration is an important feature of photogrammetric systems, because it does not require object space control and is the most common method of camera calibration in industrial applications (Fryer, 1989). The disadvantage of this method is that the extra computation cost is required and the result of calibration may be adversely affected by other features such as poor network design.

(iv). Other methods of camera calibration

(1) The plumb line method

With no radial and decentering distortion, straight lines in the object space should be straight lines in the image. Any departures from a straight line can be attributed to lens distortion (Brown, 1971). These deviations can be used to estimate the distortion parameters K_1 - P_2 by using equations 2.2 & 2.4. Figure 2.11 shows a straight line plotted in the x, y co-ordinate system. This line can be expressed by:

$$x'\cos\theta + y'\sin\theta = \rho \qquad (2.7)$$

in which ρ is the distance of the origin to the line, θ is the angle between the x' axis and the normal to the line through the origin. Co-ordinates x', y' of points on the image of the straight

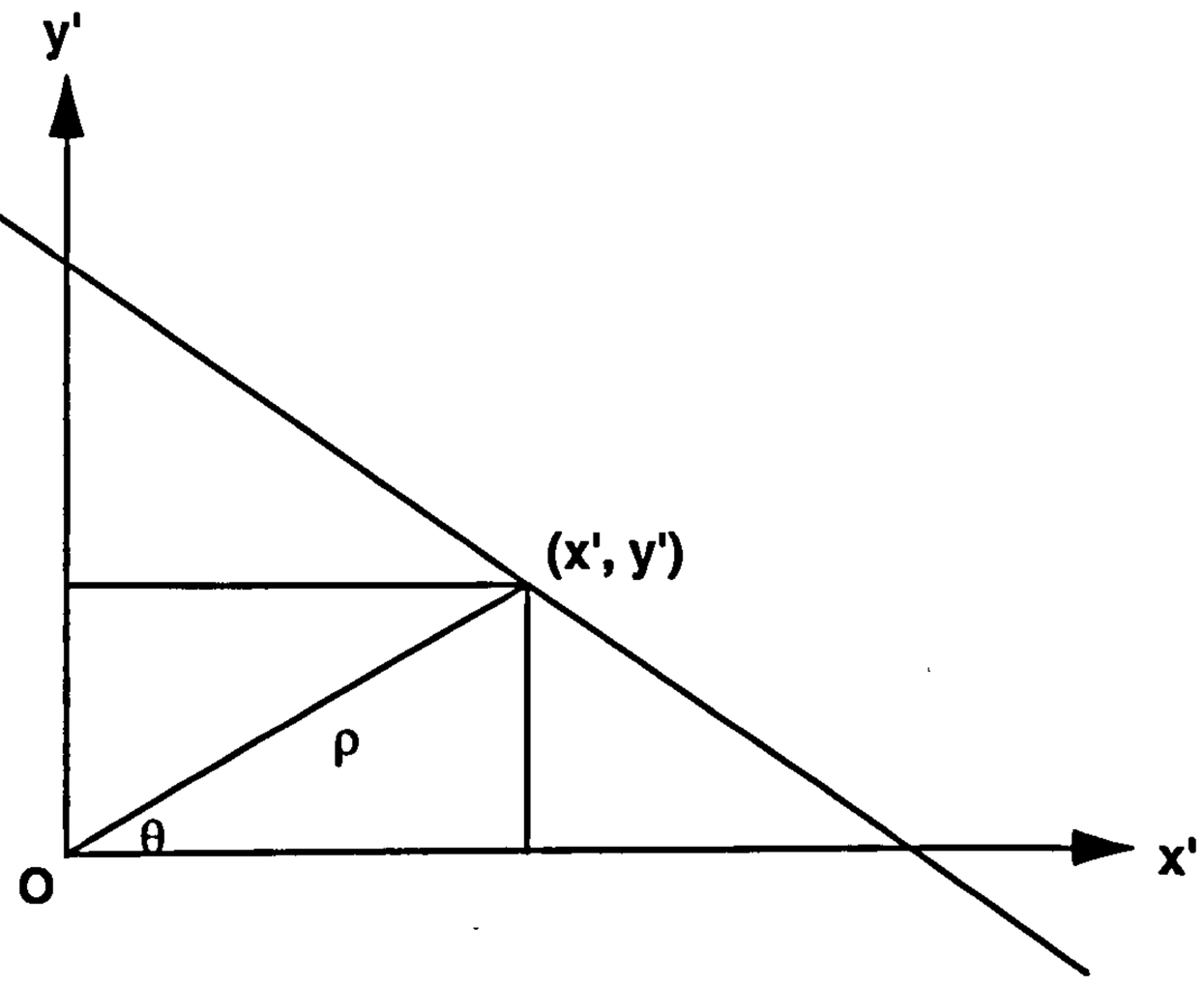

Figure 2.11 Straight line on image plane

line represent image co-ordinates after correction for radial and decentering distortion. They may be expressed as:

$$x' = (x - x_p) + x_r + x_d \qquad (2.8_a)$$

$$y' = (y - y_p) + y_r + y_d \qquad (2.8_b)$$

in which x,y are the image co-ordinates, x_p,y_p are the principal point co-ordinates, x_r, y_r are radial distortion component, x_d, y_d are decentering distortion component. Combining equations (2.8_a), (2.8_b) and (2.7), an equation of the following form can be produced:

$$f(x,y,x_p,y_p,k_1,k_2,k_3,p_1,p_2,\theta,\rho) = 0 \qquad (2.9)$$

For a discrete point this functional equation becomes:

$$f(x_{ij},y_{ij},x_p,y_p,k_1,k_2,k_3,p_1,p_2,\theta_i,\rho_i) = 0 \qquad (2.10)$$

in which x_{ij}, y_{ij} are the x,y co-ordinates of the j_{th} measured point of the ith line, θ_i and ρ_i are the angle and the distance to the ith line.

Fryer reported that in this specific case, x_p and y_p can be approximated by the centre point of the image plane without introducing significant error (Fryer, 1989). For n lines and m_i (i=0,...,n) points, there are total $2nm_i$ equations and 2n + 5 unknown parameters.

(2) Computing perspective transformation matrix method

Although the Equation (2.6) is a non-linear function of the outer and inner camera model parameters, they are linear if lens distortion is ignored (Equation 2.1) and if the coefficients of the perspective transformation matrix are regarded as unknown parameters (Haralick, 1993).

Equation (2.1) can be rewritten in perspective transformation matrix form:

$$[X\ Y\ Z]^T = R [X_0\ Y_0\ Z_0]^T + T \qquad (2.11)$$

where R is the 3 x 3 rotation matrix and T is the translation vector.

Given the 3-D co-ordinates of a number of targets and their corresponding 2-D image co-ordinates, the coefficients in the perspective transformation matrix can be computed by a least squares solution of the linear equations. The camera model parameters can then be computed by the perspective transformation matrix. Abdel-Aziz and Karara, 1971, developed a direct linear transformation (DLT) method, in which six control targets were required, to calculate the camera outer orientation parameters. Tsai, 1986, developed a two stage method,

in which both inner and outer orientation parameters as well as camera geometric distortion parameters were included.

(3) Geometric calibration method

Fischler and Bolles, 1981, used a geometric construction to derive a direct solution for the calculation of camera outer orientation parameters. This method does not compute camera inner parameters and camera distortion parameters, but it is in a closed form for the calculation of outer orientation parameters so that no iteration is required. Haralick, 1989, presented a method to determine camera outer orientation parameters from the perspective projection of a rectangle. Zeng and Wang, 1992, proposed a general solution of a closed form space resection, in which only four control targets were required to uniquely achieve the exterior orientation parameters calculation.

2.3.4. The self calibration bundle adjustment.

In digital photogrammetry, assuming the camera interior and exterior parameters are known, the spatial 3-D co-ordinates of an object target are determined by means of at least two bundles of rays, which come from two imaged targets in different image planes. Four equations will be obtained for the two rays and will result in one redundant observation for the object target co-ordinates X, Y, and Z. If further camera viewpoints and object targets are used, more bundles of rays will be formed resulting in extra variables of object target co-ordinates that will be introduced, this added redundancy will result in a better adjustment of the variables being estimated. Hence the terminology **bundle adjustment** is defined (Brown, 1958). The technique involves simultaneous least squares adjustment of all bundle of rays from all camera viewpoints to all measured image targets. Some constraints are normally used for absolute orientation when all target 3-D co-ordinates and camera exterior parameters are taken as variables. The **free bundle adjustment** is defined by using the inner constraints matrix G^t(Cooper, 1991) so that all object target co-ordinates and camera viewpoint exterior parameters can be taken as variables. The **self calibration bundle adjustment** is defined when the camera interior parameters and additional parameters are included as unknown parameters and are simultaneously estimated during this least squares procedure (Granshaw, 1980; and Fryer, 1989).

(i). The bundle adjustment

A simple camera network configuration suitable for a bundle adjustment is illustrated in Figure 2.12.

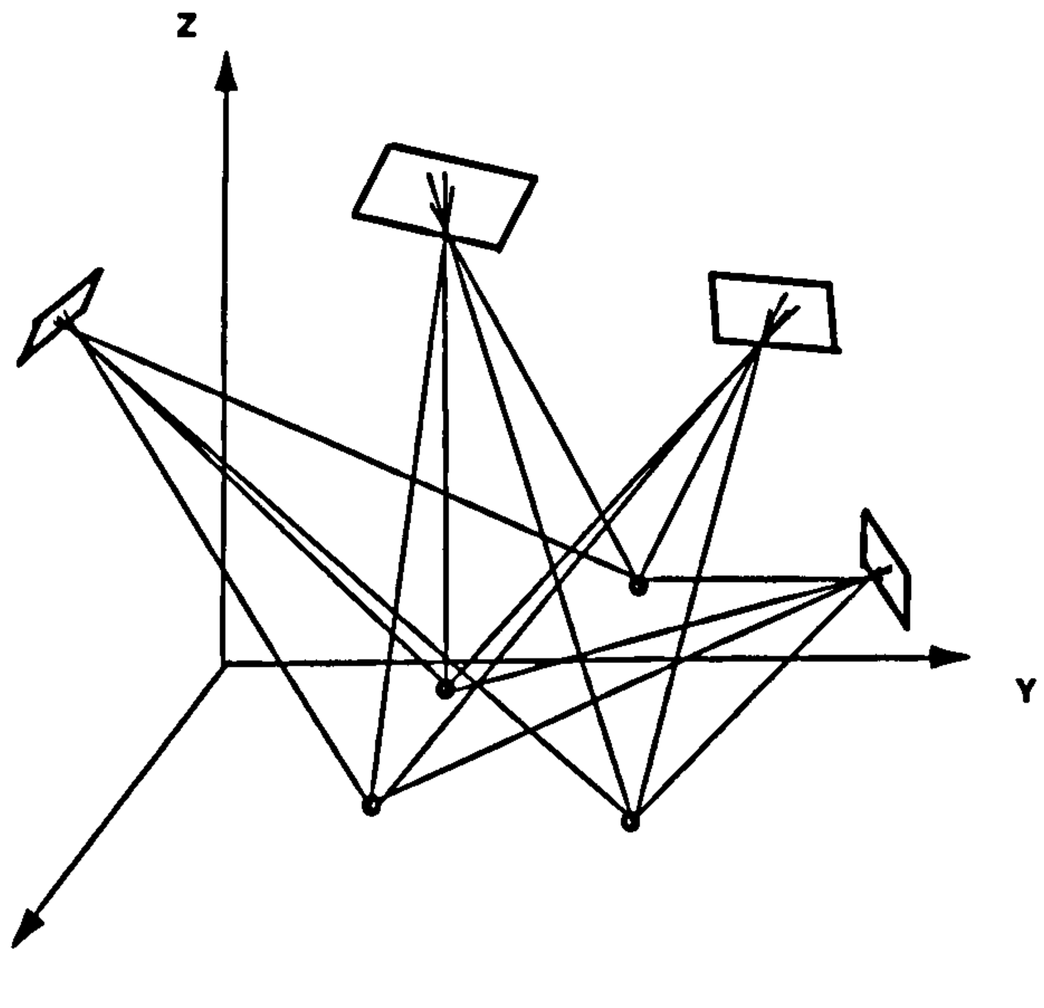

Figure 2.12 The basic configuration for the bundle adjustment

This figure shows a network where there are more than two camera viewpoints and more than two target images in each viewpoint. Each of the rays making a bundle at each target has an influence in the least squares procedure to calculate the 3-D co-ordinates of the object targets. The absolute orientation of this network can be defined by additional observations in object space, such as distances, directions, or by space co-ordinates as control targets. As the collinearity equation 2.1 is non linear if all the elements of orthonormal rotation matrix are unknowns, it has to be linearized before the least squares techniques are used.

Equation 2.1 is rewritten as follows:

$$-c\frac{m_{11}(Xa-Xo)+m_{12}(Ya-Yo)+m_{13}(Za-Zo)}{m_{31}(Xa-Xo)+m_{32}(Ya-Yo)+m_{33}(Za-Zo)}-(x-x_o)=0 \qquad (2.12a)$$

$$-c\frac{m_{21}(Xa-Xo)+m_{22}(Ya-Yo)+m_{23}(Za-Zo)}{m_{31}(Xa-Xo)+m_{32}(Ya-Yo)+m_{33}(Za-Zo)}-(y-y_o)=0 \qquad (2.12b)$$

Equation 2.12 can be represented as:

$$\mathbf{f(x,l,c)} = 0 \qquad (2.13)$$

where:

x is the vector of all parameters to be estimated, such as Xa, Ya, Za, Xo, Yo, Zo, ω, φ, κ;

l is the vector of elements which have been measured, such as x and y;

c is the vector of elements whose values are known and are regarded as constant (if

there are any).

Equation 2.13 is non-linear so that is must be linearised. This can be achieved by using Taylors' expansion and by taking the partial derivative of the equations with respect to each of these variables. Equation 2.13 can then be expressed as:

$$\mathbf{f}(\mathbf{x}_0,\mathbf{l},\mathbf{c}) + \mathbf{f}'(\mathbf{x}_0,\mathbf{l},\mathbf{c})\Delta\mathbf{x} = \mathbf{v} \qquad (2.14)$$

where

$\mathbf{f}(\mathbf{x}_0,\mathbf{l},\mathbf{c})$ is the zero-order term vector, evaluated by letting $\mathbf{x} = \mathbf{x}_0$;

$\mathbf{x}_0$ is the initial vector of variables;

$\mathbf{f}'(\mathbf{x}_0,\mathbf{l},\mathbf{c})$ is the first-order partial derivative vector of vector $\mathbf{x}$ at $\mathbf{x}_0$;

$\Delta\mathbf{x} = \mathbf{x} - \mathbf{x}_0$; and

$\mathbf{v}$ is the residual vector.

In this case, since the function can be written explicitly in each measurement, an observation equation can be written connecting each object target and its corresponding target image. Hence, two rows of equation 2.14 in j_{th} camera viewpoint and i_{th} target image can be written as (Granshaw, 1980):

$$a_{xji}\Delta X_i + b_{xji}\Delta Y_i + c_{xji}\Delta Z_i - a_{xji}\Delta X_{oj} - b_{xji}\Delta Y_{oj} - c_{xji}\Delta Z_{oj} + d_{xji}\omega_j + e_{xji}\varphi_j + g_{xji}\kappa_j$$

$$= x_{ji} - k_{xji} \qquad (2.15a)$$

$$a_{yji}\Delta X_i + b_{yji}\Delta Y_i + c_{yji}\Delta Z_i - a_{yji}\Delta X_{oj} - b_{yji}\Delta Y_{oj} - c_{yji}\Delta Z_{oj} + d_{yji}\omega_j + e_{yji}\varphi_j + g_{yji}\kappa_j$$

$$= y_{ji} - k_{yji} \qquad (2.15b)$$

where

a_{xji} - g_{xji} and a_{yji} - g_{yji} are the first-order partial derivative of the i_{th} target image in the j_{th} camera viewpoint;

x_{ji} and y_{ji} are the co-ordinates of the i_{th} target image in j_{th} camera viewpoint relative to the principal point of the j_{th} camera viewpoint; and

k_{xji} and k_{yji} are the numerical values of the first term of equation 2.12a and 2.12b determined as approximation values.

A collected linearised observation equations may then be represented in matrix form as:

$$\mathbf{Ax = b + v} \tag{2.16}$$

where

A comprises the partial differentials of the collinearity equations with respect to all the variables to be estimated;

v is the vector of target image co-ordinate residuals;

x is the vector of least squares corrections to the approximate parameters values; and

b is the vector of the all terms which can be calculated .

The observation equation solution may then be written as follows:

$$(\mathbf{A^tWA})\mathbf{x} = (\mathbf{A^tWb}) + (\mathbf{A^tWv}) \tag{2.17}$$

where the W denotes the weight matrix associated with all measurements.

and the least squares estimates of the parameters **x** are:

$$\mathbf{x} = (\mathbf{A^tWA})^{-1}(\mathbf{A^tWb}) \tag{2.18}$$

and

$(\mathbf{A^tWA})^{-1}(\mathbf{A^tWv})$ represents the error estimation vector of **x**.

However in practice, the dispersion matrix $(\mathbf{A^tWA})$ is singular with a rank defect of seven when all 3-D target co-ordinates and camera orientation parameters are variables. In the defect of seven are: three for the location of the object, three for rotation, and one for scale. To define the datum, seven arbitrary parameters can be fixed. Typically, a choice can be made from the camera viewpoint parameters, object 3-D co-ordinates, or a combination of both. Each different selection produces a different dispersion matrix **A**. However, this method is inappropriate in practice as fixing the seven parameters will directly lead to distortion of the parameters estimated by the bundle adjustment. The use of multiple camera viewpoints increases redundancy and allows the determination of the relative orientation. The free bundle adjustment, which is chosen for the bundle adjustment software design in this thesis, is an example of this approach.

(ii). Free bundle adjustment.

The free bundle adjustment uses minimum inner constraints to define the datum and thus provides a solution of collinear equations. The method was originally derived by Meissl, 1974, and was fully discussed by Cooper, 1991. In this method, constraints are provided by

the centroid of the object target co-ordinate values. The variable vector **x** is divided into two parts, $\mathbf{x_1}$ and $\mathbf{x_2}$, where the $\mathbf{x_1}$ is the vector of object co-ordinates and $\mathbf{x_2}$ is the vector of camera viewpoint parameters. The matrix **A** is also divided into two parts $\mathbf{A_1}$ and $\mathbf{A_2}$, where the $\mathbf{A_1}$ represents all the partial differentials of object 3-D co-ordinates, and the $\mathbf{A_2}$ represents all the partial differentials of the camera viewpoint exterior parameters. A seven column matrix **G** is formed to satisfy $\mathbf{G^t x=0}$. the columns of **G** are linearly independent, both between themselves and with the columns of **A**.

G is defined as:

$$G^t = \left\{ \begin{array}{ccc|ccc|c|c} 1 & 0 & 0 & 1 & 0 & 0 & \cdots & 0 \\ 0 & 1 & 0 & 0 & 1 & 0 & \cdots & 0 \\ 0 & 0 & 1 & 0 & 0 & 1 & \cdots & 1 \\ 0 & Z_1 & -Y_1 & 0 & Z_2 & -Y_2 & \cdots & -Y_n \\ -Z_1 & 0 & X_1 & -Z_2 & 0 & X_2 & \cdots & X_n \\ Y_1 & -X_1 & 0 & Y_2 & -X_2 & 0 & \cdots & 0 \\ X_1 & Y_1 & Z_1 & X_2 & Y_2 & Z_2 & \cdots & Z_n \end{array} \right\} \qquad (2.19)$$

The equation 2.16 can be rearranged:

$$\left\{ \begin{array}{cc} A_1 & A_2 \\ G^t & 0 \end{array} \right\} \left\{ \begin{array}{c} x_1 \\ x_2 \end{array} \right\} = \left\{ \begin{array}{c} b \\ 0 \end{array} \right\} \qquad (2.20)$$

From equation 2.20, it can be seen that the inner constraints are equivalent to maintain the following conditions:

$$\sum_{i=1}^{n} \Delta X_i = \sum_{i=1}^{n} \Delta Y_i = \sum_{i=1}^{n} \Delta Z_i = 0 \qquad (2.21)$$

$$\sum_{i=1}^{n} (Z_i \Delta Y_i - Y_i \Delta Z_i) = \sum_{i=1}^{n} (X_i \Delta Z_i - Z_i \Delta X_i) = \sum_{i=1}^{n} (Y_i \Delta X_i - X_i \Delta Y_i) = 0 \qquad (2.22)$$

$$\sum_{i=1}^{n} (X_i \Delta X_i + Y_i \Delta Y_i + Z_i \Delta Z_i) = 0 \qquad (2.23)$$

The physical meanings of equation 2.21, 2.22 and 2.23 can be explained as follows: equation 2.21 means that the position of the centroid of all object targets remains constant; equation 2.22 keeps constant the average distance of all **n** object targets from the centroid and equation 2.23 ensures that the average variance reference base consists of the centroid, the average

direction and average distance of all object targets from the centroid. Therefore using equation 2.20, all object target 3-D co-ordinates and all camera viewpoint parameters can be used as variables.

(iii). Self calibration bundle adjustment.

The concept of self calibration involves an extension of the collinearity equation 2.12 to include additional parameters, such as camera interior parameters. This method attempts to use the redundancy of observations to model the residual systematic errors inherent in the digital photogrammetric system. The difference between the bundle adjustment and self calibrating bundle adjustment is that self calibration attempts this modelling without requiring any additional data to be collected specifically for the purpose of modelling systematic error compensation. The main errors, as discussed in previous section, occur in the estimation of the camera lens distortion parameters and camera interior parameters, such as focal length, and principal point. If these camera interior parameter are considered, equation 2.1 is replaced by equation 2.6 and rewritten as:

$$-c\frac{m_{11}(Xa-Xo)+m_{12}(Ya-Yo)+m_{13}(Za-Zo)}{m_{31}(Xa-Xo)+m_{32}(Ya-Yo)+m_{33}(Za-Zo)}-(x-x_o)-x_{lens}=0 \qquad (2.24a)$$

$$-c\frac{m_{21}(Xa-Xo)+m_{22}(Ya-Yo)+m_{23}(Za-Zo)}{m_{31}(Xa-Xo)+m_{32}(Ya-Yo)+m_{33}(Za-Zo)}-(y-y_o)-y_{lens}=0 \qquad (2.24b)$$

For each viewpoint, there are as many as 7 parameters which can be used as variables. They are: camera constant c; principal point shift x_{shift} and y_{shift}; radial distortion parameter K_1, K_2, K_3; and decentering distortion parameter P_1 and P_2. Hence equation 2.20 is changed to:

$$\begin{Bmatrix} A_1 & A_2 & A_3 \\ G^t & 0 & 0 \end{Bmatrix} \begin{Bmatrix} x_1 \\ x_2 \\ x_3 \end{Bmatrix} = \begin{Bmatrix} b \\ 0 \end{Bmatrix} \qquad (2.25)$$

Where A_3 represents all the partial differentials of camera interior parameters and x_3 is the variable vector of camera interior parameters.

(iv). Bundle adjustment network optimisation.

Using the extended collinearity equations as a functional model in the bundle adjustment procedure, the major limiting factors are the number and location of camera positions and the precision with which the target images are measured. For the purpose of obtaining high accuracy object target co-ordinates: (1) a strong designed camera viewpoint geometry is

necessary; (2) good object target distribution is required; and (3) increased redundancy in the form of additional images at each viewpoint is desirable. Geometric network design in particular is crucial for the convergence of a bundle adjustment and for obtaining high accuracy results. Garafarend (1974) and Fraser (1989), have summarised the problem of geometric network design in terms of four interconnected stages:

(1) Zero order design (ZOD): The ZOD deals with the datum problem. It involves the choice of an optimal reference system for the object-space co-ordinates, given the photogrammetric network design and the precision of the target images. Generally, the ZOD concerns the production of an optimum cofactor $(\mathbf{A}^t\mathbf{W}\mathbf{A})^{-1}$ of the estimated parameters. In the bundle adjustment software design in this thesis, the G matrix is chosen as an inner constraint such that the datum introduces no shape distortion of the estimated bundles of rays when the free bundle adjustment is used.

(2) First order design (FOD): The FOD deals with the configuration problem. It concerns the optimal network geometry. The optimal network geometry results in an optimal design matrix A. The FOD embraces such aspects as camera radial and decentering distortion, target locations, camera selection, imaging geometry, and the influence of self-calibration in the final bundle adjustment.

(3) Second order design (SOD): The SOD deals with the measurement problem. It is mainly concerned with the maximising the precision of image co-ordinates measurement. This can be implemented by better hardware, such as high resolution cameras and framegrabbers or by software, such as using improved subpixel target location algorithms. Increased precision during SOD can be achieved by means of a weight matrix, which is produced by the search for an optimal precision distribution of the image co-ordinates. In the bundle adjustment software design in this thesis, the weight matrix **W** is formed from the covariance matrix of the bundle adjustment, which gives a high weight to high precision target image co-ordinates and a low weight the poor target image co-ordinates so that higher accuracy can be obtained.

(4) Third order design (TOD): The TOD deals with the densification problem. The TOD concerns the question of how best to enhance the precision of a network through the addition of extra object targets and viewpoints. In the bundle adjustment software for the IBM PC based photogrammetric system in this thesis, the target array density is not considered due to the limited memory available. However, the target precision can be enhanced by a "strong" convergent network geometry.

The potential for network design has been illustrated by Fraser (1992) with regard to the high precision monitoring of antenna, where one part in one million accuracy has been obtained

with high precision film cameras. In the later experiments of this thesis with multiple CCD cameras, an accuracy of one part in 30,000 has been obtained.

2.3.5. Statistical analysis of the result of bundle adjustment

In the bundle adjustment, the vector **x** of all unknown variables, such as the object 3-D co-ordinates, the exterior orientation parameters of cameras, and the interior parameters of cameras are computed by:

$$\mathbf{x} = (\mathbf{A}^t\mathbf{W}\mathbf{A})^{-1}(\mathbf{A}^t\mathbf{W}\mathbf{b}) \qquad (2.26)$$

Where

A comprises the partial differentials of the collinearity equations with respect to all the variables to be estimated;

W denotes the weight matrix associated with all measurements; and

b is the vector of the all terms which can be calculated.

The residual vector of the observations, i.e. the image 2-D co-ordinates is computed by:

$$\mathbf{v} = \mathbf{b} - \mathbf{A}\mathbf{x} \qquad (2.27)$$

The vector **v** is used to evaluate the precision of 2-D co-ordinates of each target image.

The ***a posteriori*** of the standard deviation might be estimated using:

$$\sigma_0 = \sqrt{\frac{v^T W v}{r}} \qquad (2.28)$$

Where **r** is the number of the degrees of freedom which for a free net adjustment is equal to the total number of equations plus 7 inner constraint equations, minus the total number of unknown parameters.

An evaluation of accuracy is performed by computing precision estimates of object points. The standard deviations of the estimated object co-ordinates are given by:

$$\sigma_{Xi} = \sigma_0\sqrt{q_{XiXi}}, \quad \sigma_{Yi} = \sigma_0\sqrt{q_{YiYi}}, \quad \sigma_{Zi} = \sigma_0\sqrt{q_{ZiZi}} \qquad (2.29)$$

where q_{XiXi}, q_{YiYi}, and q_{ZiZi} are the diagonal elements of the inverse of the normal matrix $\mathbf{A}^T\mathbf{W}\mathbf{A}$ at the position of the corresponding unknown variables.

The average precision of the 3-D co-ordinates of all measured object targets are:

$$\sigma_X = \frac{\Sigma\sigma_{Xi}}{n_x}, \quad \sigma_Y = \frac{\Sigma\sigma_{Yi}}{n_y}, \quad \sigma_Z = \frac{\Sigma\sigma_{Zi}}{n_z} \tag{2.30}$$

The RMS errors in object co-ordinates are computed as follows:

$$RMS_{\sigma X} = \sqrt{\frac{\Sigma(\sigma_{Xi} - \sigma_X)^2}{n_x}} \tag{2.31a}$$

$$RMS_{\sigma Y} = \sqrt{\frac{\Sigma(\sigma_{Yi} - \sigma_Y)^2}{n_x}} \tag{2.31b}$$

$$RMS_{\sigma Z} = \sqrt{\frac{\Sigma(\sigma_{Zi} - \sigma_Z)^2}{n_z}} \tag{2.31c}$$

2.3.6. Blunder detection

Blunder detection is a topic of great interest to photogrammetrists because undetected blunders can significantly distort the final solution and bias the statistical estimates used in 3-D measurement. In this system, blunders have been found to come from two sources: **(i).** wrong labelling of correspondences; and **(ii).** 2-D target location errors. Although the 3-D target matching algorithm can supply very reliable results by a two stage matching and an iterative procedure, a method is required to identify any errors that can occur. The 2-D target location errors are caused by defects in targets or by the target being partially occluded. This can cause a big shift in computed target location. However, the image residual of a bad target may be smaller than that of other good targets because the least squares adjustment has global smoothing characteristics and is relatively insensitive to individual blunders in the input data. Hence, such blunders can not be identified by a simple analysis of image measurement data residual. To detect the blunder a random sample consensus (RANSAC) method (Fischler, 1981), which has opposite the effect to the smoothing of least squares is traditionally used to detect blunders. The problem with this method is it is based on some well estimated targets being known beforehand. Iterations are then used to gradually identify the rest of the targets. After some iterations this process is able to find the best possible candidates of a certain subset of solutions. The iterations are stopped when no more good targets are found. If the same data is used, all random subsets will end up in exactly - with respect to the computing precision - the same least squares solution.

Other techniques used in blunder detection methods are based on robust estimation (Gao et al, 1992; Charles et al, 1994). Robust estimators are more reliable than the conventional least squares, where a single large blunder can cause many associated residuals to be large. There are several forms of robust estimation. They are: the L_1 norm method, which select a subset of all targets and minimises the sum of the absolute values of the residuals; the LS or L_2 norm method, which uses a least square technique and normalised residuals; and the Danish method, which uses exponential weights where measurements outside a chosen confidence interval are completely rejected. The LS method is used in this thesis to detect any blunders because it is dynamically connected with the bundle adjustment procedure. This method is described as follows.

Equation 2.26 can be rewritten as:

$$\mathbf{x = Bb} \tag{2.32}$$

where

$$\mathbf{B = (A^tWA)^{-1}A^tW} \tag{2.33}$$

therefore, Equation 2.27 becomes:

$$\mathbf{v = Ax - b = (AB - I)b} \tag{2.34}$$

and the covariance matrix of the residual is:

$$C_v = \sigma_0^2 [\, W^{-1} - A\,(A^tWA)^{-1}A^t] \tag{2.35}$$

where σ_0 **comes from equation 2.28.**

The LS robust residual for each equation is:

$$\sigma r_i = \frac{\sigma_i}{\sigma v_i} \tag{2.36}$$

where

σi is the i_{th} normal residual of each equation, and

σ_{vi} is the i_{th} diagonal element of the covariance matrix.

The LS robust residual is also called the normalised residual. By using this robust estimation for each iteration, the biggest blunders will be detected by normalising these residuals.

2.4. Theory of machine vision related to digital photogrammetry

The theory of photogrammetry is mainly concerned with the measurement of 3-D object co-ordinates by using 2-D image co-ordinate information. The theory of machine vision is primarily concerned with relations in the 2-D image space to perform tasks such as: filtering, segmentation, edge detection, feature extraction, target recognition, target location, target labelling, and image understanding. The advent of digital photogrammetric measuring systems requires many of the techniques developed in machine vision to be performed in an automatic and reliable way. The machine vision techniques which are required in a digital photogrammetric system are now discussed.

2.4.1. Low-level: image acquisition and processing

Any digital photogrammetric system will typically consist of one or more CCD cameras, a frame grabber and a computer. The digitised image, obtained from a CCD camera through an A-D converter, is stored in the memory of a frame grabber and consists of n x m pixels (for example 752 x 582). Each pixel has a known location (x,y) and a grey-level value. The digital image will be influenced by noise from a number of sources such as: non-ideal illumination, variable pixel response, poor synchronisation, quantisation error, and electronic noise. Research into these areas has been carried out by many authors (Beyer, 1992a; Haralick, 1993). The image averaging method has been commonly used to eliminate or decrease the influence of some of these noise sources, such as random noise and the temporal effects of line-jitter. In this method, a sequence of images is grabbed, and the average of the target image locations is computed. The acquisition of target co-ordinates implies a number of image processing and feature recognition processes. These processes are now discussed.

Image enhancement: The image enhancement process is needed to emphasise important features, such as targets, and suppress others. A number of linear and non-linear filters, such as the median filter, low-pass filter, edge detection filter, are available for the purpose. The selection of a filter depends mainly on the environmental parameters, such as illumination, target and background texture or reflective its characteristics.

Following any necessary filtering the next step is to segment the image at a certain grey level. In many industrial applications, the grey level of the background of the object is seldom constant over the whole image, hence, segmentation of the image at a single grey level will often give unsatisfactory results. There are many possible solutions to this problem such as: building a mathematical model of the background image and subtracting it from the image, high pass filtering, dividing the image into sections so that each subimage is processed

separately, or performing a Fourier Transform of the image, removing the low frequency components and doing an inverse Fourier Transform. Each method has its own advantages and disadvantages. In practice, the use of prior knowledge of both the shape of the targets and the structure being measured can assist in the choice of segmentation and detection algorithms. The photogrammetric measurement of a wind turbine blade section illustrates some of these processes (Figure 2.13a and b). In this case there are many equal sized targets and the background intensity changes slowly and provides good contrast between the dark targets and the light background. If the whole image is segmented above the highest background level, then some of the targets will be of reduced size, or in the worse cases, not visible at all. To reduce the problem of the uneven illumination, as shown in Figure 2.14, which is a line profile of Figure 2.13b, a local area of the image can be considered for normalisation of the background intensity level. Therefore, the whole image can be divided

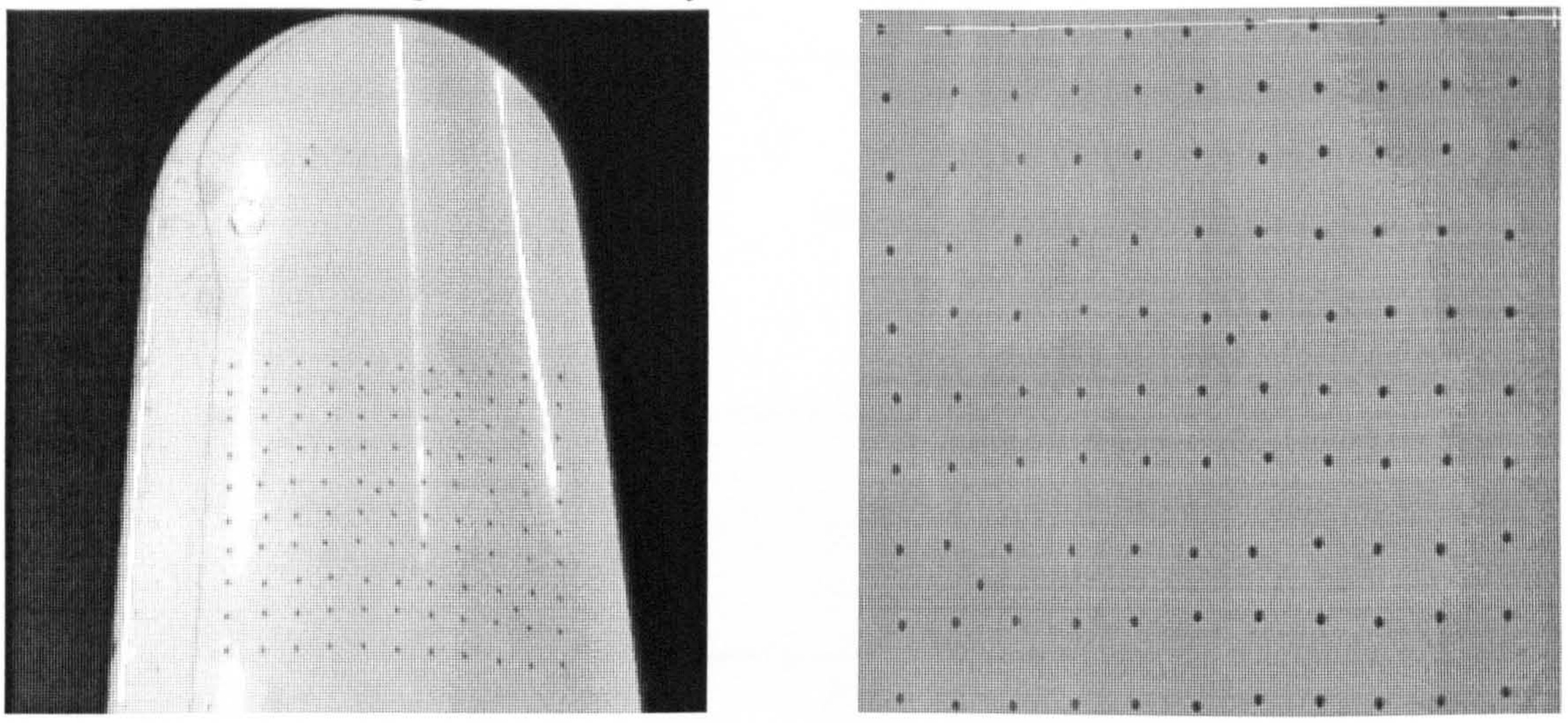

Figure 2.13 a). An original image b) A part of the turbine blade

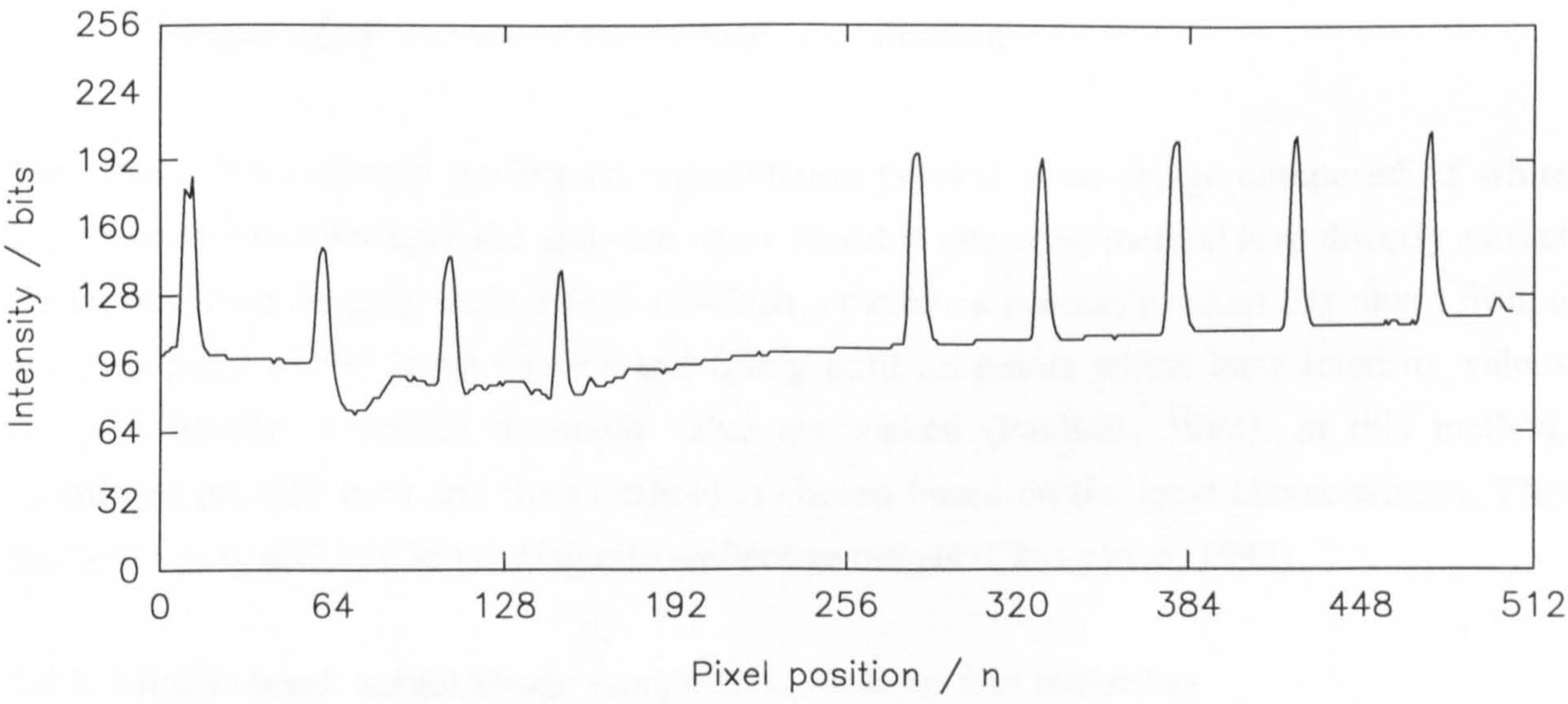

Figure 2.14 Inverted intensity profile of marked section

into subimages and the mean of all the intensity values is calculated for the whole image and the subimage. The subimage is then normalised using Equation 2.37.

$$IM[i,j] = IM[i,j] + (\mathbf{i\_mean} - \mathbf{l\_mean}) + C \qquad (2.37)$$

Where **C** is a constant, **i_mean**, and **l_mean** are the mean intensity values for the whole and subimage respectively, and IM[i,j] is the subimage array.

The advantage of this method is reliable thresholding in spite of the underlying background intensity variations. The value of **C** can be altered to adjust the image background to any desired level. Figure 2.15 shows the result of using the image normalisation, where it can be seen that segmentation will give good definition of the targets across the whole image.

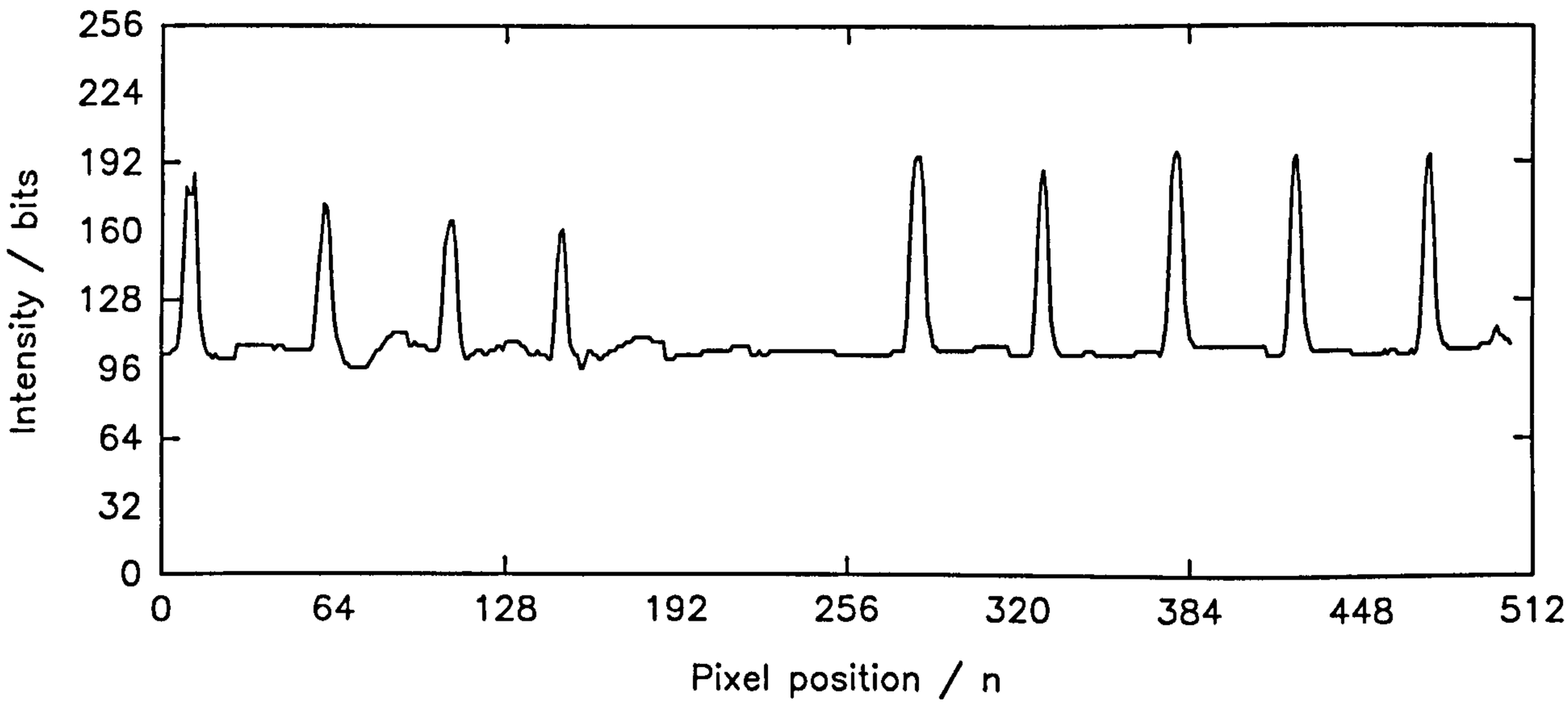

Figure 2.15 Results of local image normalisation

The result of a correctly performed segmentation process is an image composed of white targets and a black background and vice versa. Another alterative method is to directly extract the targets from the grey scale image, in which a recursive process is taken beginning from a arbitrary point of the target interior and filling until all points which have intensity values above a locally computed threshold value are visited (Pavlidis, 1982). In this method, subimages are still used and the threshold is chosen based on the local characteristics. This method is very efficient in locating retro-reflective targets (Clarke et al, 1993).

2.4.2. Middle-level: target image recognition, location and matching

The low level image processing discussed in the previous section can compensate for the

non-uniform background illumination and reflectivity. After image segmentation the process of recognising targets and locating targets to subpixel precision still has to be performed.

(i). Target image recognition

In the case of target image detection and recognition prior knowledge of the size, shape and possible orientation of the targets can be used. The recognition process is divided into three steps: **(1)** contour tracing of the object; **(2)** extraction of a structure parameter, which includes area, perimeter length, and circularity factors; and **(3)** the recognition of targets using prior knowledge and the structure parameters.

(1) Contour tracing of targets.

It is necessary to trace the contour of all objects which appear in the binary image. There are many methods can be used for this purpose such as the chain code method (Pavlidis, 1982). These are not discussed here as they are well understood and documented techniques. In the case of this study, the target appears as a black circular blob. The X,Y co-ordinates of the traced contour are extracted for use in analysis of the shape of the object.

(2) Extraction of the structure parameters

When an image is segmented there may be many objects other than the legitimate targets, so that it is necessary to find a suitable method to distinguish between targets and non-targets. Typical features which can be used are **(a)** perimeter length, **(b)** size, and **(c)** shape.

(a) **Perimeter.** The perimeter length of the subject can be calculated using the traced contour **X,Y** co-ordinates.

(b) **Area.** The area can be calculated by counting all of the pixels both inside and on the perimeter of the subject.

(c) **Shape.** A shape factor is used to express the differences between circular subjects and non-circular. A definition of the shape factor for a circular target is given in Equation 2.38.

$$Q = A/[\pi .(L / 2)^{2}] \qquad (2.38)$$

Where **A** is the area of the object, **L** is the longest distance across the object. The equation gives the ratio of the area of the subject to the area of a circle which circumscribes the subject. The nearer to a circle the object is, the closer to 1 the ratio is. The variation in the distance between pixels which are connected in x,y and the pixels connected in diagonal directions has to be compensated for. Some commercial cameras have differing scale factors in vertical and

horizontal so that there must also be an adjustment for this factor.

(3) Recognition of targets.

These three factors, allow the building of a decision function which is able to establish the likelihood of a given subject being a target. All parameters used are expressed in relative values for convenience.

$$\text{Area\_factor} = \text{ABS}((\ A - AA\ ) / AA\ ) \qquad (2.39)$$

$$\text{Perimeter\_factor} = \text{ABS}((\ P - PP\ ) / PP\ ) \qquad (2.40)$$

$$\text{Circle\_factor} = 1 - Q \qquad (2.41)$$

Where:

A is the estimated ideal target area

P is the estimated ideal target perimeter

Q is the circle factor

AA is the actual area of the object

PP is the perimeter of the object

When all of these factors are within some predetermined bounds there is a high probability of the object being a target so the object co-ordinates are stored, otherwise the object is rejected. This process is repeated for the complete image until all objects are recognised as targets or rejected.

(ii). Target location

In the previous section the recognition of the targets has been considered. In this section the subpixel location of these targets is discussed. To compute target locations the image intensity values of all pixels in a small window surrounding a target are commonly used to estimate the centroid position of the target to subpixel precision (Trinder, 1989). Many methods have been used for subpixel location of targets: such as least squares matching (LSM), interpolation, correlation, centroiding, differential, and shape fitting. LSM is a commonly used method for measuring targets to sub-pixel accuracy (Gruen, 1985). Centroiding and LSM have been used from the early days of image processing. The principle of the LSM method is that a template is constructed which has similar characteristics to those of the target image. A number of parameters are used as variables to obtain the best fit of the model target image to the real target image. These parameters will include x, y co-ordinate shifts and a number of other parameters such as scaling, rotation, image contrast and offset. For close range work, the size of the template target is typically from about 7 x 7 to 20 x 20 pixels whilst the shape of the

target may approximate to a Gaussian intensity distribution. Using physically based characteristics for the template target and parameter variable gives a high accuracy potential. However, the heavy computational cost is a disadvantage and iterative oscillation may occur when an inappropriate template is chosen (Beyer, 1992a).

Another location method which is popularly used is the centroiding method (Trinder, 1989). In this method, a small rectangular window around the target is placed such that it covers the whole target. A suitable threshold is used to eliminate background information from the target. The choice of a suitable window size can be dependent on the actual target size and object distance range. Using the intensity values within this window the precise centre of the target can be calculated using the following equations.

$$x = \frac{1}{M} \sum_{i=1}^{n} \sum_{j=1}^{m} j.g_{ij}.w_{ij} \qquad (2.42_a)$$

$$y = \frac{1}{M} \sum_{i=1}^{n} \sum_{j=1}^{m} i.g_{ij}.w_{ij} \qquad (2.42_b)$$

Where

$$M = \sum_{i=1}^{n} \sum_{j=1}^{m} g_{ij}.w_{ij}$$

g_{ij} is either 1 (target pixel) or 0 (background), w_{ij} is the grey scale value of each pixel and n, m define the window size.

A problem has been reported using the centroid method (Trinder, 1989) due to the influence of the background illumination. Targets which have a uniform background illumination will not be affected, but if there is a nonuniform background errors will be introduced. This effect is illustrated in Figure 2.16 by viewing a small section of the profile of the image shown in Figure 2.13. Although this is a single slice of the target image it demonstrates the problem.

To partially overcome such problems, a weighting factor may be introduced so that Equation 2.42 is changed into Equation 2.43.

$$x = \frac{1}{M} \sum_{i=1}^{n} \sum_{j=1}^{m} j.g_{ij}.w_{ij}.w_{ij} \qquad (2.43_a)$$

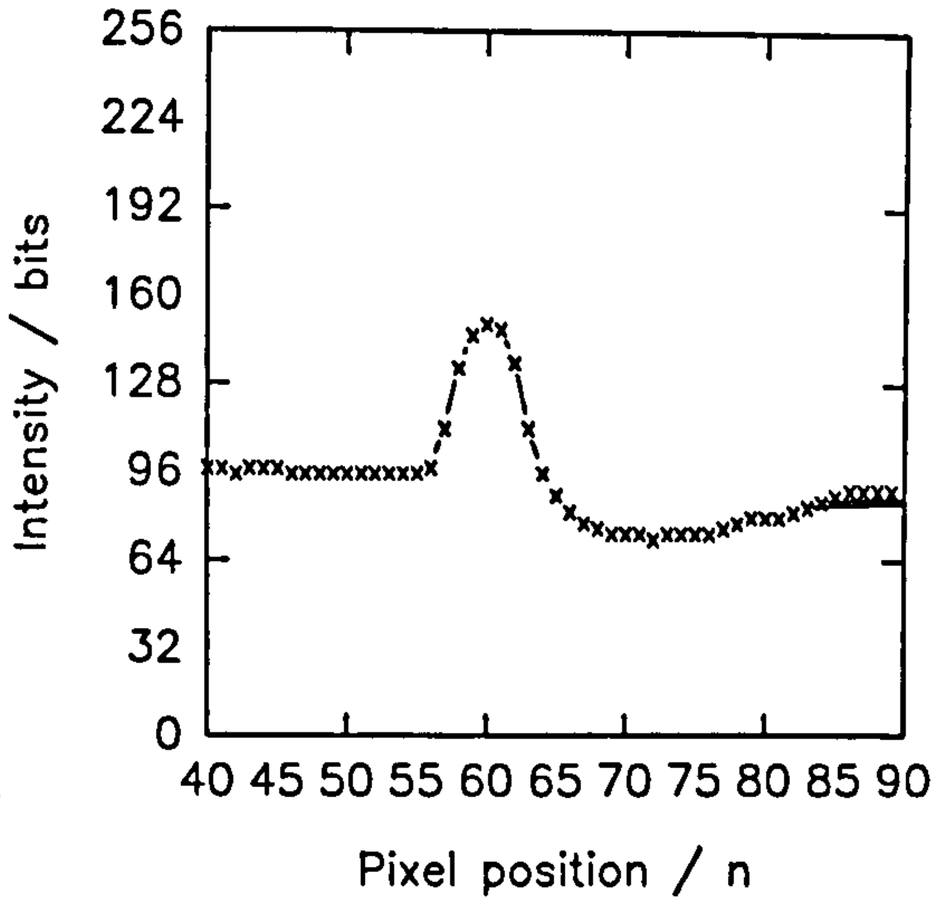

Figure 2.16 Section of target image shown in Figure 2.13b

$$y = \frac{1}{M} \sum_{i=1}^{n} \sum_{j=1}^{m} i.g_{ij}.w_{ij}.w_{ij} \qquad (2.43_b)$$

Where

$$M = \sum_{i=1}^{n} \sum_{j=1}^{m} g_{ij}.w_{ij}.w_{ij}$$

g_{ij} is either 1 (target pixel) or 0 (background), w_{ij} is the grey scale value of each pixel and n, m are the window size. In this case the higher intensity values of the target are given a greater weight in the calculation so that the influence of the background is decreased. The centroiding method works well on small circular shaped targets because the computation will give consistent results even when the targets are viewed from differing angles (Chen & Clarke, 1992; and Clarke etal, 1993).

(iii). Target correspondences

The procedures described in the previous section can be applied to images, from each viewpoint, and the location of the targets stored. Each target co-ordinate extracted in one image must be matched with its corresponding target extracted from an image using another viewpoint. The automatic solution of this "correspondence problem" is an important research area in digital photogrammetry and machine vision. The study of methods which can be used to find corresponding target images in multiple viewpoints has been undertaken by many researchers from both areas. Many techniques have been analysed, such as: area matching methods; feature matching methods; geometrically constrained matching methods; epipolar methods and so on. Baltsavias, 1991, gave a list of 34 adjectives which appear before the

word matching in the literature. This list was not exhaustive. These methods can solve many practical engineering problems and have been successfully applied in many situations. It is difficult to give an appropriate classification for all of these matching methods and so the main matching methods, which have been widely used, are described.

(1) Intensity based matching methods

Intensity based methods are based on point-to-point matching of image intensity values or matching of a surface area in one image with another. In this method, the unique intensity structure of a small part of the object is matched between various viewpoints. This method is highly reliable where there are strong intensity features to be matched.

When a template in one image is used to match with a patch in another image, this process is often called area based matching. In area based matching, cross correlation is used to determine the corresponding features between the images. One major disadvantage of the area based matching method is the computational cost of cross correlation for each image patch. To reduce the computational cost, some constraints, such as geometric constraints, coarse-fine procedures, hierarchies, can be used to improve the computation speed. These methods can be found in work by Marr, 1982; Gruen, 1988; Li, 1991; and Baltavias, 1991. More recently, the research in intensity based methods has shifted to global approaches and is more often performed in object space (Rosenholm, 1987; Heipke, 1992). The reasons for this are that the isolated matching of small image templates can be subject to blunders, especially in areas of poor or repetitive image texture, or where object surfaces have discontinuities. The object based matching method integrates the image intensity, point determination, and object surface reconstruction into a single model. The unknown quantities, such as radiometric and geometric parameters, are estimated directly from the pixel intensity values in a least squares adjustment. The method has been well described in detail by Baltsavias, 1991, and Heipke, 1992. In summary, intensity based matching methods are widely used in digital photogrammetry and the least squares method is the most common means of application for high accuracy target location with statistically based results .

(2) Feature based matching methods

In feature based matching methods the image features are extracted from the images and matched separately in a further step. In this method, image shape features, such as: points; lines; corners; arcs; or edges, are extracted by means of various operators, such as the Canny edge detector (Canny, 1983) followed by a Hough transform to extract straight line and circle information (Davis, 1992). These methods can considerably reduce the quantity of image information resulting in less computational cost than intensity based matching methods as the

task of finding corresponding features is based upon this minimised data. Another advantage of feature based matching methods is their success in dealing with occlusions as global features are decomposed into local features where local correspondences are analysed separately. An appropriate correspondence can be still established in the presence of occlusion by concentrating the contribution of local correspondences between local features extracted from different images (Grimson, 1990). However, although this method is robust it is not very accurate due to the use of an imprecise feature detection. But, feature based matching methods are widely used in machine and robot vision applications which can accept pixel level precision.

(3) Epipolar constrained matching methods

Epipolar constrained matching methods are commonly used in situations where there are few unique features or intensity characteristics. The projection of an epipolar line from a single object target onto an image can be defined as follows: when a ray of light from the object point **T** passes through the perspective centre $\mathbf{o_1}$ and projects onto position $\mathbf{p_1}$ in the image plane, these three points are defined to lie on a straight line. If this straight line is projected onto an other image ($\mathbf{V_2}$), an epipolar line is formed (Figure 2.17). This line can be used to determine whether point $\mathbf{P_2}$ originates from **T**. In the epipolar line matching method, two steps are required. The first is to estimate the orientation parameters of the cameras. These parameters are required to build epipolar line equations for each image. The second step is to match the corresponding imaged targets between images. To match a point in one image with its corresponding point in another, the image co-ordinates of this point in the first image and the orientation parameters of the two images are used to determine the relationship between

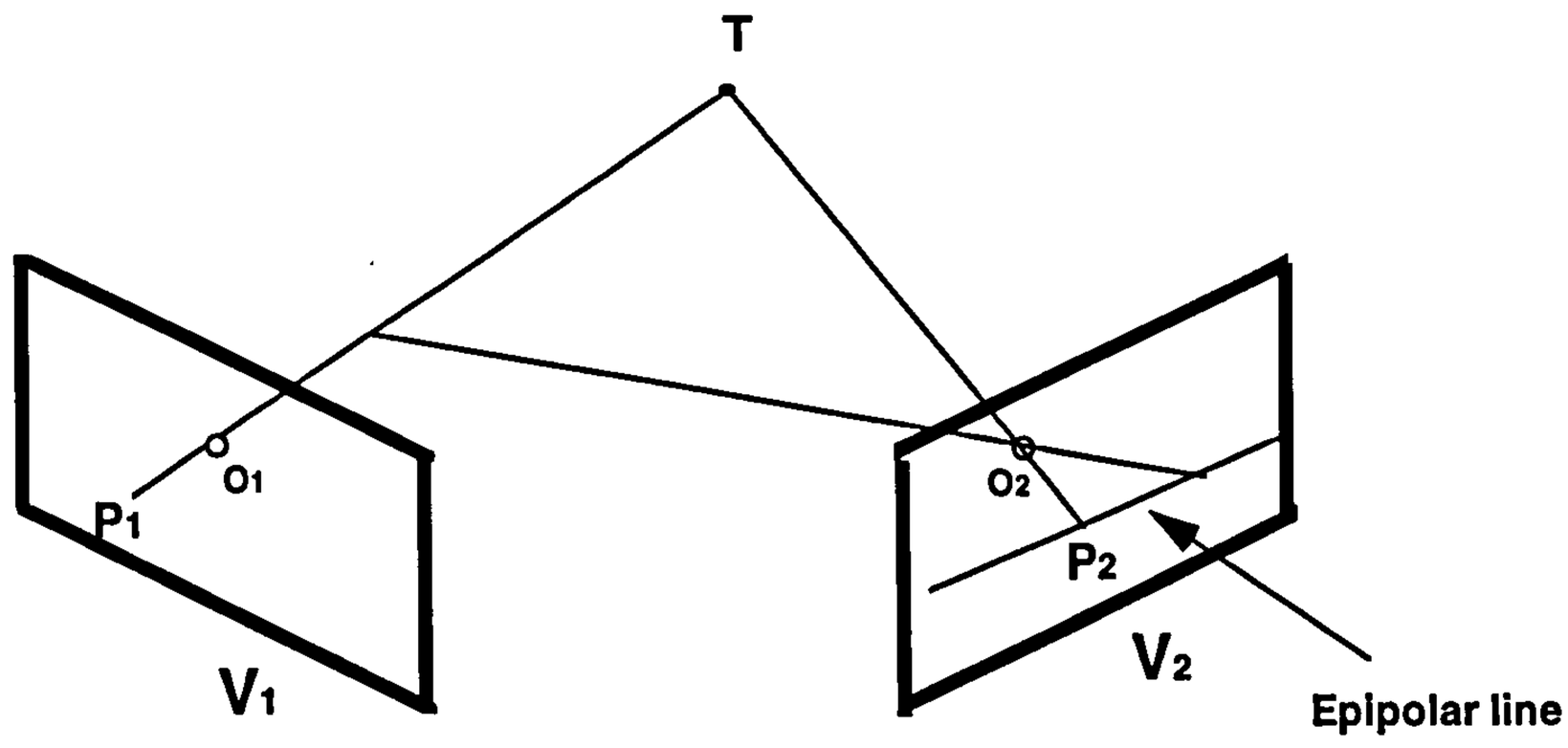

Figure 2.17 Epipolar line matching method

the co-ordinates of the point in the second image so that the matching point can be obtained. However, sometimes more than one target will satisfy the epipolar condition if another target also lies on the epipolar line. Therefore, geometric epipolar line constrained matching is not sufficient to impose an unique solution with only two viewpoints. Three or more cameras can be used to introduce more constraints to overcome some of the ambiguity problems (Ayache, 1991; Mass, 1992a). The advantage of the epipolar line method is that the method is independent of target characteristics and uses well established camera geometric properties. The algorithm is simple and easy to implement. This method can be used with intensity based and feature based matching methods as a constraint, or independently used for matching of indistinguishable targets points.

2.4.3. High-level: the use of expert systems

An expert system is one that uses the knowledge of specialists to assist an inexpert person to perform a task usually performed by an expert. The development of an expert system is of great importance to bridge the gap between the level of knowledge required to understand and use photogrammetric techniques to that possessed by the non-expert.

An expert system has the following characteristics:

- It is knowledge based. This knowledge is partly mathematical but mostly consists of a large number of logical rules.
- Reasoning based on heuristic is used.
- An aid to non-specialists is achieved providing interpretations better than those of novices.
- A variety of graphic and textual display is used to make its knowledge understandable and to justify its interpretations.
- It is flexible enough to be modified and extended frequently, without rewriting the programs that interpret the knowledge.

There have recently been some reports of photogrammetric systems using knowledge based approaches. Bammeke & Baldwin, 1992, described an expert system which has been applied to photogrammetric network design for close range measurement. Mason & Këpuska, 1992, built a prototype expert system called "CONSENS" with the aim of testing the suitability of applying conventional artificial intelligent (AI) technology to photogrammetric network design. Jansa & Trinder, 1992, presented an expert system which used close range digital photogrammetry for medical examinations in which the system knowledge base could be automatically extended and improved to aid measurement and result interpretation.

The research cited clearly indicates that the development and application of expert systems for photogrammetric are at an early stage of development, but it shows the potential of this technique.

2.5. Current trends in photogrammetry based on machine vision

The current rapid development of computer hardware and software technology are pushing digital photogrammetry into previously unreachable realms of accuracy and productivity. Further advances based on various technologies are likely to be evolutionary, with a wide range of applications to industrial problems. Digital photogrammetry is becoming more acceptable for many industrial automated 3-D measuring tasks. However, in spite of the extensive research on digital photogrammetric systems, some important limiting factors still remain. An automated digital photogrammetric system for industrial engineering measurement does not yet exist in a form where it can be installed and used by non-photogrammetrists. The current trend in digital photogrammetric systems can be divided into the following areas:

- the building of an automated and real-time digital photogrammetric systems for engineering measurement. This involves the continued development of algorithms for IBM PC-based fast image processing and object recognition, robust image matching, easy-to-use photogrammetric "black box" equipment and software, and flexible standard off-the-shelf components. Such a system using digital photogrammetric techniques is likely to be useful in many applications and make a significant impact on, for example, the automation of quality control of industrial components in manufacturing industry.
- the development of digital photogrammetric systems integrated with visual real time systems. The integration of image processing and computer graphics hardware and software will ultimately lead to combined image analysis and visualisation of dynamic changes of shape. Visualisation will combine the fields of computer graphics, image processing, machine vision, computer-aided design, and user interface studies. Such photogrammetric systems are likely to become a topic of research in their own right.

2.6. Summary

Photogrammetry and machine vision have been discussed as two distinct disciplines. However, they are closely related and there is a large area of overlap between the technologies.

The understanding of both photogrammetry and machine vision theory is very helpful for the

development and research of the 3-D measurement techniques. This thesis discusses work which combines both photogrammetry and machine vision techniques to contribute towards an automated digital photogrammetric system for 3-D measurement.

Chapter 3 Analysis of fundamental hardware characteristics of a digital photogrammetric system

3.1. Introduction

Digital photogrammetry can be used to measure the 3-D surface shape of many objects and has enjoyed rapid development during the past two decades. A PC-based photogrammetric system has been built for the purposes of research at City University. This system uses: a variety of lenses, six Pulnix TM-6CN cameras, an EPIX SVM GRB4MB framegrabber, a 486 IBM PC computer, and a variety of targets, such as naturally reflective targets, retro-reflective targets, laser targets, and projected targets.

The process of digital photogrammetric measurement may be divided into two tasks: data collection and subsequent data processing. Data collection includes the collection of the original images and any initial measurement such as target image locations. The data processing stage uses photogrammetric methods to calculate the 3-D co-ordinates of the targets on the surface of the object. A complete evaluation of all aspects of a digital photogrammetric system is extremely complex. There are several fundamental effects which may give rise to errors in the 3-D object co-ordinates estimated during the bundle adjustment process. These are:

(i) physically based effects such as:

- the influence of illumination;
- the choice of targeting methods;
- warm-up effects;
- radial lens distortion;
- decentering lens distortion;
- line-jitter; and
- quantization.

(ii) algorithmic problems such as errors in:

- target location;
- camera parameter estimation;
- target matching; and
- bundle adjustment.

Source of the features of the seven physically based error sources are analysed in this chapter. The remaining algorithmic problems will be analysed in later chapters.

3.2. The characteristics of photogrammetric error sources

3.2.1. Illumination

The surface characteristics of an object and the type of illumination play an important role in the digital photogrammetric measurement process. The use of directional illumination during image acquisition is a method often used to enhance the contrast between the target and the background. This makes the automatic recognition and location of targets easier (Low, 1991). The choice of target and lighting is application dependent, but there are some general issues that require discussion.

Incandescent bulbs are often used as they provide a simple, readily available, source of light. Such sources are cost-effective and can be easily adjusted for light intensity. They are generally used in a directional mode whereby they approximate to a point source. Consequently, strong shadows are produced on the surface of an object which may cause problems for the photogrammetric image analysis software. Additionally, incandescent bulbs emit considerable infra-red (IR) radiation. This can cause problems for some camera sensors, particularly CCD cameras, as these are sensitive to IR. Anomalies can arise because the reflection characteristics of some materials are different in the IR compared to the visible wavelength light. However, special bulbs and filters are available which can minimise the infra-red component reaching the CCD sensor.

In close range photogrammetric measurement applications, a diffuse source of light is often the most suitable. Diffuse lighting is non-directional and produces a minimum amount of shadow. Fluorescent lighting is a common means of obtaining diffuse illumination, it is especially good for providing illumination of the object surface on which a number of targets are sited. However, if retro-reflective targets are used the axial illumination is required because this can achieve high signal to noise ratio.

3.2.2. Characteristics of targets

In digital photogrammetric 3-D measurement the choice of target type is an important factor because it will influence overall measurement performance. The choice is mainly determined by the requirements of speed, precision, cost, reliability, and flexibility. There are commonly four types of targets which are available: naturally reflective targets, retro-reflective targets, laser targets, and projected targets. Each target has its own characteristics and can be chosen for different purposes. Their major properties are briefly discussed below.

3.2.2.1. Naturally reflective targets

Naturally reflective targets can be manually produced by means of a printer or by use of a card punch. This type of target is easy to produce in any size or shape and can be black against a white background or vice versa. The target is fixed to the surface of the object to be measured. These targets are very often used in deformation measurement of engineering structures where the measuring distance ranges from 10 - 300 metres (Kennie, 1990). However, there are several limitations. First, the process of individually placing large numbers of targets on the surface of each measured object makes it difficult for fast measurement of industrial objects. The repeated targeting of a surface is a tedious task and often impractical. Secondly, target contrast is often adversely influenced by uneven illumination. To overcome the problem of uneven background illumination an extra image pre-processing and contrast operation may be necessary and in such situations prior knowledge of any background intensity variations is useful in the image pre-processing stage. Figure 3.1 is a 3-D profile of natural target. It can be seen that the uneven background could cause some error in subpixel target location. Hence, a threshold value has to be chosen to minimise the background error.

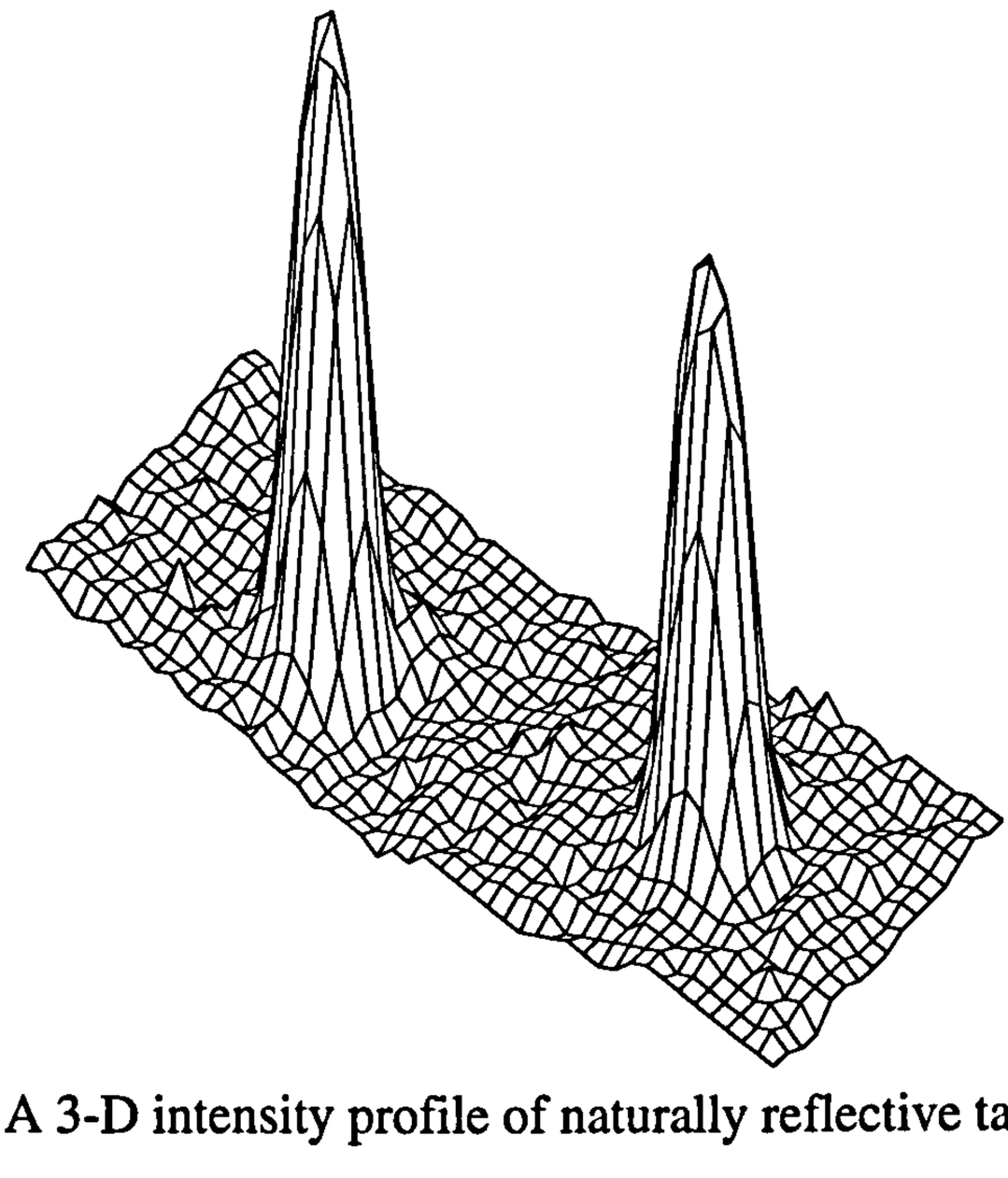

Figure 3.1 A 3-D intensity profile of naturally reflective targets

3.2.2.2. Retro-reflective targets

A retro-reflective target can be made from retro-reflective self adhesive film. The retro-reflective effect is generated by small spherical balls which cause the incident light to be

reflected back in the direction of the incident light. A very high signal-noise ratio can therefore be obtained. Figure 3.2 illustrates the structure of the retro-reflective material. The principal of reflection is shown in Figure 3.3. From this figure it can be seen that the angle of the reflected light is designed to be approximately 180 degrees compared the direction of incident light. The intensity of the light returned by the target can be changed by altering the level of illumination of the light which is approximately on axis with the camera. The resulting background noise can be minimised, even eliminated to zero level, by adjusting the

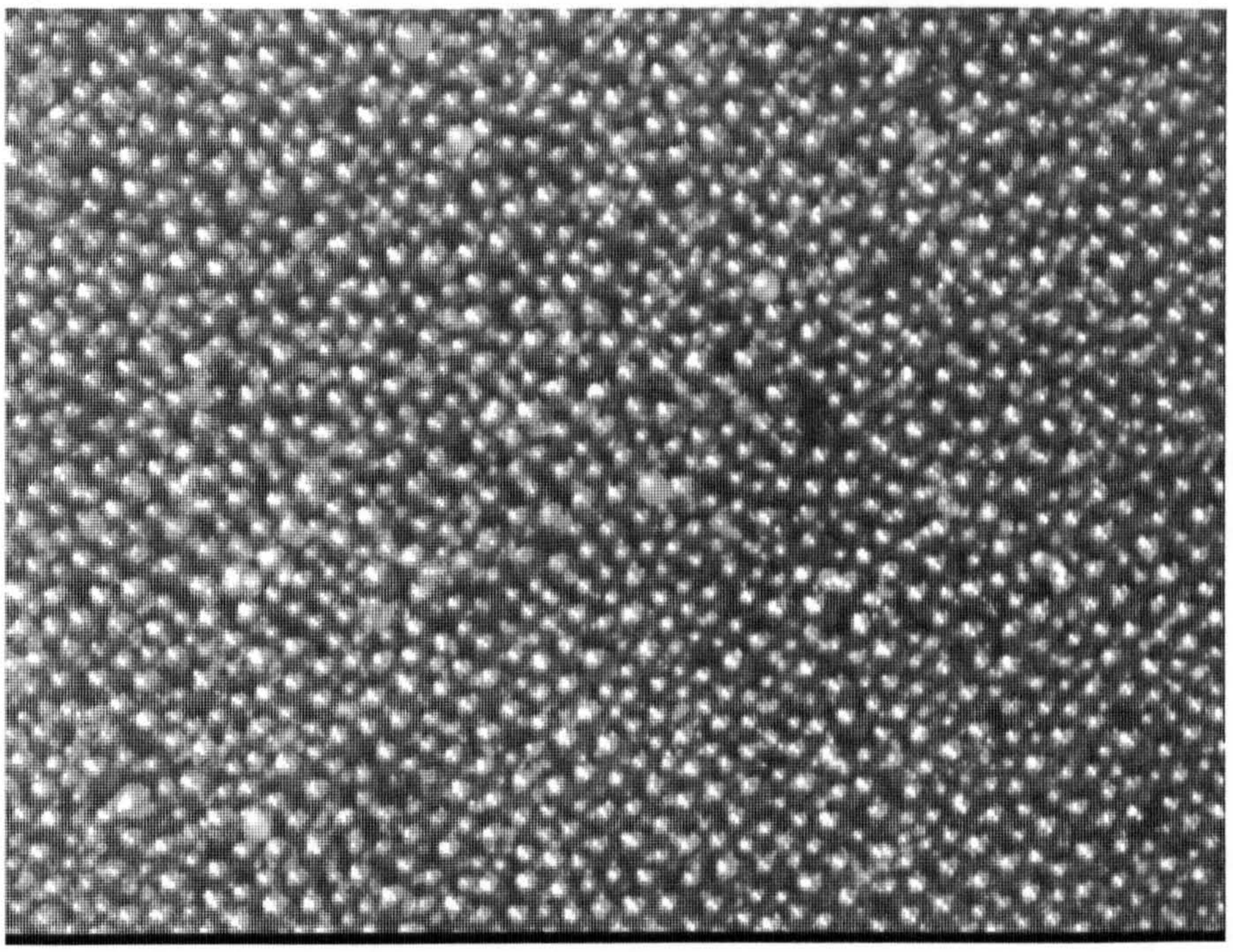

Figure 3.2 Structure of retro-reflective material

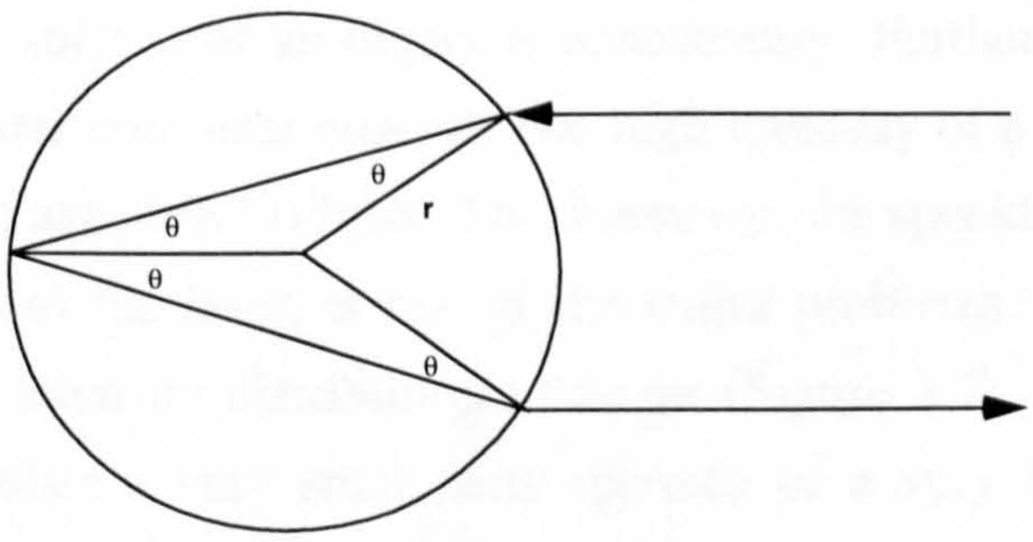

Figure 3.3 Working principal of retro-reflective material

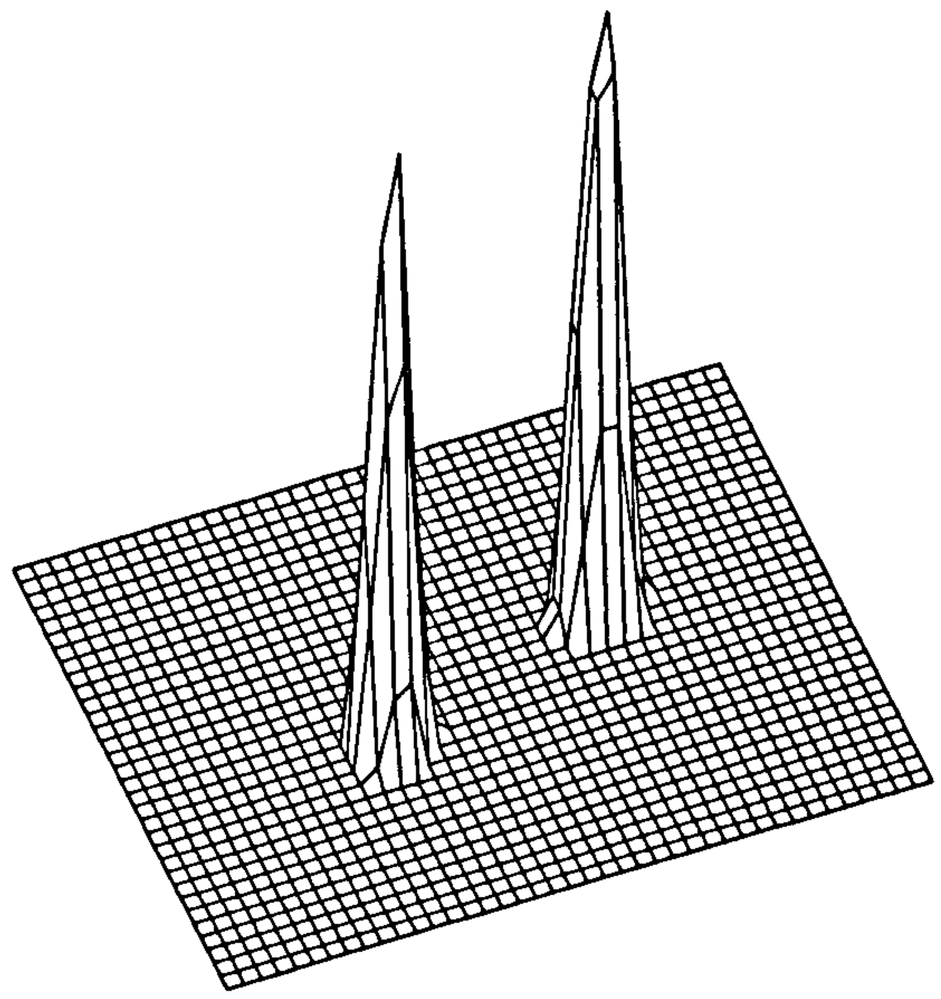

Figure 3.4 A 3-D intensity profile of retro-reflective targets

incident light to a suitable level. Figure 3.4 illustrates a 3-D intensity profile of two retro-reflective targets. The intensity values of the target have a symmetric distribution and zero background value so that very high accuracy can be obtained by a subpixel location algorithm.

3.2.2.3. Laser targets

A laser target is produced by a device such as Helium Neon (HeNe) laser which has been generally available for over 20 years. Recently, the development of cheap semi-conductor laser and integrated collimators has caused an explosive growth in use of these devices. The biggest advantage of a laser in the production of targets in digital photogrammetric measurement may be its flexibility. A modern diode laser collimator is a self contained device consisting of a diode laser, drive electronics, and a collimator. The price is reasonable (about £100 - £300 each) and is likely to continue to fall. By using laser targets the laborious process of sticking targets to a surface of an object is unnecessary. Furthermore these lasers can be switched on and off under computer control. The high intensity of a laser target can eliminate the background noise to zero level (Figure 3.6). However, the speckle, which is formed due to the coherent properties of the laser, is one of the major problems. Under certain conditions speckle will affect the intensity distribution of target (Figure 3.7). Although speckle can be minimised by using either a very small lens aperture or a very large aperture (Clarke & Katsimbris, 1994), a degradation of location performance is still present. Hence, the precision of measurement is adversely affected by this factor. However, laser targets can be used as a means of obtaining camera starting orientation parameters by using a small number of easily identified laser targets. This method will be discussed in chapter six.

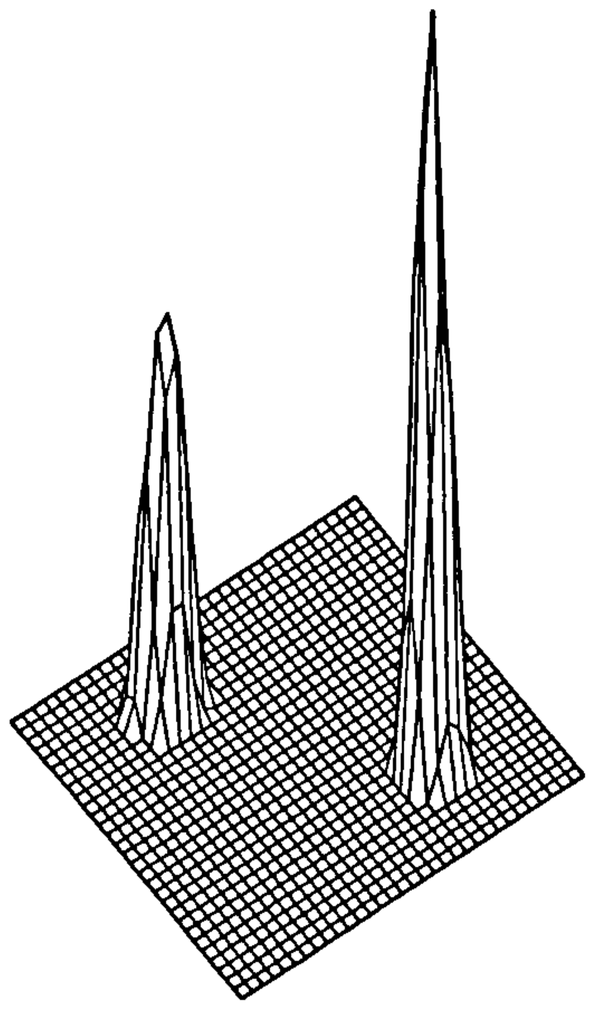

Figure 3.6 A 3-D intensity profile of laser targets without speckle

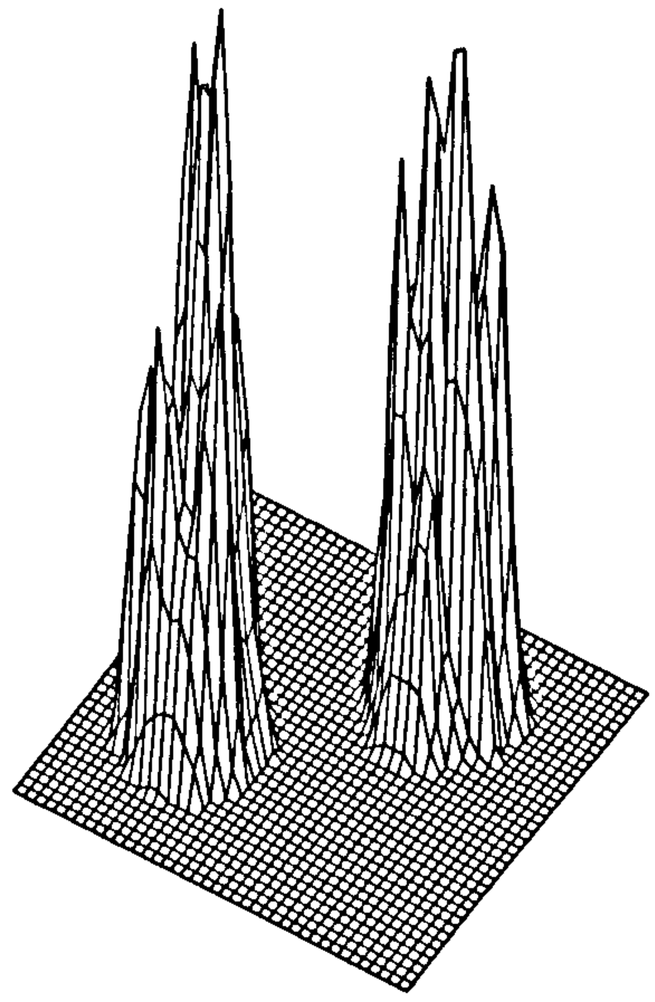

Figure 3.7 A 3-D intensity profile of laser targets with speckle

3.2.2.4. Projected targets

A projected target can be produced by a typical slide projector with an appropriate slide. This technique is often referred to as a structured light method. A suitable projection slide can be constructed using a section of black film by piercing it with small holes. The slide is then put into a projector so that the light passing through the pin holes of the film produces small spots on the surface of an object. Figure 3.5 illustrates the 3-D intensity profile of two such projected targets. By varying the density distribution and size of targets a wide variety of

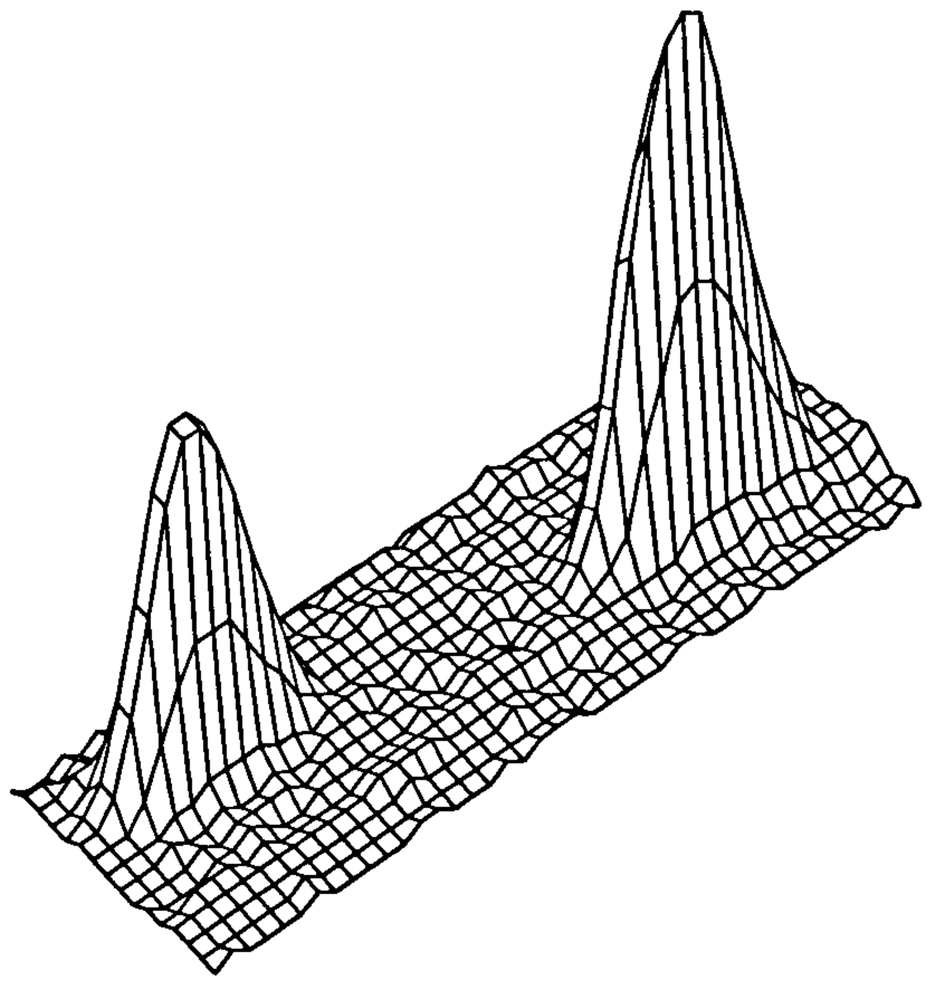

Figure 3.5 A 3-D intensity profile of projected targets

target images can be formed. However, projected targets are not ideal for the following reasons: (i) these targets are generally not as bright as retro-reflective targets or laser targets and so their signal to noise ratio is more sensitive to the level of ambient illumination. (ii) light from the slide projector may add to the background illumination if the slide is not dense enough. (iii) the surface of object has an influence on the shape of the target especially if the surface in oblique to the projector. (iv) and, the position of the targets may not be stable during the image collection period. However these targets have been widely used because of their ease of production and flexibility (Maas, 1992b).

3.2.2.5. Comparison of target characteristics

Four types of target for acquiring 2-D spatial features have been discussed. Although it is difficult to make a comparison of their relative merits, an attempt has been made, in Table 3.1. It can been seen that each of these targets has its own advantages and disadvantages. The choice of target will depend on the particular task.

Characteristics	Natural	Retro-reflective	Laser	Projected
Production speed	medium	slow	fast	fast
Precision	good	excellent	medium	medium
Processing speed	fast	fast	fast	fast
Measuring distance	far	far	< 5m	< 2m
Cost	very low	low	very high	low
Flexibility	medium	medium	high	high
Reliability	excellent	excellent	good	medium
Illumination	yes	yes	no	no

Table 3.1 Comparison of four types of targets

3.2.3. Characteristics of sensor

Image acquisition by photoelectronic sensors has evolved through a series of devices since the 1960s. The most widely used of these devices are vidicon and solid-state cameras. There are other sensor devices which use mechanical means for image scanning (e.g., the Eikonix camera, which is a 4096 x 4096 solid-state line CCD camera where the array is swept opto-mechanically, with a frame rate exceeding 2 minutes). However, with digital photogrammetric systems rapidly acquiring 2-D image data is the objective so only cameras which operate at video frame rate will be considered in this thesis. There are two types of image sensor, which can be used for 2-D image acquisition at video rate. The first is the vidicon camera, based on vacuum-tube technology in which an electronic beam scans a

light-sensitive element to produce the image pattern. The disadvantage for photogrammetric applications include the drifting of the scanning beam with time and the fact that the vacuum tube may need frequent replacement. Furthermore, this type of camera tends to be bulky, and fragile. The second type of camera is the solid-state camera, based on semi-conductor technology. Most of these cameras use charge-coupled devices (CCDs) which were introduced in 1979. The CCD sensor is composed of discrete light-sensitive elements which can be either metal-oxide semiconductors (MOS) or photo-diodes. The light energy falling on each element builds up a charge which is proportional to the integrated light intensity. This charge is collected in capacitors and then transferred from the array into an amplifier which outputs the image as a voltage train. These voltages, which are analogue quantities, are then converted into discrete numbers, for computer processing. Conversion is carried out by means of analogue to digital (A/D) converters.

3.2.3.1. Electron beam image sensors (Vidicon)

A vidicon tube is a photo conductive device which employs a photosensitive sensor layer consisting of several million mosaic cells insulated from one another on a transparent metal film (Figure 3.8). Each cell represents a small capacitor whose charge is a function of incident light. The sensor is scanned in a raster format with an electron beam resulting in for example 625 lines in accordance with the television standard. The beam is deflected magnetically by a set of coils situated outside the tube bulb. This video signal is simply a continuous analogue signal proportional to the light intensity of the focused image. The camera electronics insert synchronisation pulses (syncs.) to indicate the beginning of scan lines, fields, and frames.

The biggest disadvantage of the vidicon camera is its temperature related instability which produces large distortions. This camera has evolved and has been applied in image processing

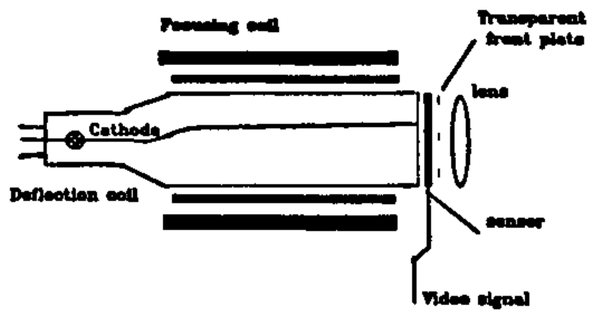

Figure 3.8 Construction of a vidicon camera

applications since the 1960s. During the 1970's and 80's vidicon cameras have been gradually replaced by solid-state cameras, especially in the fields of image analysis and measurement.

3.2.3.2. Solid-state image sensors

(i) Classification of sensors

There are two types of commercially available solid state image sensor: charge-injection devices (CID) and charge-coupled devices (CCD). The development of both sensors started in the early 1970's (Tseng at el, 1982). The difference between the two sensors is the method used to transfer the charge stored at a given pixel site. In this thesis only the CCD sensor is considered as it is by far the most widespread in photogrammetric applications. Most CCD sensors consist of metal oxide semiconductor (MOS) capacitors arranged in a regular array. The basic operation of the CCD can be described as follows: Incident light generates charge in the MOS capacitors; The charge is integrated (accumulated) by the capacitors such that the charge provides an analogue representation of light intensity, where the quantity of charge is proportional to the brightness. When a voltage is applied to the electrodes of the MOS capacitor; a shift register serially transfers the charges out of the sensor. These charges are amalgamated to form the video signal. CCD sensors can be further subdivided into two types depending on addressing methods: (i) interline transfer; and (ii) frame transfer.

(a) The interline transfer CCD is organised into column pairs of photosites (Figure 3.9a). An imaging column of photosites is adjacent to a vertical shift register, which is opaque to the photosites. Charge accumulates in the imaging column until the end of the accumulation period, when it is transferred to the opaque column. The signal then shifts vertically into a

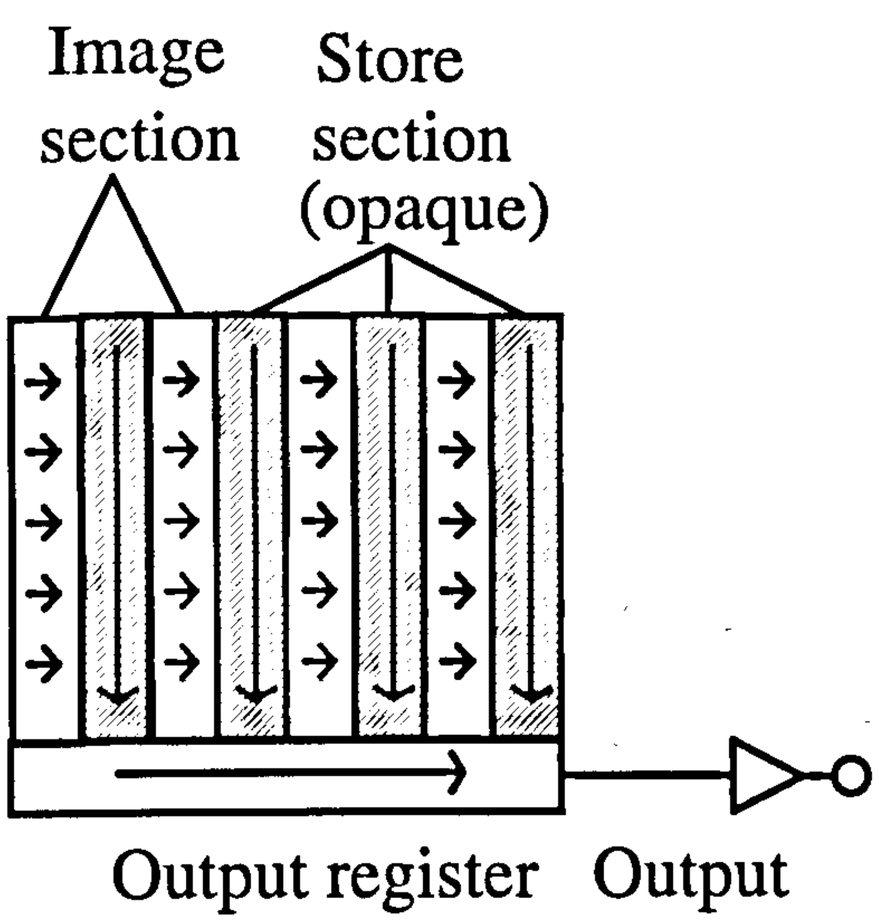

Figure 3.9 a) Interline transfer

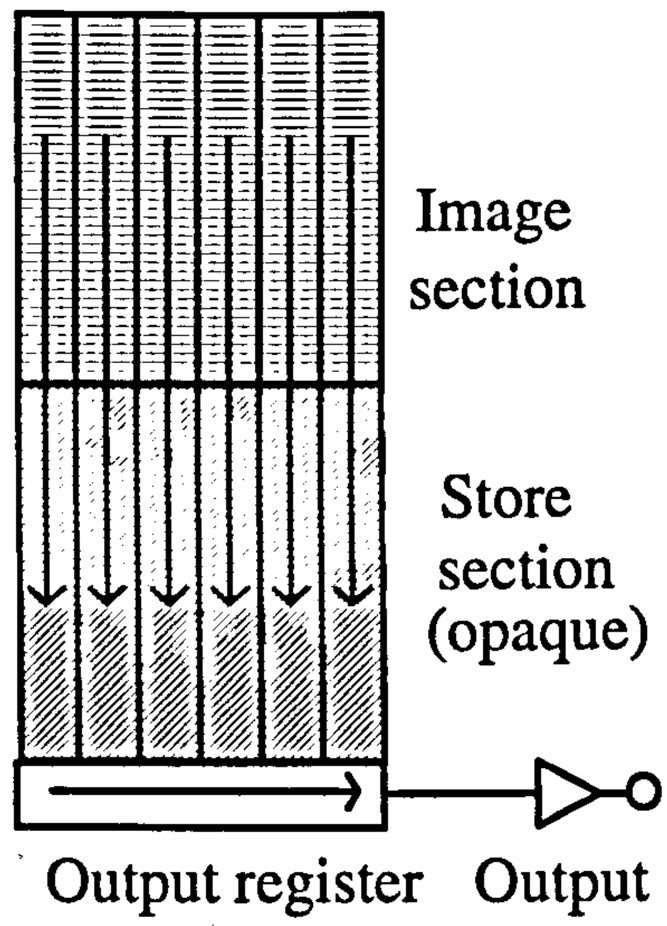

b) Frame transfer

horizontal shift register that represents the picture sequentially, line by line. The advantage of the interline transfer method is that the transfer time (to opaque storage) is short compared to the integration period. For example, in the Pulnix TM-6CN camera the transfer time is 64.0μs and the accumulation time is 40.0ms. A short transfer time is desirable because if the transfer time approached the accumulation time, solid-state sensors would tend to exhibit a locally contained spreading of the image response, called smear. Thus, the interline transfer method minimises smear. The result is an analogue voltage train that represents the image. This voltage train must be decoded by the frame grabber or monitor.

(b) In contrast to the interline transfer CCD, the frame transfer CCD uses the same capacitors for both charge accumulation and charge transportation. In the frame transfer organisation (Figure 3.9b) the sensor consists of vertical columns of CCD shift registers divided into two zones. The first zone, where charge accumulates during integration time, is photosensitive. When accumulation is complete, the whole array is transferred in parallel to the opaque storage area of the second zone.

(ii) Characteristics of Pulnix TM-6CN sensor

The characteristics of Pulnix TM-6CN camera are now investigated, as six of them have been used throughout the experiments in the thesis. A Pulnix TM-6CN camera with a 25mm Fujinon 'C' mount lens is shown in Figure 3.10. The specification of this CCD camera is illustrated in Table 3.2. From the Table, it can be seen that this camera has the following characteristics: high sensitivity, small size, high resolution, low power consumption, both

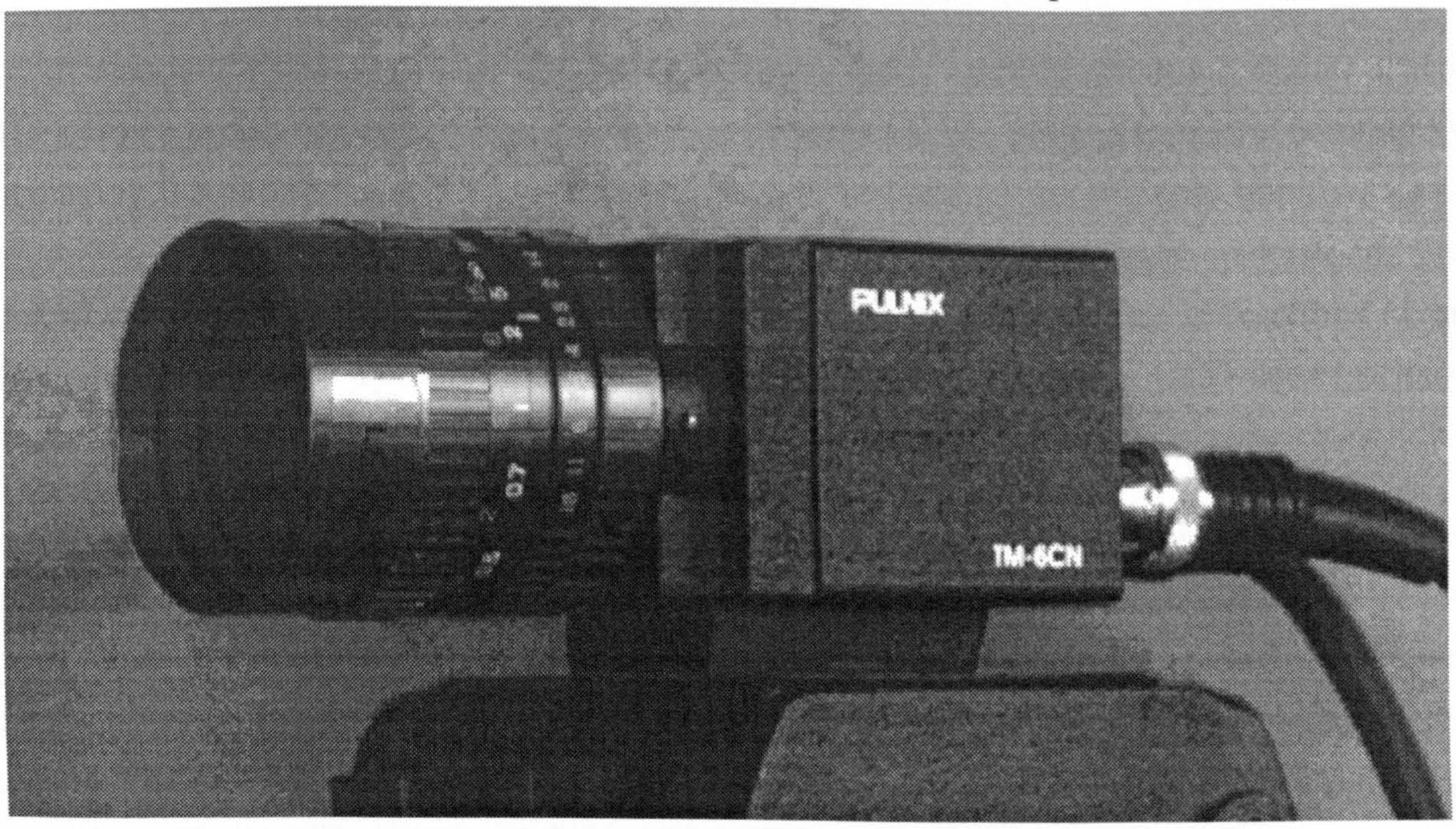

Figure 3.10 The Pulnix TM-6CN camera with a Fujinon 25 mm lens

Sensor format	1/2 inch interline transfer
Pixel	752(H)x582(V)
Cell size	8.6(H)x8.3(V) microns
Sensing area	6.41(H)x4.89(V)mm
Dynamic	67dB
Chip size	7.95mm(H)x6.45mm(V)
Timing	625 lines, 2:1 interlace (CCIR)
Clock	28.375 MHz
Pixel clock	14.1875 MHz
Horizontal frequency	15.725 MHz
Vertical frequency	50.0 Hz
Video output	1.0v p-p composite video, 75Ω
S/N ratio	50dB min.
Shutter speed	1/60 - 1/10000 sec.
Minimum illumination	1.0 lux(F=1.4) without IR. cut filter AGC: on = 16dB standard, off = 32 dB max.
Gamma	0.45 or 1
Lens	C-mount
Power requirement	DC 12V (9V min.), 2.5W
Operating temperature	-10°C to +50°C
Storage humidity	Within 70%
Vibration	7G (11Hz to 200 Hz)
Shock	70G
Dimension	45mm(W)x39mm(H)x75mm(L)

Table 3.2 Characteristics of Pulnix TM-6CN camera

CCIR standard video output and pixel clock output, and a variable electronic shutter speed. The camera is also reasonably cheap (less than £500 each). The photogrammetric community is making increasing use of CCD sensors because these cameras are not only improving and becoming cheaper, but their characteristics are also becoming better understood. An investigation of three Pulnix TM-6CN cameras combined with three lenses is described in the next section. Several common criteria to evaluate the performance of CCD cameras have been tested using this type of camera and are now discussed.

(a) Dynamic range. Dynamic range is the ratio of the maximum charge per pixel to the minimum charge packet that can still be detected. The maximum charge is limited by the capacitance of the photo diodes or the CCD registers. The dynamic range greatly determines the usefulness of a sensor, typically levels range from 300:1 to 100,000:1 depending on the sensor. The dynamic range of the SONY ICX039ALA chip used in the TM-6CN camera is quoted as 67 dB. The combined Pulnix TM-6CN and EPIX SVMGRB4MB framegrabber response at the two camera gamma settings was determinated by experiment and is illustrated

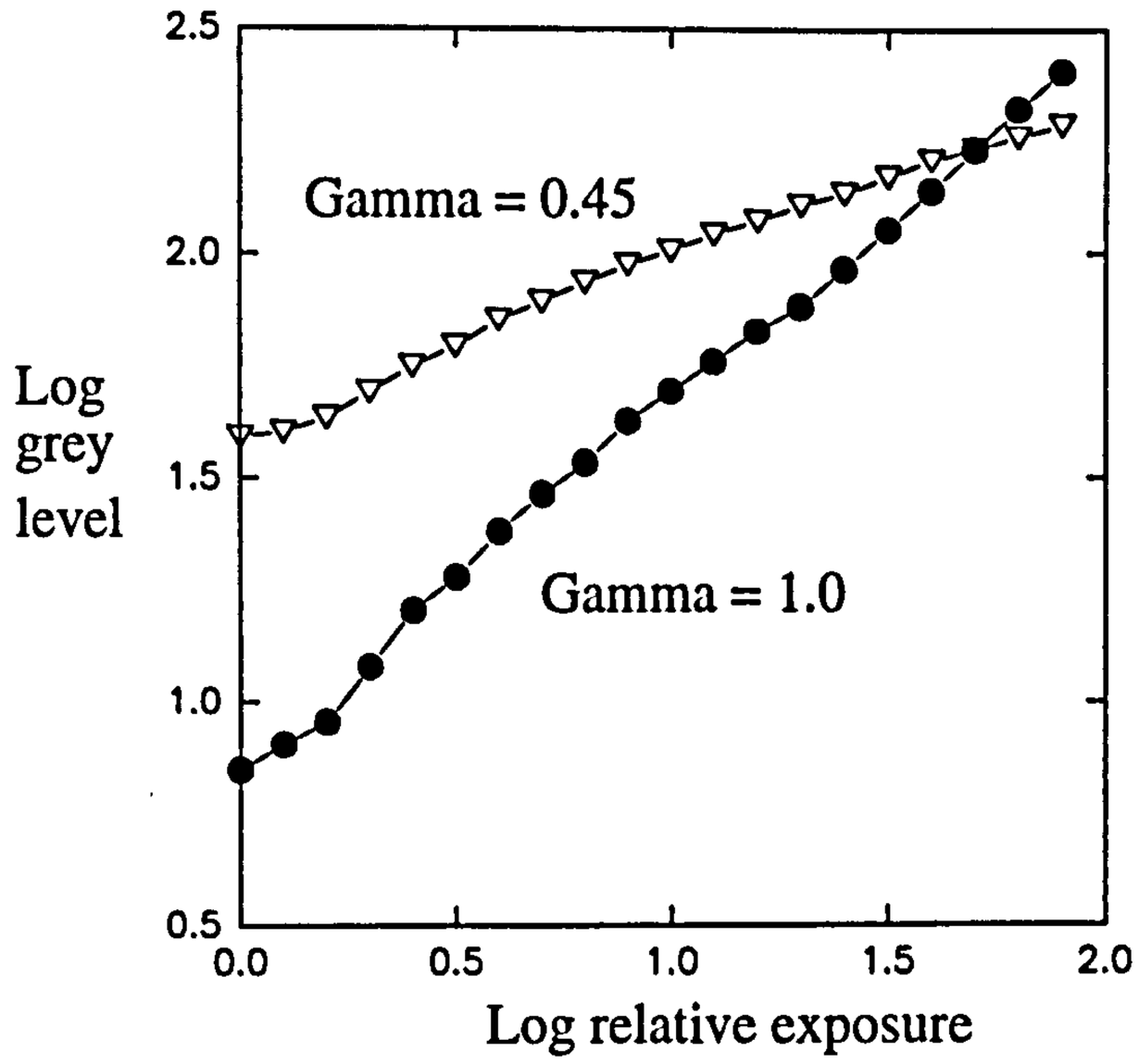

Figure 3.11 Grey level response at two gamma settings

in Figure 3.11 (Robson at el, 1993).

(b) Spectral sensitivity. Spectral sensitivity is defined in terms of the output signal generated for an input light flux at a given wavelength. The photo-sensitivity of Silicon ranges from 200 - 1100 nm, with a peak sensitivity at about 750 nm, depending on the type of silicon substrate used. The spectral sensitivity of the SONY ICX039ALA sensor used in the TM-6CN is shown in Figure 3.12. This graph includes a lens so that the spectral sensitivity curve is

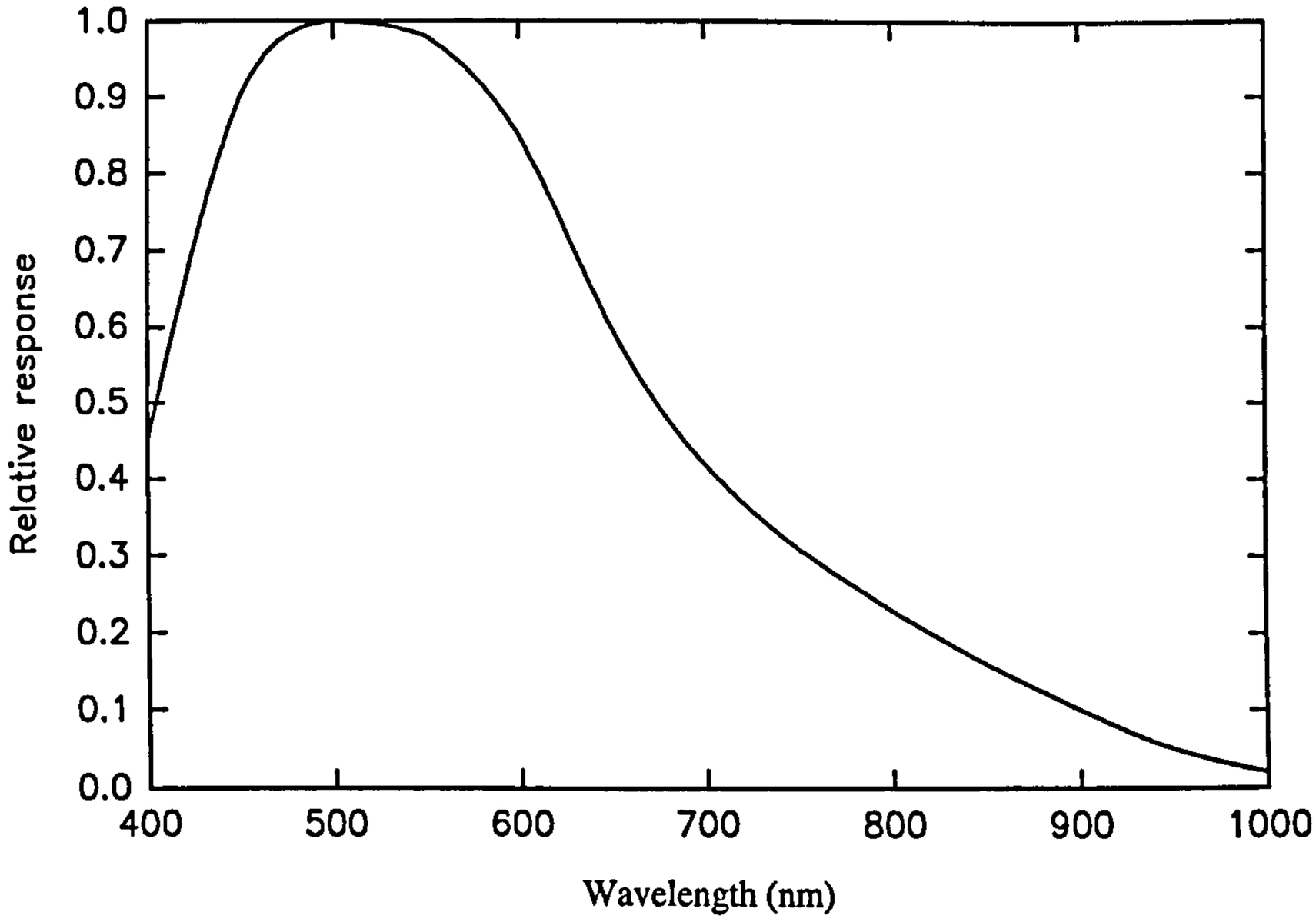

Figure 3.12 Spectral sensitivity of the sensor in TM-6CN camera

modified by the transmission properties of the lens optical elements.

(c) Pixel response non uniformity (PRNU). PRNU is defined as the variation of output signal from one pixel to another under uniform illumination. This can be caused by variations in substrate thicknesses or pixel element size. However, the framegrabber, which is connected to the CCD camera, also has characteristics of non-uniformity (Beyer, 1992). Such non-uniformities will cause errors in target location. The non uniformity of Pulnix TM-6CN cameras can be observed by using a sensor which is uniformly illuminated without the lens attached and connected to the EPIX framegrabber. The result is shown in Figure 3.13. This image, taken at a RMS grey level of 180, has been enhanced so that the 4 grey level variations cover a full 0 - 255 range.

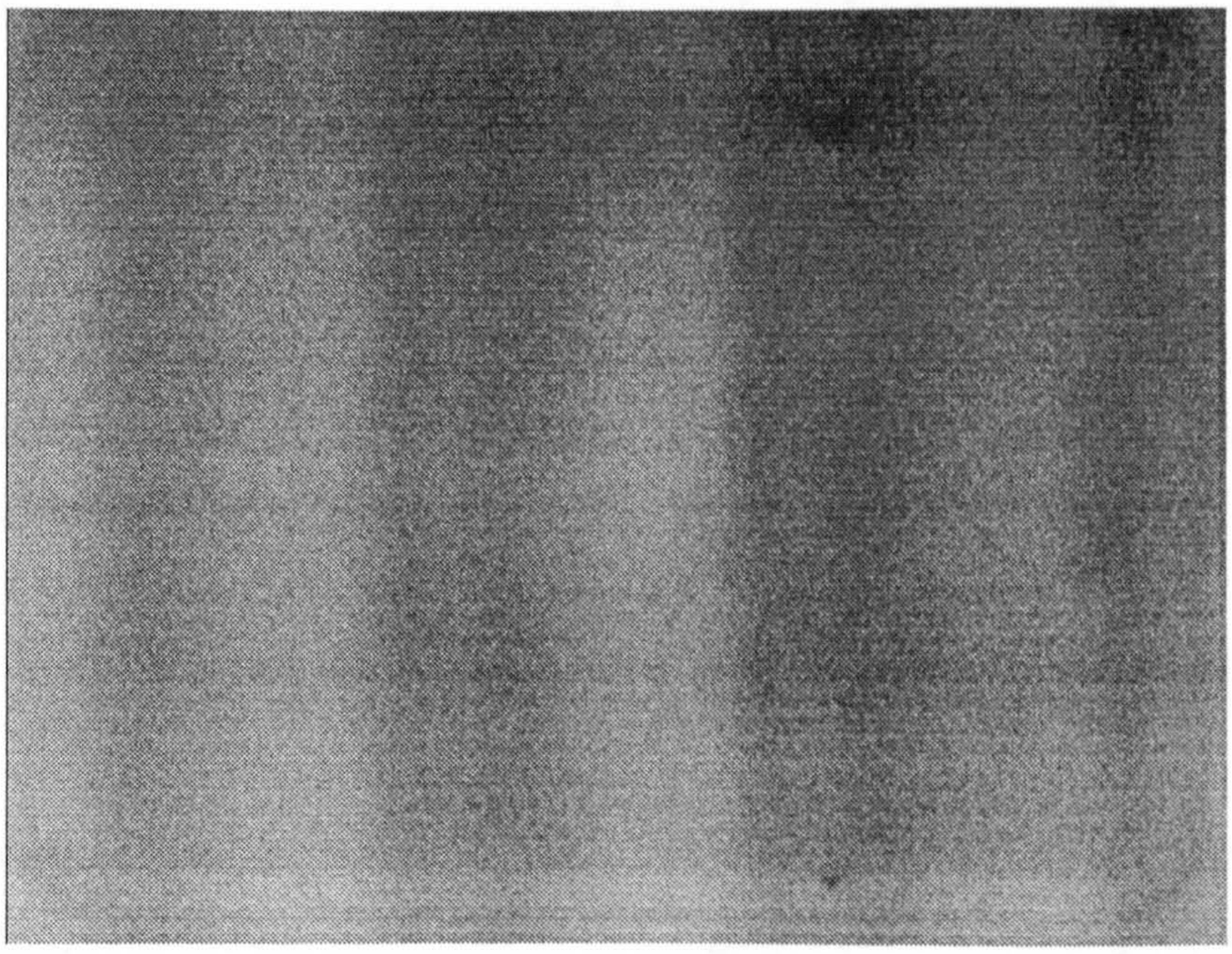

Figure 3.13 Sensor output without lens

(d) Radiometric degradation. Radiometric degradation can be derived from both the spatial resolution of each pixel, or the modulation transfer function (MTF), and the transfer of charge in sensors. The spatial resolution is largely affected by the separation between pixels and the dynamic range. The charge elements in CCD cameras are very closely spaced and the dynamic range in the scene is often higher than the dynamic range of the sensors. The excess electrons spill over to neighbouring pixels along the CCD channel, causing what is known as "blooming". This can have a serious effect on spatial resolution. To prevent blooming the camera uses a technique by which overflow drains and overflow control gates are used.

(e) Charge transfer efficiency. Change transfer efficiency (C.T.E.) is defined as the percentage of charge tranfered from pixel to pixel. It is a function of the speed of the transfer, and the transfer mechanism. The result of transferring the charge from pixel to pixel will result in a gradual difference between the first and the last pixel charges. Although recent cameras have reduced the transfer loss to better than 0.001% this is still a problem for cameras with a large number of pixels as this small loss can accumulate to an unacceptable amount.

3.2.4. Lens characteristics

The influence of lenses in digital photogrammetry cannot be underestimated as their geometric distortion can amount to several pixels, whilst over 10 intensity levels in radiometric degradation are possible. The radiometric influence of some lenses used with the Pulnix TM-6CN sensors is first discussed followed by an analysis of the geometric distortion of lenses.

The lenses, used in the photogrammetric 3-D measuring system and made by Fujinon, have a 25mm focal length with a maximum aperture of f/1.4. Three such lenses were selected for use with the three Pulnix TM-6CN cameras. The lenses use a C-mount, and have a typical covering power of 10mm ∅, to match the small area of the CCD sensor. The specifications for the C-mount are: 1" diameter: 33 threads per inch; and a flange image-plane distance of 17.536 mm.

(a) Camera output non-uniformity. The image intensity variations between different camera and lens permutations are illustrated in Figure 3.14. In this experiment, an area of white card was evenly illuminated by a pair of lamps positioned at 45° with respect to the card. From this figure, it can be seen that small RMS image intensity differences of ±2 grey levels occurred between the different lenses mounted on the same camera body. However, the camera sensors demonstrate discrepancies of up to 14 grey levels. Whilst such variations could be removed by adjusting the camera grey balance (a simple matter on the Pulnix TM-6CN), the settings should be determined with respect to signal saturation levels. During this experiment, possible image illumination fall-off at the edge of the format using wide apertures was found to be indistinguishable from the ±2 grey value variations present in all Pulnix TM-6CN images. No significant fall off in intensity was found as the Fujinon lenses are of standard construction. Image intensity non-uniformities may cause some errors in photogrammetric measurement because most locating algorithms are based on the intensity distribution of each individual target.

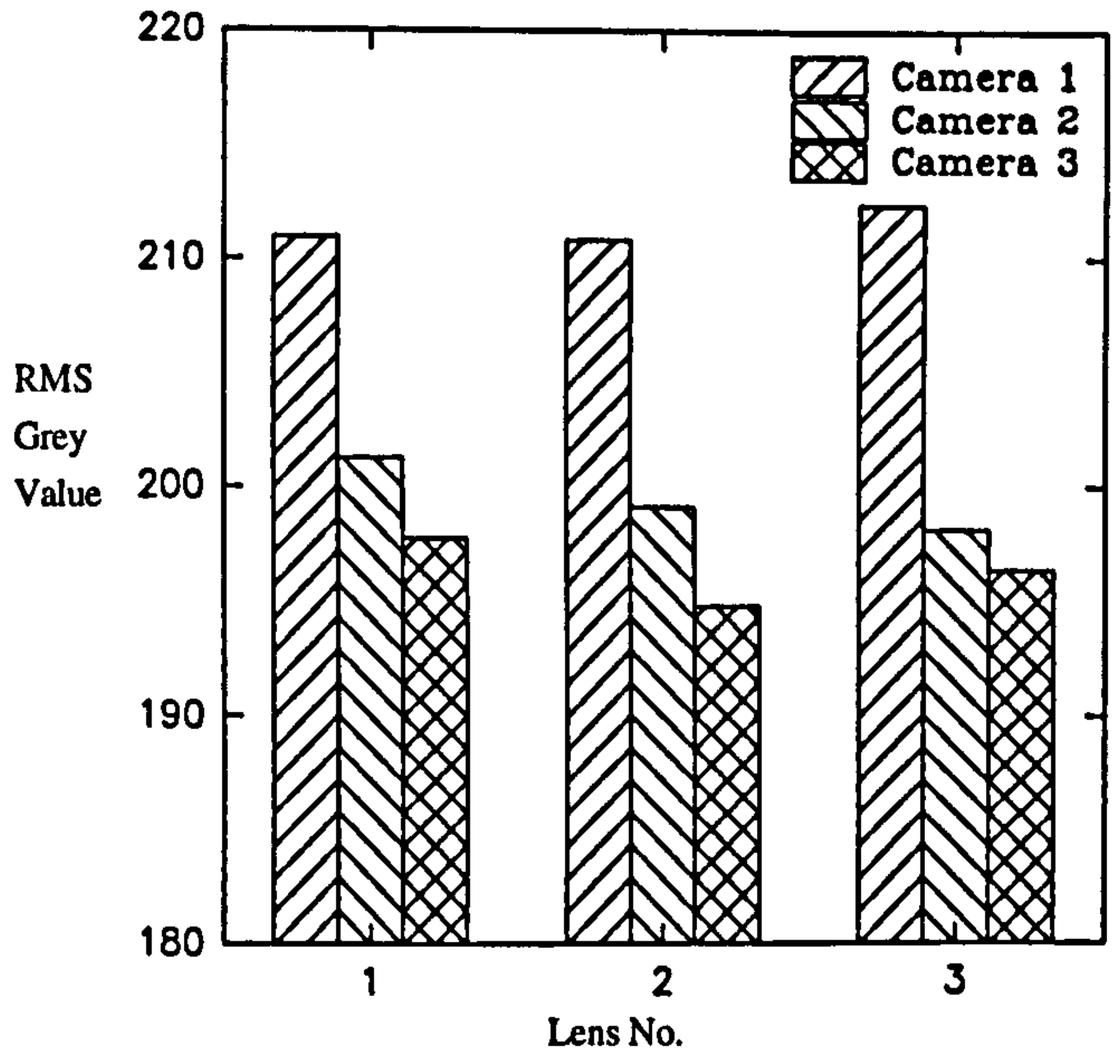

Figure 3.14 RMS grey level for three camera/lens combinations

(b) Aperture influence. The influence of varying the lens aperture whilst imaging a uniform white card with two different lenses is illustrated in Figure 3.15. It can be seen that the only significant difference occurred at f/5.6. Whilst such a difference may not be important for many applications, in an automated measuring system with multiple cameras and automated depth of field control, variations between sensors could be calibrated such that additional radiometric information is included *a priori* in the matching process.

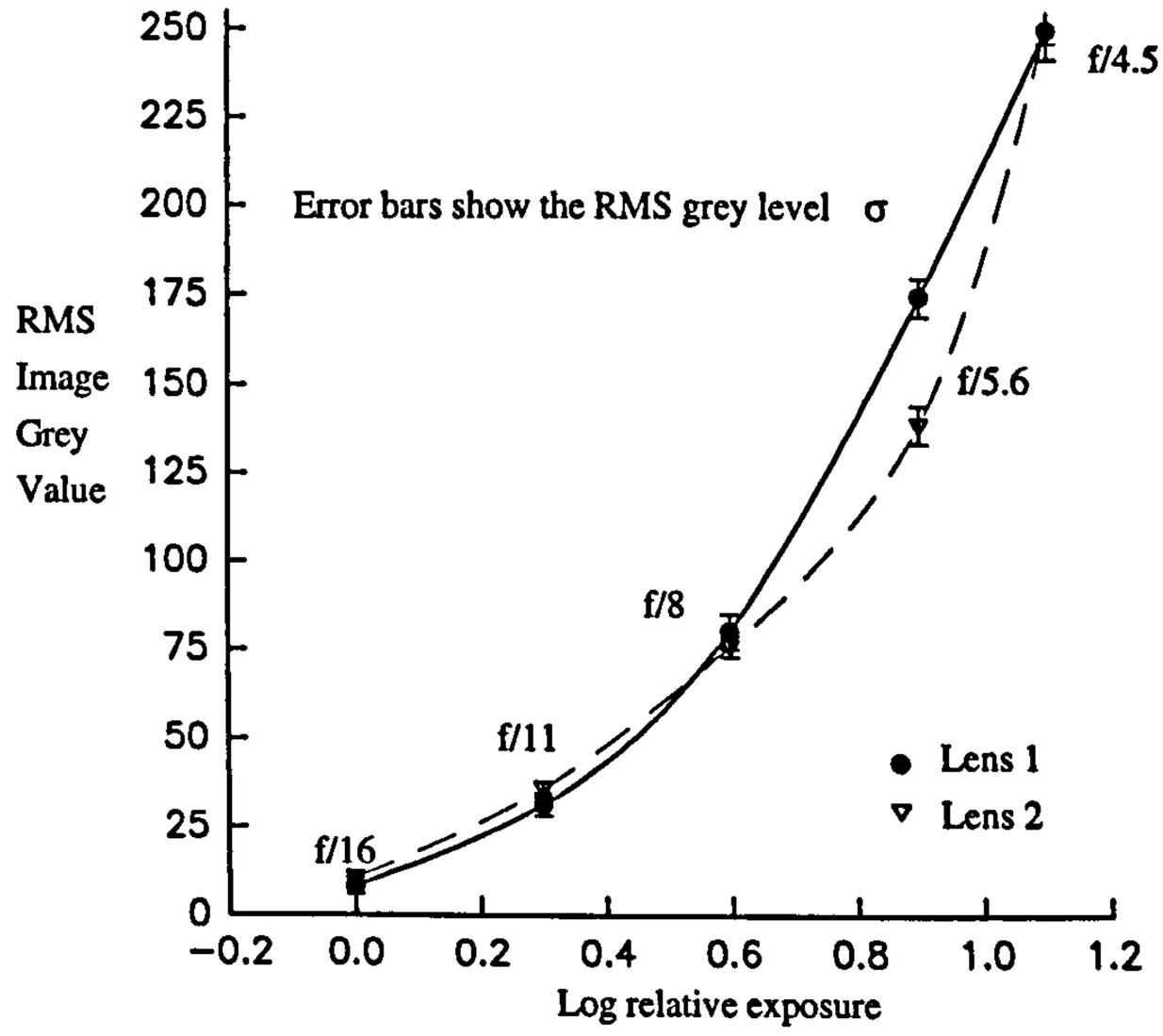

Figure 3.15 RMS grey level and lens aperture for two lenses

(c) Nyquist's sampling theorem. To recover signal information (in this case an image) in an undistorted form after a sampling process, the original information must be bandwidth limited

to half the sampling frequency. As specific spatial filters are not used, sampling above the Nyquist frequency will result in distortions to the image in the form of aliasing. However the lens can be regarded as a spatial filter since it modifies the frequency of the incident illumination patterns. The qualities of general purpose C-mount lenses vary, but the resolving power of the 25 mm f/1.4 Fujinon used in this work appears to be at least comparable to the 58 lines per mm (58 l mm^{-1})Nyquist limiting value of the sensor.

(d) Camera resolution. To evaluate the camera resolution a lens test chart (Figure 3.16) was imaged at the edge and centre of the image format for each camera and lens permutation. Visual evaluation of the patterns produced at high magnification demonstrated that there was no significant difference between the centre and the edges of the format for all permutations. Figure 3.17 shows a set of intensity profiles through three sets of line pairs. It can be seen that the spatial resolution of the system is somewhere between 38 and 60 lmm^{-1}. Such a value

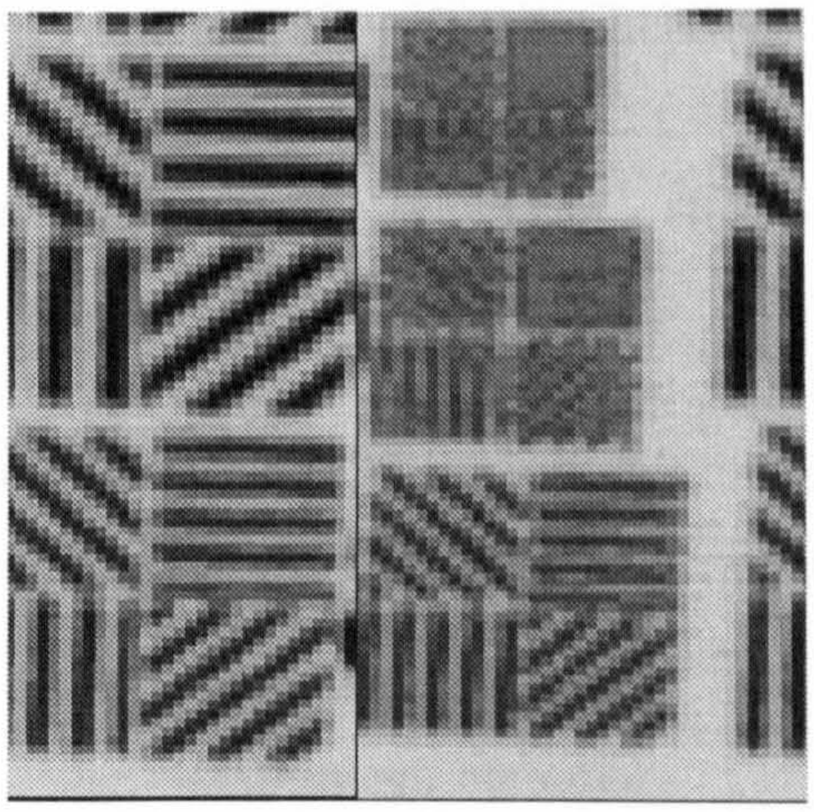

Figure 3.16 An image of a lens test resolution chart

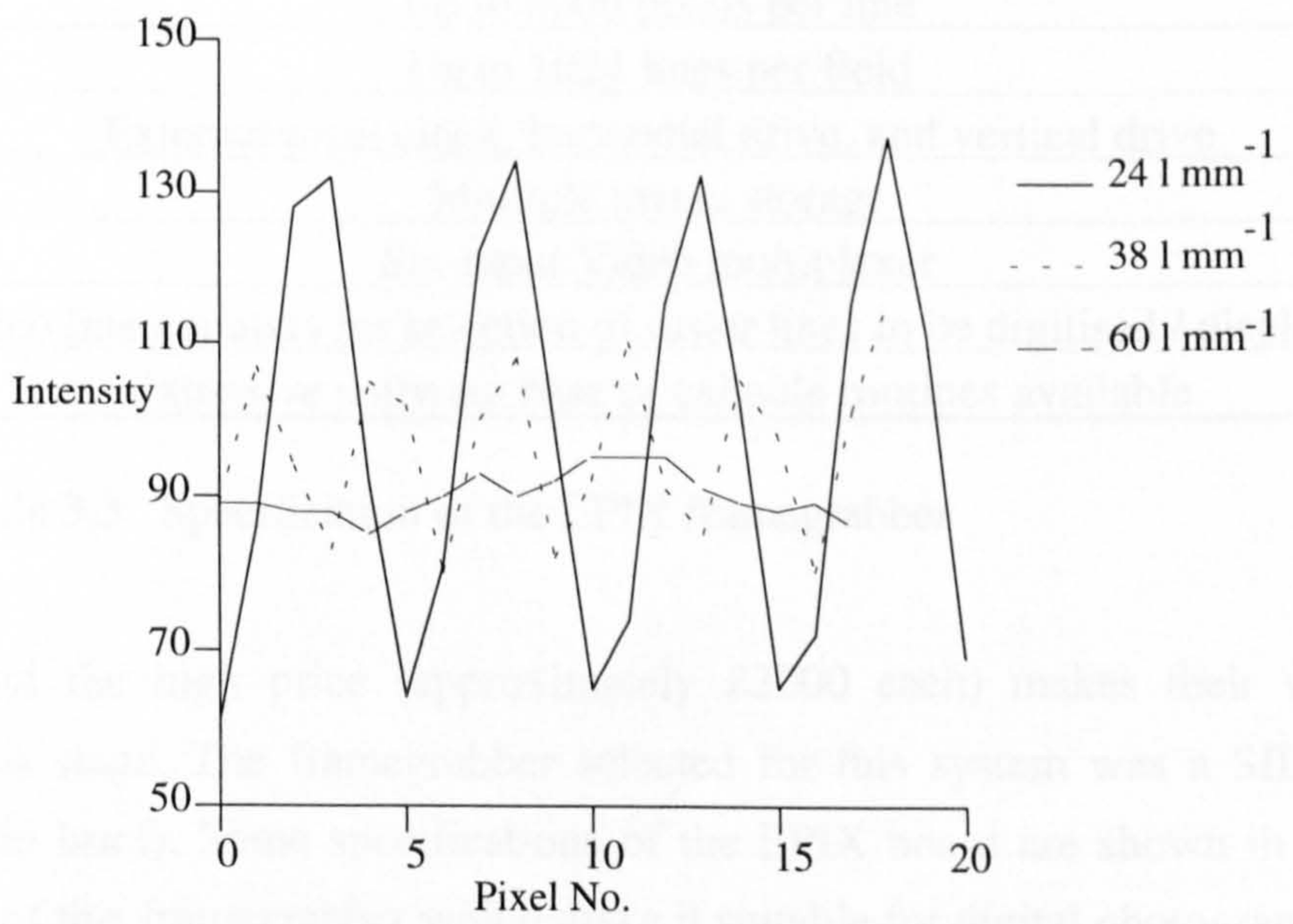

Figure 3.17 Intensity profiles through three sets of line pairs

would agree with the 58 lmm^{-1} theoretical maximum resolution given by the Nyquist theorem for the sensor. Variations in resolving power between the three lenses tested were found to be insignificant.

3.2.5. Characteristics of framegrabber

In an IBM PC based photogrammetric measurement system using cameras with an analogue output, a framegrabber is required. The basic tasks carried out by a typical framegrabber are A/D conversion, image storage, and image display (D/A conversion). Some framegrabbers incorporate some image processing hardware to make image processing quicker and easier but such functions are often not necessary for photogrammetric systems. Recently, a colour multimedia board (Andrew, 1993) has been marketed, which combines the VGA card of a PC and an integrated display of the camera image as well as image information such as text on the same monitor. However, its suitability for applications in digital photogrammetric measurement still needs to be investigated. The ability to use the camera pixel clock output to achieve pixel sync. sampling is an important specification when choosing a camera/framegrabber combination for the purposes of engineering measurement. The consequence of not using the pixel clock is to reduce the geometric accuracy of the images because of line-jitter which will be discussed later in this chapter. A digital camera may have benefits in the future as errors such as line-jitter and signal transmitting errors are overcome in

Variable sampling
4Mb image memory
Video memory address registers
752 pixels by 576 lines typical maximum resolution
Up to 8000 pixels per line
Up to 1024 lines per field
External pixel clock, horizontal drive, and vertical drive
Multiple image storage
Six input Video multiplexer
Video line counters for selection of raster lines to be digitised / displayed
Extensive software base of callable routines available

Table 3.3 Specification of the EPIX framegrabber

the design, but the high price (approximately £2000 each) makes their widespread use unlikely at this stage. The framegrabber selected for this system was a SILICON VIDEO MUX (EPIX in brief). Some specifications of the EPIX board are shown in Table 3.3. The main features of this framegrabber which make it suitable for digital photogrammetry are:

(i) Pixel clock. A typical CCD video camera uses analogue video signals to transfer the image data and the synchronisation signals from the CCD-camera to the frame grabber. Line-jitter will occur in this situation. Daehler, 1987, described this line synchronisation effect in detail and Beyer (1987, 1990) analysed the causes of line-jitter and presented some results suggesting that a pixel clock would eliminate this source of error. The EPIX framegrabber is able to accept the pixel clock from the camera so giving a one to one mapping of sensor elements to pixels and eliminating line-jitter. This will be discussed in detail in chapter 3.3.

(ii) Multiplexed inputs. In photogrammetric engineering measurement more than two cameras are generally needed. The EPIX framegrabber has a six input video multiplexer so a maximum of six cameras can be simultaneously connected to the framegrabber. This makes it possible to chose any one of the available inputs to digitise, display, transmit, process, or archive the images.

(iii) 4Mb image memory. The 4Mb of image memory allows the storage of nine images of 752 x 582 pixels such as given by the Pulnix cameras. This is convenient for rapid storage of multiple images which can then be processed at a slower rate.

(iv) Effect of cable termination. The correct cable termination is important for error free transmission. Figure 3.18 illustrates the intensity profile of an image using different cable lengths. Figure 3.18 a) is obtained using a 5m 50Ω cable where the so called "ringing" phenomenon can be clearly seen. Figure 3.18 b) is obtained using a 2m 50Ω cable where the image appears to be normal. However, both cables have an incorrect impedance of 50Ω which

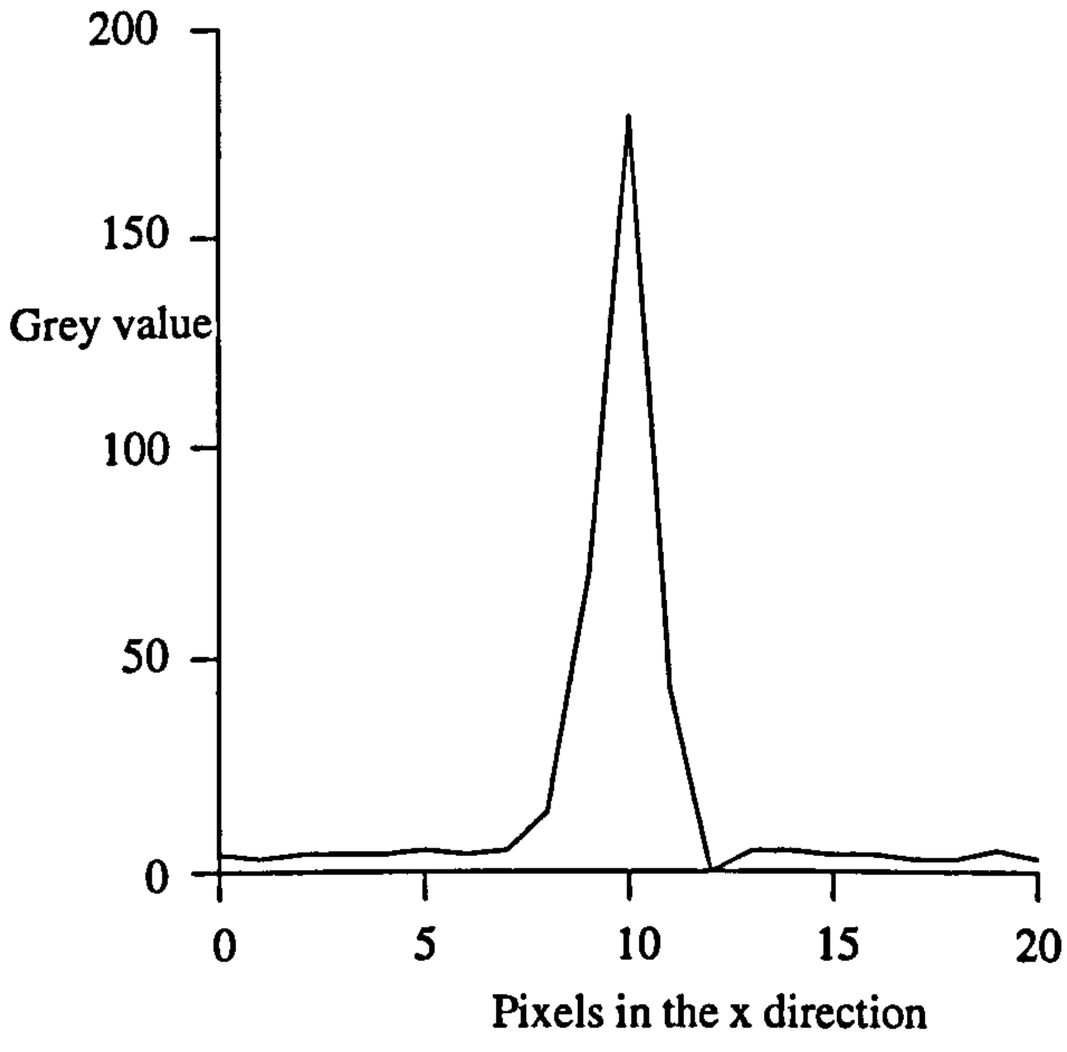

Figure 3.18 a) Using a 5m cable

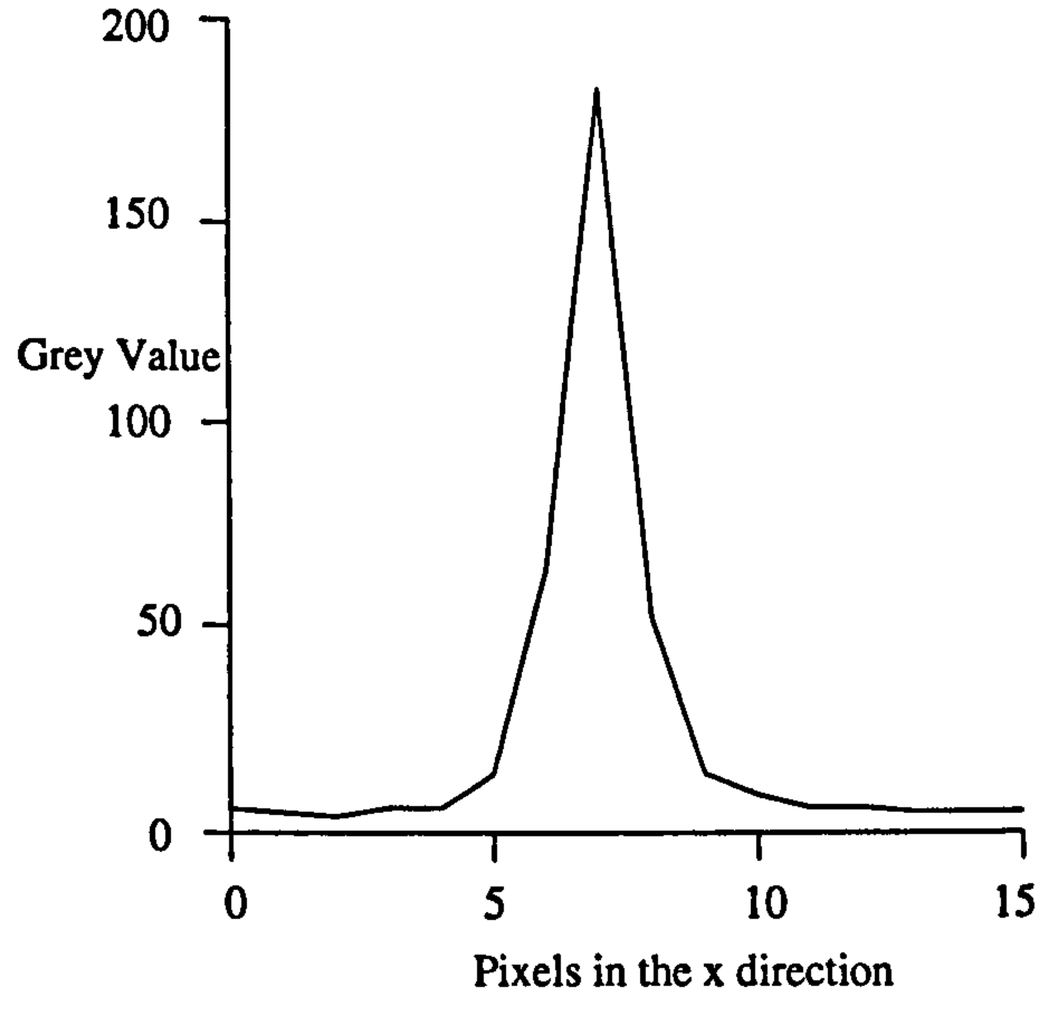

b) Using a 2m cable

results in this observation of ringing at larger cable lengths. If a correctly terminated 75Ω cable is used the video signal can be transmitted over larger lengths without distortion.

3.3. Test and calibration of hardware components

For the purpose of photogrammetric measurement it is necessary to quantify the errors and calibrate the components in a digital imaging system. Therefore the characteristics of both the Pulnix TM-6CN cameras and EPIX framegrabber have to be determined. A series of tests of temperature effects and geometric distortion for the three cameras with the framegrabber have been made.

3.3.1. Temperature effects

Changes of temperature in the CCD camera may influence its performance. This is because the CCD camera consists of electronic circuits and semiconductor electro-optical devices, which are each influenced by temperature. Such variations were assessed by "warm up" tests described in the following sections. Changes of temperature of both the camera and frame-grabber were thought to have an influence on the geometry of the images acquired. To verify this, some tests were carried out. The tests were divided into several groups: (i) evaluation of individual influence of the three Pulnix TM-6CN cameras; (ii) evaluation of the influence of the EPIX frame grabber; and (iii) evaluation of the compound influence of the Pulnix TM-6CN camera and EPIX frame grabber.

A test field was constructed on a black painted piece of flat 6mm glass, upon which 16 retro-reflective circular targets were arranged in a square such that they covered the entire

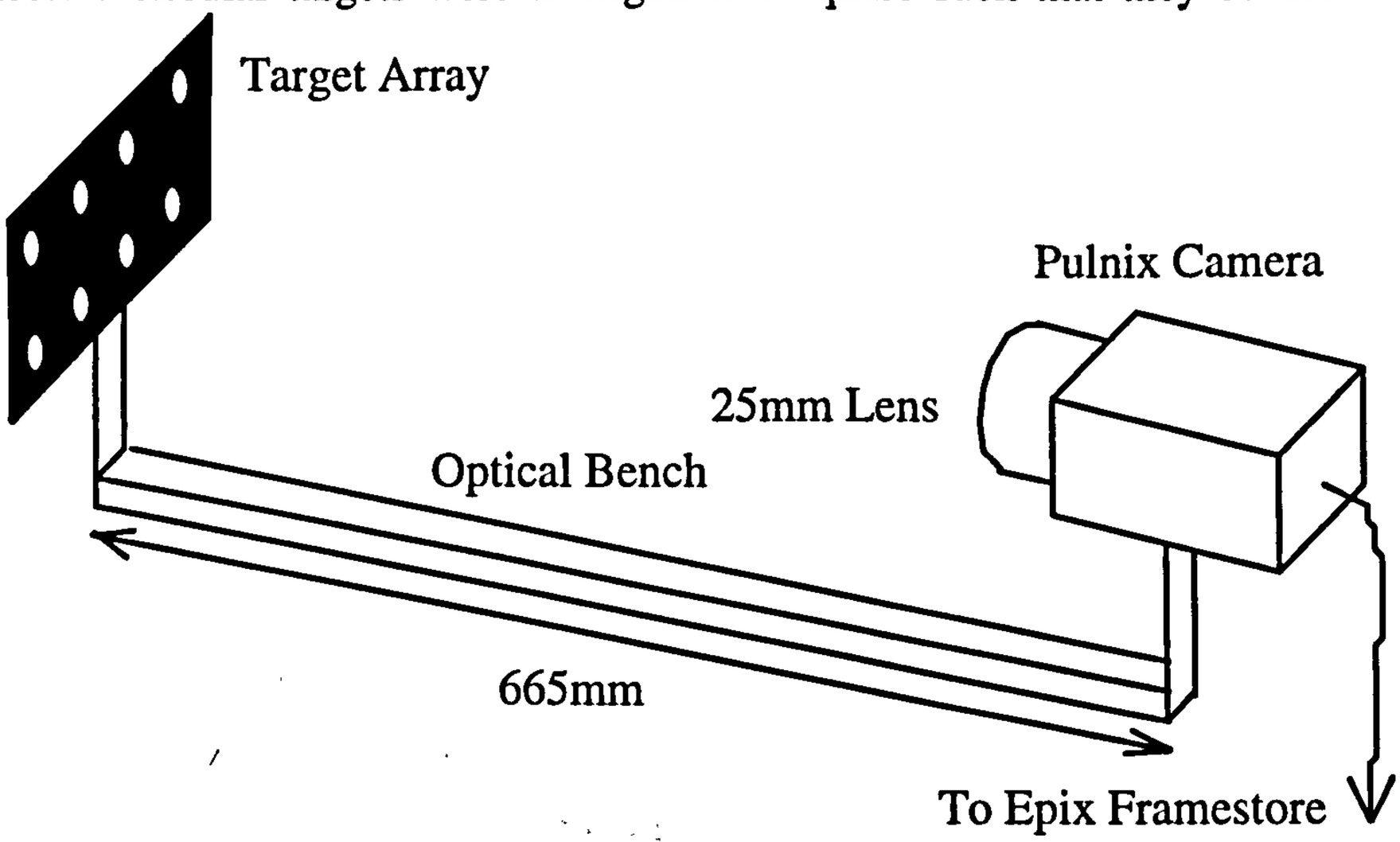

Figure 3.19 The warm-up test setup

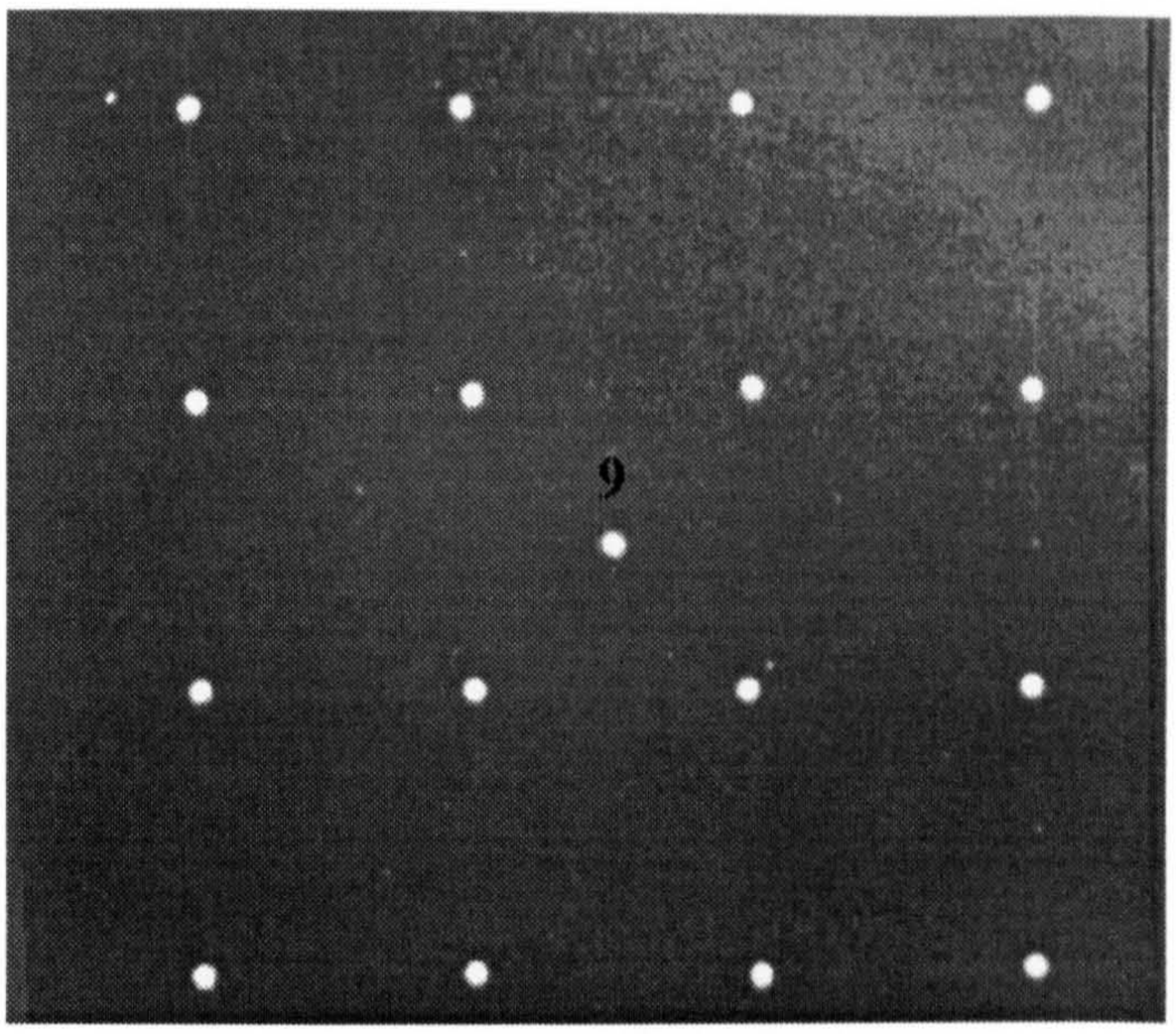

Figure 3.20 The test field used for the warm-up tests

field of view. Another target was placed in the centre of the plane. The test field was fixed on an optical bench and a Pulnix camera was fixed on an adjustable mount such that its orientation could be adjusted. The test plane was covered by a piece of black paper to remove the influences of external illumination. A diffuse source of light was placed behind the camera so that the retro-reflective targets produced a high signal to noise ratio. The distance of the test plane from the camera was approximately 665mm, resulting in the image target size of that could be covered by a 11 x 11 pixel window. The experiment setup is illustrated in Fig 3.19 and the image of the test plane is shown on Figure 3.20.

3.3.1.1. Temperature effects on camera performance

Tests were carried out by switching on the computer and the EPIX framegrabber and waiting for them to become stable (more than two hours). The camera was then switched on. A series of images were collected at varying time intervals. The x and y target image co-ordinates of the targets on the images were collected by a centroid subpixel location algorithm, in which a 25 x 25 rectangular pixel window was used. The co-ordinates of target number 9 have been used to draw a graph of the shift that occurred Figures 3.21, 3.22 and 3.23 illustrate the x, y co-ordinate shifts of target 9 over the period of warm-up for each of the three cameras. Figure 3.24 illustrates the x, y co-ordinate shift for all targets during the warm-up time.

From these figures, it can be concluded that the warm-up influence of the Pulnix TM 6CN cameras ranges between 0.1 to 0.3 pixels. The source of error may come from the electronic characteristics of camera changing with the temperature or the thermal expansion of the silicon CCD array. If the change exhibited in Figure 3.24 was caused by variations in timing,

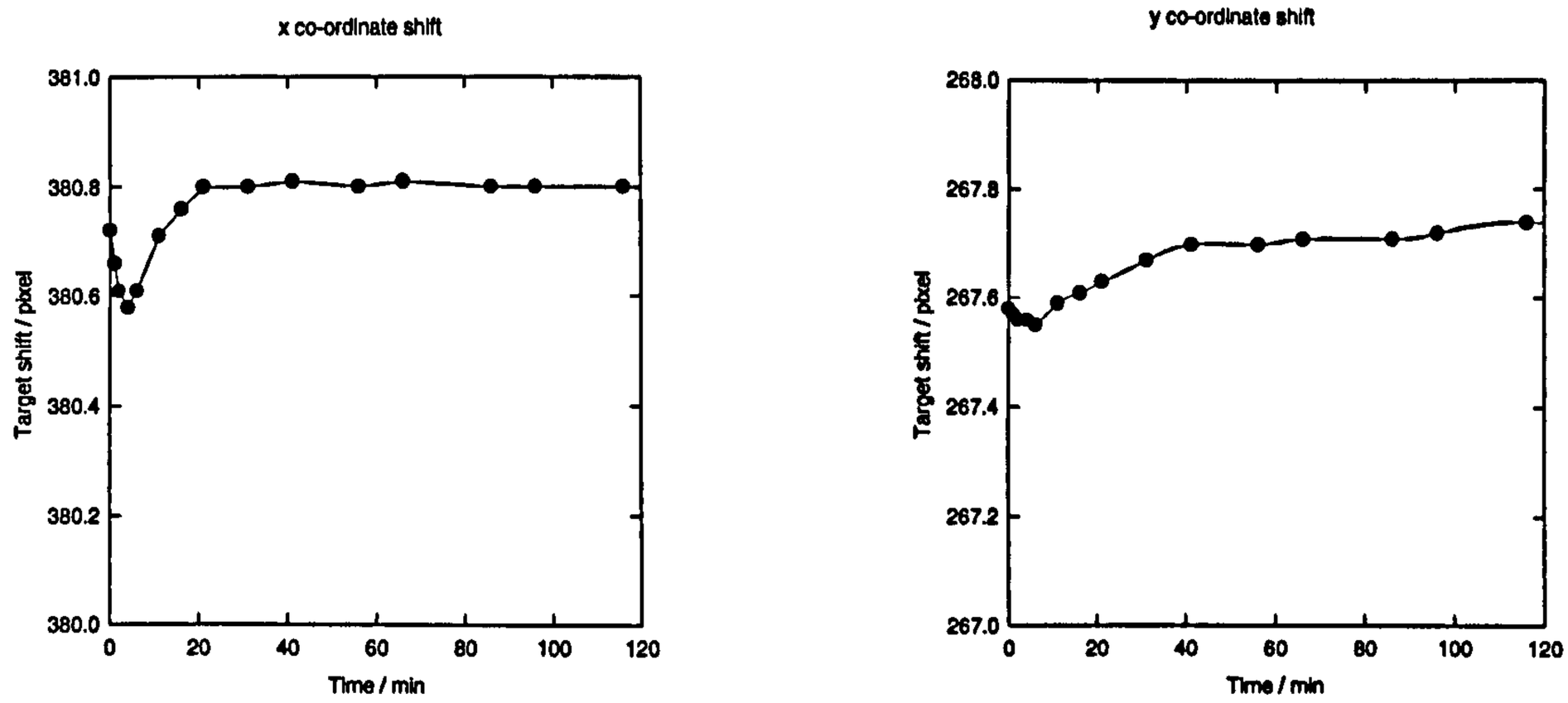

Figure 3.21 x, y co-ordinate warm-up shift for target image (camera 1)

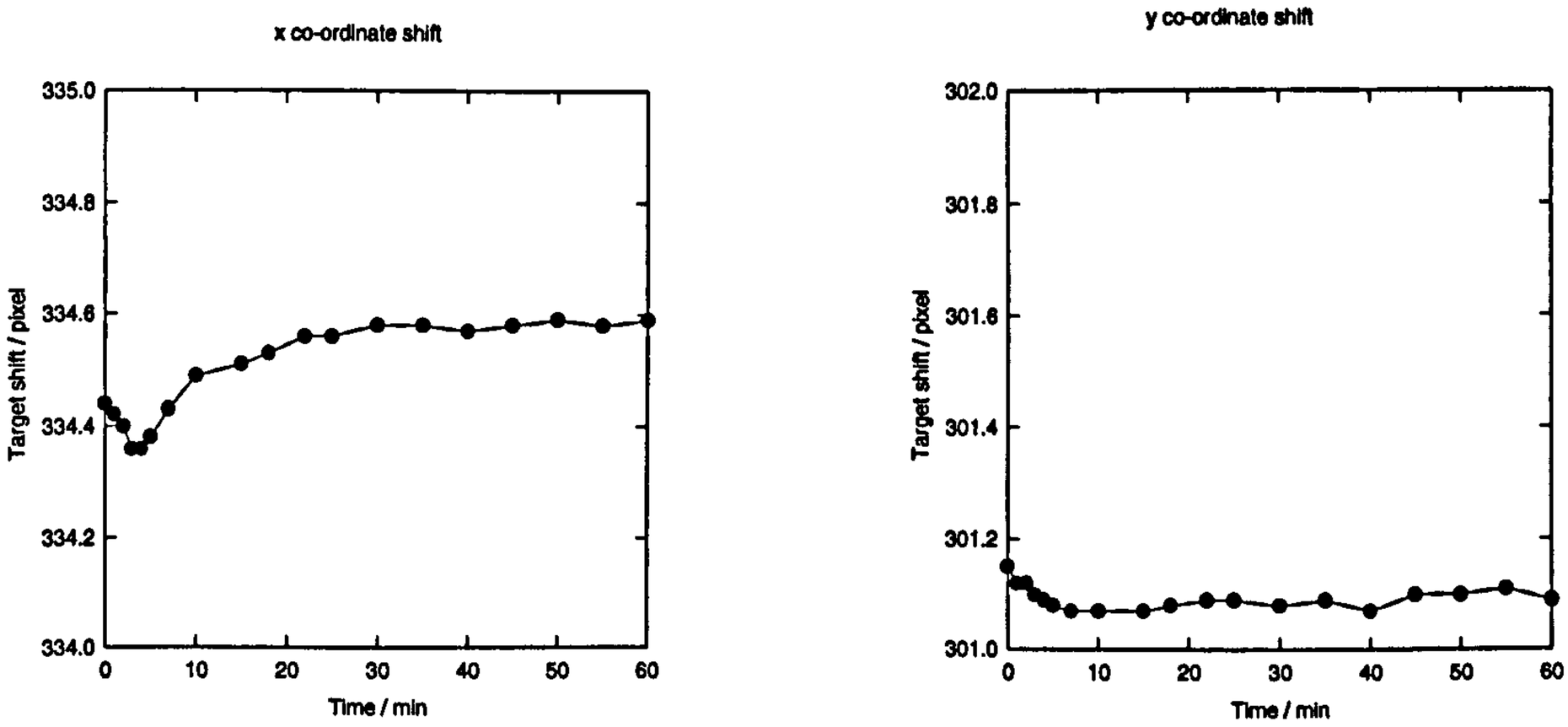

Figure 3.22 x,y co-ordinate warm-up shift for target image (camera 2)

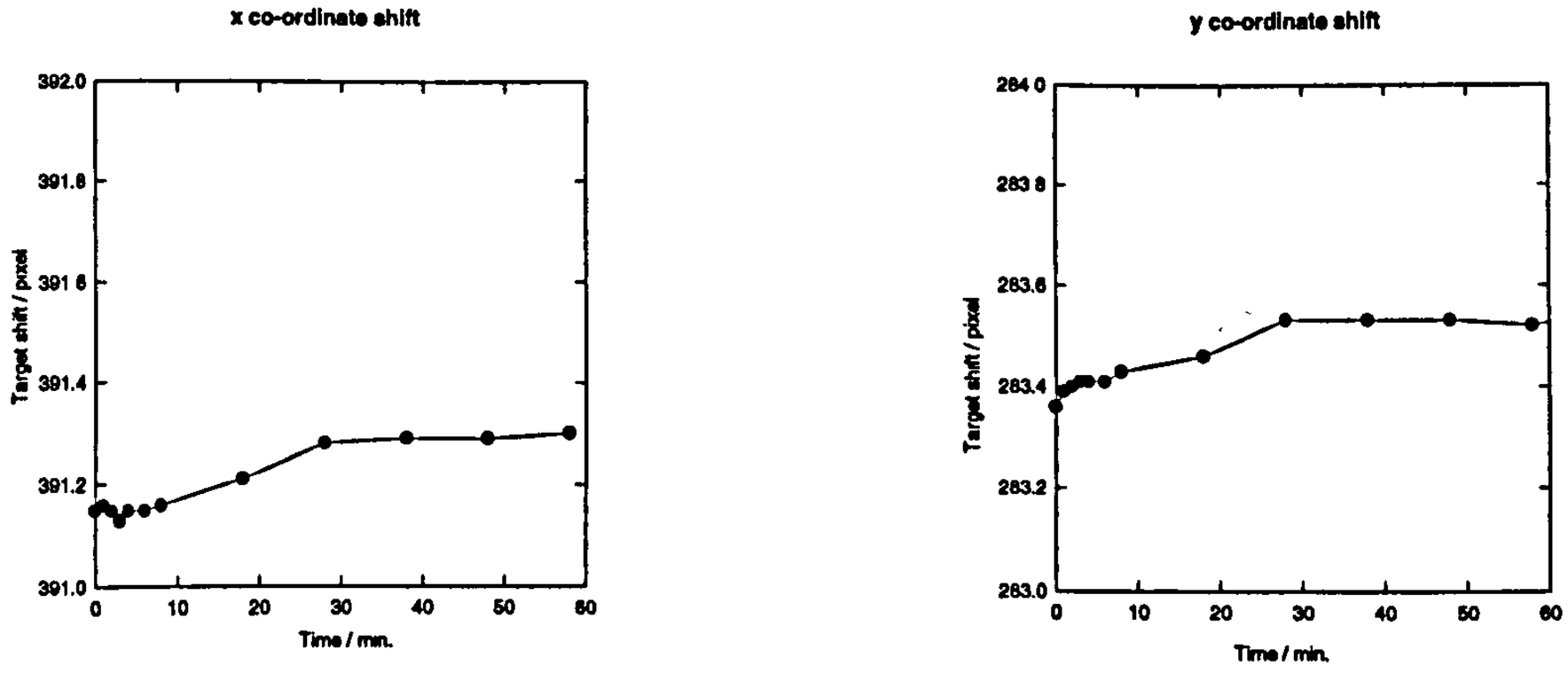

Figure 3.23 x, y co-ordinate warm-up shift for target image (camera 3)

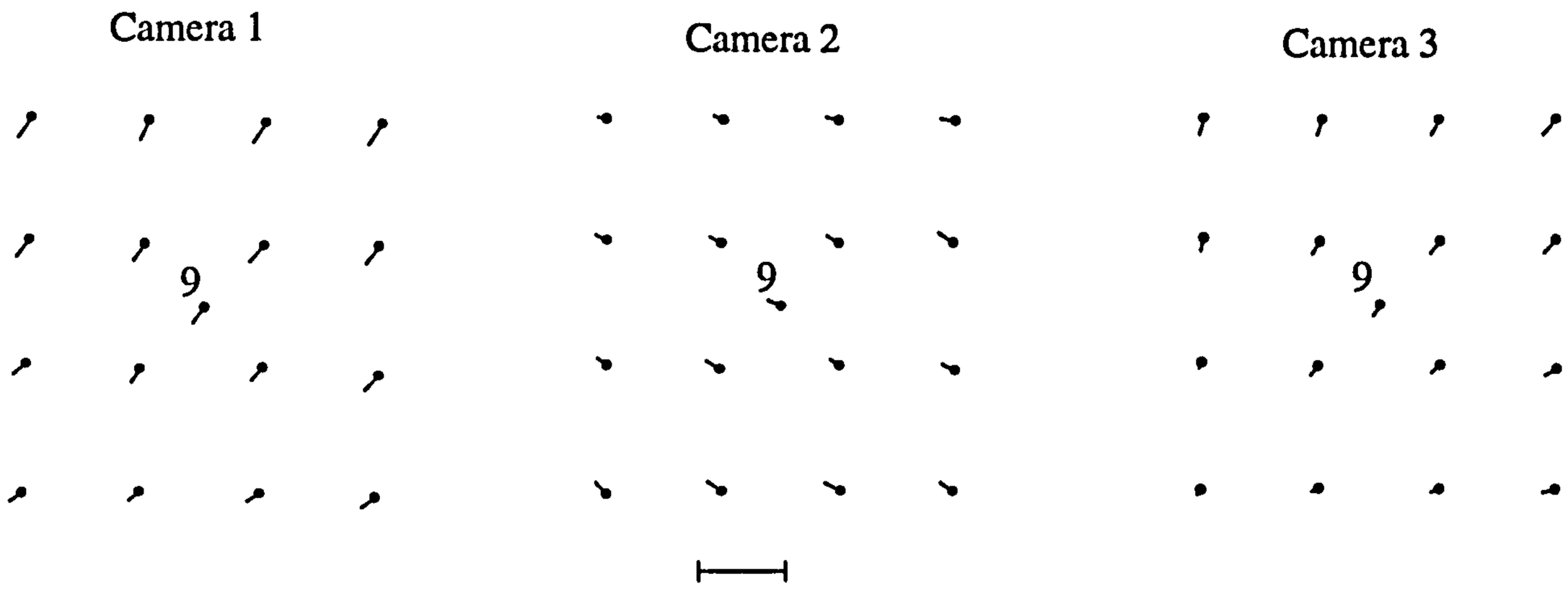

Figure 3.24 Vectors of the warm-up characteristics of the three cameras

the shifts seen would not be expected to be so systematic. A plausible, but as yet confirmed, explanation is the thermal expansion of the sensor during warm-up. Certainly the centre of expansion would not be expected to be in the same place and would vary from camera to camera. However, although the nature of the shifts appears to support this hypothesis, the degree of expansion appears to be beyond that which would be expected for the expansion of silicon over the expected temperature range. Hence, as there has been no documentation of this effect in the literature conclusive proof of the causes of this effect will require further experimentation.

3.3.1.2. Temperature effects of framegrabber

A test was carried out by switching on a camera and allowing it to become stable (more than two hours). The host computer was then switched on. A series of images were collected at varying time intervals. The camera and the test field were kept stable during this time. All the x,y co-ordinates of the target images were calculated by the same subpixel location algorithm. A shift of all targets is shown on Figure 3.25. The x, y co-ordinate shift for a single target number 9 is illustrated in Figure 3.26. It can be seen that the temperature related shift for the framegrabber is much bigger in the x direction. The shift was found to be up to more than 4 pixels in magnitude. In the y direction the shift is very small compared to the shift in x direction, about 1/20th of a pixel. The reason for the big difference is that the scanning frequency of the clock signal generated by the framegrabber has changed in relation to that of

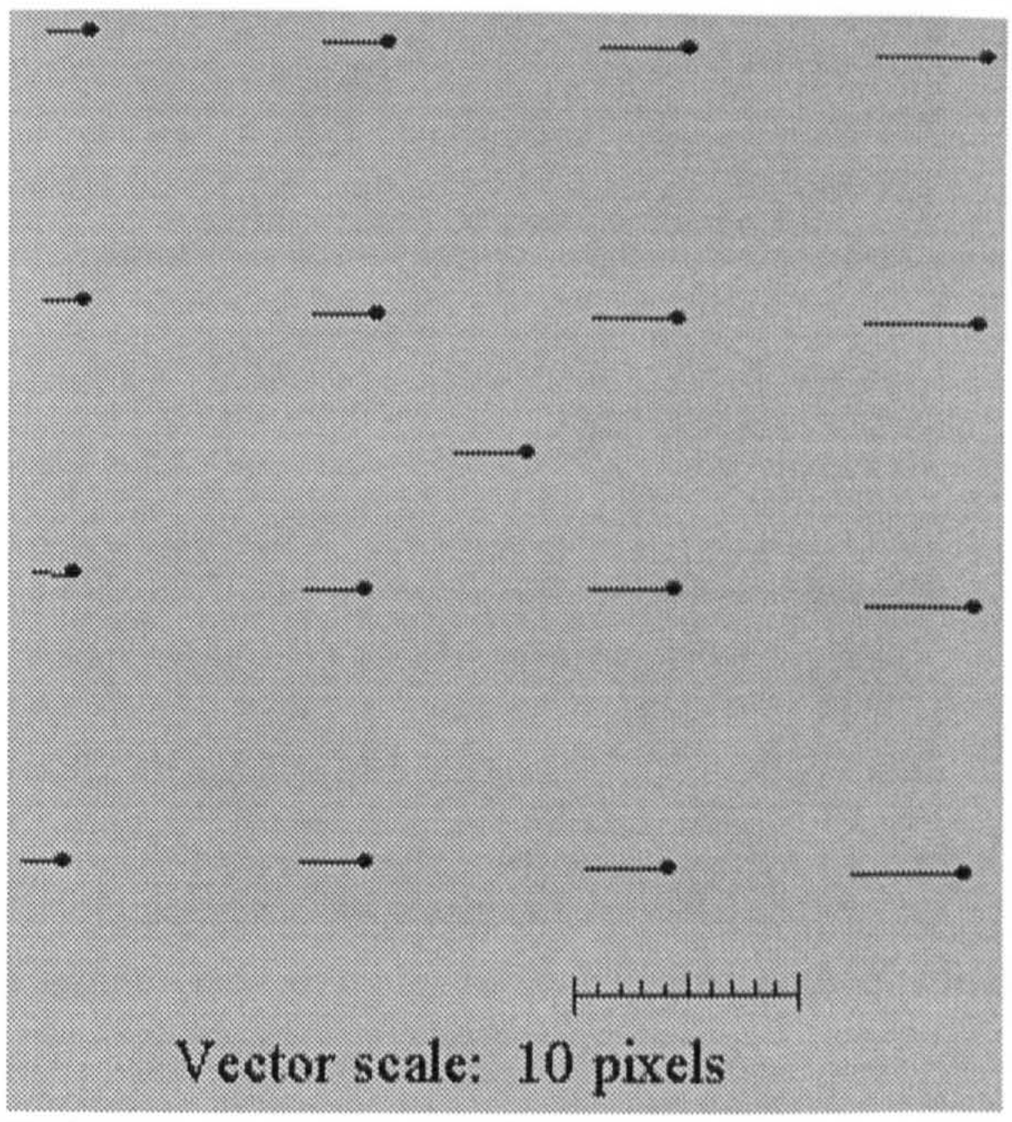

Figure 3.25 Vectors of the warm-up characteristics of the framegrabber

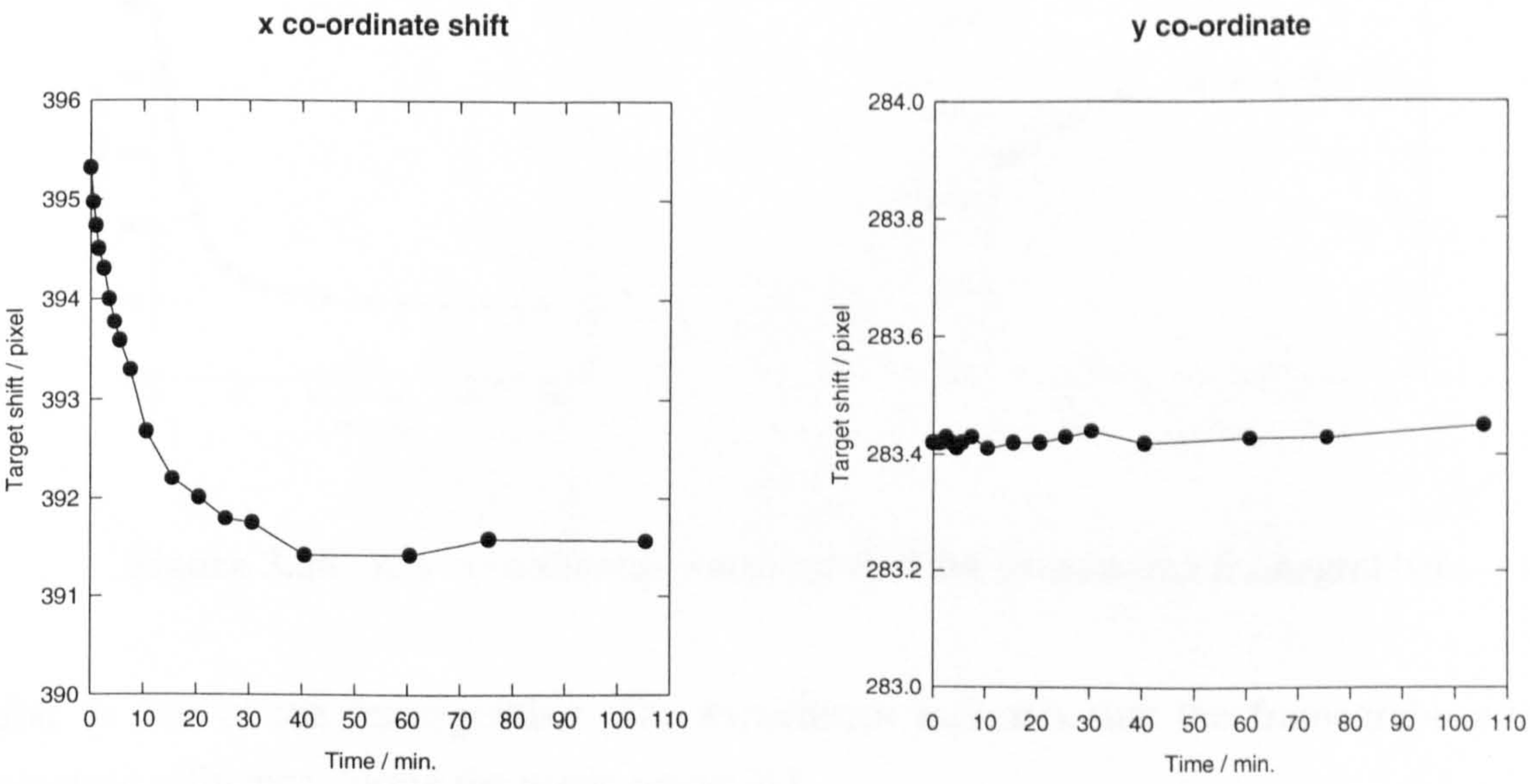

Figure 3.26 x, y co-ordinates warm-up shift for framegrabber

the camera.

3.3.1.3. Temperature effects of combined with both components

To verify the temperature effects for both the individual cameras and the framegrabber, a warm-up test which combined both components was carried out. The power supply to the camera and computer were switched on at the same time. The same steps as before were taken to collect the x, y co-ordinates of all targets on each image. The shift vectors of all targets are shown in Figure 3.27 and the x, y co-ordinate shift for a single target (number 9) is illustrated on Figure 3.28. It is can be seen that the warm-up effect of both framegrabber and camera is

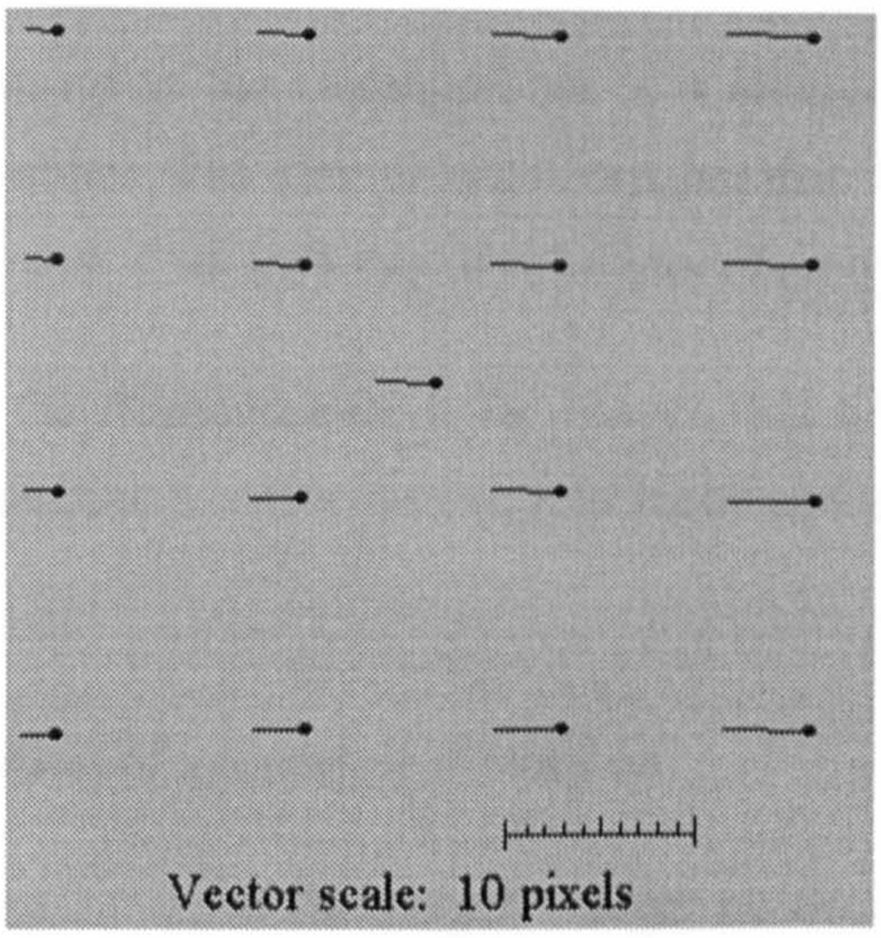

Figure 3.27 Vectors of warm-up of the camera and framegrabber

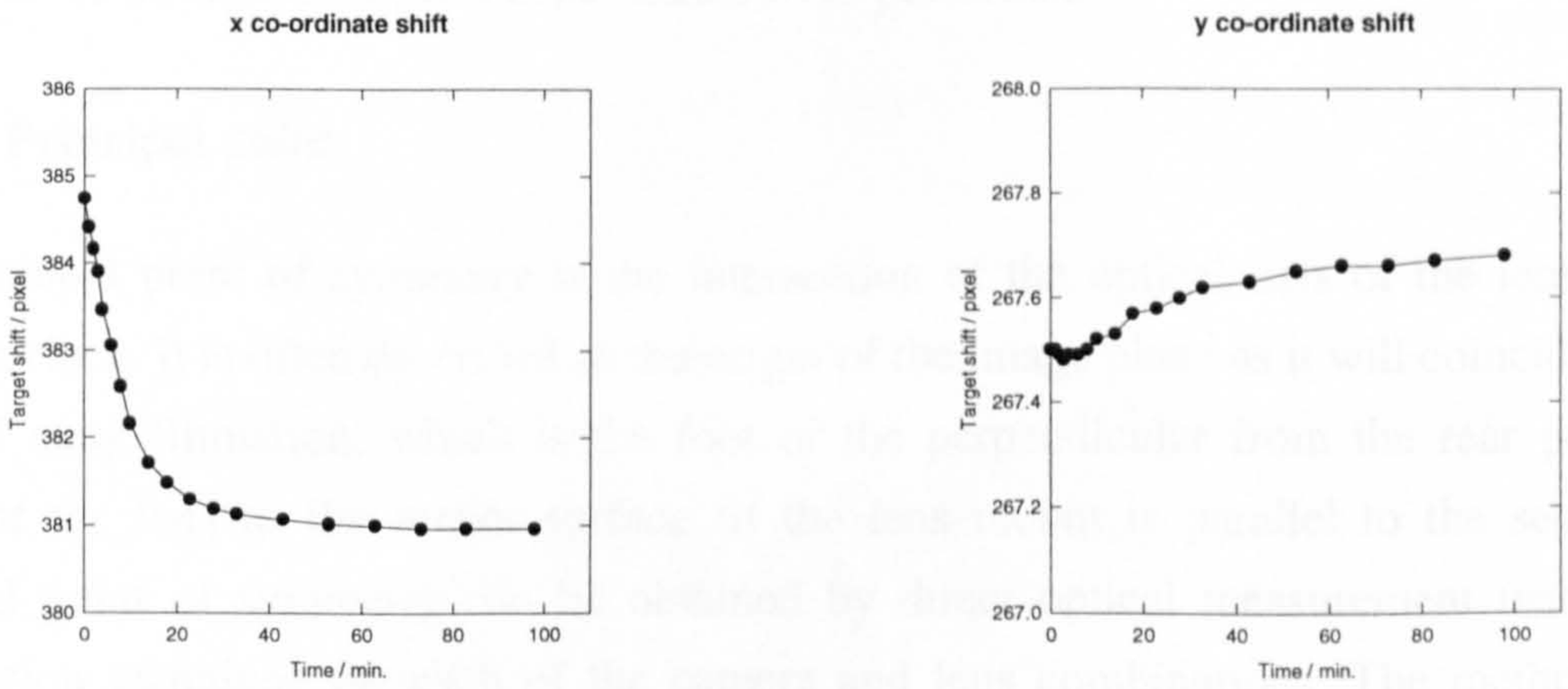

Figure 3.28 x, y co-ordinates warm-up shift for camera and framegrabber

similar to that of the framegrabber. The experiment indicates that the framegrabber is the dominating influence during the warm-up period.

3.3.1.4. Conclusion

As a result of the series experiments described in the previous sections a number of conclusions may be made concerning the warm-up effects in both camera and framegrabber components:

(i) the main effect of camera warm-up is likely to be the thermal expansion of the camera, most notably the CCD chip. The fixed point of the expansion varies from camera to camera and has the same order of magnitude for all target images. The warm-up shift for this type of camera can be up to as much as 0.2 pixels. The shift could be modelled by an affine transformation;

(ii) the main effect of warm-up in the framegrabber is a change of frequency of the clock signal generated by framegrabber. The change manifests itself in the x image direction where a four pixel shift has been noted. This shift can also be modelled by an affine transformation;

(iii) the warm-up effect of the framegrabber is far bigger that that of the camera. Although both can be modelled by an affine transformation, it is recommended that images are grabbed after warm-up.

3.3.2. Analysis and calibration of geometric distortion

The main physical sources of error in target image co-ordinates are: principal point estimation; incorrect lens distortion estimation; line-jitter; and quantization. In order to analyse these influences several experiments were performed.

3.3.2.1. Principal point

The principal point of symmetry is the intersection of the optical axis of the lens with the sensor surface. It is often described as the origin of the image plane as it will coincide with the point of autocollimation, which is the foot of the perpendicular from the rear perspective center of the lens to the sensor surface (if the lens mount is parallel to the sensor). The principal point of symmetry can be obtained by direct optical measurement using a laser illumination technique for each of the camera and lens combinations. The method used is based on a method introduced by Burner et al, 1990. The setup of the test is illustrated in Figure 3.29. A low power laser and the Pulnix TM-6CN camera (with lens removed) were mounted on an optical bench. To align the laser with the centre of the CCD array, an

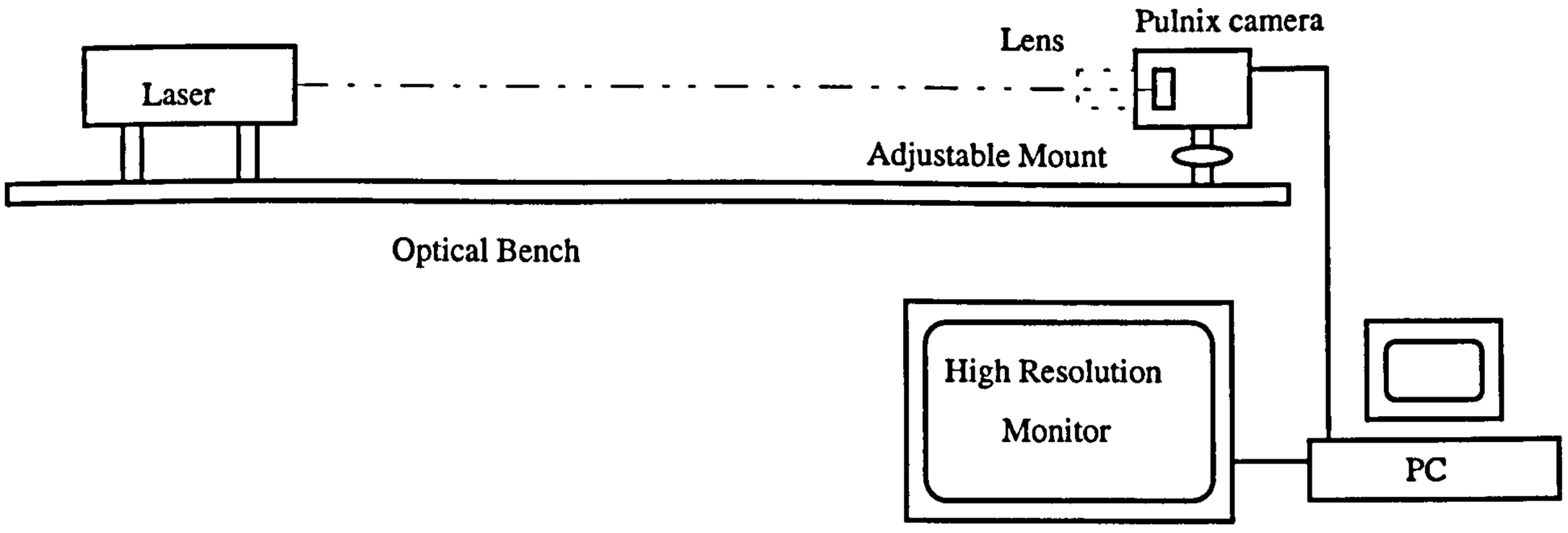

Figure 3.29 Test of principal point setting up

adjustment was made to coincide the primary reflection from the surface of the sensor with the incident beam. Because there are many similar strength reflections from the cover glass front surface, care must be taken to distinguish the correct coincidence beam. Coincidence was identified by symmetry with the diffraction pattern caused by the surface structure of the sensor. The lens was replaced and approximately focused at infinity, the beam was attenuated, and an image was grabbed. The centre of the focused spot locates the principal point of symmetry.

Three Pulnix TM-6CN cameras and three lenses were used individually to measure the principal point using this method. Table 3.4 shows the mean value from results of combination of each camera and lens. However, in a real measuring system the lens will be focused so that the principal distance and the location of the principal point will be changed. Such variations were evaluated by using one of the cameras and lenses by adjusting the lens to several different focus settings throughout its imaging range and noting the location of the principal point. Table 3.5 shows these results. From this table, it can be seen that there is a three pixel change in the principal point x co-ordinate and a 14 pixel change in the y co-ordinate.

Camera No.	Lens No.	x	y
1	1	360.5	268
1	2	354	263.5
1	3	343	275.5
2	2	351	221
3	3	346.5	293

Table 3.4 Principal point measurement

Focus Setting	x	y
Infinity	350	220
5m	349	218.5
2m	348.5	216.5
1m	349	213.5
0.5m	347	206

Table 3.5 Variation of lens focal point

3.3.2.2. Lens distortion

In order to quantitatively analyse lens distortion, several tests were carried out using plumb line methods to calculate the radial distortion parameters K_1, K_2, K_3 and decentering distortion parameters P_1 and P_2 (Fryer, 1989). The setting up of the plumb lines and the camera is shown in Figure 3.30. This plumb line method has been discussed previously in chapter two and is based on the principle that the perspective projection of a straight line from the object space should produce a straight line in the image. Any deviations from linearity can be attributed to radial and decentering distortions in the lens.

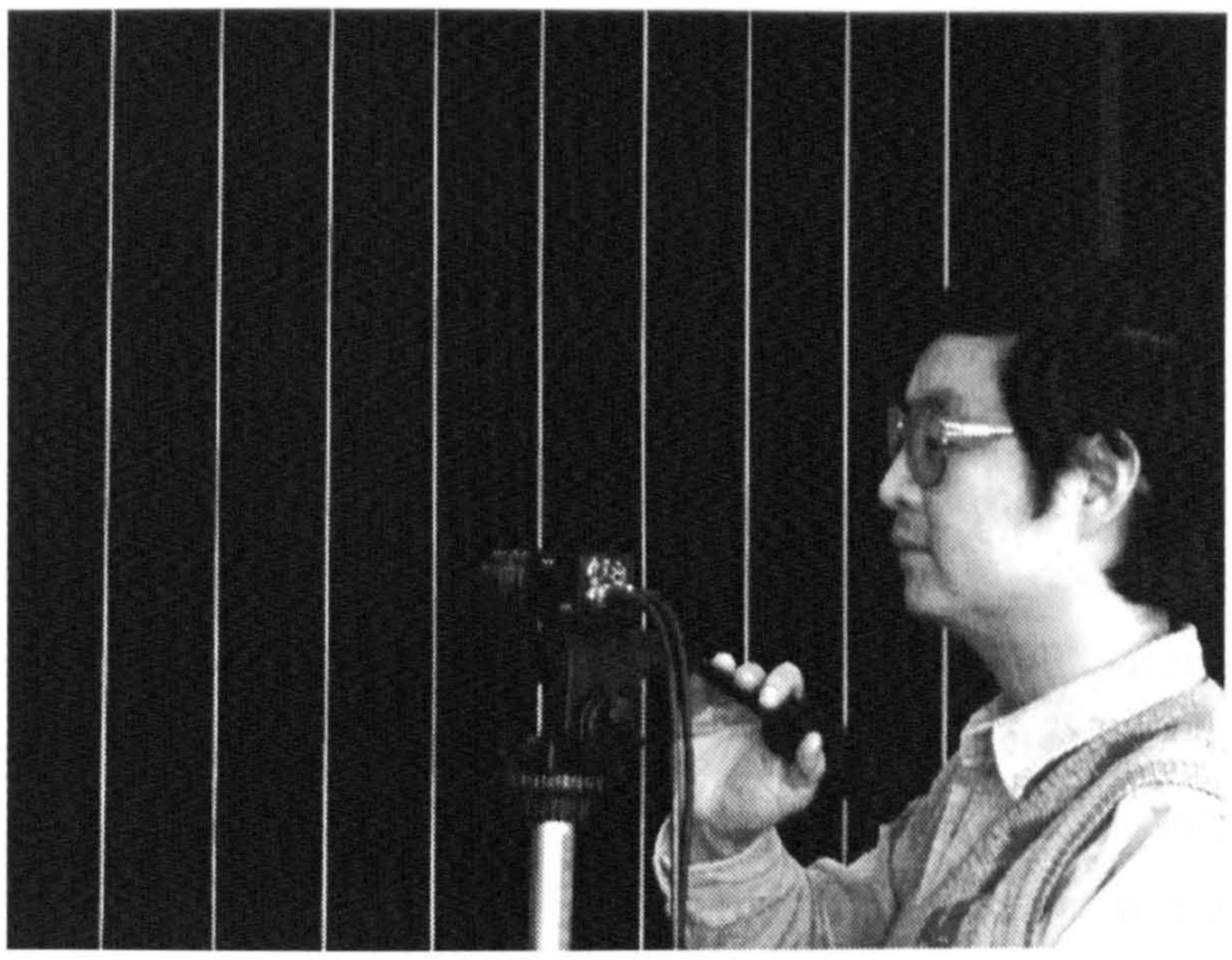

Figure 3.30 Setting up the plumb lines and camera

(i) Calculation of the parameters K_1, K_2, K_3, P_1, P_2

In order to obtain reliable results for both the parameters of radial and decentering distortion, it is necessary to obtain line imagery in both the x and y directions. For the subpixel measurement techniques to function correctly an evenly reflecting white line would ideally occupy 5-6 pixels in the image. To provide as much contrast as possible, various materials were tested. Sewing cotton line was too weak and too furry, thin wire was too stiff. Finally a builders chalk line was found to provide the best compromise, it was white, strong and flexible.

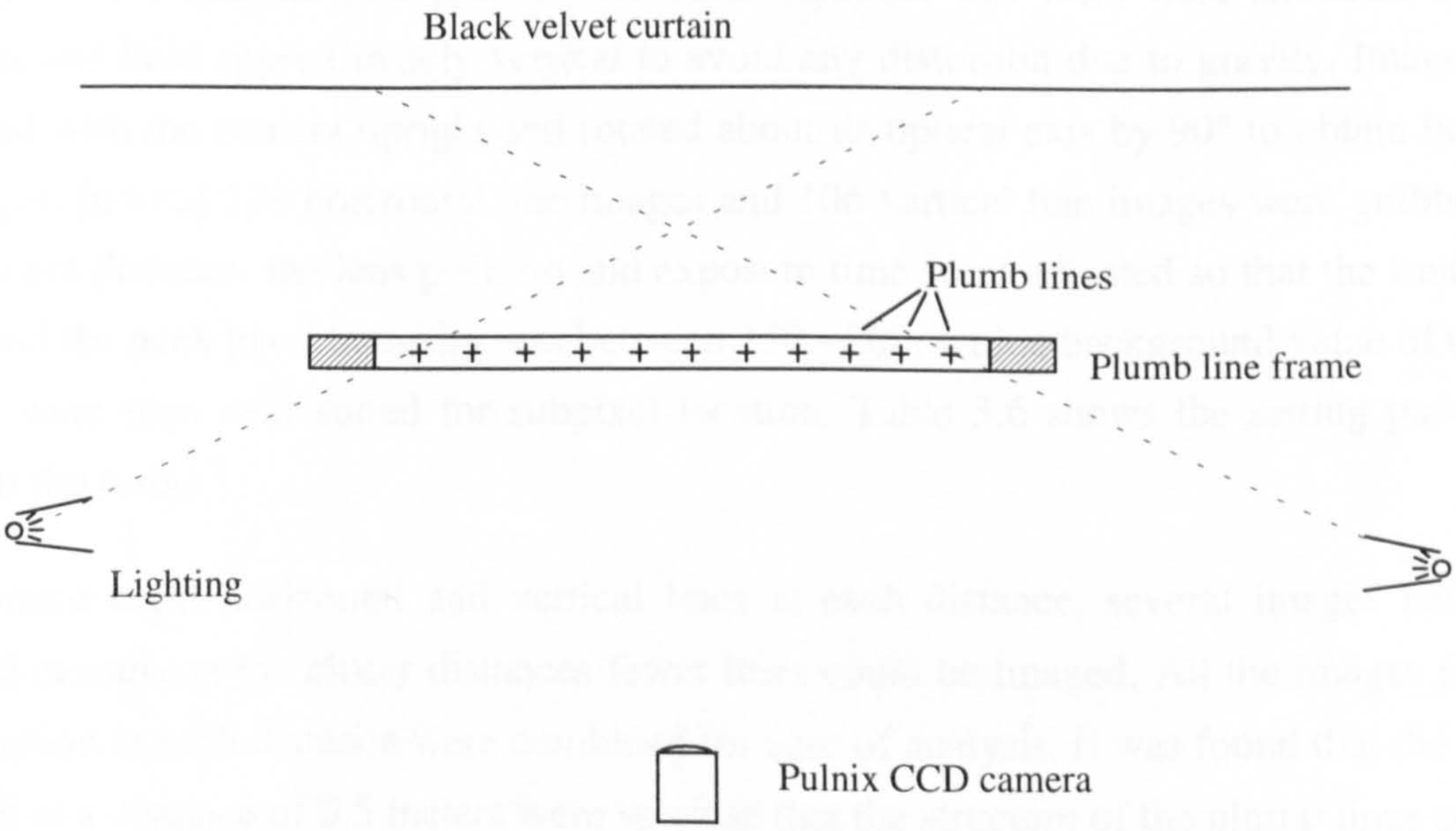

Figure3.31 The configuration of the plumb lines (plan view)

A wooden test frame was built (Figure 3.31). Ten white builders chalk lines were fixed to the frame. Although not theoretically necessary, the strings were arranged to be as parallel as possible. The background of the test frame was covered with a black velvet material so that all the ambient light falling on the background was absorbed. The distance between the plumb frame and the background was set at 1.5m so that the background would contribute little influence when light was projected onto the plumb lines.

Several illumination conditions were tested, including using two 800W halogen lamps, a fluorescent lamp, and natural daylight. The halogen lamp illumination produced strong contrast between the string image and the background. However this was found not to provide uniform illumination using just two halogen lamps, which approximated to point light sources. Furthermore the high intensity of the halogen lamps made it easy to saturate the plumbline images. Tests showed that a combination of fluorescent lamps and daylight could provide a useful results. This was because the contrast between the string and the background was sufficiently high provided the illumination was uniform. Hence, daylight was used for all the tests described in the next section.

(a) Image acquisition

The camera was fixed on a tripod. The distance between the camera and the plumbline frame was set to four distance ranges (4m, 2m, 1m and 0.5m). To look at all possibilities three cameras and three lenses were used in nine different groups. Each group was used at each of the four distances. To guarantee that eight lines were available at each image distance, several laterally shifted images were grabbed for each situation. The lines were stretched between supports and held approximately vertical to avoid any distortion due to gravity. Images were collected with the camera upright and rotated about its optical axis by 90° to obtain both sets of images. In total 136 horizontal line images and 106 vertical line images were grabbed. For each object distance, the lens position and exposure time were adjusted so that the image was sharp and the peak pixel intensity was between 150 - 200, with a background value of 0. Such images were then well suited for subpixel location. Table 3.6 shows the setting parameters used for the tests.

To produce eight horizontal and vertical lines at each distance, several images had to be grabbed because at the closer distances fewer lines could be imaged. All the images for each combination at each distance were combined for ease of analysis. It was found that the images grabbed at a distance of 0.5 meters were so close that the structure of the plumb lines could be seen. Figure 3.32 shows a zoom of an image at 0.5 meter. It is clear that location of the centroid of the line from these images would be noisy due to the structure of the plumb lines

Camera	Lens	Dist.	Aperture	Focus	ImageNo.	HoriNo.	Vert.No.
1	1	4	2.8	4.0	2	8	7
1	1	2	2.8	1.8	4	8	9
1	1	1	2.8	0.85	7	8	7
1	1	0.5	2.8	0.5	14	8	8
1	2	4	2.8	4.0	2	8	10
1	2	2	4.0	1.9	4	8	10
1	2	1	4.0	1.02	7	7	10
1	2	0.5	5.0	0.5	15	8	8
1	3	4	5.0	4.0	2	8	9
1	3	2	2.8	1.9	4	8	9
1	3	1	4.0	0.85	8	8	11
1	3	0.5	5.0	0.5	14	8	8
2	1	4	5.6	3.5	2	7	9
2	1	2	4.0	1.8	4	8	9
2	1	1	4.0	0.9	7	8	8
2	1	0.5	4.0	0.5	14	8	8
2	2	4	2.8	3.5	2	8	10
2	2	2	4.0	1.9	4	7	10
2	2	1	4.0	0.85	8	7	11
2	2	0.5	4.0	0.28	14	8	7
2	3	4	2.8	3.5	2	8	9
2	3	2	2.8	1.8	4	8	10
2	3	1	4.0	0.8	8	8	10
2	3	0.5	4.0	0.51	14	9	9
3	1	4	2.0	3.5	2	8	9
3	1	2	2.8	2.0	4	8	10
3	1	1	2.8	1.0	8	7	11
3	1	0.5	2.8	0.5	15	8	9
3	2	4	4.0	4.0	2	8	9
3	2	2	2.8	1.85	4	8	10
3	2	1	4.0	1.05	7	7	8
3	2	0.5	5.8	0.48	15	7	7
3	3	4	2.8	3.5	2	8	10
3	3	2	2.8	1.95	4	7	10
3	3	1	4.0	0.9	7	8	8
3	3	0.5	4.0	0.48	15	8	7

Table 3.6 Environment parameters for the plumb line method experiments

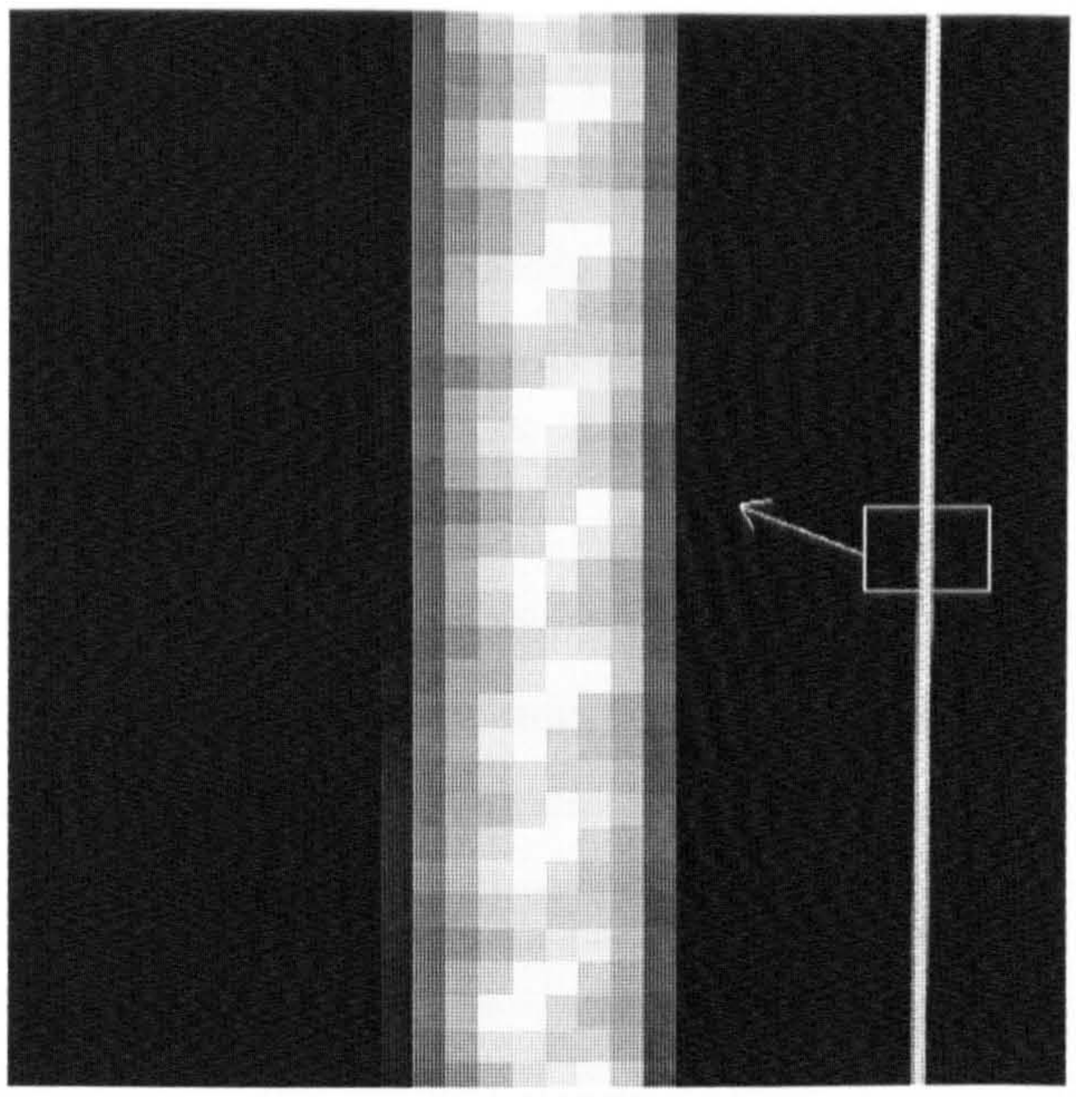

Figure 3.32 Close up view of the string at 0.5 meters

themselves and therefore could not be used for subpixel measurement. To acquire data at this distance, another thin and uniform string must be chosen for measurement. However, for most of the photogrammetric close range measurement envisaged an object to camera distance of 0.5 to 1.0 meters is unlikely so it was considered unnecessary to perform those experiments. All the images at 0.5 meters were rejected, only the images at 4, 2 and 1 meter were used to analyse the distortion of the camera lenses.

(b) Data reduction

The number of lines in each image was counted, then a limited number of points on the line were extracted using the following method. The lines were positioned as near to vertical as possible. It was not necessary to use a threshold value for the images because the background value of the image was zero. While a threshold method can remove some background noise it can cause other problems (Clarke, 1993). After each line was extracted, individual points on the lines were extracted using a sample every ten pixels. Given an image size of 752 X 576, 75 horizontal points and 57 vertical points were extracted. A program was written to automatically search the image for each camera, lens and object distance. After selecting the image file, an algorithm to search for the centre of each plumb line was applied. A subpixel location algorithm was written, in which a window size of 40 pixels was used, to locate each subpixel position on each line. The format of data extracted was stored in two groups, all horizontal lines: number, x co-ordinate, y co-ordinate; then all vertical lines: number, x co-ordinate, y co-ordinate.

A least squares program adapted from the work of D.C. Brown, 1971, and J. Fryer, 1994, was

used to calculate the lens distortion parameters. This program required the input of data in the form of vertical line data followed by horizontal. The program, originally written in FORTRAN, was re-written in 'C' so that it could more easily satisfy the requirements of these experiments. Computation of lens distortion was an iterative process. Initial values of K_1, K_2, K_3, P_1 and P_2 were set at 0. An initial RMS weighting value was also set for each of the unknown parameters, $RMS_{k1} = 1.0e^{-4}$, $RMS_{k2} = 1.0e^{-4}$, $RMS_{k3} = 1.0e^{-11}$, $RMS_{p1} = 1.0e^{-4}$, $RMS_{p2} = 1.0e^{-4}$. Generally, 3 - 5 iterations were required for convergence. Table 3.7 shows the radial and decentering lens distortion in micrometers at a radial distance of 4 millimeters and Table 3.8 summarises the mean values for radial and decentering distortion in micrometers for a radial distance of 4 millimeters where the SigX and SigY are the RMS

Camera No.	Lens No.	Dist. at 4m	Dist. at 4m	Dist. at 2m	Dist. at 2m	Dist. at 1m	Dist. at 1m
		radial distortion	decentering distortion	radial distortion	decentering distortion	radial distortion	decentering distortion
1	1	11.9	0.4	13.8	1.2	13.6	1.8
1	2	13.7	0.3	14.3	0.8	16.0	1.4
1	3	12.8	0.5	12.6	0.8	14.8	1.8
2	1	12.5	0.3	14.2	0.8	15.6	1.8
2	2	12.9	1.4	13.9	2.4	15.2	3.0
2	3	12.9	1.2	13.7	1.4	15.1	2.8
3	1	13.1	0.3	14.5	0.4	16.0	3.3
3	2	13.7	1.2	14.1	1.6	17.1	2.5
3	3	12.7	1.2	13.4	1.5	15.2	2.0

Table 3.7 Radial and decentering lens distortion in micrometers

Lens No.	Dist. at 4m	Dist. at 4m	Dist. at 2m	Dist. at 2m	Dist. at 1m	Dist. at 1m
	radial distortion	decentering distortion	radial distortion	decentering distortion	radial distortion	decentering distortion
1	12.5	0.33	14.2	0.8	15.1	2.3
2	13.4	1.0	14.1	1.6	16.1	2.3
3	12.8	1.0	13.2	1.2	15.0	2.2
Mean	12.9	0.73	13.8	1.2	15.4	2.3

Table 3.8 Mean values of lens distortion in micrometers

Camera No.	Lens No.	Dist.	K1	K2	K3	P1	P2	SigX	SigY
1	1	4	4.73e-4	-2.05e-5	-2.62e-13	-5.57e-4	2.16e-5	0.51	0.30
1	1	2	1.54e-4	4.31e-6	3.60e-17	-4.37e-5	5.62e-5	0.24	0.21
1	1	1	1.49e-4	4.48e-6	-5.32e-15	2.49e-5	1.02e-4	0.23	0.35
1	2	4	2.61e-4	-3.17e-6	-1.95e-16	1.84e-5	-5.48e-6	0.43	0.41
1	2	2	1.24e-4	6.65e-6	2.63e-14	4.21e-5	5.32e-6	0.39	0.32
1	2	1	3.11e-4	-4.23e-6	-4.89e-15	8.18e-5	3.39e-5	0.33	0.21
1	3	4	1.35e-4	2.43e-5	2.21e-14	3.35e-5	-4.69e-6	0.60	0.60
1	3	2	2.42e-4	-3.31e-6	2.37e-15	4.53e-5	-1.83e-5	0.25	0.20
1	3	1	1.67e-4	4.25e-6	2.95e-14	1.08e-4	3.76e-5	0.33	0.23
2	1	4	2.31e-4	1.16e-6	1.90e-15	4.09e-6	1.89e-5	0.35	0.23
2	1	2	2.62e-4	5.89e-8	-8.07e-16	1.84e-5	4.59e-5	0.30	0.30
2	1	1	1.77e-4	4.40e-6	-2.38e-14	9.86e05	6.54e-5	0.33	0.25
2	2	4	2.31e-4	-2.05e-6	-1.15e-14	1.63e-4	-7.66e-6	0.32	0.26
2	2	2	2.97e-4	-5.49e-6	2.64e-14	9.40e-5	-1.60e-6	0.33	0.33
2	2	1	3.26e-4	-5.95e-6	-3.48e-14	1.99e-4	2.96e-5	0.40	0.23
2	3	4	2.24e-4	-1.57e-6	8.97e-15	8.99e-5	-1.77e-5	0.30	0.18
2	3	2	2.29e-4	-1.11e-6	-3.65e-15	7.77e-5	-7.35e-6	0.31	0.27
2	3	1	1.92e-4	3.06e-6	-2.78e-14	1.76e-4	1.77e-5	0.34	0.27
3	1	4	2.08e-4	-2.15e-7	-2.10e-14	-8.23e-6	1.82e-5	0.15	0.14
3	1	2	2.99e-4	-4.95e-6	-4.45e-14	-9.07e-6	2.32e-5	0.23	0.24
3	1	1	3.62e-4	-7.12e-6	-2.38e-14	1.95e-4	8.75e-5	0.55	0.38
3	2	4	1.47e-4	4.82e-6	1.76e-14	1.10e-4	1.85e-5	0.56	0.45
3	2	2	2.66e-4	-3.21e-6	1.09e-14	6.98e-5	2.74e-5	0.28	0.30
3	2	1	3.81e-4	-7.72e-6	1.03e-14	1.56e-4	5.55e-5	0.43	0.27
3	3	4	1.76e-4	1.53e-6	8.09e-16	7.41e-5	1.03e-5	0.33	0.25
3	3	2	8.60e-5	8.79e-6	-1.09e-14	7.85e-5	4.89e-5	0.30	0.22

Table 3.9 Convergence value of K_1, K_2, K_3, P_1 and P2

errors of the parameter estimation in both horizontal and vertical directions. Table 3.9 summarises the K_1, K_2, K_3, P_1 and P_2 parameter values of the three cameras and three lenses. Figure 3.33 and Figure 3.34 shows the curves of radial and decentering distortion for the three camera and three lens combinations. Figure 3.35 and Figure 3.36 illustrate the mean results of radial and decentering lens distortion. The tests can be summarised into four results: **a)** the

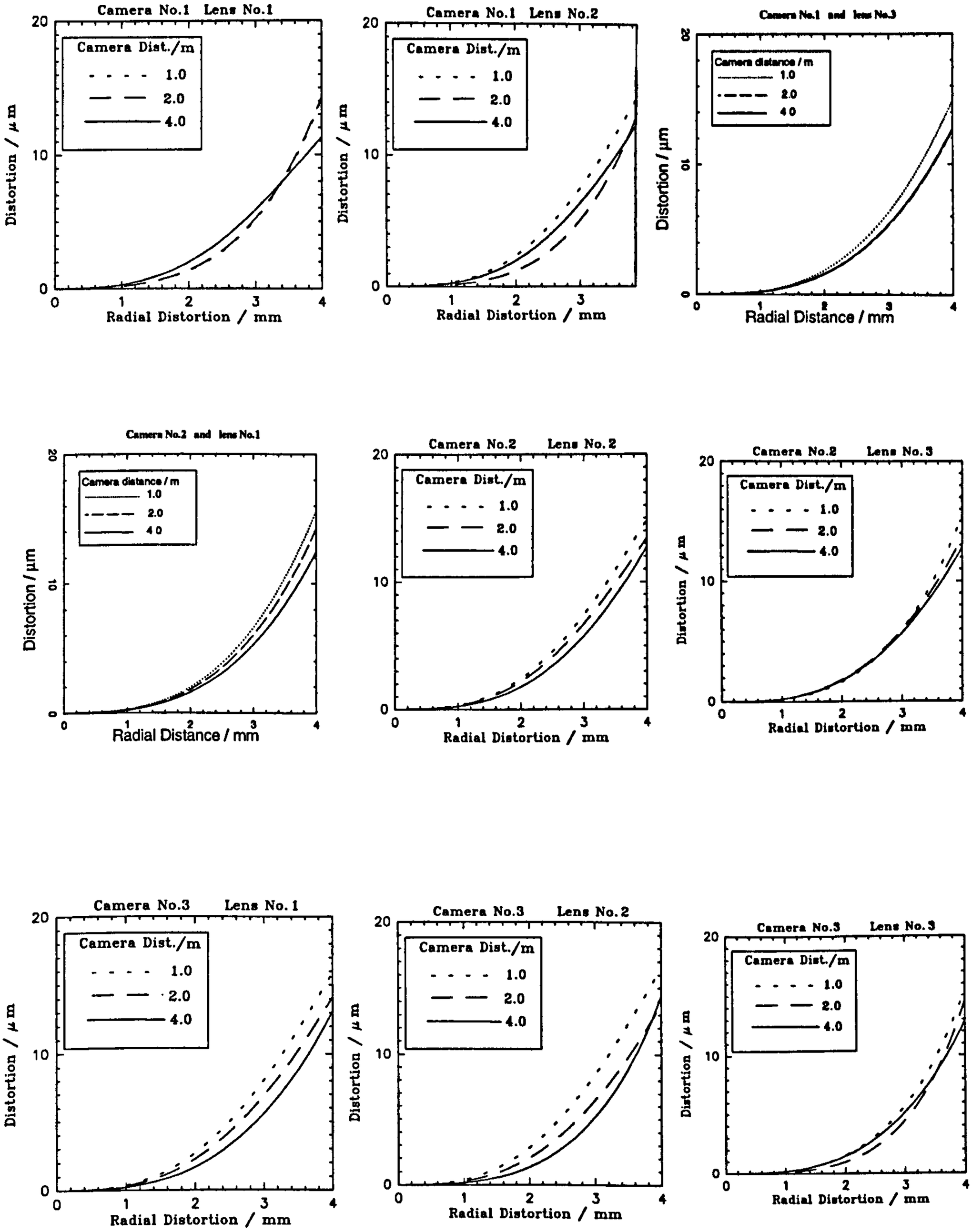

Figure 3.33 Radial distortion for three cameras and three lenses

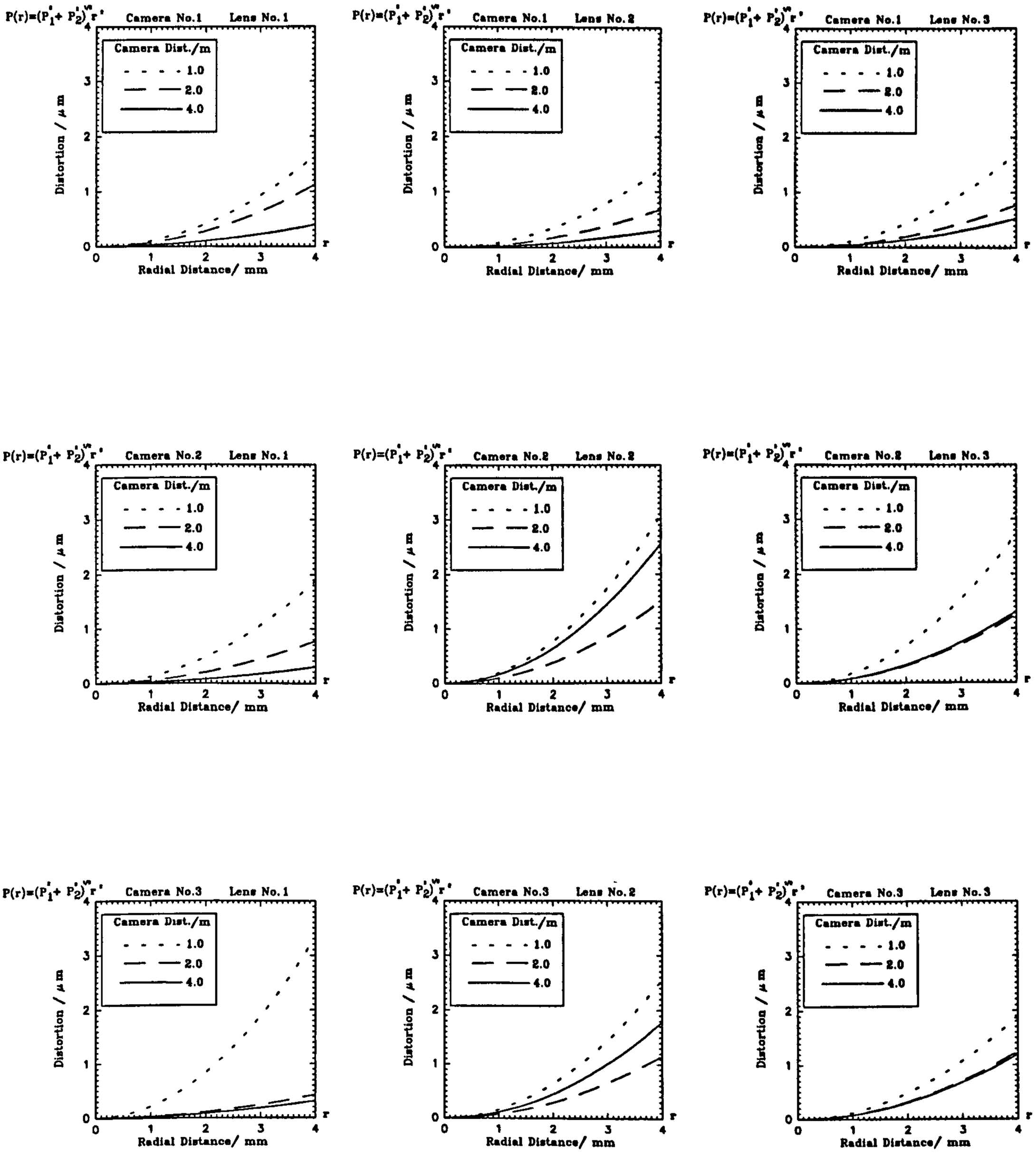

Figure 3.34 Decentering distortion for three camera and three lenses

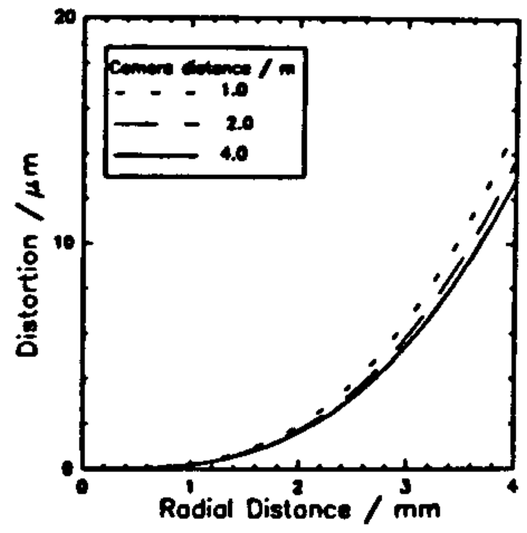

Figure 3.35 Radial distortion graph of mean results

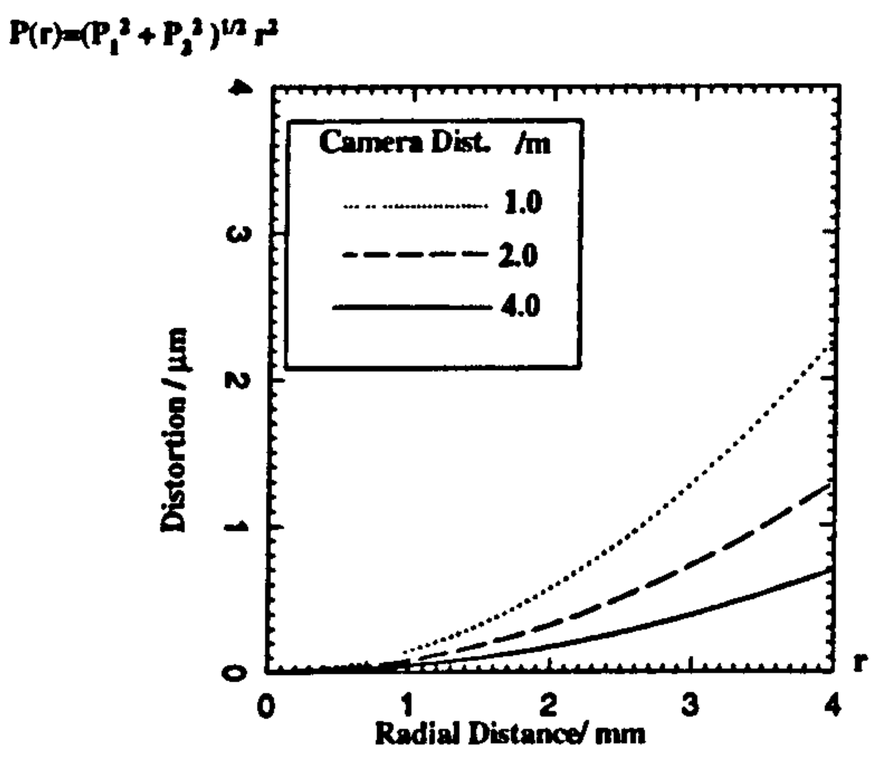

Figure 3.36 Decentering distortion graph of mean results

radial distortion is nearly one order of magnitude greater than decentering distortion; **b)** the value of the K_1 term, is one order of magnitude larger than that of the other two terms, K_2 and K_3 so that it dominates the description of radial distortion; **c)** the radial distortion within a radial distance of 2mm, where most imagery will probably be captured, is only one-eighth as large as that at the maximum radial distance of 4mm; **d)** the increase in decentering distortion at closer distances is significant.

(ii) Calculation of only K_1

The results of the previous experiments for determining the lens distortions using the plumbline method have shown that for the 25mm Fujinon C-mount lenses tested, most of the distortion is described by the K_1 term. To further analyse the role of radial distortion parameters K_1, K_2 and K_3, an experiment was conducted to determine if it was possible to use K_1 only to express the radial distortion for small format CCD cameras without a significant

Camera No.	Lens No.	Dist. at 4m	Dist. at 2m	Dist. at 1m
1	1	11.8	13.8	13.6
1	2	13.8	14.0	16.0
1	3	12.6	12.3	14.6
2	1	12.4	14.0	15.5
2	2	12.8	13.3	15.2
2	3	12.8	13.5	15.1
3	1	13.0	14.4	16.0
3	2	13.5	14.1	17.1
3	3	12.6	13.2	15.2

Table 3.10 Radial lens distortion in micrometers using K_1

Lens No.	Dist. at 4m	Dist. at 2m	Dist. at 1m
	radial distortion	radial distortion	radial distortion
1	12.4	14.0	15.0
2	13.4	13.8	16.0
3	12.7	13.0	15.0
Mean	12.9	13.6	15.3

Table 3.11 Mean values of lens distortion in micrometers using K_1

decrease in accuracy. RMS_{k1} was unchanged, RMS_{k2} set to 1.0e-11 and RMS_{k3} set to 1.0e-13 so that K_2 and K_3 could be neglected. Table 3.10 shows the radial lens distortion in micrometers using K_1 at a radial distance of 4 millimeters for different measuring distances and Table 3.11 summarises the mean values for radial distortion in micrometers for a radial distance of 4 millimeters. Comparing the result in Table 3.11 to Table 3.8, it can be seen both results are very similar. The maximum difference of about 0.2 mm at a radial distance of 4mm corresponds to 1/43th pixel, this is below the usual precision of target location. Figure 3.37 shows the results of radial distortion using these settings. It can been seen from the figure that there is the same trend in both cases. In other words, radial distortion, can for most purposes be described by the K_1 Parameter alone for the lenses used.

(iii) Calculation of K_1 by two lines

The results of the plumbline method using K_1 only with approximately ten horizontal and ten vertical lines have shown that it is feasible to estimate radial lens distortion by the first term (K_1). An experiment was designed to check the influence of calculating K_1 by using only two horizontal and vertical lines at the edge of the image format. Eight lines were recorded in both horizontal and vertical directions for each distance. From the line sets extracted at each

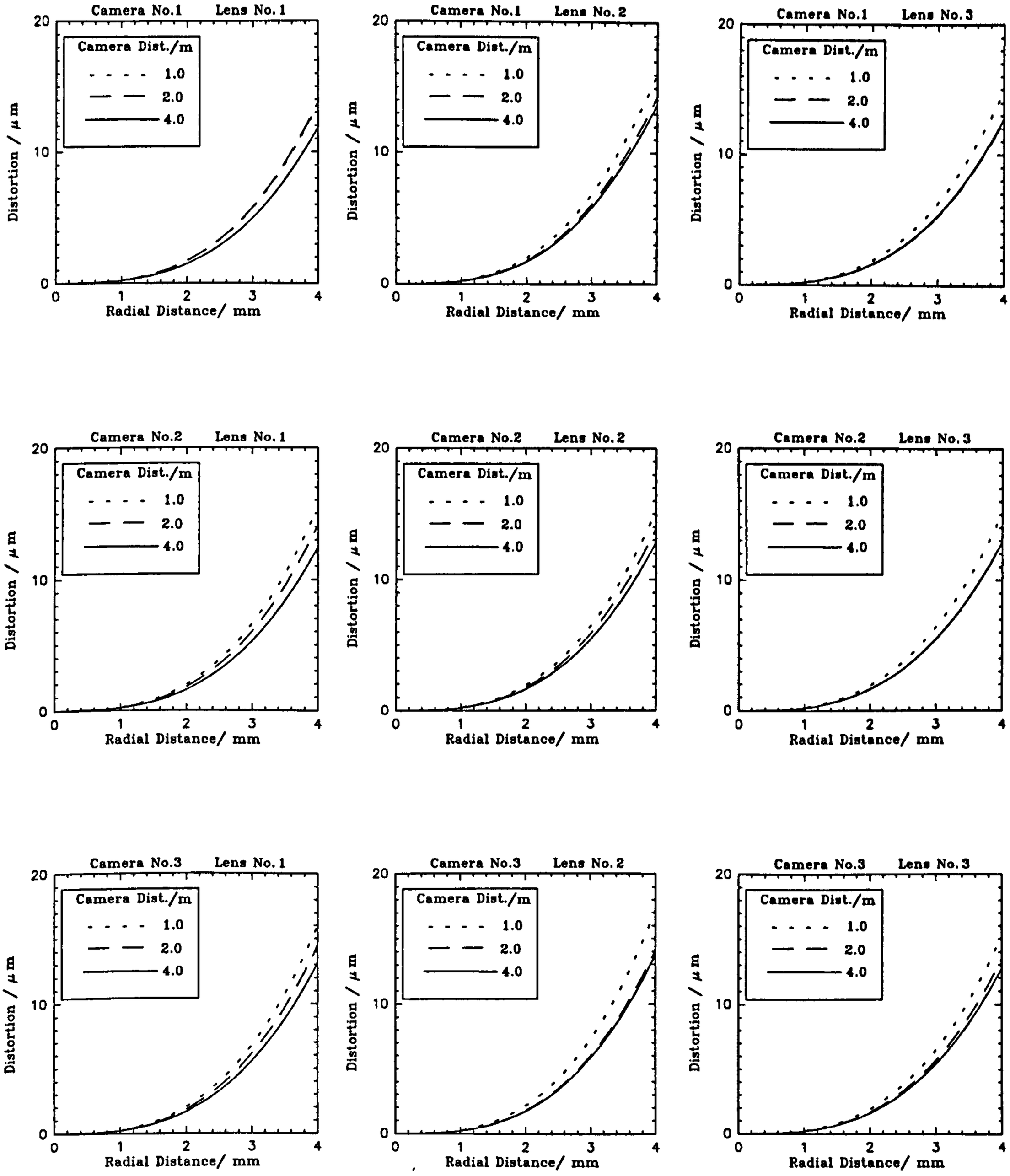

Figure 3.37 Radial distortion for three cameras and three lenses by K_1

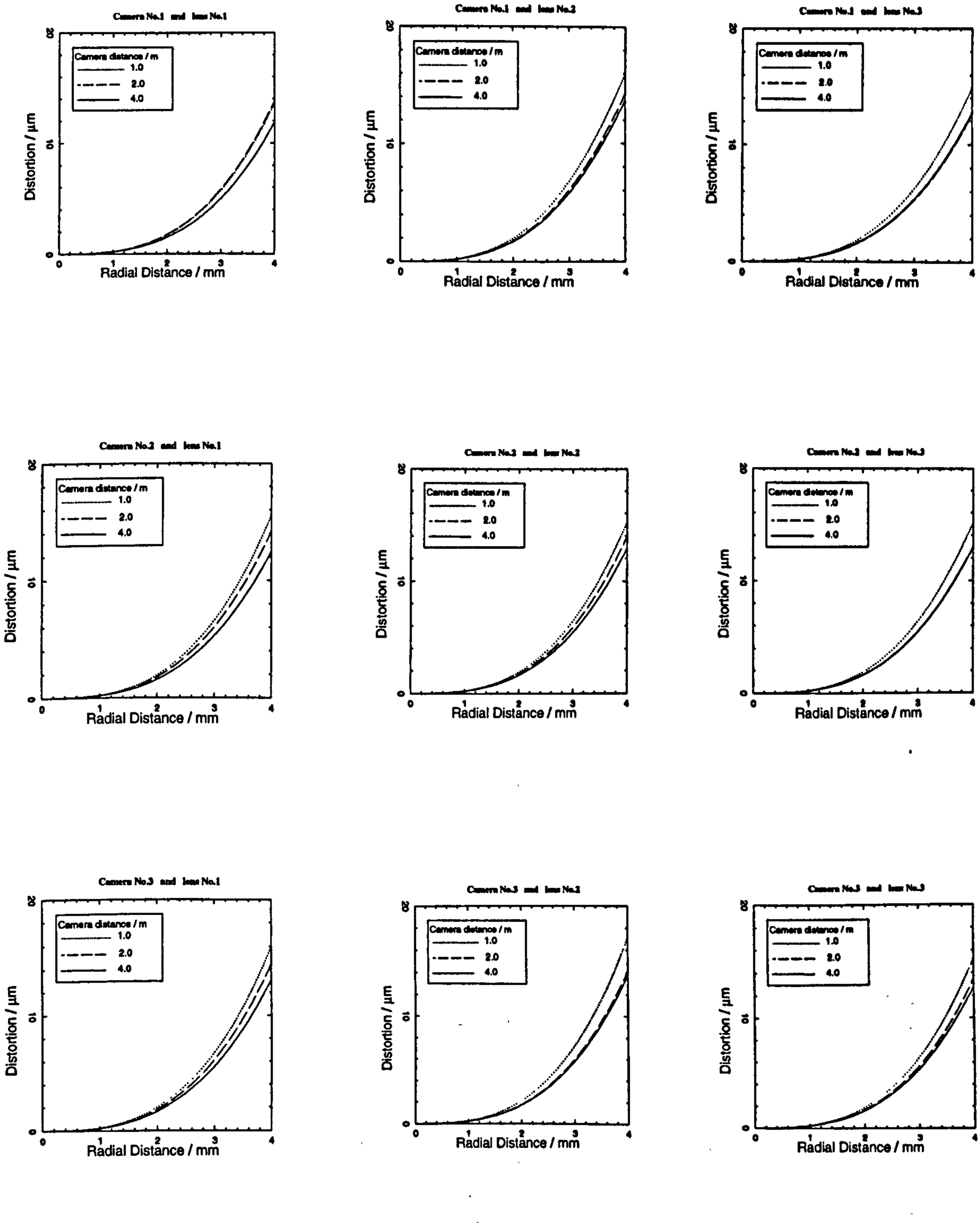

Figure 3.38 Two lines method for calculating K_1

Camera No.	Lens No.	4m	2m	1m
1	1	11.1	13.1	13.9
1	2	13.2	14.4	15.6
1	3	13.9	12.6	15.3
2	1	12.7	14.4	15.6
2	2	12.8	13.6	15.8
2	3	13.1	13.5	15.5
3	1	13.6	14.0	15.9
3	2	14.1	14.0	15.9

Table 3.12 Radial lens distortion in micrometers using only two lines

Lens No.	4m	2m	1m
1	12.5	13.8	15.1
2	13.4	14.0	15.8
3	13.4	13.4	15.3
Mean	13.1	13.7	15.4

Table 3.13 Mean values of lens distortion in micrometers using only two lines

distance, the two lines at the frame edges were extracted. The data used were again automatically processed. The results for the three cameras, three lenses and camera to object distances of 4, 2, and 1m are shown in Table 3.12. A summary of the results is presented in Table 3.13. The radial lens distortion graphs based on K_1 and only these two horizontal and

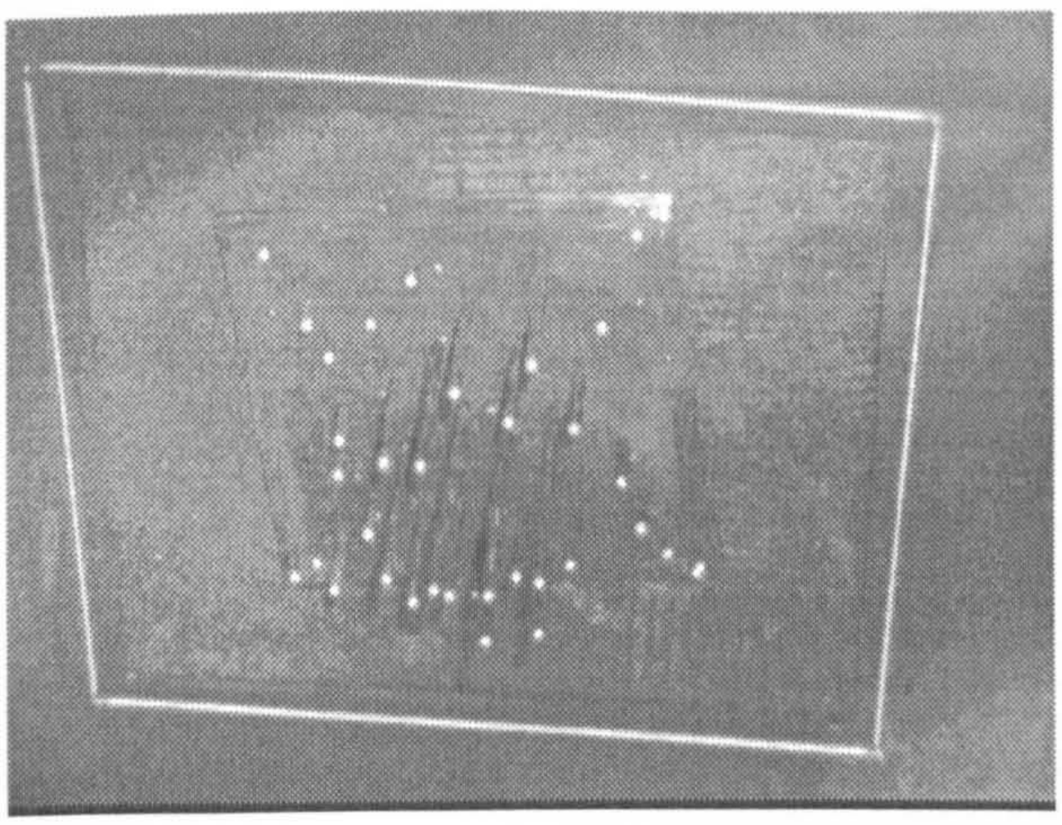

Figure 3.39 View of target test field and frame

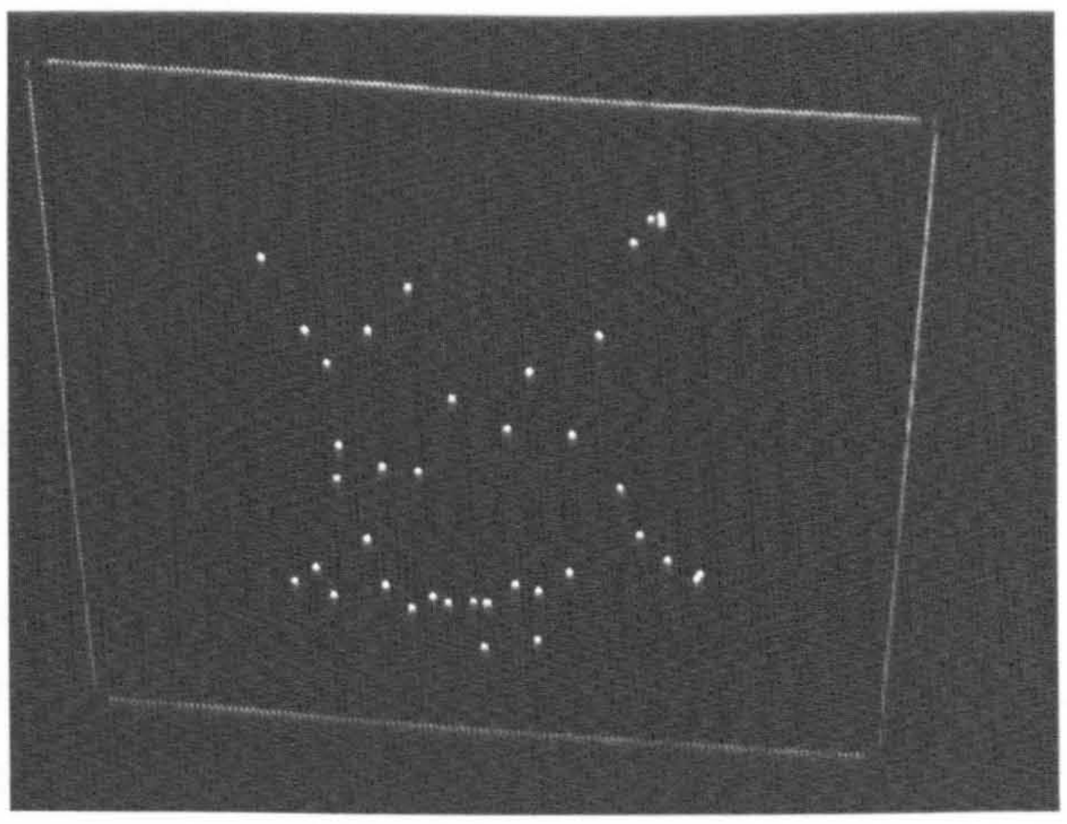

Figure 3.40 Image used to compute K_1 and bundle

two vertical lines are shown in Figure 3.38. Comparing the results with those of previous experiments, it can be seen that using two edge lines and only calculating K_1 the radial lens distortion results are comparable. Hence, the calculation of lens distortion can be simplified for most practical purposes. The advantage of this method is that the radial and decentering lens distortion can be simultaneously determined at the time of image capture. This is verified by a further experiment to investigate a quick calibration method. Figure 3.39 shows target test field and a rectangular calibration frame consisting of four lines, which can be approximately represented by two "vertical" lines and two "horizontal" lines. Figure 3.40 shows one of the images collected from different views. A number of images of the targeted test field and the calibration frame were taken. The frame line data were then extracted from the images and used in the plumbline program to estimate the K_1 parameter using the same method discussed above. The value of K_1 was 2.183×10^{-4}, similar to the results obtained before. The "on-site" calibration of lens radial and decentering distortion parameters can therefore be used to calibrate all the target image co-ordinates before placing them into the bundle adjustment procedure. To evaluate the effectiveness of ***a priori*** correction of lens distortion, two bundle adjustments were computed using the same image sets. In the first, the image co-ordinates were derived using the calibration values derived from the plumbline experiments. In the second adjustment experiment, no corrections were made. In both adjustments, self calibration was used to estimate the K_1 term. The values for K_1 produced were 2.258×10^{-5} and 2.098×10^{-4} respectively. Comparing the results to that using plumbline method for K_1 only with frame lines, the former has a small difference of 0.09×10^{-4} which is equivalent to only 0.2mm at a radial distance of 3mm, that is the maximum distance for almost all targets projected on the images. The former has a factor of 10 less than the second adjustment experiment, showing that the major systematic effect of radial lens distortion has been removed.

(iv) summary

The radial and decentering lens distortion parameters for three Fujinon 25mm lens fitted to three Pulnix TM-6CN CCD camera have been determined by the plumbline method. By analysing all these results, some conclusions can be obtained.

- all the radial distortion curves are fundamentally the same shape;
- at different object distances, the radial distortion curves appear correlated: the smaller the distance between the camera and object, the larger the radial distortion becomes. However, this change with distance is not large since even at the edge it amounts to only two and half microns;
- along the diagonal for 0 - 2mm the total distortion is less than 2 microns. At the edge of the lens, the distortion reaches about 15 microns;

- the first radial distortion parameter alone is sufficient to model radial distortion without significant error in some cases;
- compared with radial distortion, the distortion caused by the decentering distortion parameters P_1 and P_2 is much smaller. It amounts to just 10% of that caused by radial lens distortion. Therefore radial distortion plays the major role in geometric camera lens distortion;
- calculating K_1 by the plumbline method can be carried out using just two horizontal and two vertical lines attached to a lightweight frame without significant loss of accuracy;
- the use of a lightweight frame can allow the rapid calibration of the lens system on-site and on-line; and
- the accuracy using the plumbline method for calibration of lens distortion can be of the order of 1:40,000 of the object space.

3.3.2.3. Line-jitter

It is well known that one of the main geometric errors found in ordinary CCD cameras is line-jitter. The origin of line-jitter is the lack of a transmitted frequency reference between the camera and framegrabber so that a shift in the timing synchronisation (sync) takes place. A CCD camera is usually designed to comply with Vidicon camera standards which have both vertical and horizontal synchronisation (vsync and hsync) signals added to form a composite video signal (composite sync). In the framegrabber, the sync signal is separated from the composite video by a sync stripper. A Phase Locked Loop (PLL) circuit is used to generate the sampling clock frequency for the A-D converter in the framegrabber (pixel clock). The pixel clock, and stripped hsync and vsync signals are used to place the converted signal into

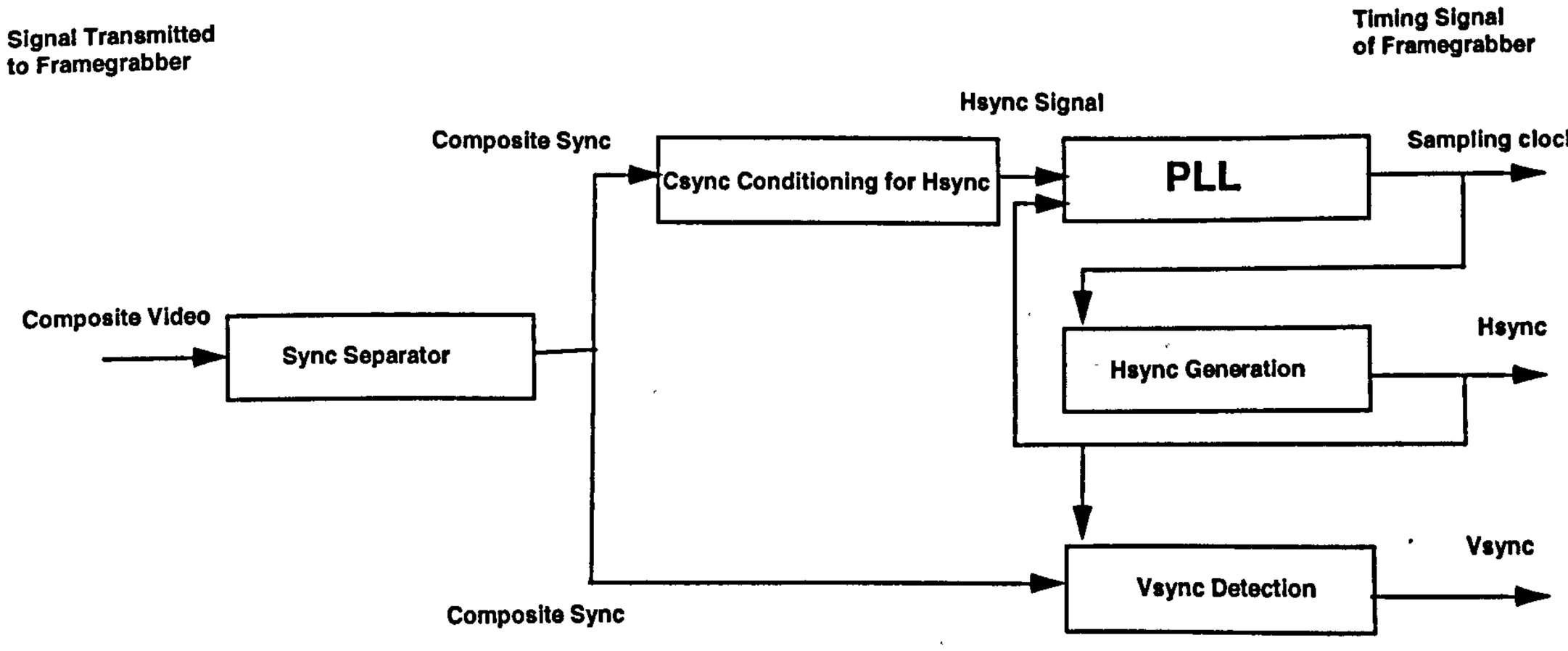

Figure 3.41 Synchronisation with composite video and PLL

framegrabber memory. This process is shown in Figure 3.41. The output of the analogue image intensity data from the CCD sensor is always at a fixed frequency 14.1815 MHz for the CCIR standard. The timing of the A-D conversion for each line always takes place at a given number of clock periods after the hsync signal is detected. Any variation of the position of the detection of the starting period gives rise to line-jitter. The result is an error in the x-direction but not in the y-direction. The problem of line-jitter has been analysed by Beyer, 1992. The nature of line-jitter is random. The error of line-jitter of many framegrabbers is between 1/4 to 1/8 of a pixel. The estimation of the effects of line-jitter have been studied by many researchers (Beyer, 1990; Raynor, 1991; Robson, 1993).

To analyse the influence of line-jitter for the combination of a Pulnix TM-6CN camera and an EPIX framegrabber, an experiment was conducted in which the test field shown in Figure 3.20 was again used. Lighting was optimised to provide even illumination across the test field, but with sufficient light to obtain optimum imaging conditions for automated subpixel location. An algorithm was written to continually grab the image and automatically locate the x and y subpixel co-ordinates. 2200 images were collected and the x, y co-ordinates saved. Figure 3.42 a) and b) shows the fluctuations occurring in the x and y directions respectively and Table 3.14 gives the RMS image co-ordinate residual standard deviation for all 2200 images. It can be seen that the difference of image shifts residuals between x and y direction is about 3 times and the contribution of line-jitter is about 0.1 pixel in this test.

There are several methods which can be used to correct line-jitter. One of the methods is the use of a pixel clock. As a one to one mapping of camera sensor output to analogue to digital converter sampling time. In this situation the camera and framegrabber are locked together so

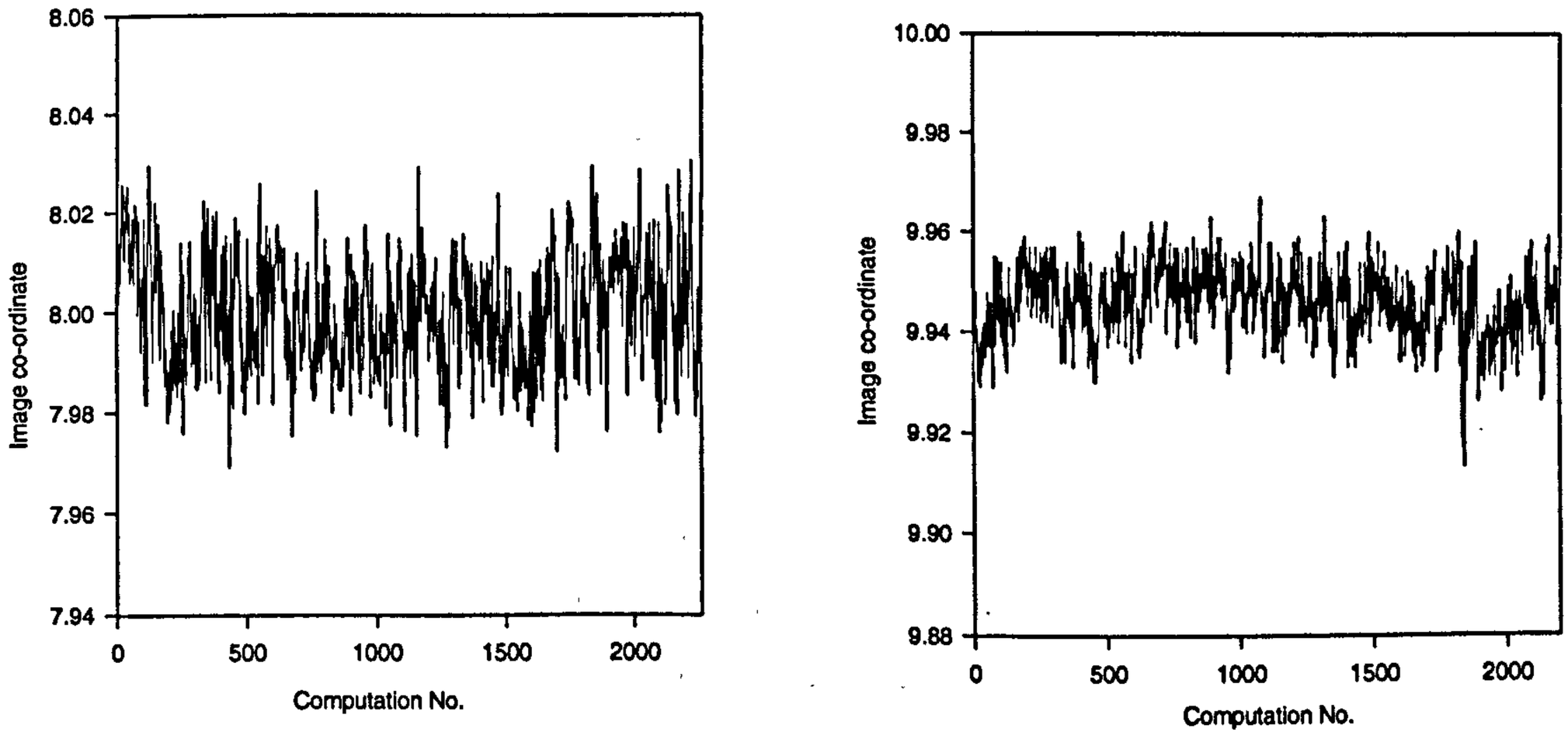

Figure 3.42 a) Subpixel errors in x direction b) Subpixel errors in y direction

RMS image shift (σ)	σx	σy
μm	0.147	0.055
pixels	1/58	1/151

Table 3.14 .RMS image co-ordinate residual standard deviation for all images

that no shift of timing synchronisation (sync) can take place. Even if there is a change in the clock rate of the camera, for instance due to the change of temperature, there will be no shift. However this method requires additional hardware between the camera and the framegrabber. Fortunately, the Pulnix TM-6CN camera provides a pixel clock output and the EPIX framegrabber, with modification, allows the use of the pixel clock and as well as horizontal and vertical sync signals. The only difficulty is that an additional electronic circuit is necessary to achieve operation and the pixel-clock has not been implemented during the research of the thesis. Another method to compensate for line-jitter is by resampling the image information and averaging over several frames. Because line-jitter is random and has zero mean, it can be reduced by this statistical method. The disadvantage is that extra computation is necessary, and the camera and object must be static during the imaging sequence.

3.4. Photogrammetric evaluation of complete photogrammetric system

The characteristics of the components necessary for a digital photogrammetric system have been analysed. To evaluate the combined performance of these components as an integrated system, a test field was constructed and a self calibration and a free net bundle adjustment were carried out. A number of experiments, which tested the three Pulnix TM-6CN cameras and three 25mm C-mount Fujinon lenses, were performed with this test object. The configuration of the test field is shown in Figure 3.43. The test field consisted of a wooden board and 74 circular retro-reflective targets. The wooden board was painted matt black and the retro-reflective were placed on it. Four additional targets were added at the corners of the base and some additional targets used to aid identification of the orientation of the test field.

A Pulnix TM-6CN camera was connected to the EPIX framegrabber and a 744x568 pixels image format was selected. The distance between the test field and the camera was approximately 1.6 metres. Lighting was placed behind the camera so that the retro reflective targets produced a high signal to noise ratio. Six images were collected from six different viewpoints located at four corners of the test field, and two looking straight down the z axis of the test field, one of which incorporated an additional ninety degree rotation. The target locations were computed from the six images using a subpixel location algorithm. Target

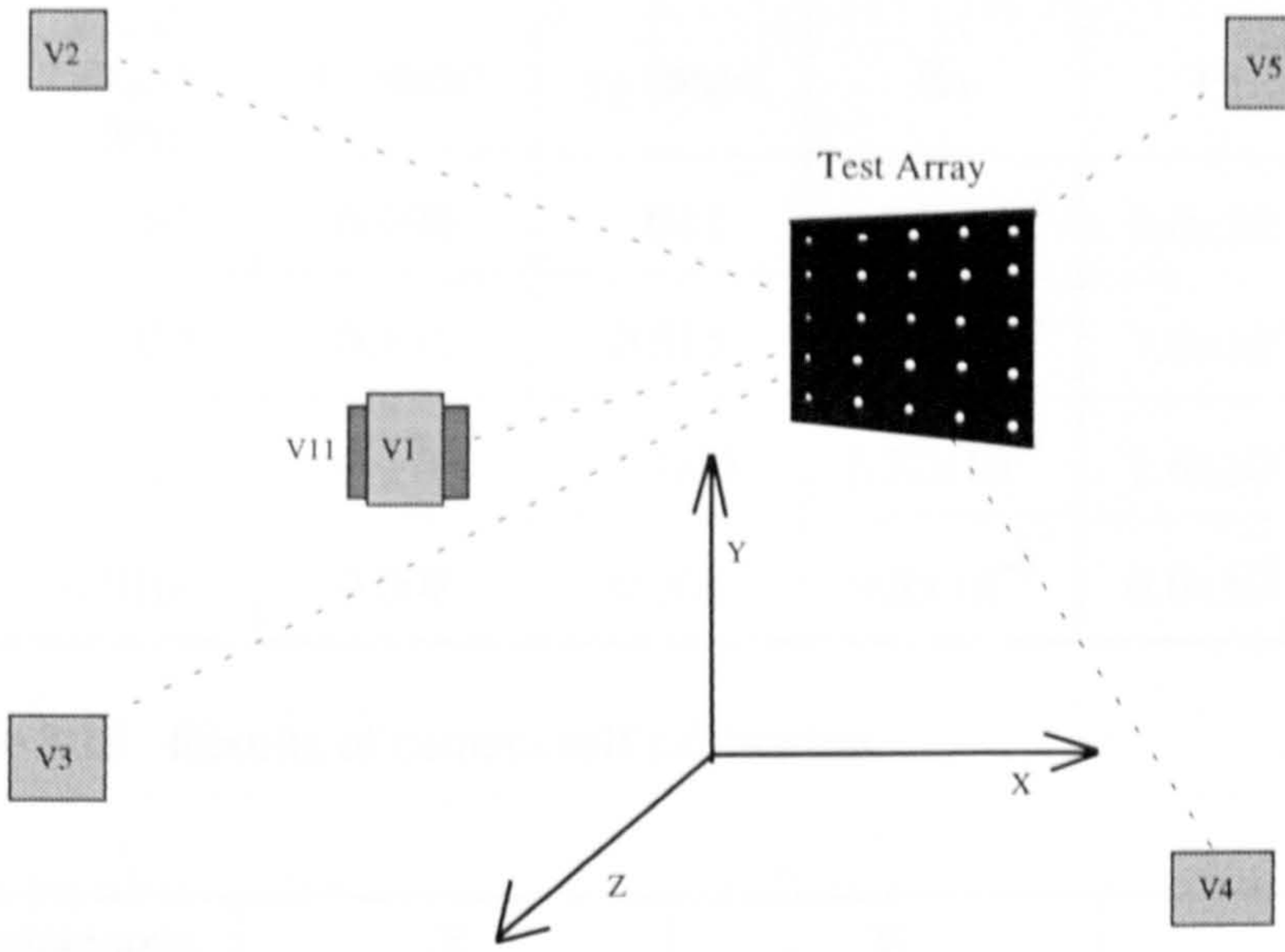

Figure 3.43 The configuration of the bundle adjustment

matching was then performed using the 3-D space intersection method. The location algorithm and the target matching method are discussed in the next chapter.

The steps in this process were as follows:

- a camera and lens was chosen from the three camera and lens sets;
- six images were collected from six positions;
- the camera exterior orientation was estimated using several control target points;
- the complete image preprocessing segmentation, target recognition, target subpixel location, and target labelling were performed;
- a bundle adjustment algorithm was then used to estimate the 3-D co-ordinates of the targets and to refine the position and orientation parameters of each camera (exterior orientation). In this step the interior orientation of the camera (focal length, principal point, K_1, P_1, and P_2) remained constant;
- the focal length was included as a parameter to be estimated in the bundle adjustment network;
- the principal offset point x_p, y_p was included as variable in the bundle adjustment network;
- parameters for radial distortion and decentering distortion were then included with an initial value of 0. The network was run as a free bundle adjustment in which the K_1, parameters of radial distortion and P_1 and P_2 parameters value of decentering distortion were determined.

By using the bundle adjustment program and the automated target matching procedure which is the major part of the thesis and derived in late chapters, the camera calibration and calculation of 3-D target co-ordinates was carried out following the steps discussed above. The camera interior parameters f, x_p, y_p, K_1, P_1, and P_2 of the three camera and lens were

Combination	Focal Length (mm)	x_p (mm)	y_p (mm)	K_1	P_1	P_2
Camera 1, Lens 1	25.107	0.096	-.041	1.63×10^{-4}	5.0×10^{-6}	4.1×10^{-6}
Camera 2, Lens 2	25.022	0.151	0.515	1.42×10^{-4}	7.0×10^{-6}	1.3×10^{-5}
Camera 3, Lens 3	25.011	0.176	-0.006	1.32×10^{-4}	1.6×10^{-5}	1.7×10^{-6}
Stand Deviation	0.010	0.008	0.008	9.8×10^{-6}	6.0×10^{-7}	7.0×10^{-7}

Table 3.15 Results of camera self calibration

Co-ordinate axis	X	Y	Z
Target RMS	0.0163mm	0.0210mm	0.0207mm
Image RMS	0.53μm(1/16pixel)	0.49μm(1/17pixel)	-

Table 3.16 System precision by using self calibration bundle adjustment

obtained from the results of the bundle adjustment. All the images in each set were used in the bundle adjustment so that a total of 895 equations and 264 variables gave rise to 631 degrees of freedom. Table 3.15 shows these results and the standard deviation of the three sets. Table 3.16 shows the RMS of target 3-D co-ordinates and image target 2D co-ordinates.

The results of the self calibrating bundle adjustment show that all the parameters for the principal point offset, radial and decentering lens distortion obtained from the integrated digital photogrammetric system are of the same order as those determined in the individual component tests. The object precision obtained from this test was of the order of 1:50000.

3.5. Summary

This chapter has discussed tests to evaluate the fundamental characteristics of components for a digital photogrammetric system.

Warm-up effects were investigated, and demonstrated that the framegrabber has a large influence compared to any warm-up effects in the cameras. A shift of up to four pixels was found in the x image direction of the EPIX framegrabber due to the mismatch of frequency between framegrabber and camera during warm-up. A 0.2 pixel shift was found to occur in the Pulnix TM-6CN camera during the warm-up period, possibly due to thermal expansion of the sensor. It is therefore recommend that the warm-up time for the CCD camera and the

grabber is at least one hour, since after that only 0.01 pixel shifts were observed.

An investigation into the location of the principal point demonstrates that there is a significant co-ordinate difference between the principal point and the center of chip array. Lens distortion calibration demonstrated that K_1 was the dominant factor for lens distortion in the Fujinon 25mm lenses. Using a frame test field is a feasible method to quickly estimate the lens distortion on line with similar accuracy to conventional off line calibration and self calibration methods.

As a result of the tests carried out in this chapter it is hoped that there is potential to increase the accuracy of the integrated digital photogrammetric system further, by reducing individual component errors, for example concentrating on the use of a pixel clock, averaging target co-ordinates, improving the target locating algorithms, and improving the bundle adjustment procedure. An automated procedure could also be obtained by solving the problem of initially estimating the camera orientation and performing image target matching automatically. This will be described in later chapters.

Chapter 4 Automatic 3-D object measurement

4.1. Introduction

A system based on digital photogrammetry combined with machine vision has great potential for industrial measurement, inspection and quality control. The systems that need developing will be operated not only by photogrammetrists, but also by engineers, or other non-expert users who can be expected to have no knowledge of photogrammetry. Therefore, automation of as many tasks as possible is essential in these systems.

The automatic determination of camera exterior orientation is one of the fundamental tasks in a machine vision system, a robot system, or a digital photogrammetric system. In the first section of this chapter, the techniques and methods of automatically estimating camera orientation parameters, i.e. both rotation and position parameters, are discussed. In particular the general solution of a closed form space resection is considered because this can lead to an algorithm for automatic estimation of camera orientation parameters. Two implementations of the closed form space resection are examined. The first method is an automatic frame extraction method, in which a three line frame is used for an automatic and rapid extraction of the orientation parameters. Implementation of the method by using machine vision techniques, such as line thinning, line tracing, and least squares line fitting, are described. The second method uses an automatic laser spot extraction method. This method uses several (typically four) lasers which can be controlled by computer to be on or off so that the identification of each target image is easy to compute. The two methods are further discussed within the context of a multiple camera digital photogrammetric measurement system. Several practical experiments are performed and evaluation of each method is made. The potential for measurement automation using this algorithm is also discussed.

In digital photogrammetry difficulties are often experienced when automatically matching features from multiple camera views. This is particularly true where the features are geometrically and radiometrically similar such as occurs with retro-reflective targets which may have no distinguishing features. The correspondence of several control targets can be established by several methods, such as an automatic frame extraction method or an automatic laser spot extraction method. However it is not possible to match the number and density of targets often required for 3-D measurement by these special methods.

The traditional epipolar line method is founded on the intersection of straight lines in the image plane and can solve correspondences between targets. However, for success the method requires accurate camera orientation parameters. In this chapter an alternative target matching

technique to the epipolar line method is developed based on the initial estimations of the camera orientations. This method, which is combined with a bundle adjustment process, is based on a 3-D intersection and an "epipolar plane", as opposed to the 2-D intersection of the epipolar line method. The theory of the approach is described and discussed. Comparisons are made between the established epipolar line method and the derived 3-D matching method. Some results from both simulation and practical testing are given and critical evaluation is made of the techniques.

4.2. Automatic estimation of camera orientation

4.2.1. Overview of methods for estimation of camera orientation

At the same time as the development of automated industrial inspection, digital photogrammetric measurement systems have emerged as a subject area on their own. Many digital photogrammetric measurement operations, such as target matching, tracking, high accuracy measurement, industrial part inspection, and so on, are based on the prior estimation of the camera orientation and location in 3-D space. However, obtaining initial camera orientation estimation is a major problem. This is especially true if an automated digital photogrammetric measuring system is to be built.

In the Cartesian co-ordinate system, the position of a camera is represented by six spatial degrees of freedom (three for translation and three for rotation). The task of camera orientation estimation is to calculate these parameters so that the co-ordinates of a target in 3-D space can be transformed into the image plane of a camera based on these parameters. There are four decomposed co-ordinate systems which complete the transformation of a target from the co-ordinate system of a 3-D object to the co-ordinate system of a 2-D image plane (Haralick, 1993). These co-ordinate systems are called object frame, camera frame, image frame, and image plane respectively as shown in Figure 4.1. These four co-ordinate systems are connected by co-ordinate transform matrices. To determine these transformation matrices it is necessary to start by matching corresponding features between image plane and object frame. A correct calculation of the relationship cannot be obtained if there are not enough corresponding features between the image and object.

The implementation of the object to image plane transformation requires low level computer vision for identification of target images. Furthermore, a knowledge of perspective geometry, co-ordinate transformations, vector space geometry, and some artificial intelligence strategies for searching, matching and space resection are required for the transformation. There are many existing techniques to solve the camera orientation problem. Several commonly used

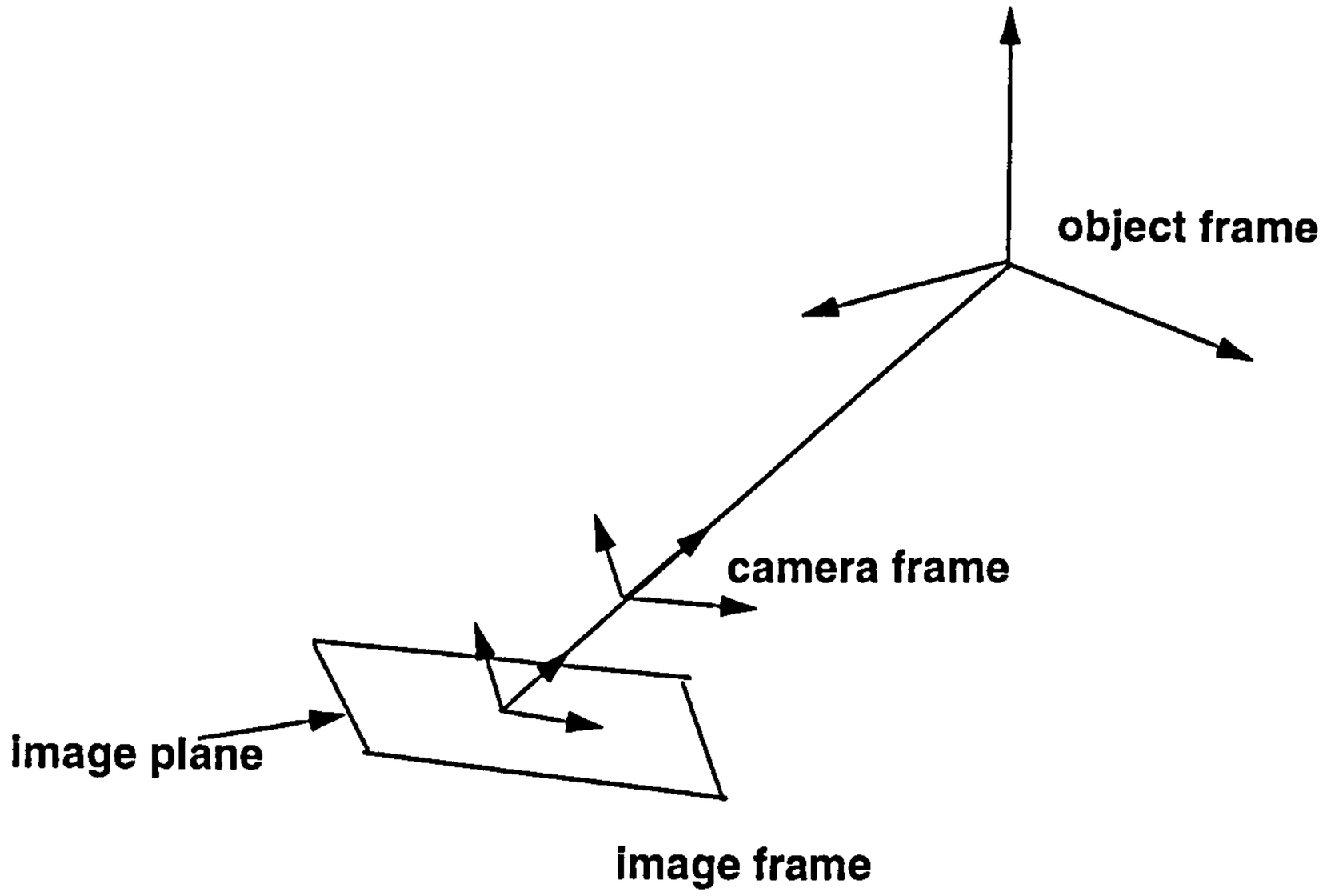

Figure 4.1 Perspective transformation

techniques are: **i)** perspective transformation method; **ii)** a non-linear optimisation method; **iii)** vector calculation of geometric constraints method.

4.2.1.1. Perspective transformation method

There are several common methods for projecting 3-D objects onto a 2-D image plane. All points on an object can be projected into the image plane along lines which converge to a position called the center of projection. This method is called perspective projection. Some researchers have shown that a human' eye model for 3-D viewing is similar to the perspective projection. Therefore, the method which has been developed by computer vision experts is the perspective projection model.

A target in the object frame will form a 2-D target image in camera image plane. The basic projection geometry is shown in Figure 4.1 and the relationship between co-ordinate systems is expressed in Equation (4.1).

$$\begin{bmatrix} 1 & 0 & 0 & 0 \\ 0 & 1 & 0 & 0 \\ 0 & 0 & 1/c & 1 \end{bmatrix} \begin{bmatrix} 1 & 0 & 0 & 0 \\ 0 & 1 & 0 & 0 \\ 0 & 0 & 1 & -c \\ 0 & 0 & 0 & 1 \end{bmatrix} \begin{bmatrix} r_{11} & r_{12} & r_{13} & 0 \\ r_{21} & r_{22} & r_{23} & 0 \\ r_{31} & r_{32} & r_{33} & 0 \\ 0 & 0 & 0 & 1 \end{bmatrix} \begin{bmatrix} 1 & 0 & 0 & -X0 \\ 0 & 1 & 0 & -Y0 \\ 0 & 0 & 1 & -Z0 \\ 0 & 0 & 0 & 1 \end{bmatrix} \begin{bmatrix} X \\ Y \\ Z \\ 1 \end{bmatrix} = \begin{bmatrix} x^* \\ y^* \\ t^* \end{bmatrix} \qquad (4.1)$$

where

r_{11} - r_{33}: are 3 x 3 orthonormal rotation matrix,

X, Y, Z : object space co-ordinate,

Xo, Yo, Zo: projection center position,

c: camera constant, and

x*, y*, t*: co-ordinates of image frame.

Equation (4.1) can be rewritten as:

$$\mathbf{T_p \bullet T_2 \bullet T_r \bullet T_1 \bullet X = x^*} \tag{4.2}$$

The image co-ordinates in the image plane are defined as:

$$\begin{bmatrix} x \\ y \end{bmatrix} = \begin{bmatrix} x^*/t^* \\ y^*/t^* \end{bmatrix} \tag{4.3}$$

where x and y are the co-ordinates of points in the image plane.

The sequence of operations to transform a point in the object frame to a point in the image plane is as follows: The original co-ordinates of a 3-D point in the object frame are transformed to the center of perspective projection by $\mathbf{T_1}$. They are then transformed to the camera frame by rotation matrix $\mathbf{T_r}$. The co-ordinates of the points in the camera frame are transformed to the image frame by matrix $\mathbf{T_2}$. The target co-ordinates of the point in the image frame are obtained by Tp. The x, y co-ordinates of the point in the image plane are finally obtained by equation (4.3).

Although the equations characterising the transformation from the 3-D object co-ordinate system to the 2-D image co-ordinate system are non-linear functions of the exterior parameters, they are linear if the coefficients of the 3 x 4 perspective transformation matrix are regarded as unknown parameters. Given that the 3-D object co-ordinates of a number of targets and the corresponding 2-D image target co-ordinates are known, the coefficients in the perspective transformation matrix of linear equations can be calculated. Thence the camera model parameters can be computed. The main advantage of this method is that it is a linear equation solution and no non-linear optimisation is needed. The main disadvantage of this method is that lens distortion cannot be considered. Sometimes lens distortion is unacceptably large when performing 3-D measurement (Luh and Klassen, 1985) and so this method will be unacceptable. The method of obtaining this transformation has been widely used in computer vision especially for robot vision where subpixel precision is not necessary (Haralick, 1980, 1993; Karara, 1979; and Ayache, 1991).

4.2.1.2. A non-linear optimisation method

The perspective transformation method discussed in the previous section is efficient when the

camera lens distortions are ignored and non-linearity is overcome by regarding the coefficients of the 3 x 4 perspective transformation matrix as unknown parameters. However, there are some cases in which the camera lens distortion has to be estimated and so some alternative approaches are required. The use of non-linear optimisation methods is a common situation. Non-linear optimisation is an iterative technique and is considered an efficient method to deal with the estimating transformation by minimisation techniques.

A popular example is the Direct Linear Transformation (DLT) method developed by Abdel-Aziz and Karara (1971). The DLT method was originally developed to solve linear equations. However, it was later found that unless lens distortion is ignored, a nonlinear search is needed. In the handbook of non-topographic photogrammetry, Karara, 1979, commented on the DLT method: "**When originally presented in 1971 (Abdel-Aziz and Karara, 1971), the DLT basic equations did not involve any image refinement parameters, and represented an actual linear transformation between comparator co-ordinates and object-space co-ordinates. When the DLT mathematical model was later expanded to encompass image refinement parameters, the title DLT was retained unchanged**". The derivation of the DLT begins with the collinearity equation. After algebraic manipulation of equation (2.6), the following equations are obtained:

$$\frac{L_1X+L_2Y+L_3Z+L_4}{L_9X+L_{10}Y+L_{11}Z+L} = x - x_{lens} \qquad (4.4\ a)$$

$$\frac{L_5X+L_6Y+L_7Z+L_8}{L_9X+L_{10}Y+L_{11}Z+L} = y - y_{lens} \qquad (4.4\ b)$$

where

$$L_1 = (x_p m_{31} - c m_{11}) / L$$
$$L_2 = (x_p m_{32} - c m_{12}) / L$$
$$L_3 = (x_p m_{33} - c m_{13}) / L$$
$$L_4 = x_p + c\,(m_{11}Xc + m_{12}Yc + m_{13}Zc) / L$$
$$L_5 = (y_p m_{31} - c m_{21}) / L$$
$$L_6 = (y_p m_{32} - c m_{22}) / L$$
$$L_7 = (y_p m_{33} - c m_{23}) / L \qquad (4.5)$$
$$L_8 = y_p + c\,(m_{21}Xc + m_{22}Yc + m_{23}Zc) / L$$
$$L_9 = m_{31} / L$$
$$L_{10} = m_{32} / L$$
$$L_{11} = m_{33} / L$$
$$L = -\,(m_{21}Xc + m_{22}Yc + m_{23}Zc)$$

There are two possible ways of using the DLT method(Wong, 1975). The first performs a direct solution, and the second uses non-linear optimisation.

(i) Direct solution

The direct solution procedure uses the approximation that all the object space point co-ordinates are known and are assumed to be without error. If the first radial lens distortion term is used, the equations for this method can be written as (Mcglone, 1989):

$$L_1X + L_2Y + L_3Z + L_4 - xXL_9 - xYL_{10} - xZL_{11} - (x - x_p)K_1r^2A - x = v_x \qquad (4.6_a)$$

$$L_5X + L_6Y + L_7Z + L_8 - yXL_9 - yYL_{10} - yZL_{11} - (y - y_p)K_1r^2A - y = v_y \qquad (4.6_b)$$

where

$$A = L_9X + L_{10}Y + L_{11}Z + 1$$

The equations can be solved directly for the DLT parameters by a linear least squares technique. Although the solution is only an approximation, it is still widely used by the computer vision community for quickly acquiring an estimation of the camera orientation.

(ii) Iterative solution

For the consideration of precision, the DLT equations are linearized with respect to the parameters, and the solution is obtained by least squares in an iterative manner. Let the v_x and v_y represent the residuals for the equations. Each iteration will compute corrections to the estimated parameters which are converging to the true values during the iterations. In this situation, equation (4.6) is rewritten as:

$$v_x - L_1X / A - L_2Y / A - L_3Z / A - L_4 / A + xXL_9 / A + xYL_{10} / A + xZL_{11} / A + (x - x_p)K_1r^2 + x / A = 0 \qquad (4.7_a)$$

$$v_y - L_5X / A - L_6Y / A - L_7Z / A - L_8 / A + yXL_9 / A + yYL_{10} / A + yZL_{11} / A + (y - y_p)K_1r^2 + y / A = 0 \qquad (4.7_b)$$

Since equations (4.7) are non-linear, a linearized equation can be obtained by applying Newton's method and, subsequently, a least squares iterative procedure is followed to optimally estimate the unknown parameters. The main advantages of the method are: a calibrated camera is not needed and the camera interior parameters can be solved at the same time of calculating the exterior parameters. The main disadvantages are: a good initial estimation to start the first iteration is necessary.

4.2.1.3. Geometric vector method

The two methods of estimation of camera orientation parameters discussed previously are based on least squares techniques. The second method is an iterative procedure. In this section, a solution is discussed based on a closed form space resection. This method was originally derived by Fischler, 1980, to provide a basis for an automatic camera orientation solution algorithm. This method was improved by Zeng, 1992, who gave a general solution of closed form space resection for four object control targets. This method can be divided into two steps: i) the calculation of the camera location parameters; and ii) the calculation of the camera rotation parameters.

i) Calculating the camera location parameters

Suppose there are three control targets on the surface of an object and the correspondence between them and the target images in image plane is known (Figure 4.2). Let x_i, y_i, be the

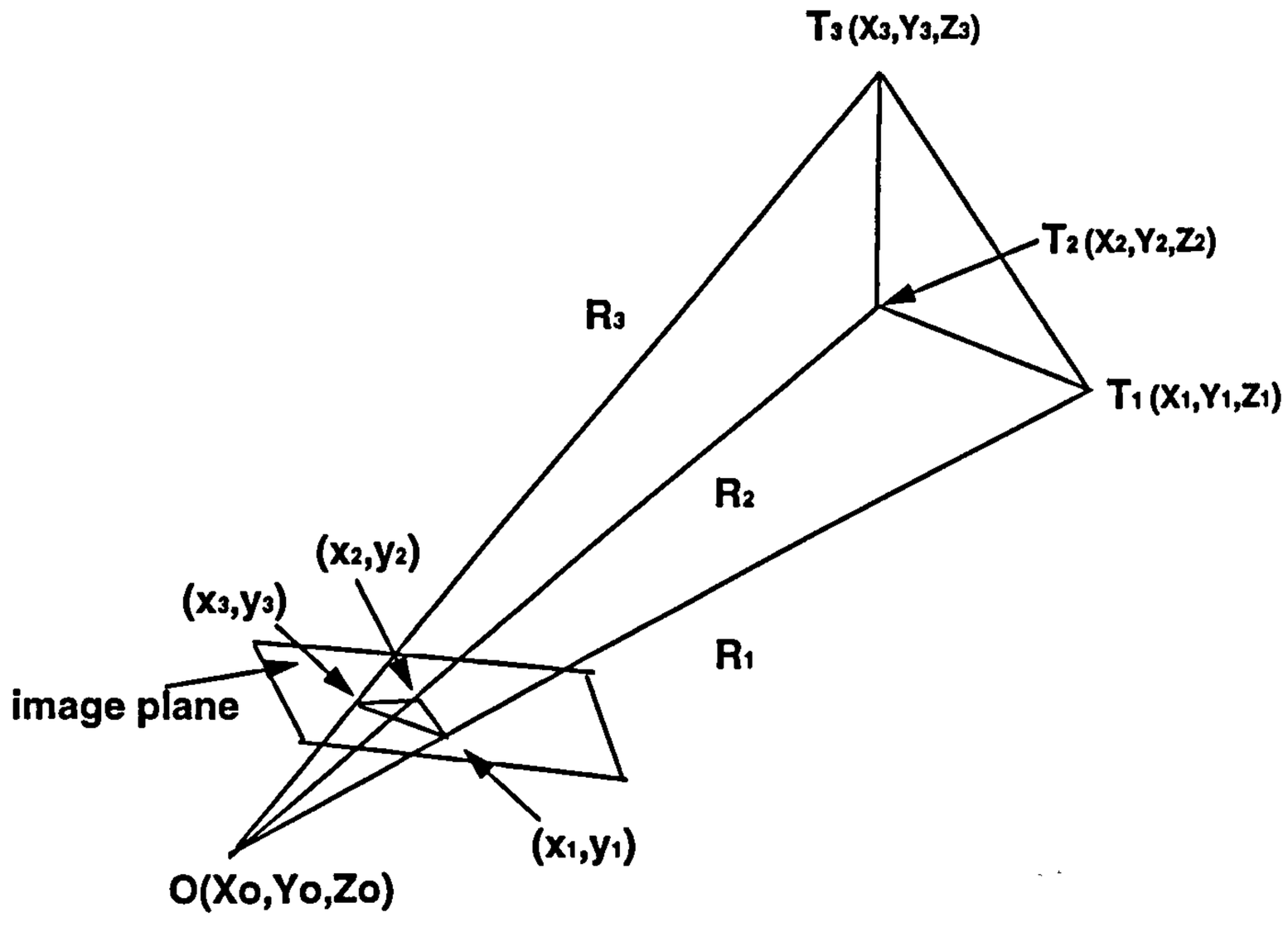

Figure 4.2 The geometry of camera location

image co-ordinates; c the camera constant; Xi, Yi, Zi the co-ordinates of object control targets; X_o, Y_o, Z_o the co-ordinates of camera location; and R_1, R_2, R_3 the distances between the camera location point and the object control targets respectively. Therefore, an equation can be written:

$$\begin{aligned}(X_1 - X_o)^2 + (Y_1 - Y_o)^2 + (Z_1 - Z_o)^2 &= R_1^2 \\ (X_2 - X_o)^2 + (Y_2 - Y_o)^2 + (Z_2 - Z_o)^2 &= R_2^2 \\ (X_3 - X_o)^2 + (Y_3 - Y_o)^2 + (Z_3 - Z_o)^2 &= R_3^2\end{aligned} \qquad (4.8)$$

The values of R_1, R_2, and R_3 can be obtained by solving a quadratic equation derived by the geometry constraints for x_i, y_i, c, Xi, Yi, Zi, (Zeng, 1992). The camera location parameter X_o, Y_o, and Z_o can be calculated by equation 4.8. Two solutions for X_o, Y_o, and Z_o are obtained from the equation. A fourth object control target can be used to obtain another two solutions. The solution for the camera location parameter values will be the solution which is the same between the two sets.

ii) Calculating the camera rotational parameters

Following the camera location computation the camera rotational parameters are calculated. The rotational matrix is often constructed with algebraic parameters to overcome the singularity problem when computing the trigonometric functions (Thompson, 1959). Hinsken, 1988, derived a complete set of formulae as following:

$$R = \begin{bmatrix} d^2+a^2-b^2-c^2 & 2(ab+cd) & 2(ac-bd) \\ 2(ab-cd) & d^2-a^2+b^2-c^2 & 2(bc+ad) \\ 2(ac+bd) & 2(bc-ad) & d^2-a^2-b^2+c^2 \end{bmatrix} \tag{4.9}$$

where $a^2 + b^2 + c^2 + d^2 = 1$ (4.10)

The physical meaning of a, b, and c is shown in Figure 4.3.

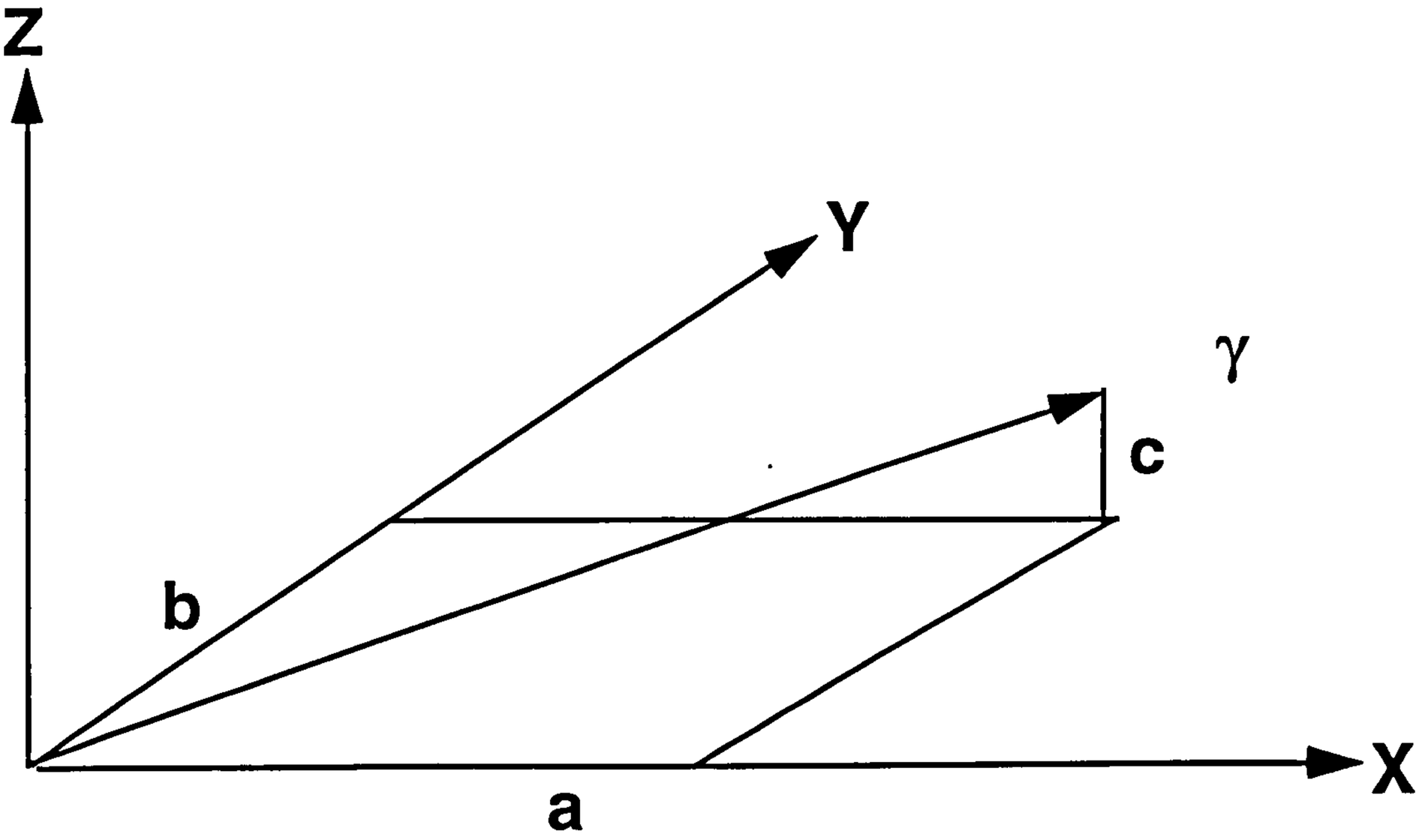

Figure 4.3 The physical meaning of a, b, c

If M is defined as:

$$M = [a\ b\ c\ ]^{T}$$

Then,

$$RM = M \tag{4.11}$$

From this equation, it can be seen that the M remains unchanged after transforming M by R. After the transformation of R is performed, the co-ordinate system is rotated by an angle γ around vector M (the rotation axis), and this can be expressed as

$$|M| = L_m = \sqrt{a^2 + b^2 + c^2} = \sqrt{1 - d^2} = \sqrt{(1 - \cos\gamma)/2} \tag{4.12}$$

The rotation angle γ is directly related to the rotation parameter d. The direction vectors of the rotation axis (p,q,r) can be obtained from two pairs of object and image targets so that a, b, and c can be calculated from the following equations:

$$a = p\sqrt{(1 - d^2)/(p^2 + q^2 + r^2)}$$

$$b = q\sqrt{(1 - d^2)/(p^2 + q^2 + r^2)} \tag{4.13}$$

$$c = r\sqrt{(1 - d^2)/(p^2 + q^2 + r^2)}$$

Using the geometric vector method can give rise to a number of equations which are used to estimate the camera orientation parameters. No nonlinear search and iteration is needed. However, this method will not work under certain condition such as when a fourth object control target lies on the so called critical surface (Zheng, 1992), in this case no unique solution can be obtained. Zheng also indicated that any targets lying on this critical surface will allow two solutions so that an infinite number of target locations are able to satisfy the two solutions. Therefore the conclusion presented by Fischler, 1980, who suggested that six targets in arbitrary positions will always produce an unique solution, is overturned. However, four coplanar object control targets can provide a unique solution, Such a method has been used in the experiments for this thesis without problem.

4.2.1.4. Comparison of the methods

Although there are many alterative methods of finding camera orientation parameters, such as the two stage method (Tsai, 1987), the two plane method (Isaguirre and Summers, 1985), the 3 x 3 matrix extraction method (Melen, 1993), the three methods described have been widely used in both the computer vision and photogrammetric communities. The relative advantages

of each of these methods are difficult to quantify because they are dependent on the application. The choice of method for a particular task will depend on the features of the methods. Table 4.1 gives a general comparison of the methods.

Characteristic	Method 1	Method 2	Method 3
Requiring control target number	>=6	>=6	4
Computing cost	low	high	low
Precision	med.	high	med.
Expertise	low	high	low
Reliability	high	med.	med.
Requiring starting values	No	Yes	No
Subject restriction	No	No	plane

Table 4.1 Relative merits of the three methods

In the three methods discussed previously, the correspondence between the object targets in 3-D space and the imaged targets in the image plane is assumed to have been established so that the methods can be directly used to estimate the camera orientation parameters. However, in an automated system, the correspondence must be automatically obtained. In another words, for automatic estimation of camera orientation parameters, it is necessary to recognise the targets in the image and determine their identification automatically. Two implementations are presented for automatic estimation of camera orientation and target 3-D co-ordinates and are discussed in following sections. They are: i) an automatic frame extraction method; and ii) an automatic laser spot extraction method.

4.2.2. Implementation by an automatic three sided rectangle method

It is a difficult task to automatically find the correspondence between a target placed on an object and its imaged position. At least four targets and their corresponding target images are required to estimate the camera orientation parameters with the geometric vector method. The four targets could be projected to any position in the image plane depending on both the spatial orientation of the camera and the spatial positions of the four targets. An interactive method has been traditionally used to identify the correspondence between targets and their target images. If an automatic procedure to identify the correspondence is required, it is necessary to have unique features for each of the targets to enable identification. In this thesis two methods are investigated to implement an automatic procedure. The first is an automatic three rectangle extraction method, and the second uses laser diode collimators.

4.2.2.1. The building of the test frame

As discussed in the beginning of this chapter, each object target must be properly distinguished in an automatic system. Feature extraction by image processing methods is a very powerful tool. A simple test field was constructed with the aim of using image processing techniques to extract unique feature points. A three side rectangle was constructed using three lines of a size suitable to frame the object to be measured. The three sided rectangle test field is shown in Figure 4.4. A three side rectangle provides four unique features, the two intersection points and two the termination points, labelled 100, 101, 102, 103 in Figure 4.4. If the 3-D co-ordinates of the four points are known, and the corresponding

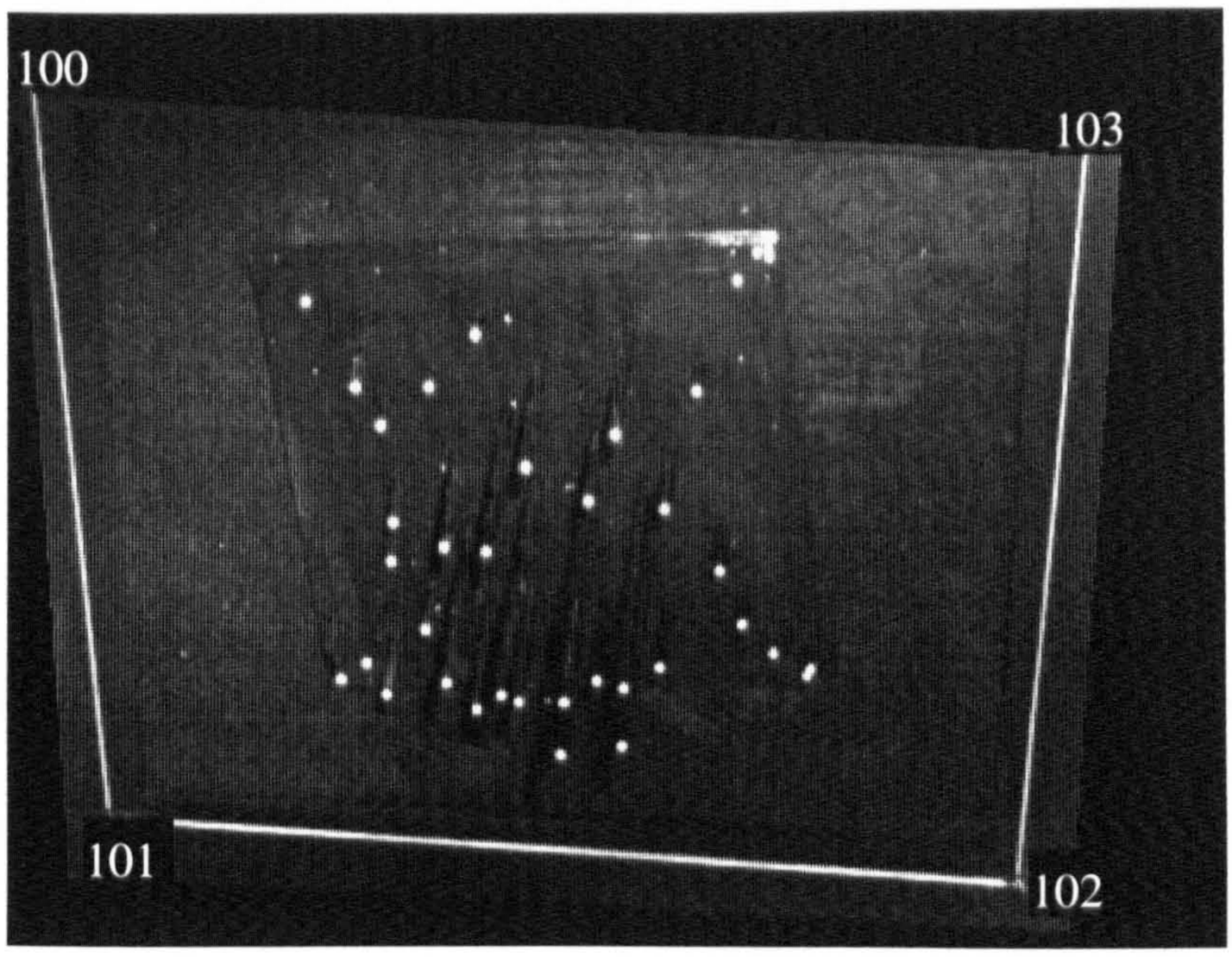

Figure 4.4 The three side rectangle for orientation

image co-ordinates are known, the camera orientation parameters can be estimated by the geometric vector method discussed in the previous section. The task of detecting and extracting the four image points and finding their corresponding object locations is now discussed. The sequence of operations is as follows: **i**) the detection and extraction of line segments; **ii**) the fitting and merging of line segments; and **iii**) the determination of the co-ordinates of the intersection and termination points.

4.2.2.2. Segmentation and extraction of line segments

The first step is the segmentation of the rectangle sides. The method for the segmentation used in this application is a single level method, because in addition to the line other features such as targets should be extracted at the same time. The local image normalisation method discussed in chapter 2.4.1 may be used if the grey levels of the background of the object are

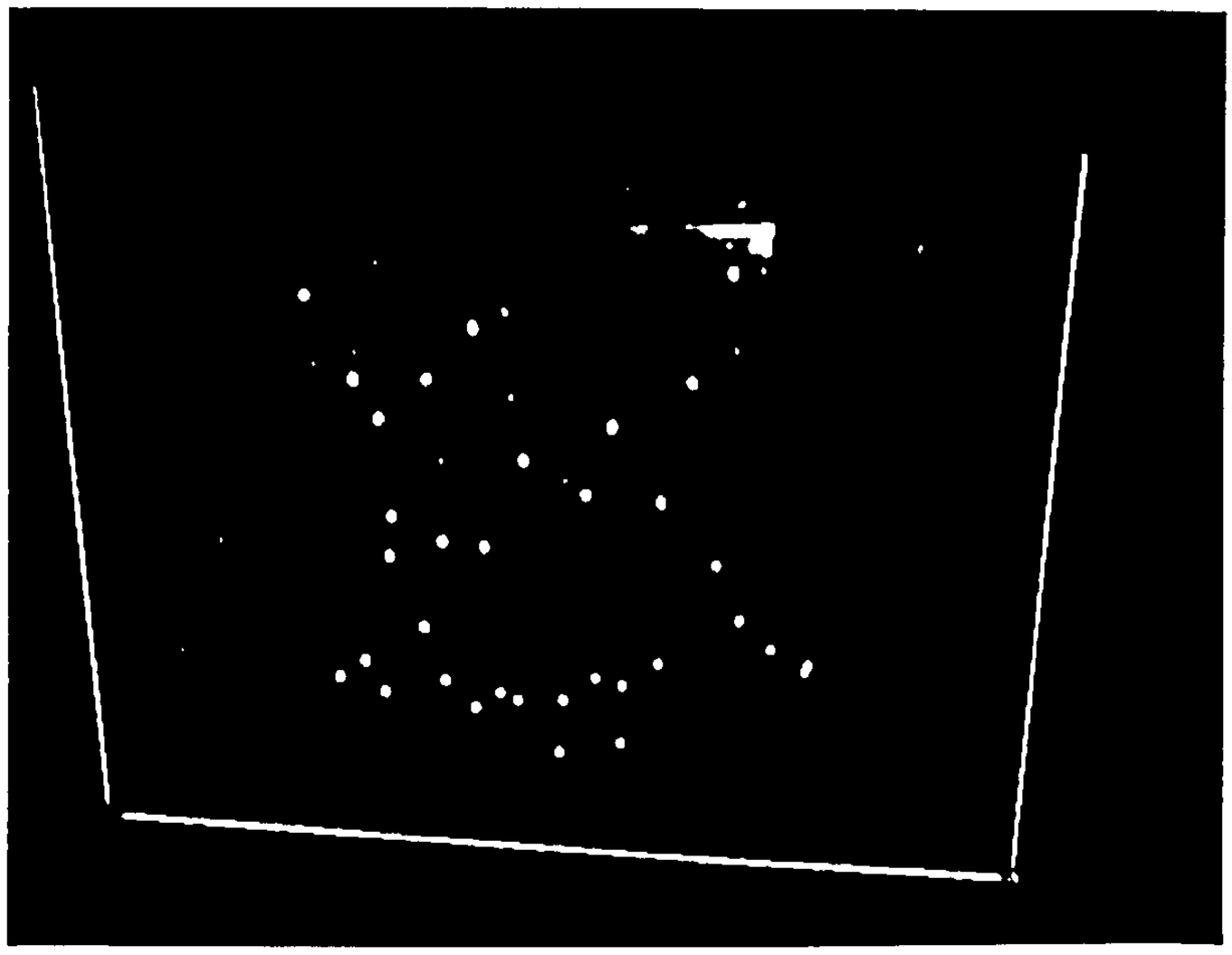

Figure 4.5 The result of segmenting the frame in test field

not constant over the whole image. Figure 4.5 shows the result of segmentation. The next step is the extraction and isolation of the rectangle sides. The rectangle sides have a variable width and so an extension of the Pavlidis thinning method, (Pavlidis, 1982), which is more efficient for the extraction of line segments is used.

Thinning algorithms have been widely studied by those in image processing and pattern recognition because they offer a way of simplifying image features. In the case of the rectangle sides, thinning is required in order to change the segmented line structure from a variable width to a single skeleton line so that a line can be fitted to the data and the parameters of the line extracted. The steps for this algorithm are as follows: A binary image is created by setting all pixels which are above a threshold to 1, and all other pixels to 0. Following the segmentation process the geometric relationships between the remaining pixels are analysed. A procedure is used whereby the neighbours of each pixel are checked according to pattern defined in Figures 4.6a and b. This results of these tests will be that either

	A	A	A			A	A	A	
	0	P	0			A	P	0	
	B	B	B			A	0	2	

A	A	C
0	P	2
B	B	C

Figure 4.6 a) Pattern one b) Pattern two

a pixel is marked as skeletal = 2, or discardable = 3. The marking of pixels with a 2 or 3 is necessary while the algorithm loops. Any pixels marked with a three are deleted after each loop. Four loops are required to thin the line by one pixel. Many loops are required to obtain the final one pixel wide skeleton. A full description of this method may be obtained from Pavlidis, 1982.

Two modifications of the Pavlidis's thinning algorithm have been carried out to reduce the necessary computation: **i)** using a status variable to represent the deletable pixels in each loop; and **ii)** using a stack technique to store the high intensity pixels.

i) The use of a status variable

A problem with the standard thinning algorithm is that in each loop only one of the four neighbours of a pixel is checked to decide whether it is part of the skeleton or an unwanted pixel. Furthermore, the whole image must be checked twice to guarantee a correct result. The first check is performed on the whole image to judge whether pixels are skeletal or unwanted at which time the pixels are marked by setting them to 2 for a skeletal pixel and 3 for unwanted. The second check keeps the skeletal pixels and deletes all the unwanted pixels. This process is repeated until a final result is obtained. The algorithm, although reliable, is not efficient. A modification to the algorithm has been written whereby a status variable D is defined to store the unwanted pixel information. The method works as follows: Assume that image pixels are 255 and background 0. The initial value of D is set to one. For each loop D is increased by one. The use of the patterns in Figure 4.6a) and b) is modified: **(1)** For Figure 4.6a), at least one of each group of pixels marked with A and B must be not less than D. **(2)** For Figure 4.6b), at least one of the pixels marked C must be not less than D; if both pixels labelled C are not less than D, then the value of the pixels labelled A and B can be any value, otherwise at least one of the members of each pair marked A or B must be not less than D. After finding all the skeletal pixels, all pixels less than D are finally deleted. This method can save half of the computation time.

ii) The use of a stack technique

In the image the number of pixels lying on the three sides of the rectangle (object pixels) is far less than those in the background typically 1 - 5%. For example, in Figure 4.5, the number of pixels representing the object (three line rectangle, targets, and some noise) are only 5023 comparing with 433152 in total for the 752 x 576 image. If during each loop all of the image is checked, a lot of time is spent performing the background checking. To improve efficiency a stack technique is used. First, the whole image is scanned and all the co-ordinates of object pixels are pushed onto a stack, which is represented by an array. Second, each pixel is popped

from the stack in sequence where it is matched with the patterns in Figure 4.6a) and b) and the status variable D. The remaining pixels are put back onto the stack. The process continues until the final result is obtained. Consequently, the whole process involves only object pixels and the number is decreased by each loop so that a considerable number of "empty operations" are saved. Figure 4.7 illustrates the final result of the thinning algorithm.

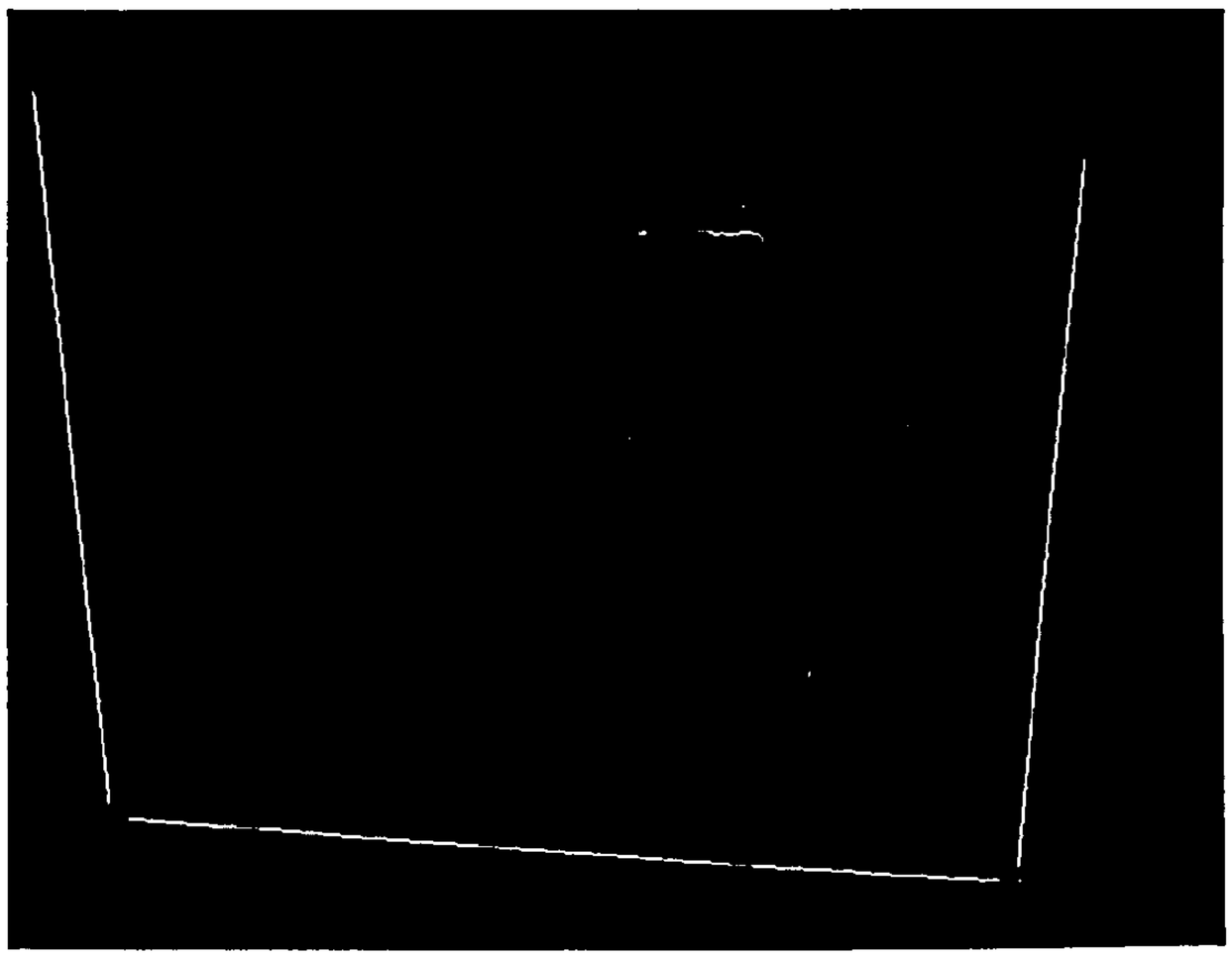

Figure 4.7 The result of thinning the image in Figure 4.5

4.2.2.3. Recognition, merge, and fit of line segments

The recognition of line segments is simple because all the segments are expressed by skeletal lines. A program was written to trace along the skeletal line. The trace begins at a termination point of a line, that is a pixel which only has one pixel in its eight neighbouring positions. The co-ordinates of each pixel are traced and the number of line segments recorded. Any line whose length is above a threshold (normally larger than 30 pixels) is taken as a legitimate segment. A least squares technique is used to fit a straight line to the line segments using the recorded co-ordinates of each segment so that a line equation can be obtained. The next process is to merge the straight line segments because each line of the three sided rectangle may be incomplete due to occlusion. This is a simple task as broken line segments forming from the same line have nearly equal coefficients (slope and intercept). After merging the lines, a least squares method is applied to the segments and obtain equations of the sides of the three sided rectangle.

4.2.2.4. Determination of the co-ordinates of the intersection and termination points

The properties of the three rectangle sides have to be determined after their equations have been obtained. Two rectangle sides are approximately parallel and this feature can be used to

distinguish the two rectangle sides from the third side. The co-ordinates of the two intersection points between the two parallel rectangle sides and the third side can then be calculated by solving two groups of equations, the solutions are the co-ordinates of the intersection points labelled as 101' (x_1, y_1) and 102' (x_2, y_2). The co-ordinates of the two termination points can be obtained by calculating the distances between the two terminations of each parallel rectangle side to the intersection point with the third side. The points with the larger distance are the termination points. The two termination points are labelled as 100' (x_0, y_0) and 103' (x_3, y_3) respectively. Although at this stage four image points have been recognised and extracted, their correspondences to the real targets must be decided. It is possible to correspond with the object targets 100, 101, 102, 103 in order of 100', 101' 102', 103', or 103', 102', 101', 100'. In this case, object labelling of targets is defined by a right handed rule. Subsequent image target labelling is made to correspond with this convention by the following method: Assume the vector $\overline{\mathbf{ap}} = \overline{\mathbf{100'101'}}$, $\overline{\mathbf{bp}} = \overline{\mathbf{100'102'}}$, then the relationship between 100', 101' and 102' can be defined as:

$$T = |\, \boldsymbol{ap} \times \boldsymbol{bp} \,| = \begin{vmatrix} \boldsymbol{i} & \boldsymbol{j} & \boldsymbol{k} \\ x_1 - x_0 & y_1 - y_0 & 0 \\ x_2 - x_0 & y_2 - y_0 & 0 \end{vmatrix} \tag{4.14}$$

If T > 0, the order of the image targets is correct, so

100 = 100', 101 = 101', 102 = 102', 103 = 103'.

If T < 0, the order of the image targets is reversed, so

100 = 103', 101 = 102', 102 = 101', 103 = 100'.

The final result of finding the correct correspondences is shown in Figure 4.8. The four image

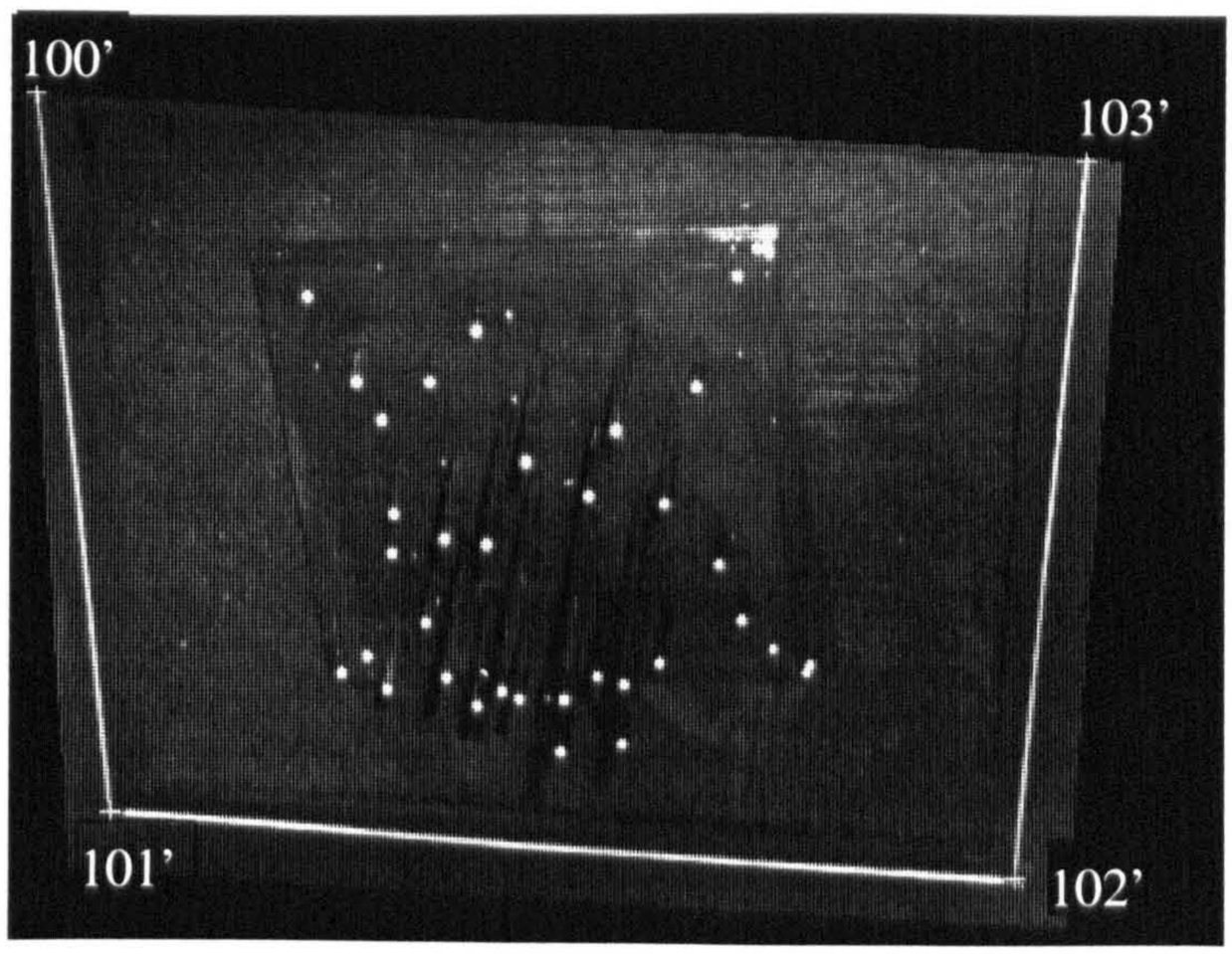

Figure 4.8 Determination of the four points

targets are converted from pixel to millimeter units, since the camera pixel size is known. The geometric vector method described in section 4.2.1.3 is then used to obtain estimates of the camera orientation parameters.

4.2.2.5. Evaluation of the method

The three sided rectangle method for estimation of camera orientations has been successfully tested by placing three cameras in three different positions to give differing viewpoints of the three sided rectangle (Figure 4.9). The characteristics of this method can be summarised as follows:

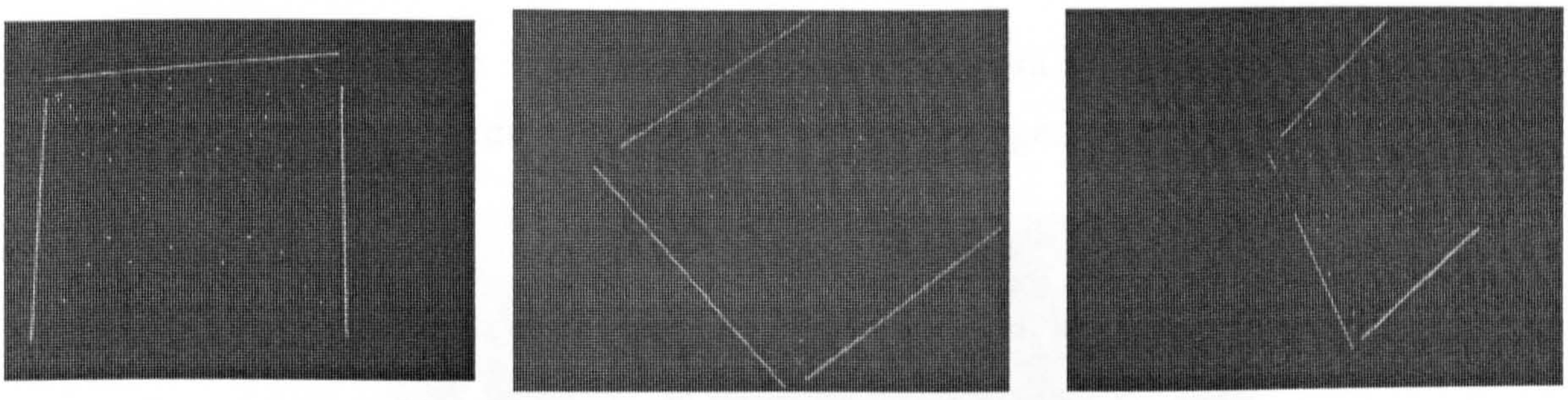

Figure 4.9 Results of different viewpoints for three cameras

Reliability. Because the method is based the extraction of rectangle sides, it can be made very robust. A robust line detection algorithm is used and because of the strong image features the reliability of determination of the four points is usually very high. Even if there are some occlusion as shown in Figure 4.9, a solution can be still obtained by line segment detection and the subsequent combination of these broken line segments. However, problems can be experienced if the occlusion takes place at both termination points. This will cause an incorrect solution due to an error in the end position.

Speed. The speed of the algorithm depends on the width of the rectangle sides because the thinning algorithm, which performs four loops per pixel layer, is still computationlly expensive even with the optimisation discussed in this section. For the examples shown in Figure 4.9 the task of estimating the camera orientation parameters was completed in about 20 seconds.

Accuracy. The main influence on accuracy results from the thinning algorithm using a pixel units. Although the two intersection points have subpixel accuracy, the two determination points have only pixel level accuracy. However, the level of accuracy obtained is sufficient

for the purposes of providing starting values for the camera orientation parameters.

4.2.3. Camera orientation by an automatic laser spot extraction method

As discussed in chapter 3, a laser target has the advantage of flexibility. A diode laser is an active light source and can be switched on or off. A diode laser collimator is able to project a small, highly intense spot of light onto a surface. An experiment was conducted to investigate the use of lasers as control points in an automatic procedure to estimate the camera orientation parameters. This method is discussed in the following section.

4.2.3.1. The laser spot projection system

Four lasers are used for the automatic estimation of camera parameters. The configuration of the system is shown in Figure 4.10. These lasers are arranged to be parallel to each other. The

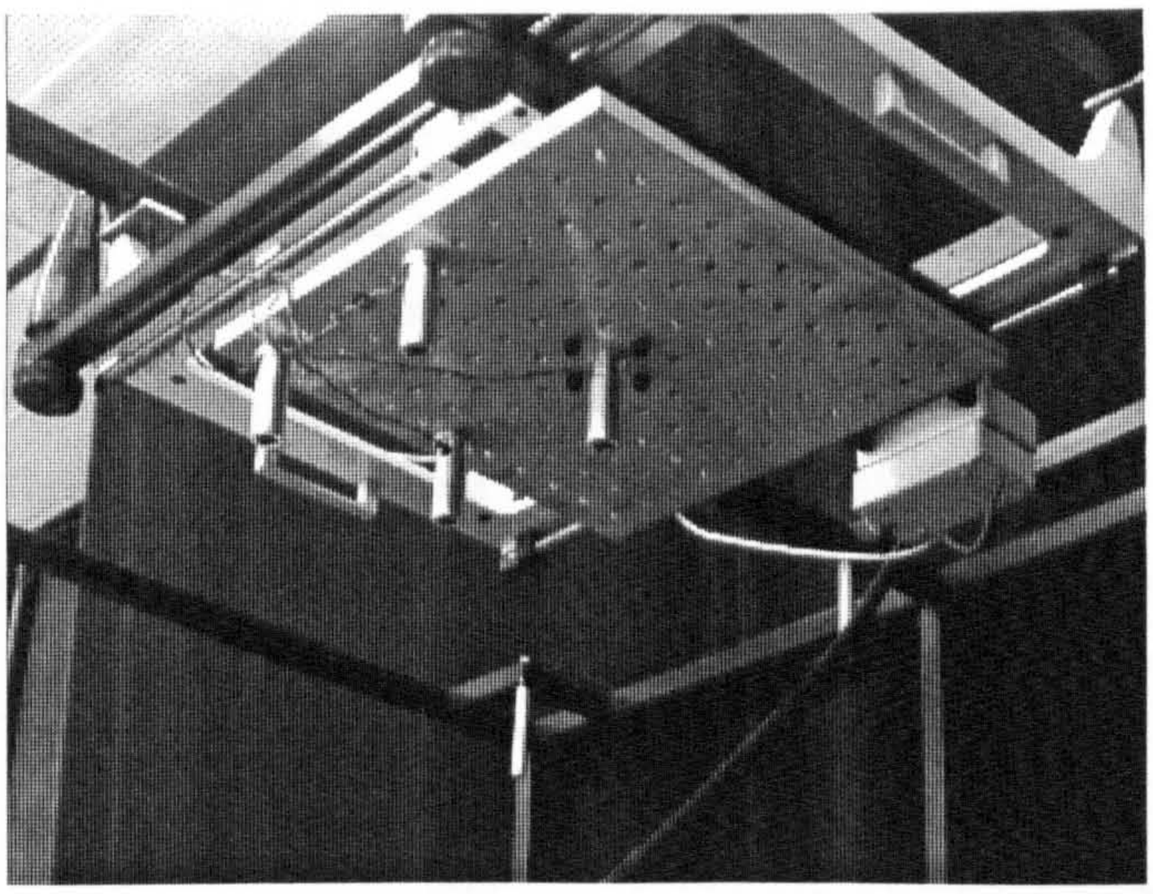

Figure 4.10 Configuration of the laser diode system

lasers were fixed vertically into four holes on an aluminiums plate, which has number of holes arranged in an array so that the four lasers could be adjusted to variable positions depending on the size of object measured. The aluminium plate was fixed to a Maxtascan scanning table which has two rails that allows precise movement in both x and y directions. The movement of the Maxtascan table is controlled by computer through a parallel I/O card which is used to drive the two motors. The correspondence between the laser spot in object space and the laser target images in image plane can be obtained by switching the specified lasers on and off.

4.2.3.2. Extraction of the laser target images

The simplest way to extract the laser target images and identify their correspondences is to

switch one laser on at a time. An image is grabbed when the laser is switched on. The co-ordinates of the laser spot image can be obtained by a centroid subpixel location algorithm. The laser is then switched off and the next laser switched on. All 2-D co-ordinates of the four laser target images can be sequentially obtained. The distances between each pair of the four lasers are constants as the lasers are fixed. If the lasers project onto a plane that is perpendicular to the lasers, the 3-D co-ordinates of the four lasers can be defined using the known distances between each pair of lasers. The camera orientation parameters can then be estimated by the geometric vector method. The object is then placed into the cameras field of view after obtaining the camera orientation parameters and the 3-D measurement of the object is able to proceed as normal.

This procedure requires five images to be grabbed in sequence, one for each of four laser spots and one for the object measured, and requires the lasers to be turned on and off. An alterative implementation of this method is adopted in which only two images are grabbed for the four lasers so that the lasers are only turned on and off twice. First, one laser is switched on to obtain the correspondence of the laser spot and its co-ordinates in the image plane. Second, the remaining three lasers are switched on, and the co-ordinates of these three laser spots are captured. Third, the co-ordinates are analysed to find the correspondences of the laser spots in the object space. As the co-ordinates of the first laser spot image and its correspondence with the object space spot has been determined, these are labelled 100' and 100 as shown in Figure 4.11 a) and b). The four object space laser spots can then be defined

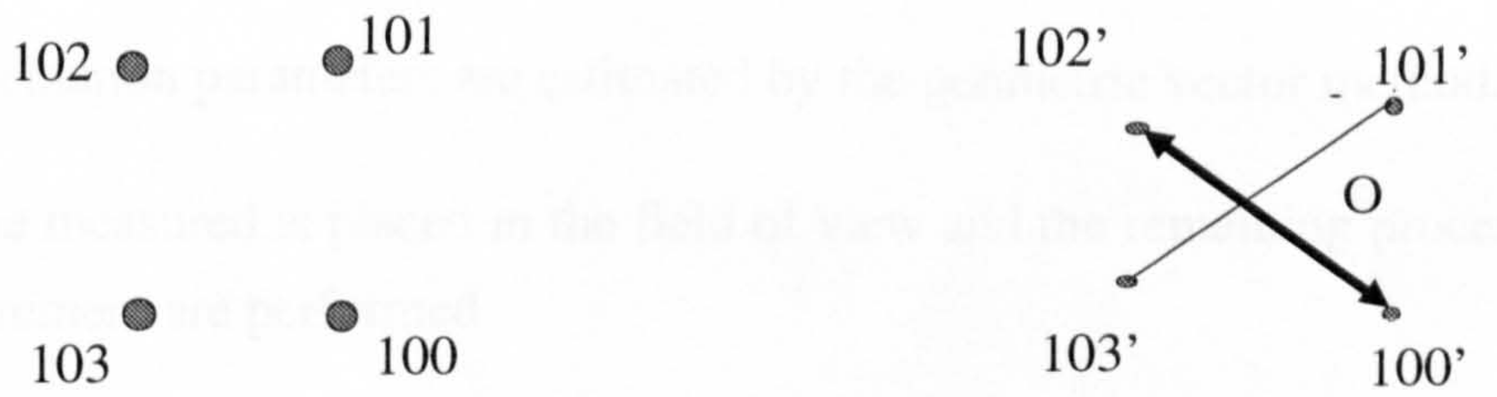

Figure 4.11 a) Laser spots in space plane b) Laser spot images in image plane

as 100, 101, 102, 103 in a counter-clockwise direction. The imaged spot 102' that corresponds to the object space spot 102 can be found using the fact that the cross over point 'O' of the line (100', 102') and line (101' ,103') should lie between the two termination points of the two lines (Figure 4.11b). This method is implemented by arbitrarily choosing one of the three imaged spots as a hypothetical 102'. The co-ordinates of hypothesis O are

obtained and the condition is tested. It can be verified that only the true 102' satisfies this condition. After this correspondence is found for the target image 102', the 101' and 103' can be distinguished by using a right handed rule, in which the z axis is defined as the direction leaving the image plane. Hence, only the three spots 100', 101', and 102' are necessary to satisfy the right handed rule. The co-ordinates of the four spot images are then converted into millimeter units followed by the application of the geometric vector method to obtain estimates of the camera orientation parameters.

The steps for the automatic procedure of estimation of camera orientation parameters using the laser spot extraction method can be summarised as follows:

- The four laser collimators are adjusted to a position where the object measured is going to be placed and the cameras adjusted accordingly. The 3-D co-ordinates of laser spots are produced. The object is then replaced by a plane.

- A laser, labelled 100, is switched on and an image is grabbed. The 2-D co-ordinates of this laser spot image, labelled 100', are calculated by a subpixel location algorithm. The laser is then switched off.

- The remaining three lasers are switched on and an image is grabbed. The 2-D co-ordinates of the three laser spot images are calculated by the subpixel location algorithm.

- The 102' spot image is identified by the method discussed in this section.

- The 101' and 103' spot images are then identified by right handed rule.

- The camera orientation parameters are estimated by the geometric vector method.

- The object to be measured is placed in the field of view and the remaining processes of 3-D measurement are performed.

4.2.3.3. Evaluation of the method

This method of automatic laser spot extraction for estimation of camera orientation has been successfully tested in a number of experiments in which a camera was placed in a number of differing positions. The characteristics of this method can be summarised as follows:

Reliability. Because this method is based on the projections of the lasers, it is robust as the laser spots provide high contrast images compared to the background illumination so that the spot images are easy to detect and locate.

Speed. The method is quick as no iteration is necessary during image processing. The whole procedure is completed in a few seconds for all the processes including switching the lasers, grabbing images, locating the spot images, identifying the correspondences, and estimating the orientation parameters of each camera.

Accuracy. One of influences on accuracy is the precision of the estimation of the 3-D co-ordinates of the lasers spot and the possibility of the surface not being planar. Another influence for accuracy is caused by laser speckle. Laser speckle may cause as high as half a pixel error even when a subpixel location algorithm is used (Clarke, 1994).

4.3. A 2-D epipolar line matching method

The previous sections have discussed methods to automatically calculate the camera orientation parameters of each individual viewpoint. The next task to be performed in an automatic digital photogrammetric system is the matching of each target image with the corresponding target images obtained by the other cameras. In digital photogrammetric 3-D engineering measurement there has been considerable research into the subject of target matching (Baltsavias, 1991). In chapter two the main matching algorithms of intensity and feature based methods were discussed. Intensity based matching takes a grey scale image of a target or a pattern and uses correlation or least squares matching methods to achieve the high precision location of any matching targets or patterns (Heikpe, 1992). Feature based matching methods use the physical structure of targets in a binary image, such as area, perimeter, or degree of circularity. These features are extracted to determine legitimate matching targets (Blake, 1990). Both methods require some prior knowledge about the targets to succeed. However, there are seldom enough unique features in each target to allow successful matching when the target is viewed from differing angles and distances. This is especially true of circular retro-reflective targets which are often used for high accuracy measurement. Consequently, feature based methods are not useful in finding target correspondences in differing views, however, such methods can be used in target recognition. In the situation where point-like targets are used which have few unique features or intensity characteristics, epipolar line matching methods are commonly used to match the corresponding targets.

4.3.1. Introduction to the epipolar line matching method

For the purpose of this discussion it is assumed that at least two cameras are used. The geometric relationship between an object target projected onto two images planes is shown in Figure 4.12.

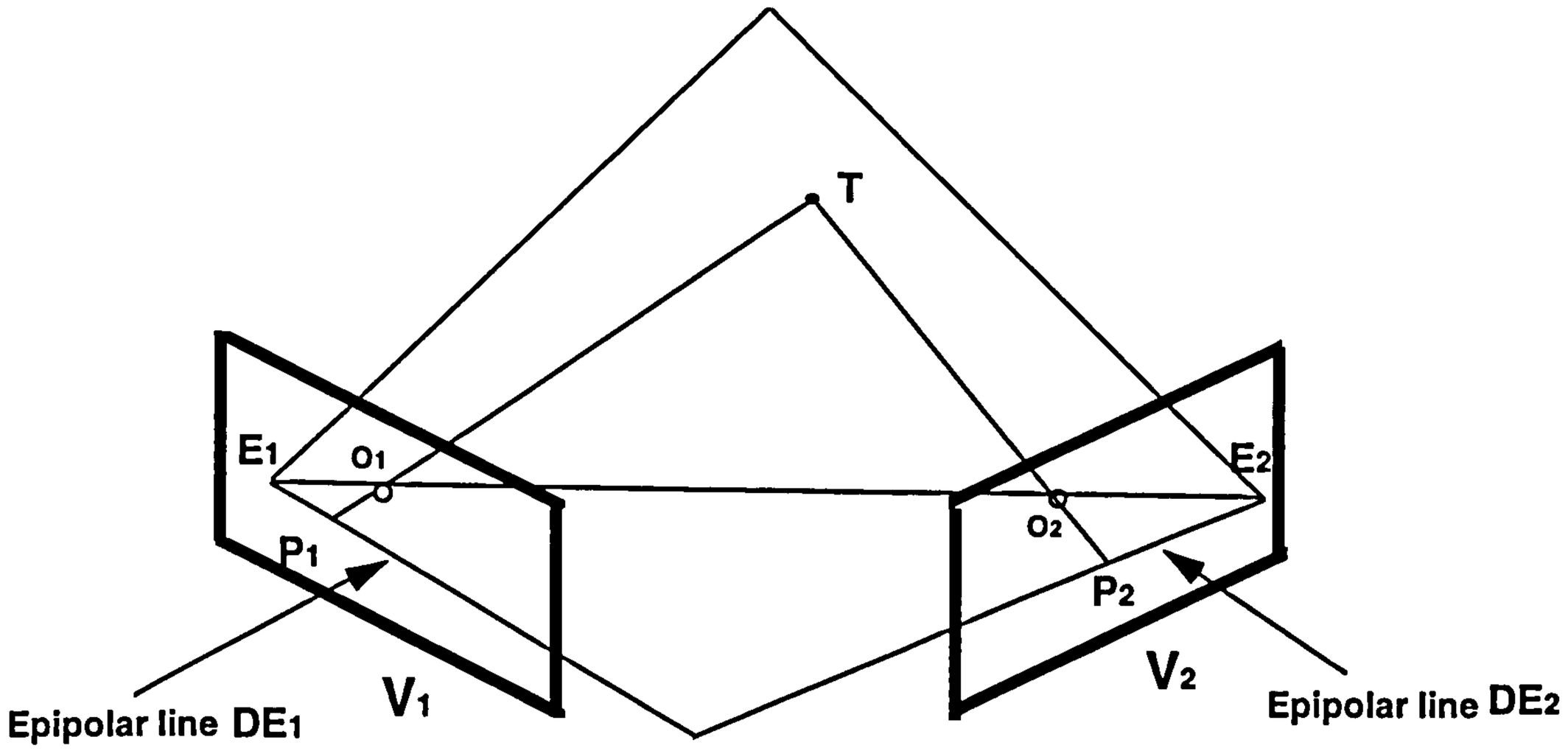

Figure 4.12 Geometric relation of target images between two viewpoints

Definition 4.1: When a ray of light from the target T passes through the perspective center O_1 and projects onto position P_1 in the image plane, these three points lie on a straight line by definition. If this straight line is projected onto another image (V_2), an epipolar line DE_2 is formed. In the same way, the conjugate epipolar line DE_1 can be obtained from the line projection of T passing through the perspective center O_2 and position P_2.

Definition 4.2: The image point E_2, which is the projection of O_1 in V_2, is defined as the epipole of V_2. In the same way, the conjugate epipole E_1 is define as the projection point of O_2 in V_1.

These two definitions allow the epipolar line of each object target on each image plane to be constructed by two image points, the epipole on that viewpoint and the projection of the object target on that image plane. However, in practice, the 3-D co-ordinates of an object target are usually unknown and only the 2-D co-ordinates of the target image at the image plane are available. To form the epipolar line of the target image in other image plane, an alternative method is now defined:

Assume the distortion of all cameras is negligible and that the orientation parameters of all cameras are exactly known. For each target image in the image plane of V_1, two equations can be obtained by using the collinearity equations as described in equation 2.1:

$$x_1 - xo = -c\frac{m_{111}(X - Xo_1)+m_{112}(Y - Yo_1)+m_{113}(Z - Zo_1)}{m_{131}(X - Xo_1)+m_{132}(Y - Yo_1)+m_{133}(Z - Zo_1)} = f_{11}(X,Y,Z) \qquad (4.14a)$$

$$y_1 - yo = -c\frac{m_{121}(X - Xo_1)+m_{122}(Y - Yo_1)+m_{123}(Z - Zo_1)}{m_{131}(X - Xo_1)+m_{132}(Y - Yo_1)+m_{133}(Z - Zo_1)} = f_{12}(X,Y,Z) \qquad (4.14b)$$

where only X, Y, Z are unknown.

Two equations can be built by projecting the object target (X, Y, Z) to the other image plane as:

$$x_2 - xo = -c\frac{m_{211}(X - Xo_2)+m_{212}(Y - Yo_2)+m_{213}(Z - Zo_2)}{m_{231}(X - Xo_2)+m_{232}(Y - Yo_2)+m_{233}(Z - Zo_2)} = f_{21}(X,Y,Z) \qquad (4.15a)$$

$$y_2 - yo = -c\frac{m_{221}(X - Xo_2)+m_{222}(Y - Yo_2)+m_{223}(Z - Zo_2)}{m_{231}(X - Xo_2)+m_{232}(Y - Yo_2)+m_{233}(Z - Zo_2)} = f_{22}(X,Y,Z) \qquad (4.15b)$$

where the X, Y, Z and x_2, y_2 are unknown.

Combining the four linear equations in equation 4.14 and 4.15 and eliminating the variables X, Y, and Z, the 2-D epipolar line equation can be obtained as:

$$y_2 = ax_2 + b \qquad (4.16)$$

where a and b are coefficients computed directly from the equation 4.14 and 4.15. The physical meaning of this equation is shown in Figure 4.13.

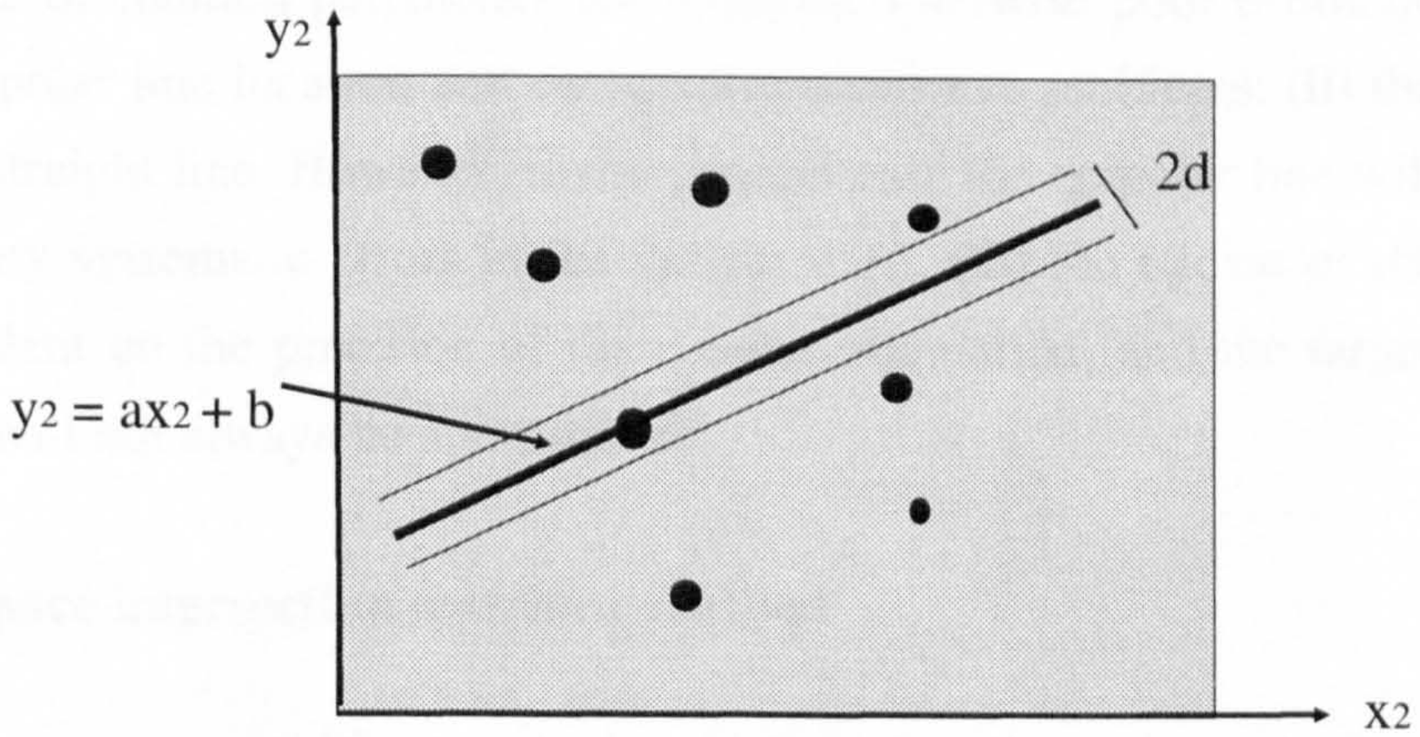

Figure 4.13 Epipolar line in image plane 2 for a target image in image plane 1

To match a target image point in one image with its corresponding target image point in the other, the process is as follows:

The co-ordinates of a target image point in the first image plane are calculated using a subpixel location algorithm. These data are used to determine the coefficients of the epipolar line equation 4.16 in the second image plane by using equation 4.14 and equation 4.15. All target images in the second image are tested with equation 4.15 and the target image that satisfies the equation is considered a correct match.

When the algorithm is used, errors in target location and camera parameters will require that a tolerance band is used, otherwise no target image will exactly satisfy the equation. The tolerance band limits, of distance d from the epipolar line, are used on both sides of the epipolar line as shown in Figure 4.13. If the target image tested lies outside of the tolerance, the target image will be rejected. If the target image lies inside of the area, the target image will be accepted as the correct corresponding target image.

The previous discussion describes a successful match but ambiguities may occur if more than one target images lies inside of the epipolar tolerance area. This problem can easily occur with large numbers of targets and a high range disparity between targets. With two cameras these ambiguities are unsolvable. However, such ambiguities can be reduced by increasing the number of cameras (Maas, 1992a). This will discussed in chapter five.

4.3.2. Discussion

The epipolar line method is founded on the intersection of straight lines in the image plane to solve correspondences between targets. However, the method has some limitations: **(i)** accurate camera orientation parameters are required otherwise poor estimation will cause an error in the epipolar line location and cause correspondence problems; **(ii)** the epipolar line is modelled as a straight line. However, in the general case the epipolar line will be distorted by the lens, and any systematic errors in the system used; **(iii)** the choice of the tolerance band value is dependent on the precision of the camera orientation, and the target image location algorithm, but will not always be appropriate.

4.4. The 3-D space intersection matching method

In this section, a new matching method, which is based on the epipolar line method, is developed. This method uses a 3-D intersection and epipolar plane, as opposed to the 2-D intersection of the epipolar line method. In this method, collinearity equations are directly used so that additional parameters, such as camera lens distortion parameters, are included

and target matching is performed in 3-D space. Because target matching is performed in 3-D space, the tolerance value can be closely related to errors in 3-D co-ordinate estimation.

The method is formally, discussed in this chapter followed by an optimisation of the method in the next chapter.

4.4.1. The 3-D space intersection matching principle

A 2-D image is formed of a targeted object in 3-D space world when light rays from the targets are projected through the camera lens onto the sensor. The co-ordinates x_i and y_i of the various target images can be estimated as discussed in chapter two. These measured image positions are not likely to be exactly correct, but will contain some error caused by image intensity variations, the distortion of the lens, the low spatial resolution of the sensor, and any systematic errors in the method used. Some of these discrepancies can be modelled by careful use of additional parameters included within the functional model, hence equation 2.6 is rearranged to include additional parameters:

$$\frac{(Xa-Xo)}{(m11((x-xo)+x_{lens})+m21((y-yo)+y_{lens})+m31(-c))}=\frac{(Za-Zo)}{(m13((x-xo)+x_{lens})+m23((y-yo)+y_{lens})+m33(-c))} \quad (4.17a)$$

$$\frac{(Ya-Yo)}{(m12((x-xo)+x_{lens})+m22((y-yo)+y_{lens})+m32(-c))}=\frac{(Za-Zo)}{(m13((x-xo)+x_{lens})+m23((y-yo)+y_{lens})+m33(-c))} \quad (4.17b)$$

This equation satisfies a 3-D line equation in vector form:

$$\frac{Xa-Xo}{p}=\frac{Ya-Yo}{q}=\frac{Za-Zo}{r} \quad (4.18)$$

Where

$$p=(m11((x-xo)+x_{lens})+m21((y-yo)+y_{lens})+m31(-c))$$

$$q=(m12((x-xo)+x_{lens})+m22((y-yo)+y_{lens})+m32(-c))$$

$$r=(m13((x-xo)+x_{lens})+m23((y-yo)+y_{lens})+m33(-c))$$

Equation(4.18) is the equation of a 3-D line. The intersection of two 3-D lines define a point in 3-D space. If a target lies on the surface of a 3-D object, the 3-D line equation describes a ray projected from this target through the perspective centre of the lens. If all of the targets from another image are projected through the perspective center of another camera lens, provided the exterior orientation parameters are reasonable, then one of these rays will ideally

be close to the single projected 3-D line thereby, identifying the correct corresponding target. If additional targets are considered in the same way, further target image candidates for correct correspondences will be found. The 3-D lines will not intersect at a single point due to small errors in the parameters modelled by equation 2.6, and due to target location errors. However, the correct corresponding target ray is likely to fall, within some tolerance, close to the object target Xa,Ya,Za. The principle of the 3-D space matching method is illustrated in Figure 4.14 for the two projected rays of a matching target.

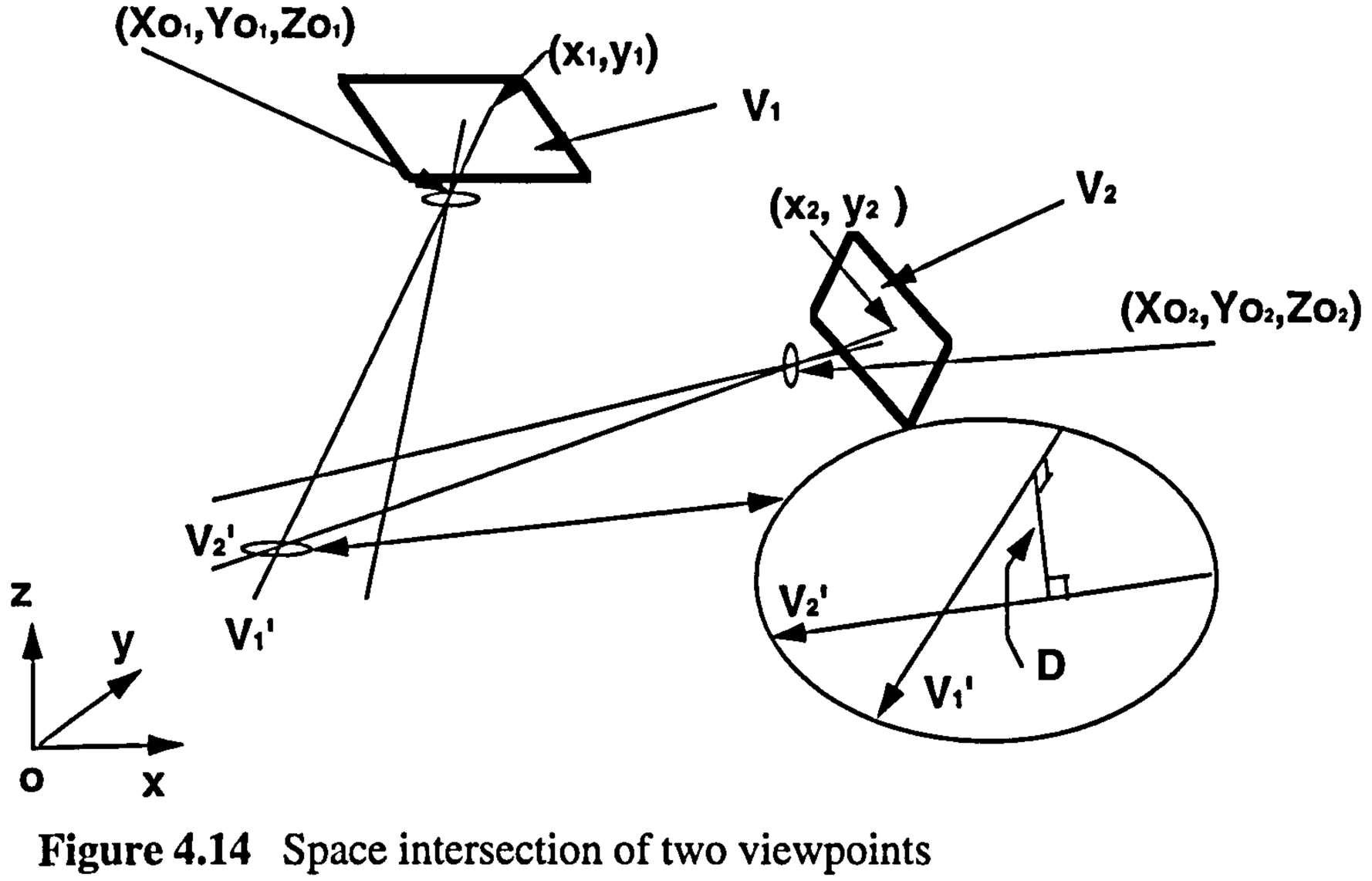

Figure 4.14 Space intersection of two viewpoints

Using two camera viewpoints as an example (Figure 4.14), it can be seen that whilst the two rays are not likely to intersect at a single point in space because of the errors mentioned previously, the distance D can be calculated directly from equation 4.18:

$$D = \left| \begin{array}{ccc} Xo_2-Xo_1 & Yo_2-Yo_1 & Zo_2-Zo_1 \\ p_1 & q_1 & r_1 \\ p_2 & q_2 & r_2 \end{array} \right| / \sqrt{\left(\left| \begin{array}{cc} p_1 & q_1 \\ p_2 & q_2 \end{array} \right|^2 + \left| \begin{array}{cc} q_1 & r_1 \\ q_2 & r_2 \end{array} \right|^2 + \left| \begin{array}{cc} r_1 & p_1 \\ r_2 & p_2 \end{array} \right|^2 \right)} \qquad (4.19)$$

where

p_1,q_1,r_1 and p_2,q_2,r_2 are vectors of equation 4.18 for two cameras.

The 3-D co-ordinates of a point Xa, Ya, Za can be estimated by 3-D space intersection by substituting x_1, y_1, x_2, y_2 into equation 2.6 since all camera orientation parameters are known. The method of computing the unknowns Xa, Ya, Za is as follows:

Xa, Ya, Za are defined by equation 4.20:

$$\begin{bmatrix} Xa \\ Ya \\ Za \end{bmatrix} = (A^t W A)^{-1} A^t W b \tag{4.20}$$

where

$$A = \begin{bmatrix} m_{11}+m_{31}\frac{x^{(1)}}{c} & m_{12}+m_{32}\frac{x^{(1)}}{c} & m_{13}+m_{33}\frac{x^{(1)}}{c} \\ m_{21}+m_{31}\frac{y^{(1)}}{c} & m_{22}+m_{32}\frac{y^{(1)}}{c} & m_{23}+m_{33}\frac{y^{(1)}}{c} \\ m_{11'}+m_{31'}\frac{x^{(2)}}{c} & m_{12'}+m_{32'}\frac{x^{(2)}}{c} & m_{13'}+m_{33'}\frac{x^{(2)}}{c} \\ m_{21'}+m_{31'}\frac{y^{(2)}}{c} & m_{22'}+m_{32'}\frac{y^{(2)}}{c} & m_{23'}+m_{33'}\frac{y^{(2)}}{c} \end{bmatrix} \tag{4.21}$$

$$b = \begin{bmatrix} (-m_{11}-m_{31}\frac{x^{(1)}}{c})Xo_1 + (-m_{12}-m_{32}\frac{x^{(1)}}{c})Yo_1 + (-m_{13}-m_{33}\frac{x^{(1)}}{c})Zo_1 \\ (-m_{21}-m_{31}\frac{y^{(1)}}{c})Xo_1 + (-m_{22}-m_{32}\frac{y^{(1)}}{c})Yo_1 + (-m_{23}-m_{33}\frac{y^{(1)}}{c})Zo_1 \\ (-m_{11'}-m_{31'}\frac{x^{(2)}}{c})Xo_2 + (-m_{12'-m32'}\frac{x^{(2)}}{c})Yo_2 + (-m_{13'}-m_{33'}\frac{x^{(2)}}{c})Zo_2 \\ (-m_{21'}-m_{31'}\frac{y^{(2)}}{c})Xo_2 + (-m_{22'}-m_{32'}\frac{y^{(2)}}{c})Yo_2 + (-m_{23'}-m_{33'}\frac{y^{(2)}}{c})Zo_2 \end{bmatrix} \tag{4.22}$$

where

m_{11} - m_{33} are the rotation matrix elements of viewpoint one,

$m_{11'}$ - $m_{33'}$ are the rotation matrix elements of viewpoint two,

Xo_1, Yo_1, Zo_1 are position parameters of viewpoint one,

Xo_2, Yo_2, Zo_2 are position parameters of viewpoint two,

$x^{(1)} = (x_1 - x_0) + x_{lens1}$,

$y^{(1)} = (y_1 - y_0) + y_{lens1}$,

$x^{(2)} = (x_2 - x_0) + x_{lens2}$,

$y^{(2)} = (y_2 - y_0) + y_{lens2}$,

and

W is a weight matrix, usually taken as the covariance matrix (equation 4.23).

$$W = \begin{Bmatrix} \frac{q_0}{q_1} & 0 & 0 & 0 \\ 0 & \frac{q_0}{q_2} & 0 & 0 \\ 0 & 0 & \frac{q_0}{q_3} & 0 \\ 0 & 0 & 0 & \frac{q_0}{q_4} \end{Bmatrix} \qquad (4.23)$$

where

q_0 is the global variance,

and

q_i (i = 1, 2, 3, 4) are the local variance.

Equations 4.19 to 4.23 represent the situation where there only two viewpoints exists. If more than two viewpoints are used, the relevant changes in these equations have to be made. Assuming there are **n** viewpoints, equation 4.20 remains is the same but the matrices **A**, **b**, and W are changed. The new equations are as follows:

$$A = \begin{bmatrix} m_{11}^{(1)} + m_{31}^{(1)}\frac{x^{(1)}}{c} & m_{12}^{(1)} + m_{32}^{(1)}\frac{x^{(1)}}{c} & m_{13}^{(1)} + m_{33}^{(1)}\frac{x^{(1)}}{c} \\ m_{21}^{(1)} + m_{31}^{(1)}\frac{y^{(1)}}{c} & m_{22}^{(1)} + m_{32}^{(1)}\frac{y^{(1)}}{c} & m_{23}^{(1)} + m_{33}^{(1)}\frac{y^{(1)}}{c} \\ \cdots & \cdots & \cdots \\ m_{11}^{(n)} + m_{31}^{(n)}\frac{x^{(n)}}{c} & m_{12}^{(n)} + m_{32}^{(n)}\frac{x^{(n)}}{c} & m_{13}^{(n)} + m_{33}^{(n)}\frac{x^{(n)}}{c} \\ m_{21}^{(n)} + m_{31}^{(n)}\frac{y^{(n)}}{c} & m_{22}^{(n)} + m_{32}^{(n)}\frac{y^{(n)}}{c} & m_{23}^{(n)} + m_{33}^{(n)}\frac{y^{(n)}}{c} \end{bmatrix} \qquad (4.24)$$

$$b = \begin{Bmatrix} (-m_{11}^{(1)} - m_{31}^{(1)}\frac{x^{(1)}}{c})Xo_1 + (-m_{12}^{(1)} - m_{32}^{(1)}\frac{x^{(1)}}{c})Yo_1 + (-m_{13}^{(1)} - m_{33}^{(1)}\frac{x^{(1)}}{c})Zo_1 \\ (-m_{21}^{(1)} - m_{31}^{(1)}\frac{y^{(1)}}{c})Xo_1 + (-m_{22}^{(1)} - m_{32}^{(1)}\frac{y^{(1)}}{c})Yo_1 + (-m_{23}^{(1)} - m_{33}^{(1)}\frac{y^{(1)}}{c})Zo_1 \\ \cdots \quad \cdots \quad \cdots \\ (-m_{11}^{(n)} - m_{31}^{(n)}\frac{x^{(n)}}{c})Xo_n + (-m_{12}^{(n)} - m_{32}^{(n)}\frac{x^{(n)}}{c})Yo_n + (-m_{13}^{(n)} - m_{33}^{(n)}\frac{x^{(n)}}{c})Zo_n \\ (-m_{21}^{(n)} - m_{31}^{(n)}\frac{y^{(n)}}{c})Xo_n + (-m_{22}^{(n)} - m_{32}^{(n)}\frac{y^{(n)}}{c})Yo_n + (-m_{23}^{(n)} - m_{33}^{(n)}\frac{y^{(n)}}{c})Zo_n \end{Bmatrix} \quad (4.25)$$

$$W = \begin{bmatrix} \frac{q0}{q1} & 0 & .. & 0 \\ 0 & \frac{q0}{q2} & .. & 0 \\ .. & .. & .. & .. \\ 0 & 0 & .. & \frac{q0}{qn} \end{bmatrix} \quad (4.26)$$

Using equation 4.20 and matrices **A** and **b** in equation 4.24 and 4.25, the co-ordinates of an object target can be estimated based on its projections. The distance D_i from the estimated point to the **n** space projection ray can be formalised as:

$$D_i = \begin{vmatrix} i & j & k \\ p_i & q_i & r_i \\ X_a - Xo_i & Y_a - Yo_i & Z_a - Zo_i \end{vmatrix} / \sqrt{(p_i^2 + q_i^2 + r_i^2)} \quad (4.27)$$

where

p_i, q_i ,r_i are vectors of equation 4.18 for the **ith** viewpoint.

i, j, k are unit vectors of the three axes X, Y, and Z.

The sign is chosen to keep D_i positive. The physical meaning of the equation 4.26 is shown in Figure 4.15.

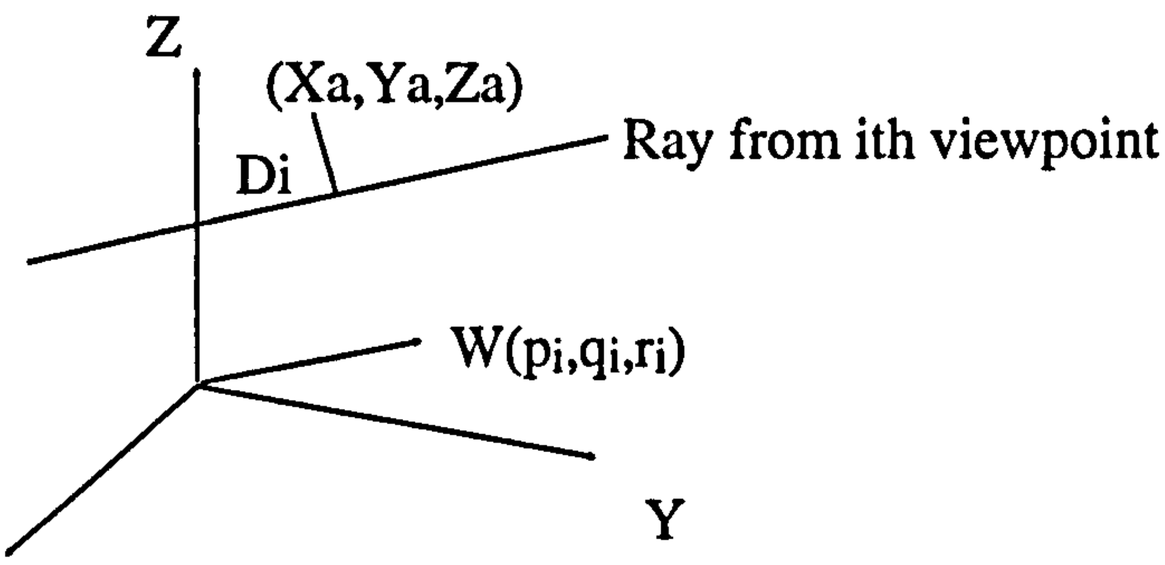

Figure 4.15 Space intersection of **nth** viewpoint

4.4.2. Discussion

If all of the targets in the original image are analysed using this method the corresponding targets from other images can be found. For all correctly corresponding targets, D should be small and lie within the pre-determined tolerance band. For other non-corresponding targets, the value of D will depend on the spatial distribution of the targets, and will generally be much larger than that for the correctly corresponding targets. The value of the tolerance band has to be selected so that it excludes all of the incorrect targets while encompassing the correct ones.

Compared with the epipolar line method, there are two important differences between the methods:

(1) The epipolar line method uses the projection of an epipolar line whilst the 3-D spatial method is the space intersection of points between two views. The advantage of using 3-D rather than 2-D epipolar projections is that additional parameters can be easily included (equation 4.17) in the computation. The epipolar line method can compensate for lens distortion and other error sources, by correcting the original data, or using additional parameters. However, this requires the predetermination of these additional parameters which is not always convenient.

(2) The threshold values for judging correspondences between image views are different. The 3-D space method uses the standard deviation of targets in 3-D space whilst the epipolar method uses the residuals from the collinear equations. It will be shown in later chapters that the 3-D space method can be dynamically connected with the bundle adjustment so that the

object tolerance value can be chosen according to the computed RMS errors of the 3-D co-ordinates of the object targets. The advantages of this method will be investigated in detail in the next chapter.

4.5. Summary

In this chapter, two automatic methods have been discussed for the estimation of camera orientation parameters and target matching. In particular, the general solution of a closed form space resection was considered. A three side frame method and a laser spot extraction method were used to develop an automatic and rapid extraction of the camera orientation parameters. Implementation of the three sided rectangle method by using line thinning, line tracing, and a least square line fit was described. The laser spot method was implemented using switching and some simple logic. Experiments were described and evaluations made of the techniques.

Two target matching methods for multi-viewpoints were introduced, the 2-D epipolar line matching method and a new 3-D space intersection matching method. The latter method converts the traditional epipolar line matching method in 2-D to 3-D space so that several benefits can be achieved: (i) collinearity equations are used in which the camera additional parameters are included; (ii) the matching takes place in 3-D space so that the tolerance value is based on the RMS errors of the computed 3-D co-ordinates of object target; (iii) the estimation of co-ordinates of the 3-D object targets results directly from the matching procedure; and (iv) the method can be combined with the iterative bundle adjustment which will be discussed in the next chapter.

Further discussion of these automatic methods in the next two chapters will concentrate on several aspects: (i) the combination of 3-D space intersection matching with the bundle adjustment; (ii) the optimisation of this matching method for multiple viewpoints; (iii) the theoretical analysis of sources of error caused by ambiguity, occlusion, target image location, and errors of viewpoint orientation estimation; (iv) the integration of image processing, target location, computing target correspondences, and the self calibrating bundle adjustment into a single software package as a step towards an automatic photogrammetric measuring system.

Chapter 5 Optimisation of the multiple camera 3-D matching method

5.1. Introduction

A study of the methods which can be used to find corresponding target images in multiple viewpoints has been undertaken by many researchers from the areas of machine vision and photogrammetry. Many techniques have been analysed, such as: area matching methods; feature matching methods; geometrically constrained matching methods; and epipolar methods. Such methods have been successfully applied in many situations. However, all of these methods can be limited by practical problems which can be categorised into three types:

- Noise: There will be many sources of error in the measurement system. These include errors in the estimation of: lens distortion; the functional model; target image location; and camera orientation parameters. Such errors will affect the target matching process.

- Occlusion: Occlusion occurs when targets are fully or partially obscured by other object features. In intensity based or feature based methods, occlusion may result in false identification of targets. In the epipolar based method, occlusions result in the target being projected on to some viewpoints and not others.

- Ambiguities: Target images in intensity or feature matching methods can appear similar in shape and appearance so that an incorrect or ambiguous match is made. In the epipolar constrained matching method targets may be imaged too close together or lie on the same epipolar line (plane) so that false matches may be made.

The key to the design of target matching algorithms is in overcoming the problems caused by these three errors. At the same time the computation cost of the matching algorithm must be taken into account since it increases exponentially as the number of viewpoints increase. The following criteria will be used to judge the performance of a matching method.

Efficiency: A good matching method must be as efficient as possible. This should be measured both in terms of run time efficiency and in terms of computational complexity.

Correctness: The method should find the correct matches. This means that it should not miss any correct matching and not make false matches in the presence of occlusion or potential ambiguities.

Robustness: A matching method must continue to be reliable with increasing noise in the image data and estimated parameters, and where multiple views, partial object

coverage, and weak network geometries are present.

The primary method of obtaining discrete points on a object to be measured is by placing circular retro-reflective targets. In such a case simple intensity or feature based methods are not appropriate. Therefore, the epipolar constrained method is investigated as it provides an alternative to the method proposed in this thesis.

In this chapter, a 3-D target matching method is developed in which the estimated camera orientations are iteratively improved by combining the bundle adjustment procedure during the matching procedure. Furthermore, the random search matching process is converted to a space tree search process. The computation cost is radically decreased by adding constraints and introducing optimised search strategies. Methods of overcoming the errors caused by occlusion, ambiguities, and noise are discussed and their influences on system performance are estimated and analysed.

5.2. Iterative 3-D target matching with network and constraints

As discussed in the previous chapter, the use of the epipolar method to match the correspondent target images requires that the camera orientation parameters are accurately defined. These parameters are difficult to obtain with suitable precision in an unconstrained environment as they are usually obtained to high precision through a bundle adjustment which cannot occur until the correspondence problem has been solved. This problem with the epipolar method and poor knowledge of the network geometry can be overcome by combining the bundle adjustment technique with epipolar target matching. One of the advantages of the bundle adjustment is that it can iteratively calculate the 3-D co-ordinates of target positions to high precision and at the same time improve camera exterior orientation and lens distortion parameters.

In this section, the 3-D matching technique is optimised to improve target image correspondence performance. The technique is founded on the well established bundle adjustment procedure. In the first iteration of the matching procedure, a few target image matches are determined using the initial approximations of the camera viewpoint parameters discussed in chapter 4 and an initial 3-D tolerance. A bundle adjustment is then computed and the refined camera orientation parameters are fed back into the matching algorithm, with a new 3-D tolerance, where new targets are found. By these means the process can be refined and repeated, as the network is strengthened, until all target correspondences are found.

The 3-D tolerance band from which space distance D between two rays is chosen can be obtained using the existing target standard deviation computed during the bundle adjustment.

Hence, the relationship between the tolerance threshold and the 3-D co-ordinate standard deviation in the object space is a complete reflection of the 3-D co-ordinate estimation errors at each iteration of the bundle adjustment.

There are several advantages which can be gained by using the RMS object co-ordinate standard deviation as the basis for generating a tolerance factor: It has a clear physical meaning; and since the solution becomes more and more refined as new targets are gradually introduced the RMS will become smaller and the tolerance value will consequently reduce as the geometric structure of the network improves.

The shortest distance between ray projected (equations 4.27) can be used as a direct test of correspondence because the equation describes the intersection error in the 3-D space.

In the matching procedure, it is important to avoid errors due to target ambiguities and occlusions. Two stages are used to improve reliability: **a global uniqueness constraint** which uses multiple viewpoints to match all targets except where an occlusion or ambiguity occurs (stage one) and; **a local uniqueness constraint** to overcome such problems by selecting a subset of the viewpoints (stage two).

The two stage method can make the matching procedure more robust by gradually introducing additional targets. Using multi-viewpoint constraints for target correspondence can improve the reliability of matching by initially only matching the targets appearing on all viewpoints and rejecting all occluded and ambiguous targets. The iterative process allows the strengthened network to support the matching procedure. Occlusions are overcome by adding more viewpoints. Ambiguities are solved by isolating the view, on which more than one target have the same space intersection.

5.2.1. Global uniqueness constraints

Definition 5.1: An epipolar plane is defined as the space plane $P_{11}T_1P_{21}$' constructed by two space rays, along which space target T_1 projects on two image planes at P_{11} and P_{21} (Figure 5.1).

From this figure, It can be seen that the epipolar plane intersects the two image planes along two epipolar lines. Ambiguities will take place if a target lies on, or near, any other target's epipolar plane. This epipolar plane includes all ambiguous situations, for example, target T_2 is an ambiguity of target T_1.

Suppose **n** targets on the object space are projected on **m** viewpoints. There will be **m** sets of

The matching process is carried out to find G(M) from any set G(P). Each element in G(M) must be tested and the group rejected if two targets are found on the same epipolar plane. Some ambiguities can be solved at this stage. In Figure 5.2, targets T_1 and T_2 lie on the epipolar plane of viewpoints V_1,V_2, so that T_1 and T_2 are ambiguities between V_1 and V_2. However, if the global uniqueness constraint is applied to viewpoints V_1, V_2, and V_3, then: $M_1 = \{P_{11},P_{21},P_{31}\}$ and $M_2 = \{P_{12},P_{22},P_{32}\}$ are unique matching groups, consequently both sets can be accepted. In Figure 5.3, targets T_1 and T_2 lie on the epipolar plane of viewpoints V_1,V_2 and V_1,V_3. Such a situation cannot be solved with a global uniqueness constraint since the two groups, $M_1 = \{P_{11},P_{21},P_{31}\}$ and $M_2 = \{P_{11},P_{22},P_{32}\}$, both contain target T_1 so that no unique matching group exists. Targets in occlusion, (Figure 5.4) cannot be matched with the global uniqueness constraint because no group G(M) can be found. A solution can be obtained by another method which will be described in stage two.

The use of multiple views and global uniqueness constraints based on groups of target images means that matching reliability can be increased. This is because in real situations, camera orientations are only approximately known. However, the situation can be more complicated, for example, some correct targets can lie outside the tolerance and some incorrect targets can lie inside. In such a case a mismatch will result. Such problems can be reduced by adding more viewpoints, and by refining the unknown parameters of camera orientation for instance.

The bundle adjustment technique is very sensitive to any misidentification of homologous target image points. If such an adjustment is to converge only legitimate targets can be introduced into the adjustment network. In addition a solution depends on reasonable initial estimates of camera and 3-D object co-ordinate starting values. The usual method of using a bundle adjustment software package is to introduce the stronger elements first to gain good target and camera orientation parameters and then to gradually add in any remaining target image measurements. Consequently bundle adjustment procedures are generally iterative until all targets are introduced and the lowest possible root mean square residual (RMS) is gained. If any targets are incorrectly labelled, an increased RMS will result when their measurements are introduced into the network. Often the system will not converge until the offending target(s) are identified and either correctly labelled or rejected.

5.2.2. Local uniqueness constraints

This stage of the matching process is designed to remove any remaining ambiguities and occlusions. The process is carried out between pairs of images. On completion of stage one, there will generally be a large number of matched targets. These targets are included in the bundle adjustment network to enhance the geometry and to strengthen the network.

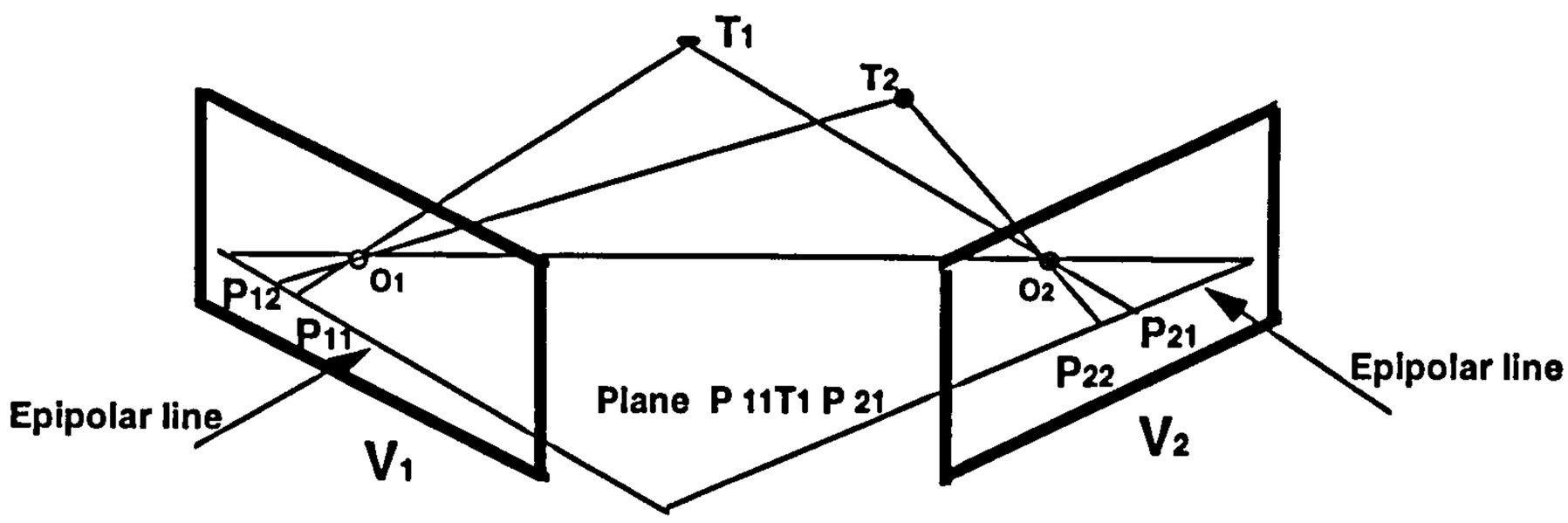

Figure 5.1 Epipolar plane.

target images $V_i = \{P_{ij_i}, (j_i = 1,...,m_i)\}(i=1,...m)$ respectively. The uniqueness algorithm can be described as follows: There is a group of target images G(P), one target image from each viewpoint, where G(P) is defined in definition 5.2.

Definition 5.2: G(P), is a set consisting of one target image in each view:

$P = \{P1j_1, P2j_2,...Pmj_m\}$ $(P1j_1 \in V_1, P2j_2 \in V_2,... Pmj_m \in V_m)$

where $V_1, V_2,...V_m$ are complete set of points in each view and the notation $j_1, j_2,... j_m$ represents one of the target images in $P_1, P_2,...P_m$ respectively.

Further, there will be a subset of points: G(M), where the minimum distance between the reprojected rays will satisfy the 3-D object space tolerance. G(M) is defined as definition 5.3.

Definition 5.3: G(M), is a set containing one target image from each view where

$M = \{P1j_1, P2j_2,...Pmj_m\}$ $(P1j_1 \in V_1, P2j_2 \in V_2,... Pmj_m \in V_m)$,

which satisfy $D_{ij} < \delta$ $(i=0,...m, j=0,...m, i \neq j)$ and $G(M) \in G(P)$.

where D_{ij} is the distance between point P_i and P_j, and d is the tolerance value.

When the set M is composed of $\{P1j_1, P2j_2,...Pmj_m\}$ the set is termed a pre-selected matching group. If another group $M' = \{P1j_{1'}, P2j_{2'},...Pmj_{m'}\}$ exists in which at least one target image corresponds to one of the target images in group M then at least two targets lie in the same epipolar plane. In such situations, both of the target images in group M and M' will be rejected as non-matching target images. If the target image in M does not appear in any other whole set, M is a matching group and labelled.

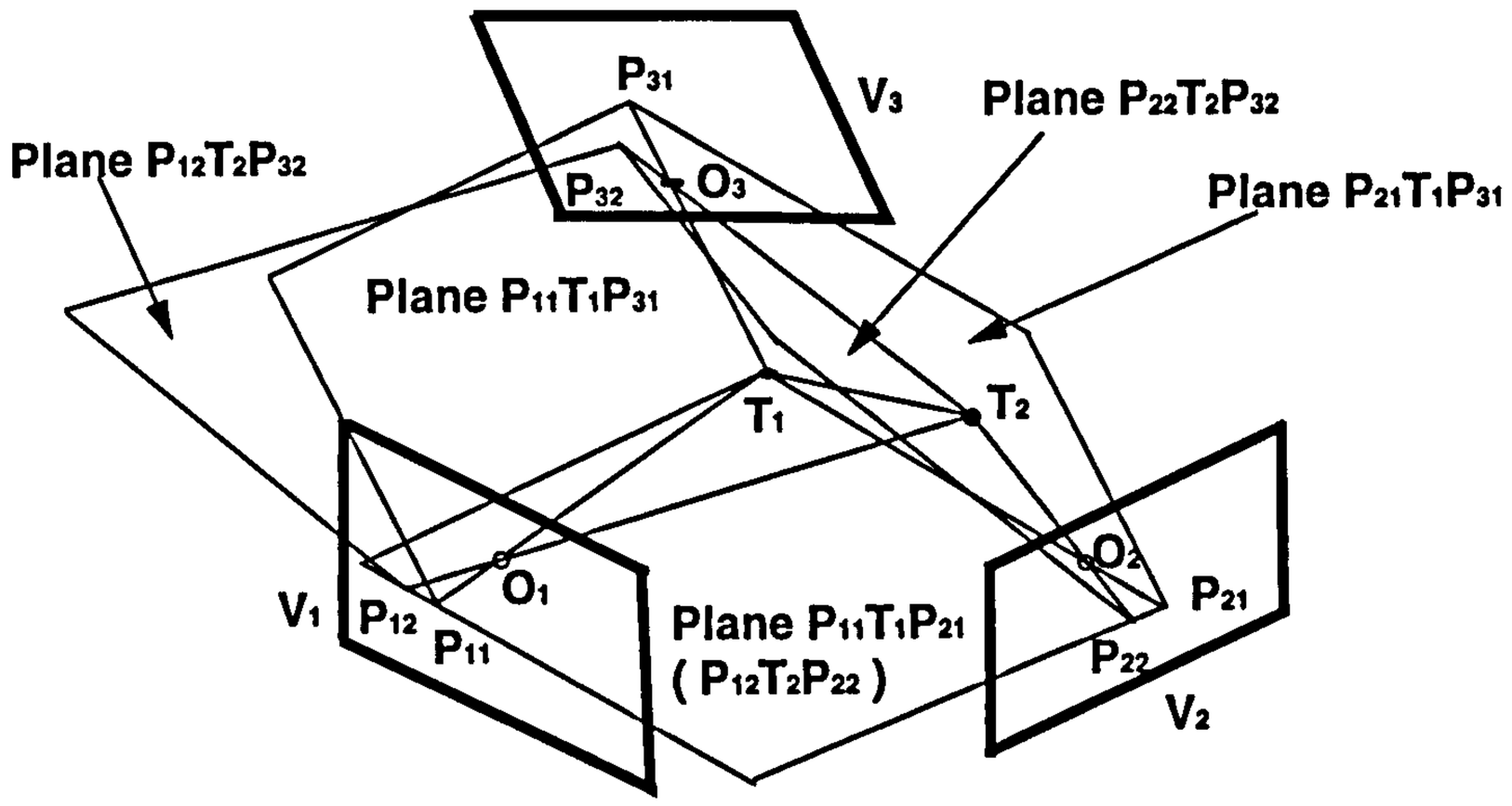

Figure 5.2 Two targets on the epipolar plane in viewpoints V_1, and V_2.

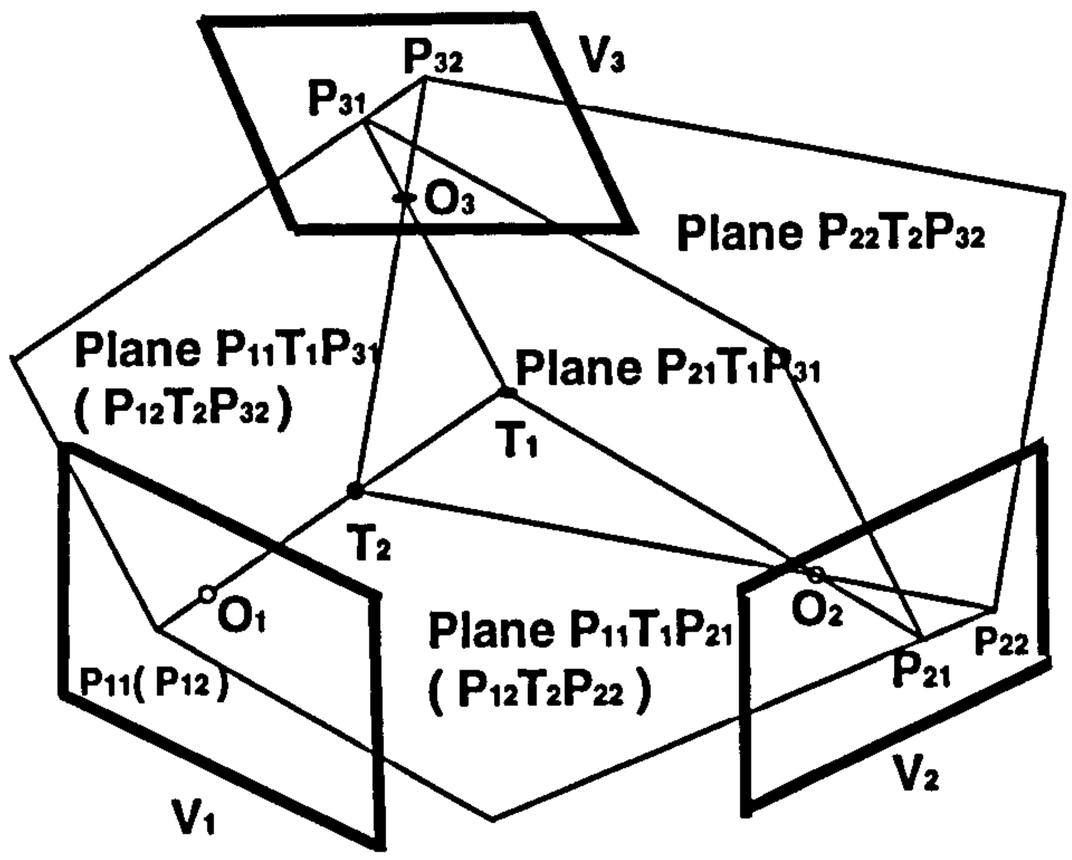

Figure 5.3 Two targets on the same epipolar planes in viewpoints V_1, V_2 and V_2, V_3.

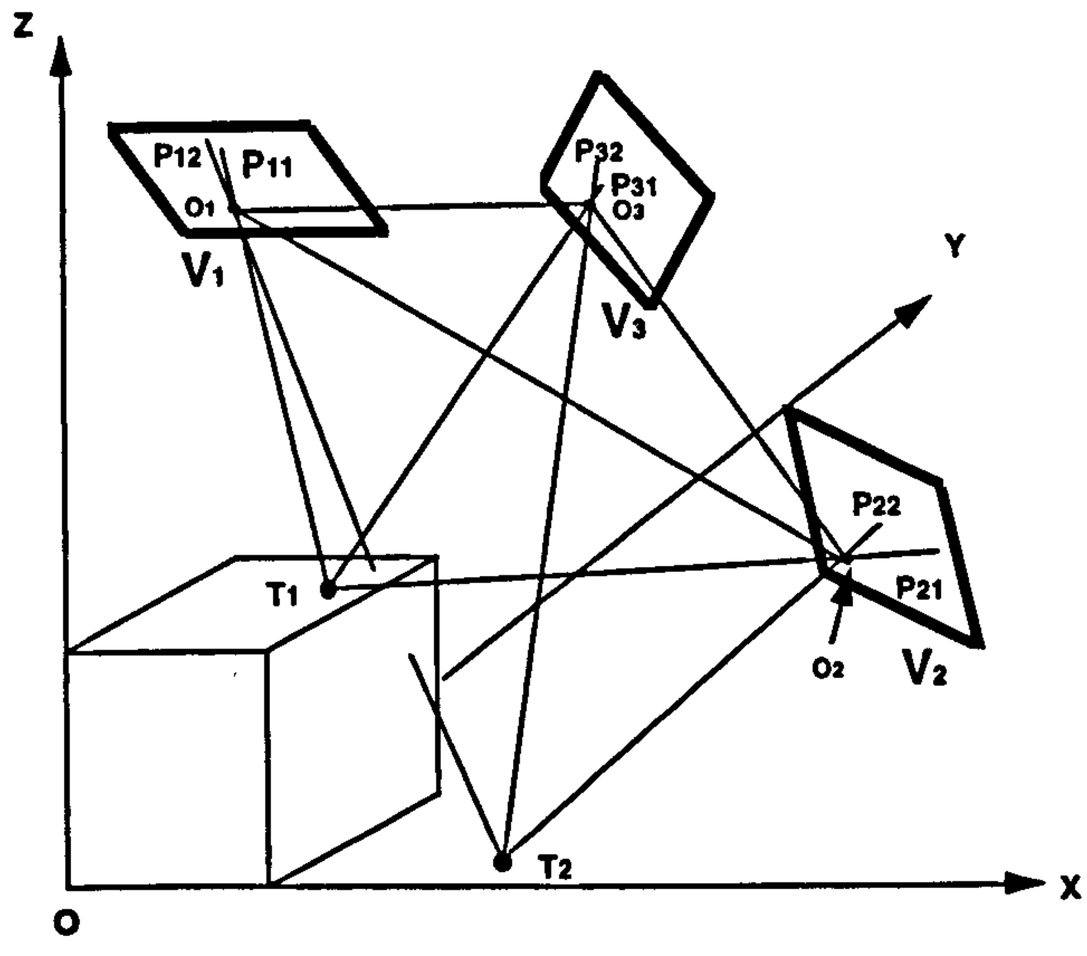

Figure 5.4 An object target occluded in viewpoint V_1.

Consequently most of the estimated parameters including any camera inner orientation parameters will have good estimations. Targets which have not been matched in stage one will have been rejected because of: occlusion in at least one image; ambiguities; or singular target images. If following stage one, the object space RMS standard deviation is small, a small tolerance can be chosen. Consequently combinations of two camera viewpoints can be used to match the remaining targets.

Initially a two point group M is found, where:

$$M = \{P_{ik},P_{jl}\}\ (i \mathrel{!}= j,\ i=1,2...,m,\ j=1,2,...,m,\ k=1,2,...,m_i,\ l=1,2...,m_j)$$

If another group M' can be found, where $M' = \{P_{ik'},P_{jl'}\}$ and in which $P_{ik'}=P_{ik}$ or $P_{jl'}=P_{jl}$, both groups M and M' must be rejected as non-matching points. If only one G(M) exists, M is a matching group and labelled. For ambiguous targets such as T_1 and T_2 (Figure 5.3), which lie on the epipolar plane of V_1,V_2 and V_1,V_3 and remain from stage one, it is possible to obtain correspondences with V_2 and V_3. Target T_2 occluded in viewpoint V_1 (Figure 5.4) can be matched by isolating viewpoint V_1 and using V_2 and V_3. However matching reliability will decrease in such cases where only two viewpoints can be used.

Theoretically, after this stage, all targets will be matched except for any targets which appear in only one image, which are indeterminate. However, under practical conditions, with very dense target arrays, problems of multiple ambiguities, for a single master image point can still occur (Maas, 1992).

The target matching procedure can be summarised by the following:

(1) The camera orientation parameters are automatically estimated by either the three side rectangle method or the laser spot extraction method, both described in chapter four, to give the starting values for camera viewpoints.

(2) A target is selected in the master image and the distance 'D' computed for all of the targets in slave images.

(3) The distance 'D' for each of the rays from the slave images is compared with the selected tolerance value. If any of the distances are within the tolerance the targets are noted as a possible match, if there is only a single value it is stored as a correct match.

(4) Procedures (2) and (3) are repeated for all targets within the Master image.

(5) Successful Xa,Ya, Za target co-ordinates are loaded into the bundle adjustment which is

recomputed. As the network gets stronger and the parameters are refined, the 3-D tolerance value is reduced and procedures (2)-(4) are repeated until all possible target matches are found and the parameters converge to pre-determined limits.

(6) The method discussed in stage two is used to match any remaining target images.

The benefits of the full 3-D method of matching combining with a bundle adjustment procedure mean that: (i) initial camera parameter estimations are not required to a high accuracy; (ii) initial values are improved by bundle adjustment based procedures; (iii) target matching tolerances can be changed during the bundle adjustment process according to a statistically derived formula; (iv) targets can be progressively introduced into the measurement network enabling a more robust correspondence matching technique; (v) the procedure is founded upon a flexible, functional model, with a statistical basis and hence, can use all available information.

5.3. Matching as a space search process

5.3.1. Local point pair matching as a tree search problem

The epipolar matching method uses the geometric relationship between the image co-ordinates, the object co-ordinates, and the orientation of the camera in each viewpoint. However, if the object is reasonably flat, a simple method which does not need camera orientation parameters can be applied. This method, which may be called global matching or affine transformation, is based on knowledge of the network geometry along with the assumption of nearly flat object (Chen and Clarke, 1992). However, To find the corresponding target images of object targets on the surface of an arbitrary shape, the 3-D epipolar geometric constraints derived in chapter four can be used. Two stages have been developed to improve the matching procedure. However, in stage one, the global uniqueness constraint requires that all of the target images in all of the viewpoints must be thoroughly searched to determine the pairs of rays which satisfy the tolerance ($D_{ij} < \delta$) criteria. Such a search procedure is inefficient, consequently methods of refining the search procedure and the implementation of uniqueness constraints through ***a priori*** knowledge must be considered.

As an example the case of Figure 5.5 is considered. Even in such a simple case, there are a number of possible combinations. A simple search method is described as follows:

- choose a target image in viewpoint one;
- choose any target image from viewpoint two;
- choose any target image from viewpoint three;

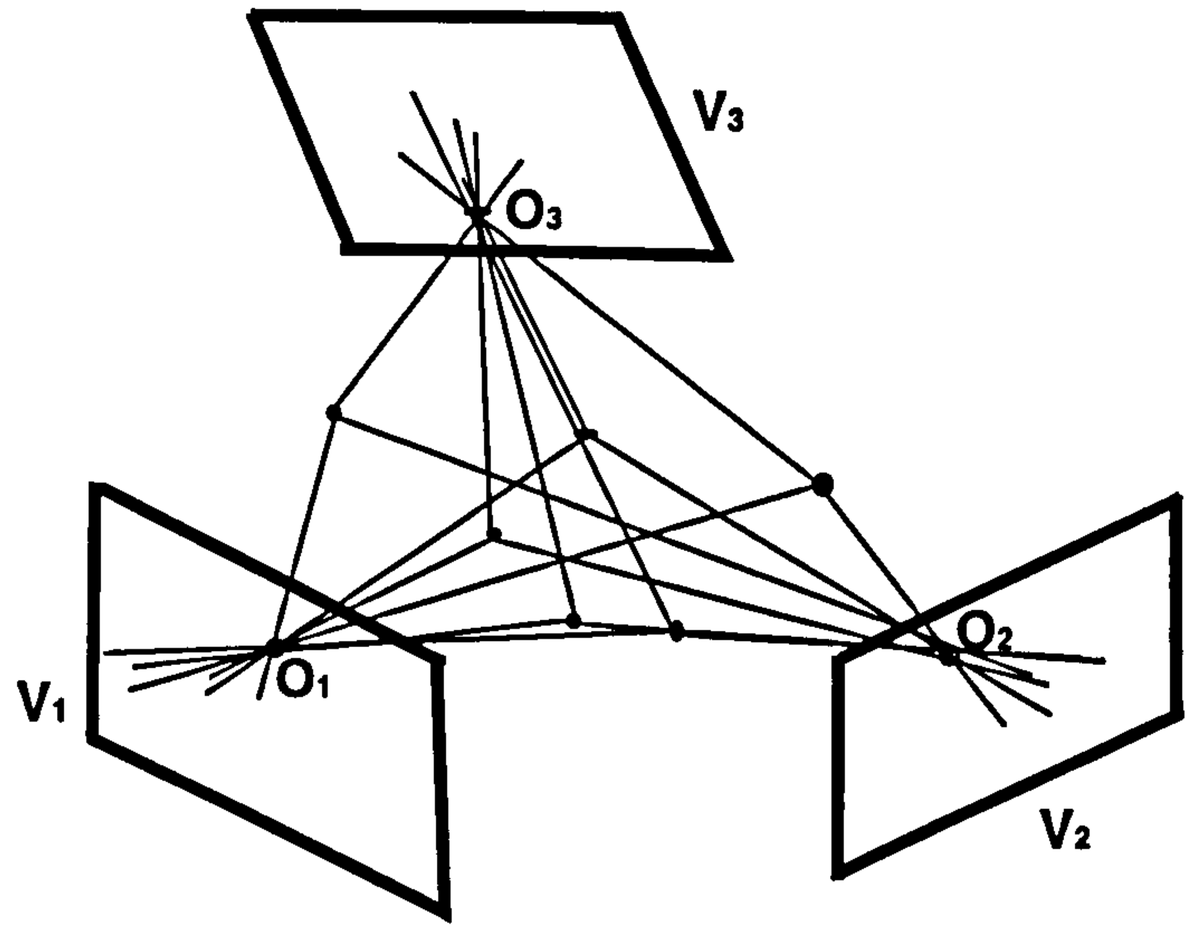

Figure 5.5 Principle of 3-D space matching.

- using the three target images chosen, calculate the distance between any two target images out of the three combinations. The target image group in which all the measured distances between rays satisfy the distance judgement is temporarily accepted as a corresponding target image group, and later accepted permanently as a corresponding target image group if none of the target images in this group are candidates in any other group;

- choose another target image in viewpoint one and repeat the above three steps.

For 3 viewpoints and 6 targets, there are 6 x 6 x 6 combinations of grouped target images. For each groups two target images need to be chosen from a three target image group, so there are 3 combinations. Therefore, a total of N = 3 x 6 x 6 x 6 = 648 combinations of distance calculations are necessary, where N represents the total matching number. Generally, if there are **m** viewpoints, **n** target images in each viewpoint (if the number of targets are equal in each viewpoint), then $N = C_m^2 * (C_n^1)^m = \frac{1}{2} * m * (m-1) * n^m$. These permutations are shown in Figure 5.6.

One way to optimise the search method is to concentrate on the group being matched. For example, the previous method can be rearranged into a matching tree (Figure 5.7). Each level is a viewpoint and the nodes are the target images in each viewpoint. If the node does not satisfy the geometric constraints, i.e., it does not correspond with the node in the level above it, the node can be removed and all the nodes below it do not need to be considered any further. This can be more efficient.

It can be seen from Figure 5.6 and Figure 5.7 that the multiple viewpoint matching process is a tree search process and by using the same terminology used in pattern recognition

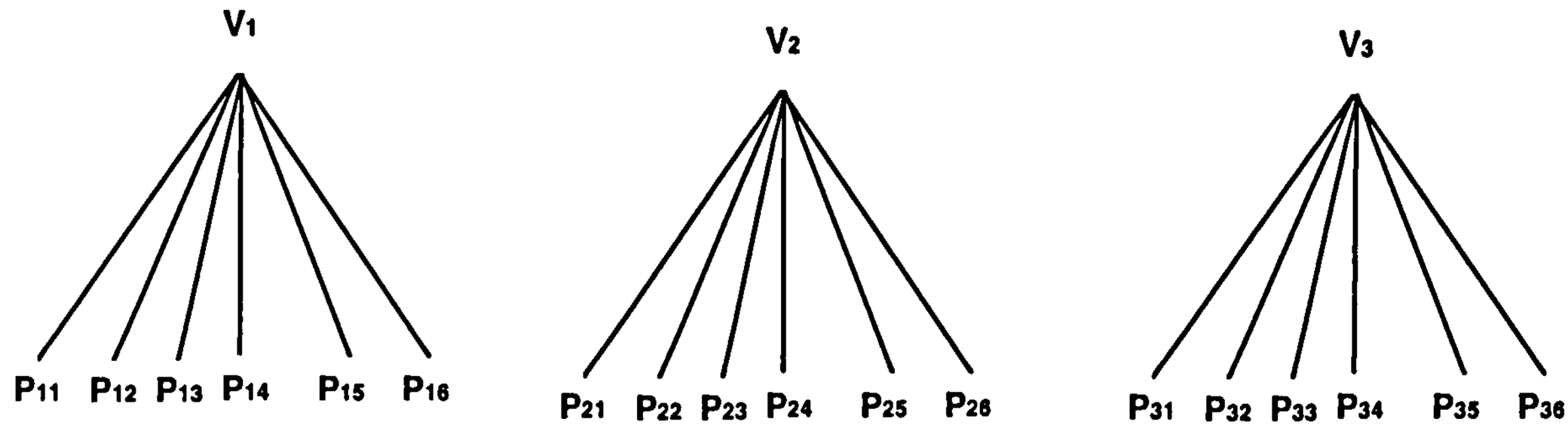

Figure 5.6 Matching combinations.

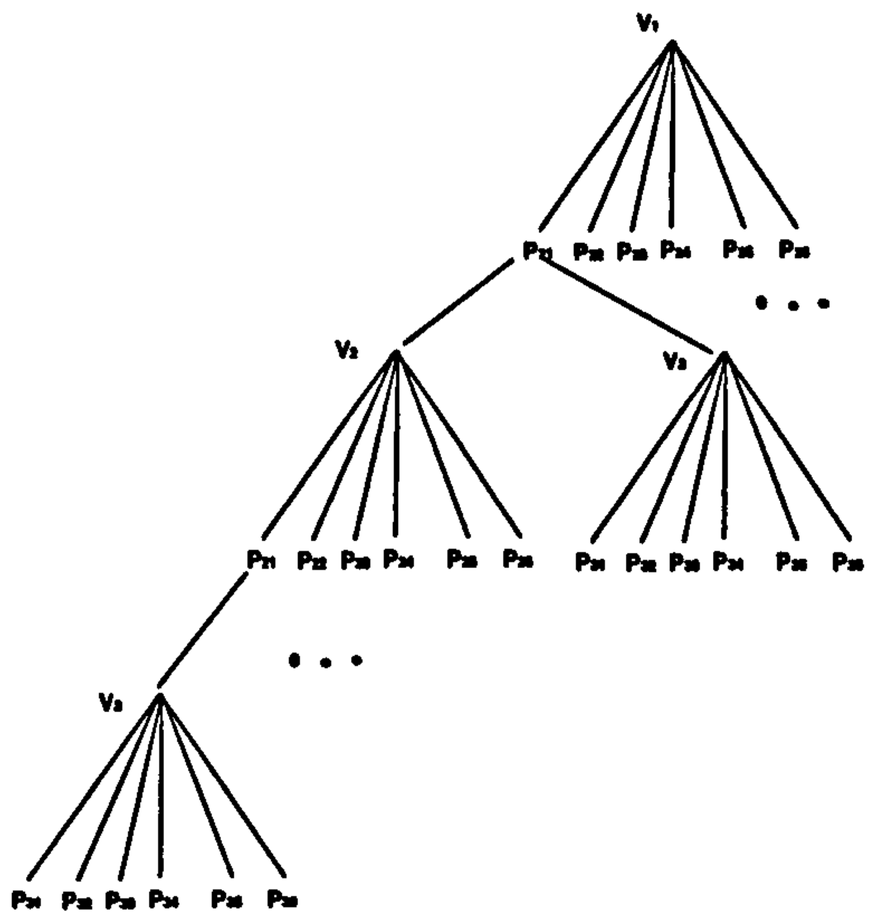

Figure 5.7 Tree search for matching.

techniques (Grimson, 1990), it is called a "matching tree search process". At each node of the tree a judgement is made concerning the matching. Such tree searches are the subject of research in artificial intelligence (Winston, 1990), and such searching methods can be directly applied to the matching process in this case.

5.3.2. Searching in the correspondence space

In this section the search space necessary to find the correct matching of the targets is discussed. The search is carried out in multiple dimensional space which consists of a set of viewpoints, each viewpoint represents a co-ordinate axis (Figure 5.8). The target images in each viewpoint are expressed by discrete co-ordinate labels on each axis. The plane of any

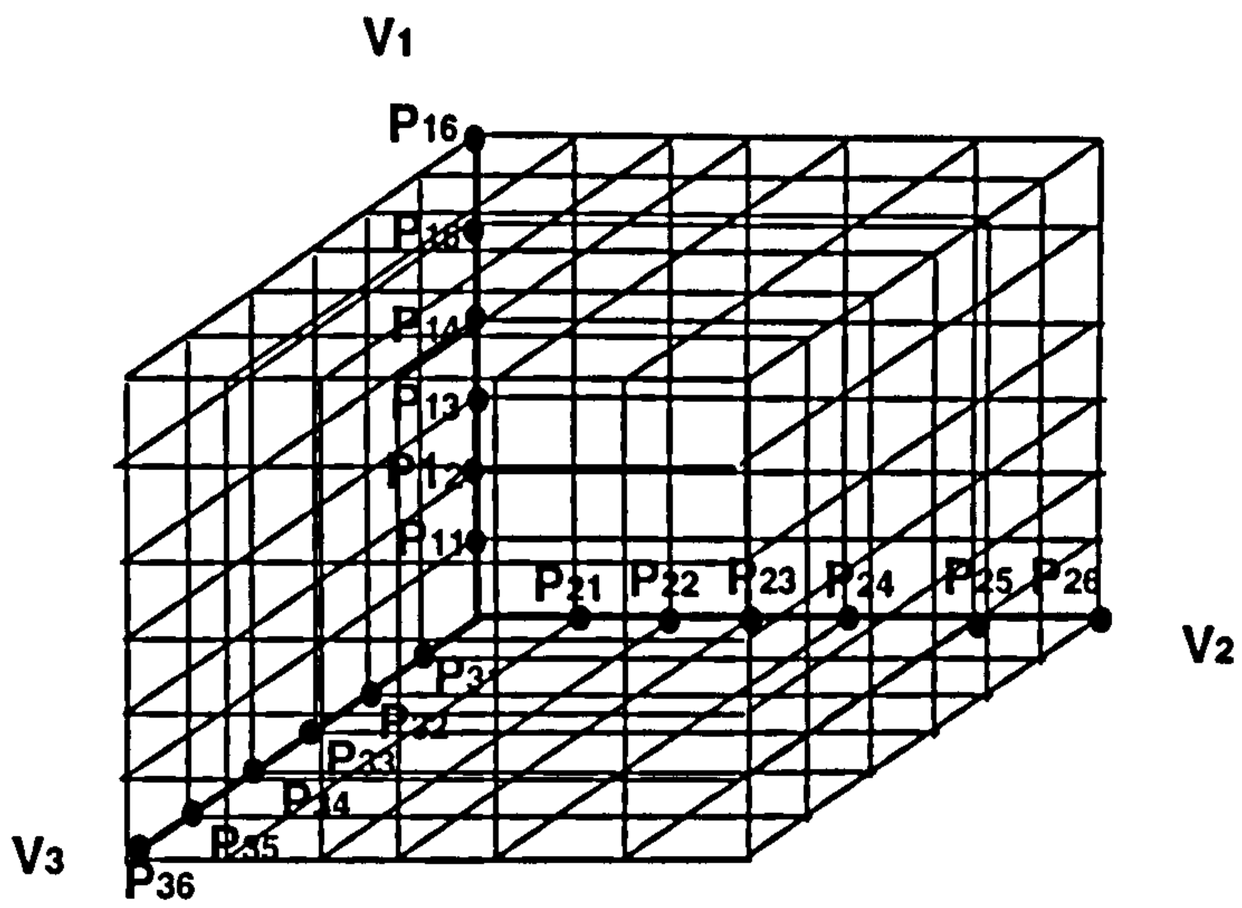

Figure 5.8 Matching space.

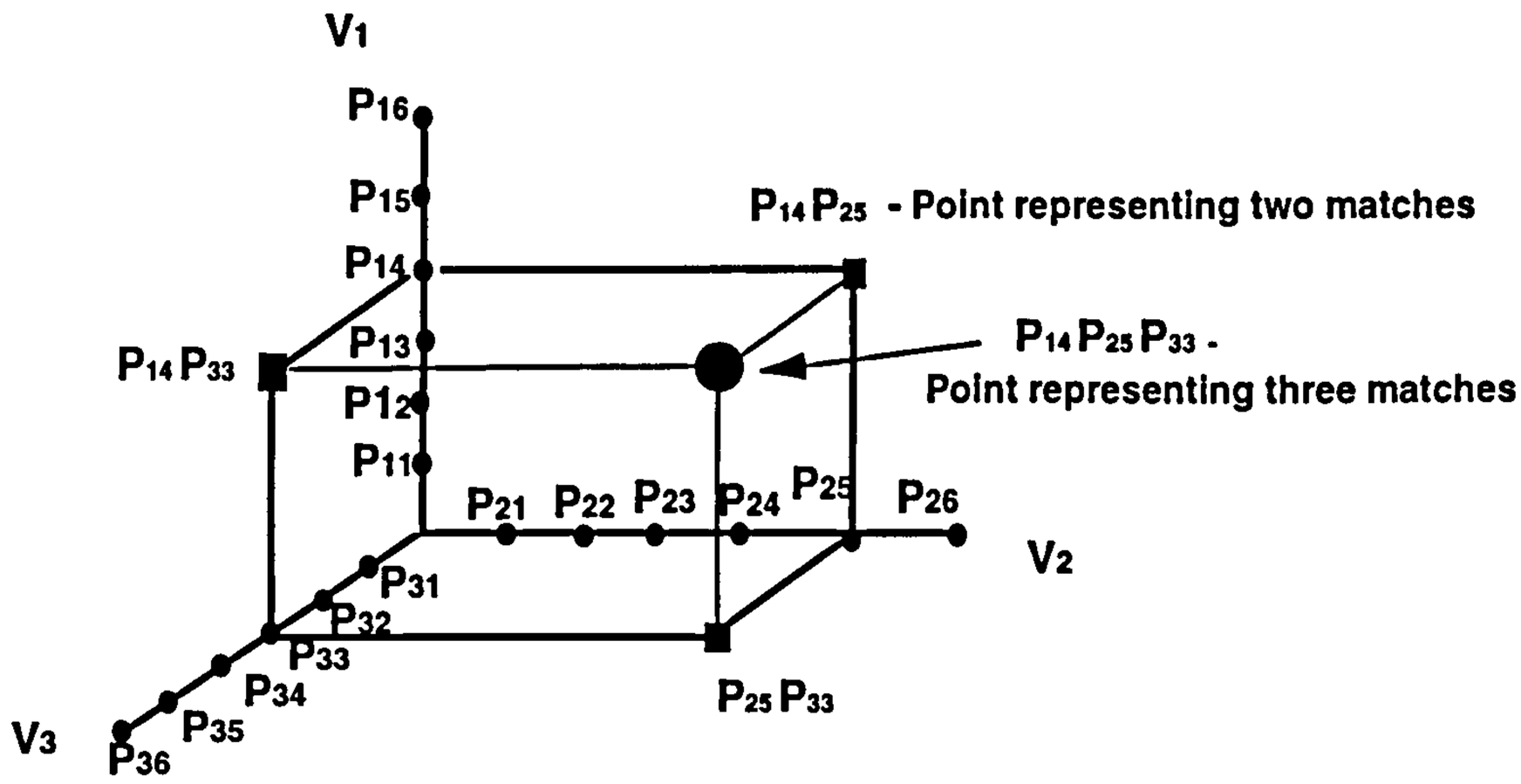

Figure 5.9 Matching points.

two axes expresses a possible match between two target images, such as those planes containing $P_{14}P_{25}$, $P_{25}P_{33}$, and $P_{14}P_{33}$ as shown in Figure 5.9. In the same way, matches among three target images are represented by the point $P_{14}P_{25}P_{33}$. This example can be represented graphically, but the extension to four matches or to greater than three viewpoints cannot. However, the methodology can be extended to **n** viewpoints. Hence the point in the **'n'** dimensional graph can be decomposed to any two axes representing just two viewpoints. If all the target images match, the target has been correctly identified in each of the viewpoints. Therefore, a straightforward way of finding the matches in the correspondence space is simply to test all the discrete points in some orderly manner. Since the correspondence space defines all possible matches, testing all nodes will ensure that all possible matches will be found. The problem with this simple approach is that for most

realistic situations, the matching space is too large for the approach to be practical. If there are 'm' viewpoints and each viewpoint has 'n' target images, then there are n^m discrete spatial points and $C_m^2 * n^2$ discrete plane points. Even with an implementation using a fast hardware design and with parallel architectures, the computational load is too large to be performed in a reasonable time period. If it is not practical to consider all of the nodes in the correspondence space, other alternative methods are needed which will minimise the number of searches without missing any valid targets. Fortunately most of the nodes in the correspondence space are generally unmatched. The key is to efficiently identify nodes which can be ignored without explicitly testing them all. If such a method can be found the computation requirement can be reduced. This can be carried out by considering individual components of a point representing two target images, say (P_{11}, P_{25}) in Figure 5.10. If there is no match, any

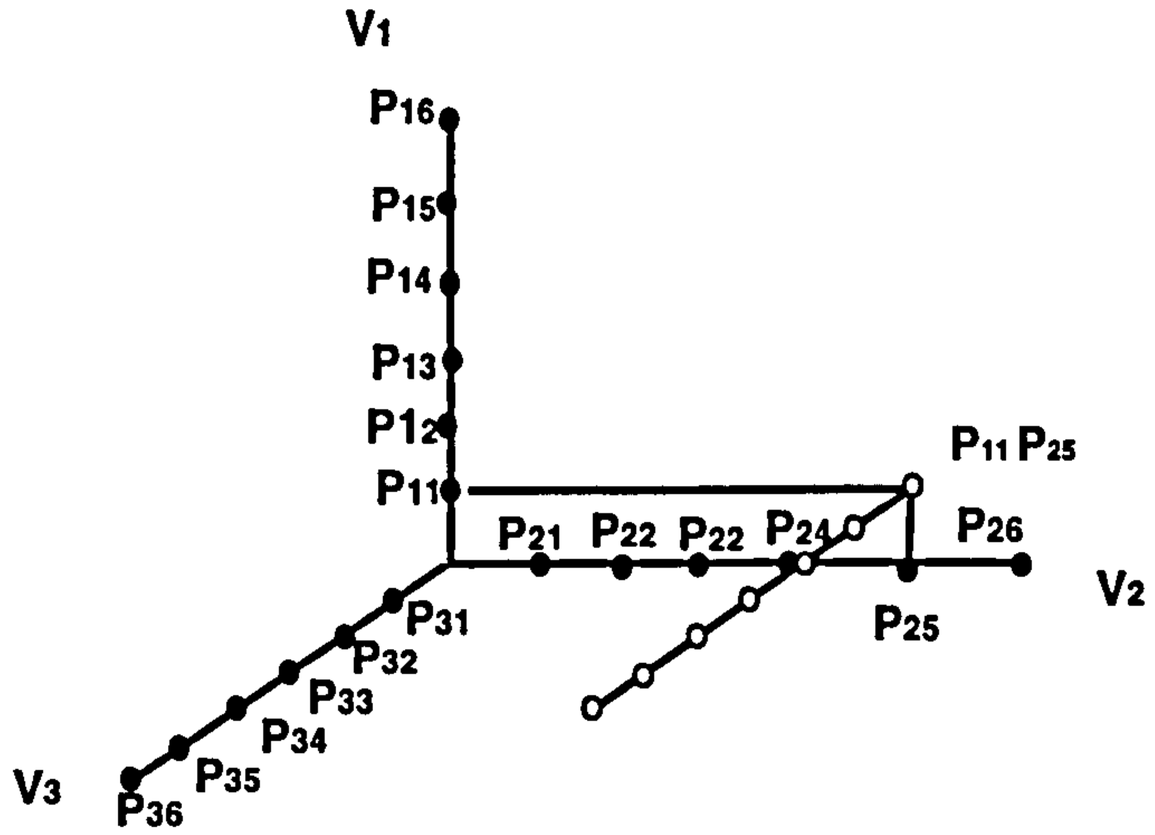

Figure 5.10 Part of unmatching subspace.

point on the axis V_3, which is parallel to the line connected to $P_{11}P_{25}$ will not satisfy the matching criteria. In such a situation, the entire matching subspace, which includes all the space nodes on the subspace, can be ignored. Similarly, for any additional viewpoints, all of the subspace accessed by passing through node $P_{11}P_{25}$ can be ignored. Such constraints can be continually used, dropping subspace whenever a non-matching group is found. This process can reduce subspace such that only a small subspace region, which has the potential for correct matching, will remain for further searching (Figure 5.11). By this method, the computation cost is reduced by isolating those portions of the search space which contain possible matches. A key aspect of this approach is the method used for searching the correspondence space in a suitable way. Several variations used for the search process and a robust search method will be discussed in following sections.

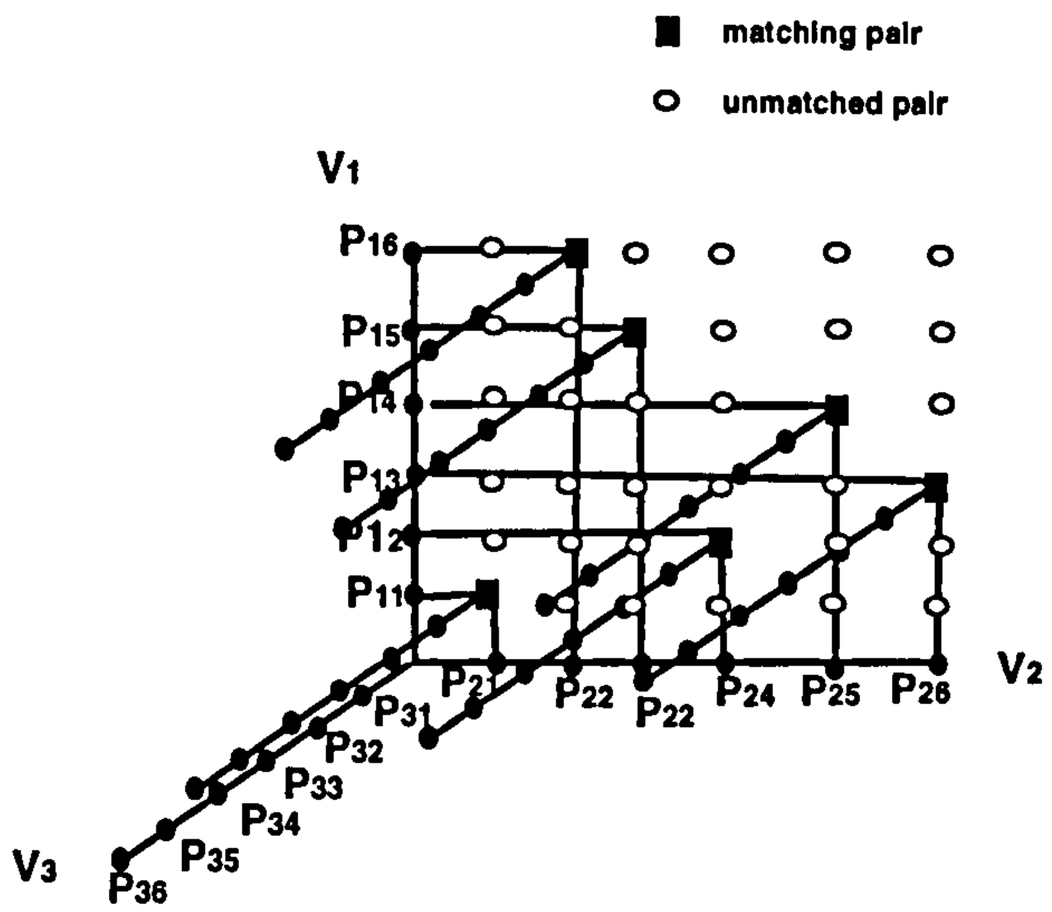

Figure 5.11 Matching subspace.

5.4. Global consistency search, hypothesis-testing, and heuristic methods

5.4.1. Global consistency searches

In the previous section, the process of matching target images in multiple viewpoints was converted into that of searching correspondence space. As a consequence, tree search methods can be used to find target correspondences. Artificial intelligence methods and model-based recognition methods have been researched over many years and many optimisation techniques have been developed (Grimson, 1990). One of these methods, the tree search, can be used in the context of target matching.

In section 5.2, the matching process was divided into two stages, stage one where the correct match was defined as globally consistent and unique, and stage two where the correct match was defined as locally consistent and unique in two viewpoints. The two stage method can produce a robust matching result. However, this method is limited to the situation where occlusions occur in every viewpoint. In this section a method is developed where a postulated correct match can be globally consistent or pseudo-globally consistent. Pseudo global consistency occurs when null targets are used to continue the tree search method when no matching targets are found in a particular viewpoint.

5.4.1.1. Depth first search

For simplicity and without losing generality, 3 viewpoints and 6 target images in each viewpoint are chosen as an example (Figure 5.12). A target image at the root level can be

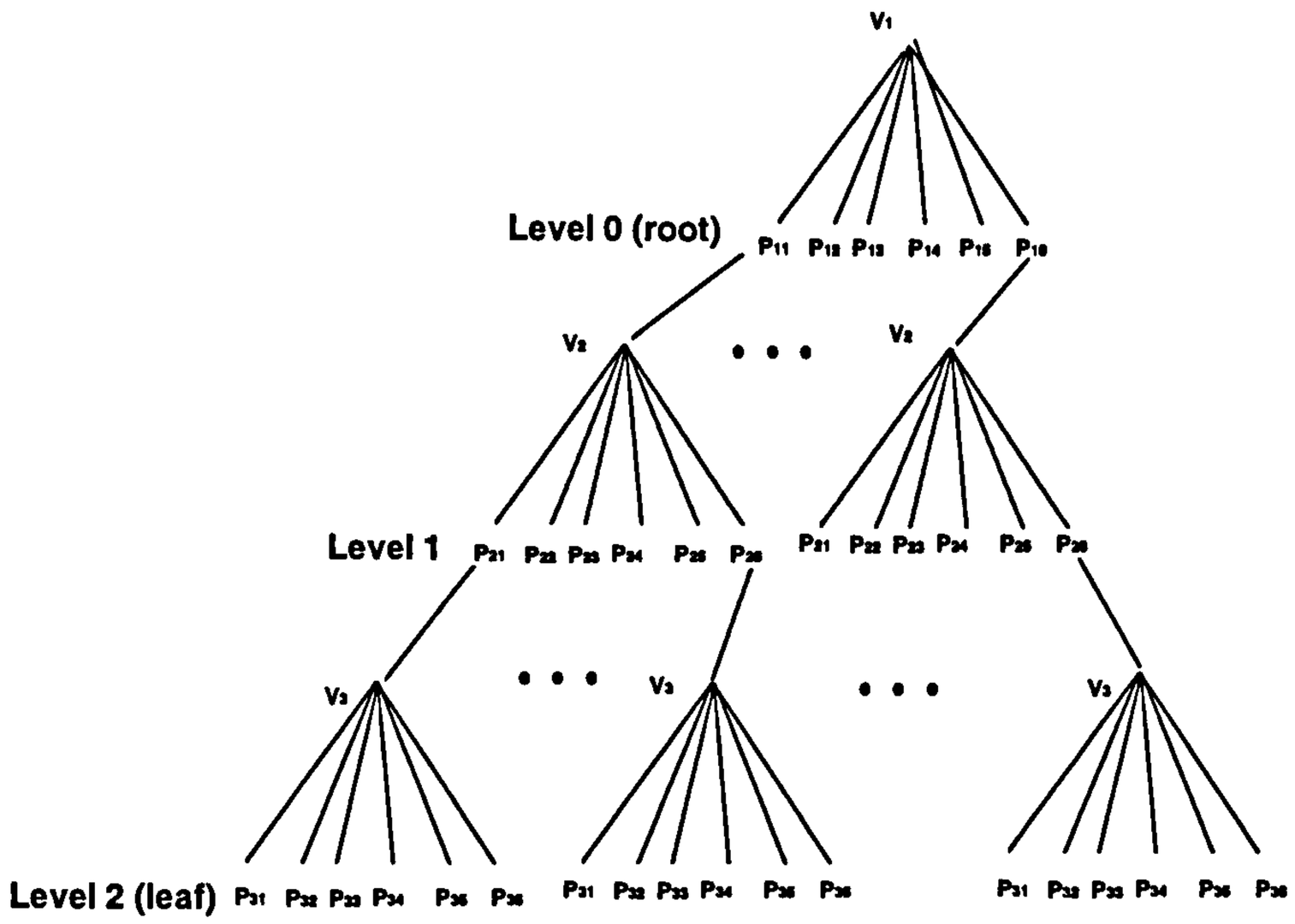

Figure 5.12 Depth first search.

chosen. The search processes toward to the leaves of the tree by passing through each level. A judgement is made between the root target image and one of the target images at level 1 (Figure 5.12). If the matching candidate is not satisfied another target image at level 1 is selected. This process continues until a target image at level 1 is encountered which satisfies the matching condition. A judgement is then made between this target image at level 1 and one of the target images, which are leaves at level 2 in this example. Tests are continued until a matching condition at this level is met. The group of target images can be expressed as: $P = \{P_{1i},P_{2j},P_{3k}\}$ ($P_{1i} \subseteq V_1$, $P_{2j} \subseteq V_2$, $P_{3k} \subseteq V_3$). The process of depth first tree backtracking is an efficient search method since the search will terminate when any node that is not matched with its upper level node is met. The search will then go back to check another parallel node. By terminating useless searches computation time can be saved. At the leaf pairs $\{P_{1i},P_{2j}\}$ and $\{P_{2j},P_{3k}\}$ may be found to be matching pairs, but an additional judgement is necessary for $\{P_{1i},P_{3k}\}$ so that global consistency can be satisfied. Generally, if there are **m** viewpoints, an extra C_m^2 - (m-1) = $\frac{(m-1)(m-2)}{2}$ matching judgements will be required after finishing (m-1) node matching judgements.

5.4.1.2. Width first search

The width first search method is illustrated in Figure 5.13. The method is similar to the depth first search method except for the different tree structure. A target image in viewpoint 1 is held fixed. After a matching pair $\{P_{1i},P_{2j}\}$ is found, the matching pair $\{P_{1i},P_{3k}\}$ between viewpoint 1 and viewpoint 3 are searched instead of searching $\{P_{2j},P_{3k}\}$. The advantage of the width first search method is that the software implementation requires only a single loop

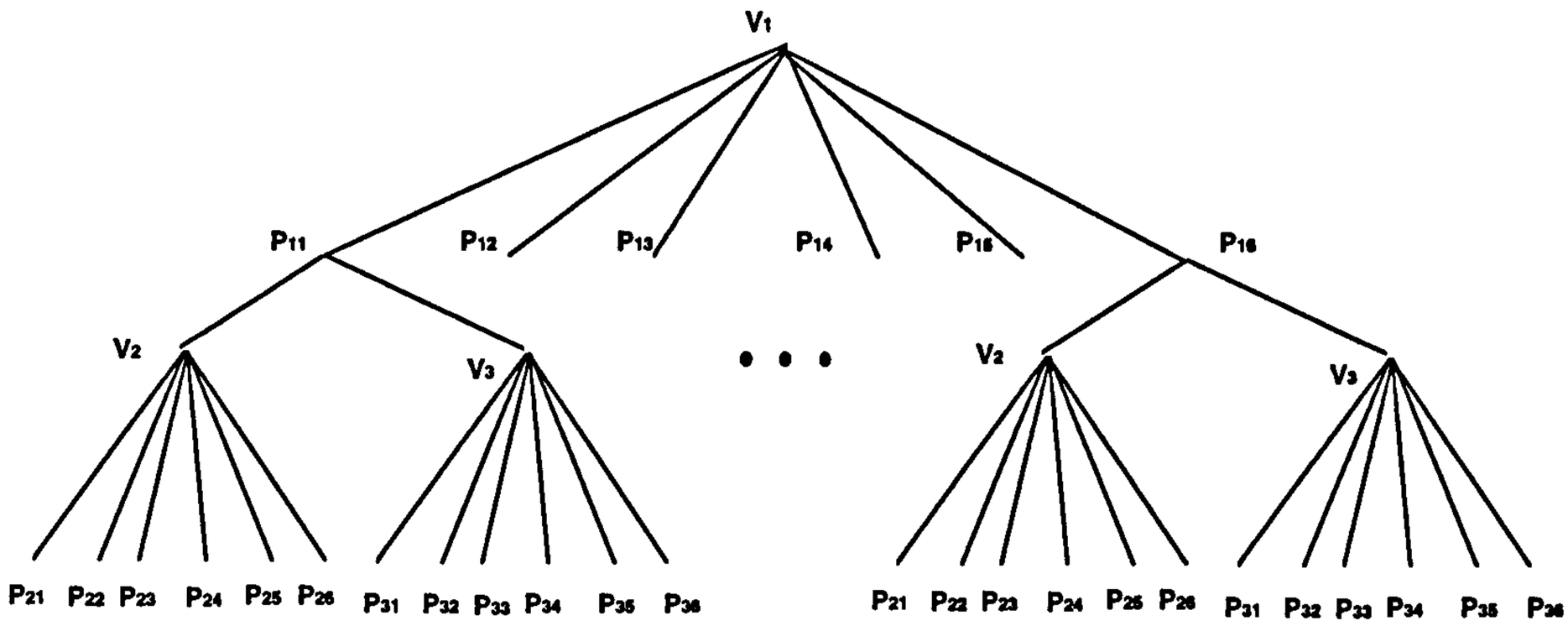

Figure 5.13 Width first search.

process to realise the search. Another difference in this method is that only the target images in V_3 are leaves. Therefore, when the search reaches any target image in V_3 and it is consistent with the node of V_2, the search obtains a possible matching group. The width first search is implemented in this thesis.

5.4.2. The introduction of pseudo targets images to deal with occlusion

The matching methods described in the previous section search along each node of the matching tree. Search criteria are based on a local minimum matching constraint of two target images. The process is continued until a leaf is encountered. At each leaf a prior match group is obtained. This method assumes that all targets are imaged in every viewpoint. However, if some of the projections are occluded, then a condition will arrive where no leaf of the tree will produce a consistent matching group. As a consequence, the constrained search method is likely to terminate its movement down each path before reaching a leaf and to finish prematurely, then a prior matching group will not be found. One answer to this problem is to extend the search method to allow for occlusions, while preserving the constrained tree tracking testing properties. Such a method can be based on the introduction of an imaginary type of target image: the pseudo target image.

At each node of the matching tree, an extra branch corresponding to the pseudo target image is added. This is shown in Figure 5.14 in the width first search mode. This pseudo target image is denoted by a "*" to distinguish it from the actual target image P_{ij}. The star indicates that the pseudo target to which it is matched is to be excluded from the final object space

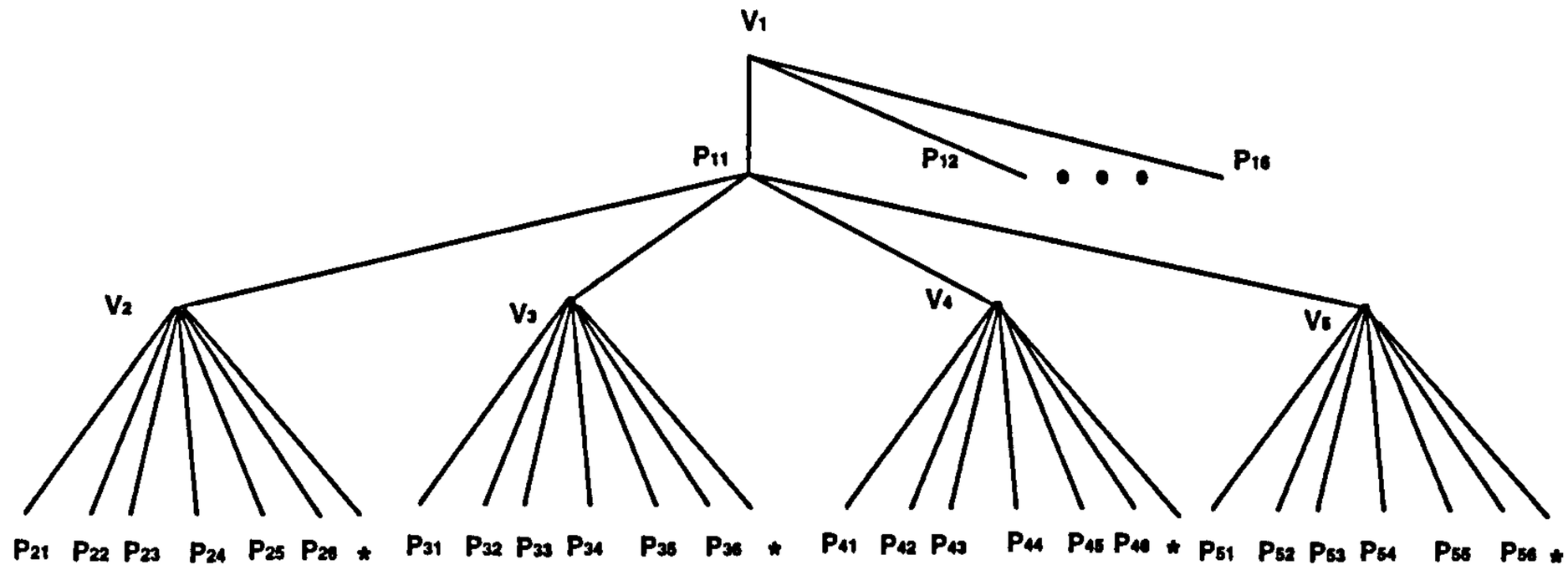

Figure 5.14 Pseudo target expression

match, and treated as spurious data. To make this addition to the matching scheme, relationships between the group of matching target images and the pseudo target image must be defined. Since the pseudo target image is excluded, it cannot affect the current matching, hence, any constraint involving the target image matched to the pseudo target image will be consistent.

With the addition of the pseudo target method it is possible for the constrained search matching to overcome occlusion problems. For example, given five viewpoints, and a target which appears in all of the viewpoints except viewpoint 3. The correct matching group should

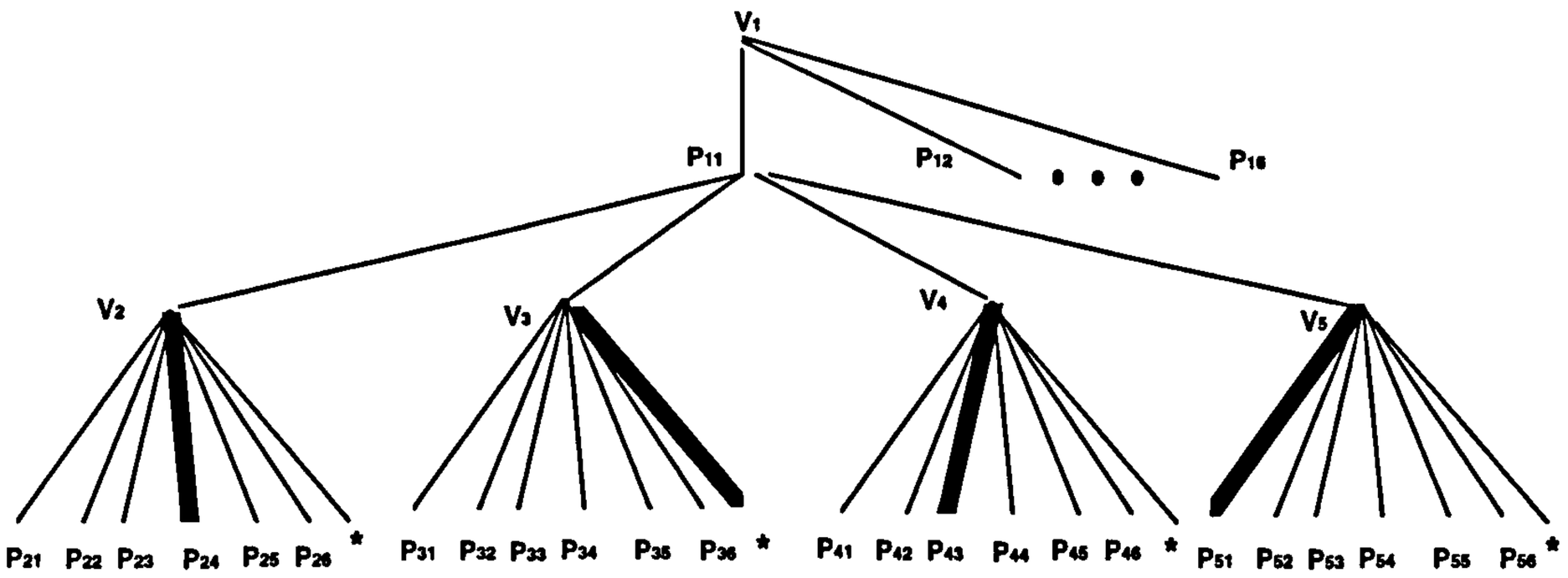

Figure 5.15 Search through pseudo target.

be M = {P_{11},P_{24},P_{43},P_{51}}. One valid matching group through the depth first search tree is shown in Figure 5.15, which passes all the viewpoints by including both the real matching target images and some pseudo target images. Hence, a hypothetical match group is obtained: P = {P_{11},P_{24},*, P_{43},P_{51}}. It can be seen that the only difference is that the number of matching target images in the match group is less than the number of viewpoints. To allow fewer target images than the number of viewpoints to be used as a correct matching group a viewpoint threshold is defined as m_t ($1 < m_t \leq m$). By this definition, even when some target images are occluded, they can be accepted as a legal matching group of target images as long as the number of matched target images is equal to or larger than m_t. Therefore, after the search arrives at a leaf and a hypothetical match group is obtained, the number of the real target images in the hypothetical match group m_r, is counted. If $m_r > m_t$, then the m_r is a real match group and is accepted. If $m_r < m_t$, the hypothetical match group is false and is rejected.

5.4.3. Sub-global uniqueness constraints

In the previous section, global uniqueness constraints in multiple views were used to overcome the problem of ambiguities and to obtain a reliable solution. The global uniqueness constraint implies that the target must be projected into the image plane of each viewpoint only once. The matched target images in one matching group should not occur in another matching group, otherwise they are ambiguous and must be rejected. Targets occluded in some viewpoints also do not satisfy the global uniqueness constraint. For some cases, all targets will be occluded in at least one view. In these cases, the pseudo target is a suitable solution to overcome the occlusion problem and allows the matching algorithm to continue working. Therefore, the global uniqueness constraint has to be redefined into a sub-global uniqueness constraint. Furthermore, the introduction of a pseudo target may also cause a reduction of the number of projections of each target. If the minimum acceptable number of projections is reduced in the match process, unreliability may result. An important question is how many viewpoints are sufficient to give correct and reliable matching. The cases of two, three, four or more viewpoints are now considered.

Two viewpoints.

It is not possible to reliably match target images projected from the same target, by using just two viewpoints and searching for the target images which lie on the epipolar plane. For a given target image in one viewpoint, there exists an infinite number of possible homologous target images in the other viewpoint. These possible homologues are on the epipolar plane of the target image. In general two viewpoints are not enough. Although the problem of occlusion of targets in one viewpoint can be solved by using a combination of any other two

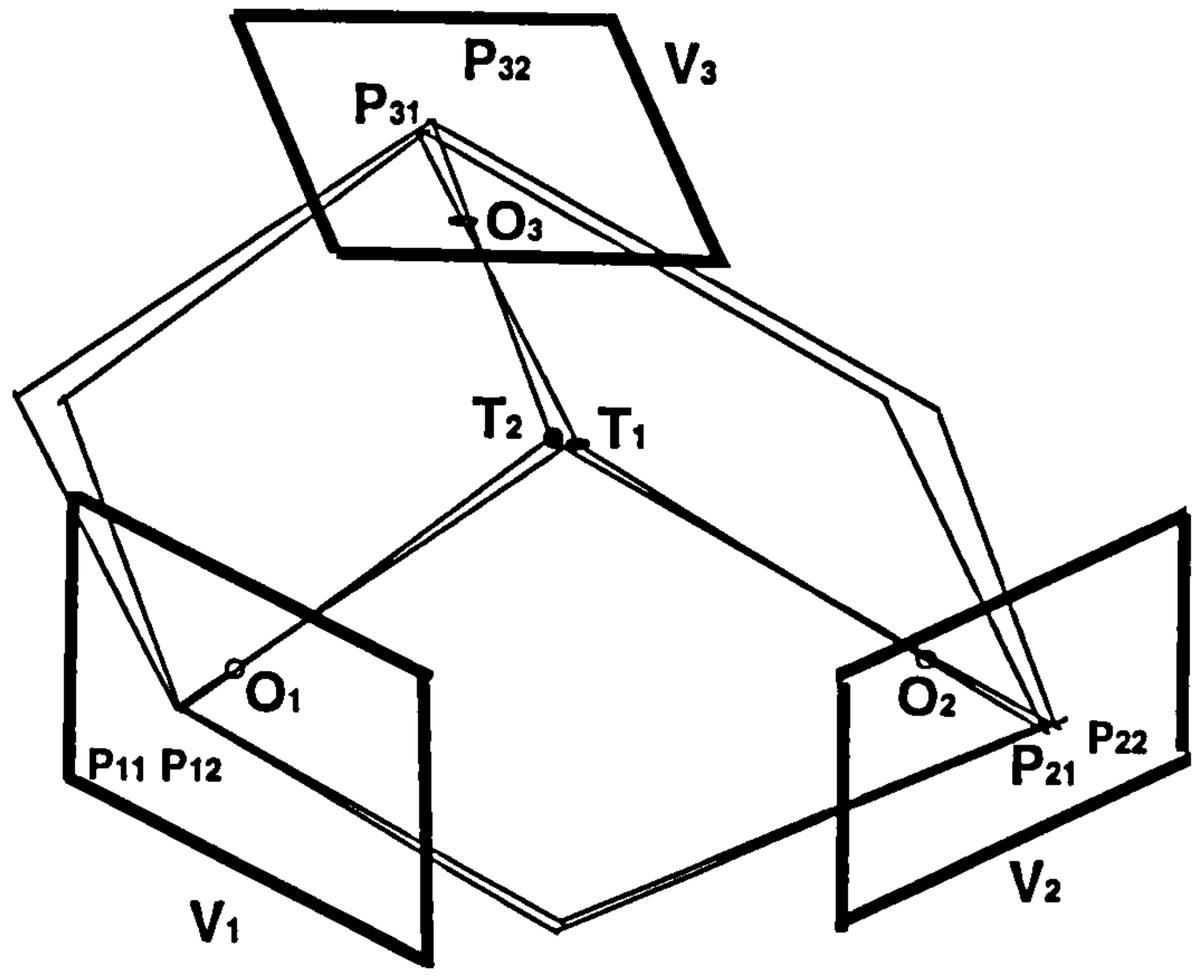

Figure 5.16 Unsolvable case one.

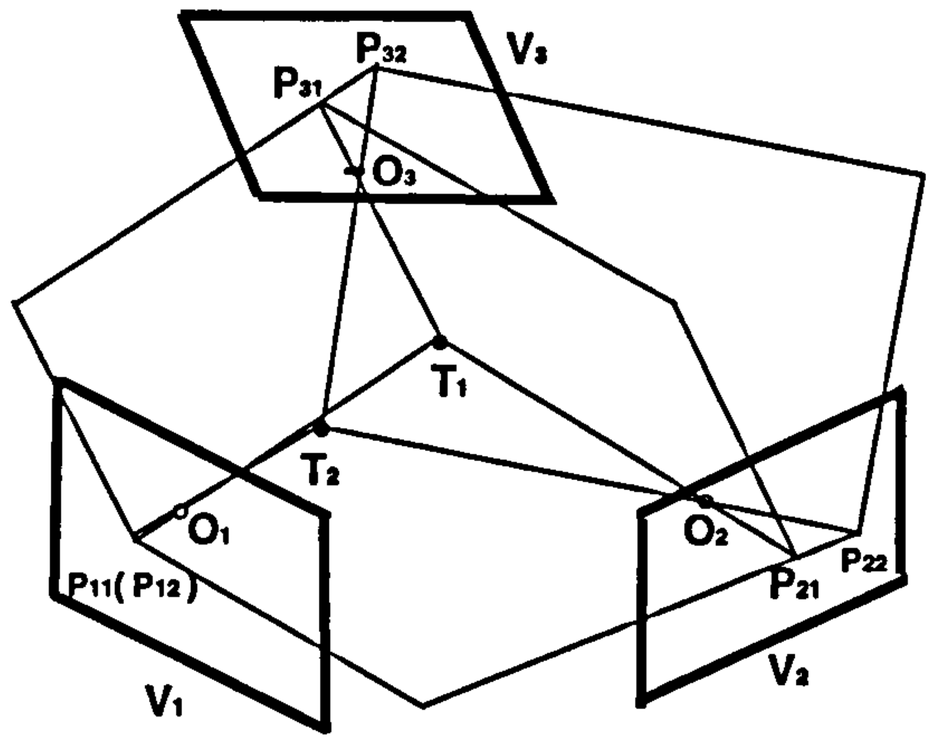

Figure 5.17 Unsolvable case two.

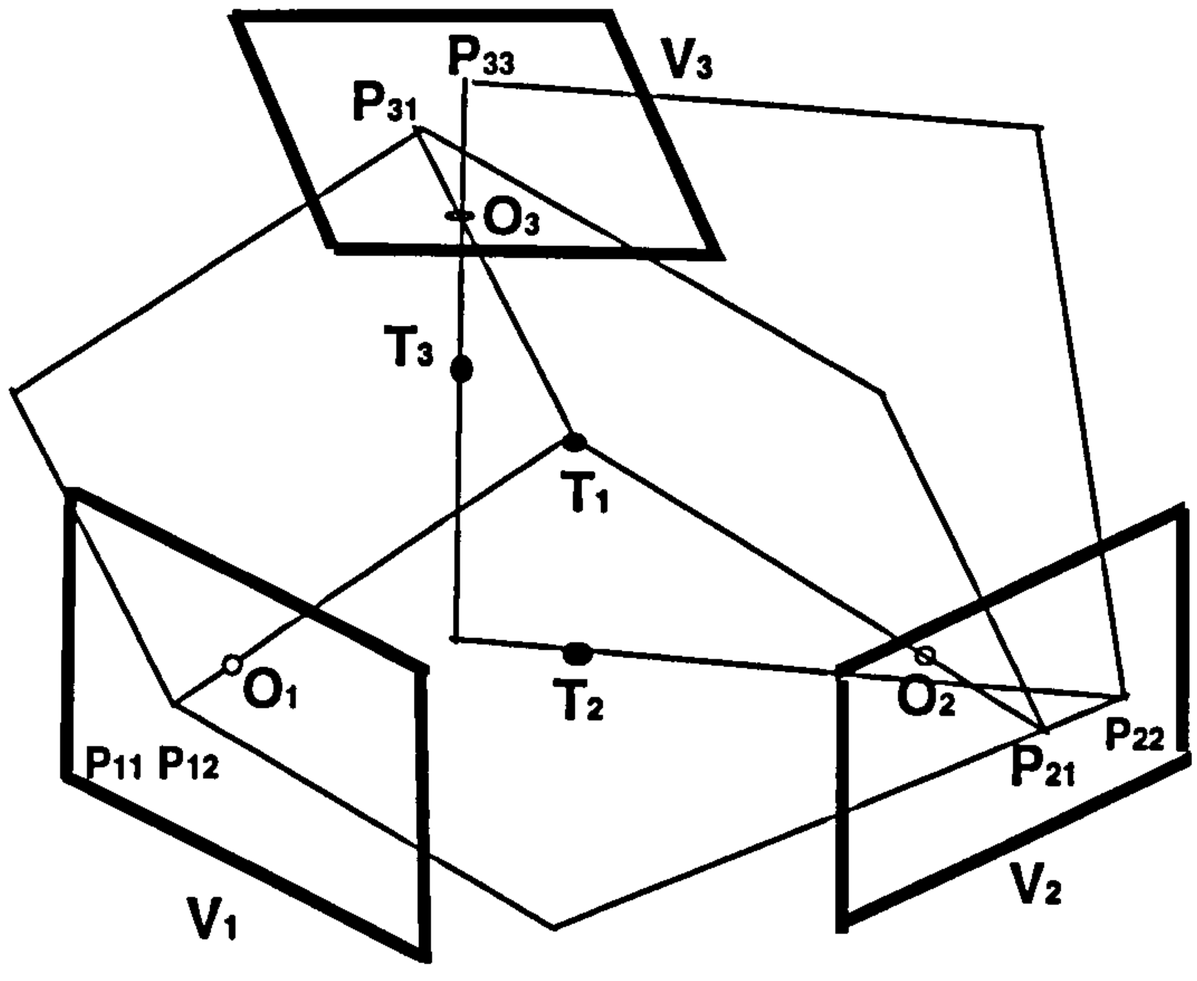

Figure 5.18 Unsolvable case three.

viewpoints, the ambiguities still remain. Any target image which lies on the epipolar plane of another target image will be ambiguous and there is no way to distinguish between them in 3-D space.

Three viewpoints.

The use of three viewpoints with the global uniqueness constraint will enable correct target matching performance. Many ambiguous target images can be correctly matching by the combination of three viewpoints, as analysed in the previous section. This combination can drastically reduce the number of ambiguities that can occur with just two viewpoints (Mass, 1992). Under these circumstances, in which camera orientation parameters are exactly known, any remaining unsolvable, but detectable ambiguities may be separated into several cases:

1). Two target images are physically too close (Figure 5.16)

2). Two target images are in line with respect to one camera view (Figure 5.17)

3). Several ambiguities coincide (Figure 5.18)

The first case can be avoided by ensuring targets on the object surface are an appropriate distance apart. The second case may be solved by isolating both target images that are too close in the image plane, but a serious ambiguity will occur if this is not detected. Furthermore, in both of these cases there will be additional problems if the camera parameters are not accurately known. The third case can be solved by using information from more viewpoints. Therefore, three viewpoints can provide reliable matching of target images in many, but not all circumstances.

Four viewpoints.

Many target images which remain unsolvable for the three viewpoints case can be solved using four viewpoints. The targets which are too close or are occluded in a single viewpoint can be successfully matched by using the targets appearing in the remaining three viewpoints and hence ambiguity problems can be overcome. The problem illustrated by case one is not solved by additional viewpoints. Four viewpoints are more reliable especially in a noisy environment, since the non-heuristic geometric constraints, that is, the epipolar plane constraints are predominant during the match procedure. The algorithm is similar to that used with three viewpoints. Four viewpoints are desirable as a minimum combination if multiple viewpoints are available. However, the situation is much more complicated in applications when the camera orientation parameters are not exactly known. This situation will seriously affect the performance of matching and will be discussed later in this chapter.

More than four viewpoints.

As more viewpoints are included reliability increases and the estimated 3-D target co-ordinates can be computed more accurately. However, some occluded targets will be missed as the global uniqueness constraint is not suitable for this situation, and the computation necessary will increase as the number of viewpoints increases. To overcome the first problem the sub-global uniqueness constraint is used. In this case the increase in computation is not as large as that when the optimised search algorithms of hypothesis-testing and heuristic methods are introduced.

5.4.4. Hypothesis-testing and heuristic methods

When a leaf is arrived at by either the depth first search or the width first search method, it cannot be guaranteed that the group $P=\{P_{1i},P_{2j},P_{3k}\}$ is a matching group, i.e. P = M. The extra group $\{P_{1i},P_{3k}\}$ or $\{P_{2j},P_{3k}\}$ must be checked. If **m** viewpoints are used, (m-1)(m-2)/2 extra checks are necessary. The extra number of matches required has a square relation to the number of viewpoints. However, a more efficient method can be used to verify the group and is discussed in the next section.

Whenever a depth first search or width first search is used, a set of hypothetical matching groups is produced. In each search method, the consistent nodes are used to decide the search path since the ultimate solution to the search requires consistency. When searching the matching tree, each leaf of the tree that is reached defines a possible matching group. However, not all matching groups will be correct. Figure 5.19 is an example of incorrect

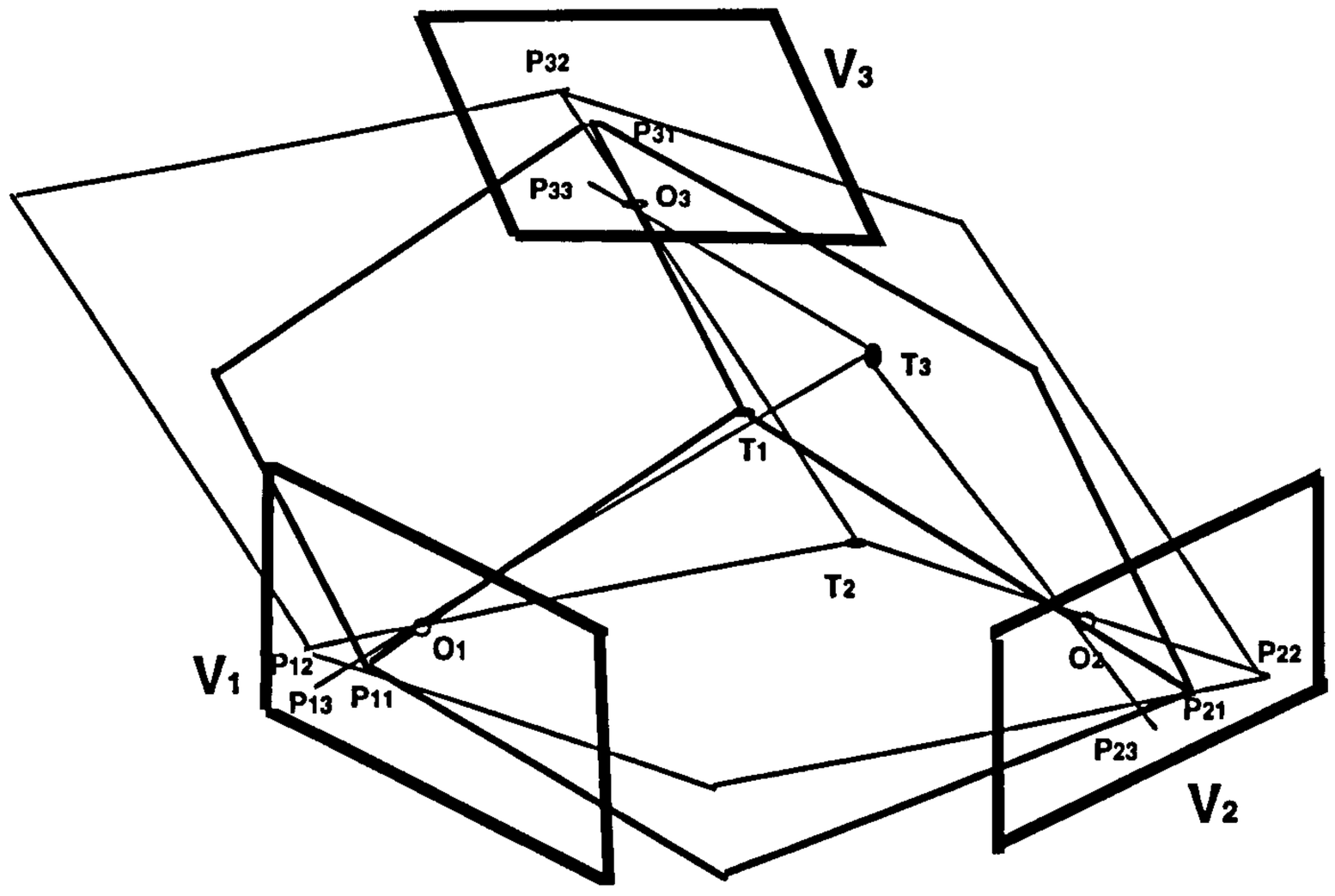

Figure 5.19 Incorrect matching.

matching. From this figure, T_1 and T_2 lie on the epipolar plane of $P_{11}T_1P_{21}$. T_2 and T_3 lie on the epipolar plane $P_{22}T_2P_{32}$. The group of target images $P = \{P_{11}, P_{22}, P_{33}\}$ will be one of the possible search results, but not necessarily the correct matching set. The correct match can be found by testing every possible group combination, unfortunately this is time consuming. A hypothesis-testing method is proposed to optimise the search time. When the search reaches a leaf, the group of target images covered by the search is considered as a hypothetical matching group. Using this group of target images, a least squares technique is used to estimate the co-ordinates of the corresponding target, i.e. the spatial position of the target. However, it is not sufficient simply to compute the object position. All the target images in the group must be checked to ensure they are the image plane projections of this target in object space. This check is carried out by using the spatial target position to verify the correctness of the match. After verifying the correct match, the 3-D target co-ordinates can be used as initial values for the subsequent bundle adjustment procedure.

A description of the method is now given:

(i) Hypothesise the existence of a matching group:

Using the search method discussed above, a group of target images, consisting of target images from the top level (root) to bottom level (leaf), is found. This group is termed a hypothetical matching group.

(ii) Refine the spatial position of the hypothetical matching group:

Using the hypothetical matching group, which is the group $P = \{P_{1i1}, P_{2i2}, \ldots P_{min}\}$ where ($P_{1i1} \in V_1$, $P_{2i2} \in V_2$,... $P_{min} \in V_m$), the 3-D co-ordinates Xa, Ya, Za can be estimated by a 3-D space intersection using least squares estimation.

(iii) Test the hypothetical matching group:

Given the spatial target co-ordinates from the estimation process (ii), the testing process can be specified.

- Let the set of parings $P = \{P_1, P_2, P_3, \ldots P_m\}$ ($P_1 \in V_1$, $P_2 \in V_2$, $P_3 \in V_3$,...$P_m \in V_m$) denote the hypothetical matching group. Given such a group, the method described in the previous section is used to solve for the target spatial co-ordinates.
- For each target image in each viewpoint P_i, the ray P_iO_i passing through the viewpoint perspective centre O_i and the ray TO_i between the estimated space target

and viewpoint perspective centre O_i are computed.

- The minimum spatial distance between the two rays P_iO_i and TO_i is then computed.
- This minimum distance must then be tested to check that it is less than the derived error bounds. If all target images in the group satisfy the test the matching set is taken as being globally correct and accepted as an authentic correct matching group. If any of the target images do not satisfy the test, the matching group is discarded.

By these means a global consistency can be enforced in the search. Such an approach is particularly appropriate when the matching group consists of many viewpoints. With this method a limited number of match judgements are used to compute the object space co-ordinates of each target, which can then be used to guide the search for additional consistent pairings.

A general optimised algorithm has been developed based on the theory discussed in the previous sections that can match targeted points, such as retro reflective circular targets, using images from multiple viewpoints. The performance of this algorithm is analysed through simulations and experimental tests later in this thesis.

5.4.5. Optimised 3-D target matching algorithm

The goal of the 3-D matching algorithm is to find the correspondences of target images seen in multiple viewpoints correctly and completely. The matching tree is constructed and the heuristic tree search is carried out to find the prior matching group. Pseudo targets are used to by-pass any target occlusions and to force the tree search to reach the leaf of the tree. The hypothesis-testing method is used to confirm the correct matches and initial 3-D targets co-ordinates are computed. These matched targets are then placed into a bundle adjustment to accurately and reliably measure and reconstruct the 3-D co-ordinates of points on the object. The 3-D target matching algorithm proceeds in several stages:

1. Initialisation: Given the orientation parameters of each viewpoint derived in chapter 4, the search tree is initialised and a search strategy is built.
2. Search and hypothesis: The search proceeds through the tree, passing each node in turn. The match condition is determined according to the epipolar plane constraints. Searching is continued until a leaf of the tree is found. The group of nodes are then marked as a hypothetical match set.
3. Refine: Using the hypothetical matching set of target images, the location of the corresponding target in the object space is computed by least squares techniques.

4. Validation and verification: The validity of the match set is tested using several conditions. Firstly, each of target images in the hypothetical match group is investigated independently, each should be a projection from the same target in the object space (within some error bounds). Secondly, each target image is compared with all other matched target images in the matching list. If any of the target images in the group violate the sub-global uniqueness constraint at the same level, both the group and the set in the matching list are labelled as non-usable matching sets. If these checks are passed, the set of matching target images is placed into the matching list and the object space location of the target computed to provide starting values for subsequent bundle adjustment.

5. Repetition of steps 2, 3 & 4 allows the search process to be repeated using different levels of combinations, that is, from the maximum number of viewpoints to the chosen minimum number of viewpoints (four in most cases).

6. Addition of the new target co-ordinate sets to the bundle adjustment to refine the camera parameters.

5.4.5.1. Initialisation algorithm

The procedure for the initialisation is shown in Algorithm 5.1.

The algorithm is described by a pseudo C code. Such code can be easily converted into C language source code for programming.

In algorithm 5.1, the matching algorithm is initialised by determining camera starting values,

Algorithm 5.1 (Initialisation)

Procedure Initialisation

- Get the orientation parameters of each viewpoint
- Allocate an array for storing search tree nodes

For each viewpoint V_i ($i=1,\ldots, m_{i-1}$)

For each viewpoints V_j ($j=i,\ldots, m_i$)

- Determine the space distance from the two space rays
- Put the distance value into the appropriate tree node

Endfor

Endfor

Endprocedure Initialisation

Algorithm 5.2 (Search and Hypothesis)

Procedure Search_Hypothesis

For each viewpoint V_i (i=1,...,m_i-m_s)

- Label each unmatched target image

For each target image P_{il} in viewpoint V_i (i=1,...,m_i-m_s)

For each viewpoint V_j (j=i+1, m_i)

For each target image P_{jk} in viewpoint V_i(i=1,...,m_i-m_s)

- Compare the distance $D\{P_{il},P_{jk}\}$ between $\{P_il,P_{jk}\}$ with δ

If $D\{P_{il},P_{jk}\} < \delta$

then put Pjk into the hypothetical matching group, break ;

else continue searching with the next target image in this viewpoint

Endfor

if no hypothetical matching target image group is found in this viewpoint

then use pseudo target image

else increase the matching count

Endfor

if matching count > m_s

then a hypothetical matching group exists

3D_Estimation

Validation_Verification

else search next target image in viewpoint V_i

Endfor

Endfor

Endprocedure Search_Hypothesis

Algorithm 5.3 (3-D Targets Position Estimation)

Procedure 3D_Estimation

- use of the hypothetical matching group as the projection of an object space target
- put the estimated orientation into collinear equation for intersection
- determine the object space co-ordinate {X,Y,Z} of the 3-D target by least squares (space intersection)
- put {X,Y,Z} co-ordinates into the library of object space target initial values

Endprocedure 3D_Estimation

Algorithm 5.4 (Validation Verification)

Procedure Validation_Verification

For each viewpoint Vi (i=1,...,m_i)

- Check the distance d between the object space target and the ray created by the target image in this viewpoint

  If $d < \delta$

  then next target image

  else the hypothetical match group is invalid, return

Endfor

For each viewpoint Vi (i=1,...,m_i)

- Check the global uniqueness constraint
- Check the target image with the library of matched groups

  If the target image exists in the library

  then it violates the constraint, put both groups into non-matching library, break;

  else check next target image

Endfor

- Verification success, put the group into the matching library

Endprocedure Validation_Verification

allocating memory for nodes and building the matching tree. Each node is represented by the distances between two projected target images from each individual viewpoint.

5.4.5.2. Search and hypothesis

This procedure is illustrated in Algorithm 5.2.

5.4.5.3. 3-D target position estimation

This procedure is illustrated in Algorithm 5.3.

5.4.5.4. Validation verification

This procedure is illustrated in Algorithm 5.4.

5.5. Evaluation of the method by simulation and experiment

To evaluate the matching method developed in this thesis several experiments were designed to analyse the matching performance under a variety of conditions. These experiments include both simulation and practical tests.

5.5.1. Evaluation by simulation

In order to quantitatively analyse the performance of the 3-D optimised matching algorithm, a computer simulation software package has been written. By simulating the conditions which give rise to matching problems, the performance of the algorithm cam be rigorously analysed by concentrating on one error source and isolating other error sources.

5.5.1.1. The simulation package

A simulation package has been written for the Microsoft Windows^{TM} environment. The appearance of the computer simulation system is shown in Figure 5.21. The advantage of building this simulation package is that it is not only useful for testing the 3-D matching algorithm, but the bundle adjustment algorithm or other photogrammetric algorithms can also be analysed. In the system, a number of cubes of random size, position, and rotation, can be created. On each side of each cube a number of targets can be randomly distributed. All relevant parameters, such as: the number of cubes; the number of targets on each side; the cube size; or the viewpoint position; are variable. By changing the position of the viewpoint, various views can be generated of the object such that ambiguities, occlusions and single

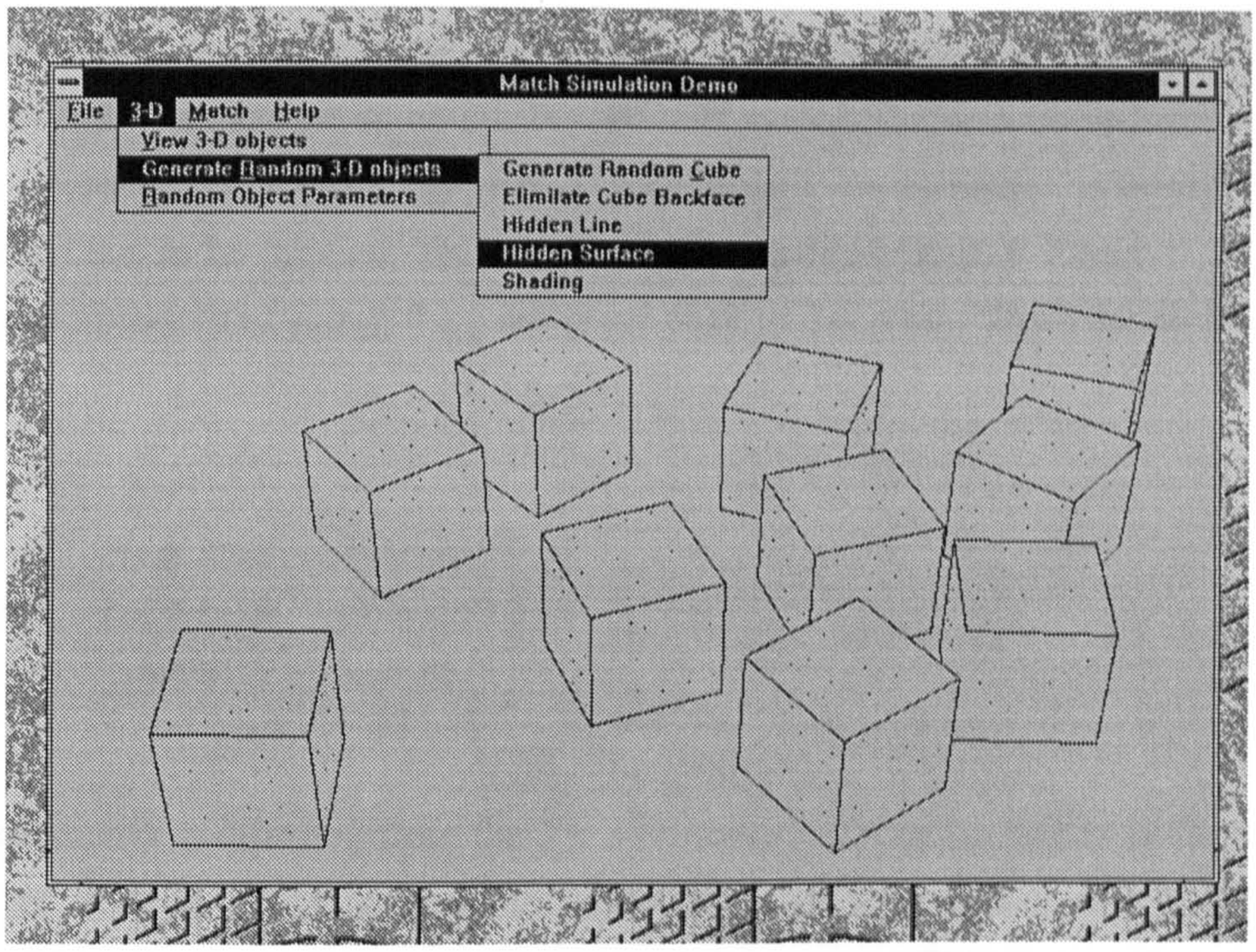

Figure 5.21 The simulation system under Microsoft Windows^{TM} environment

projections are likely to occur. For simplicity, the three rotation parameters are dependent on the three position parameters by constraining each camera view to point straight towards the origin of the co-ordinate system which the cubes are randomly created around. For convenience some modules in the simulation system, such as hidden lines and targets of cubes, are based on the viewing transformation of Ammeraal, 1992, who uses a spherical co-ordinate system to build the viewing transformation. The three rotation parameters ω, φ, and κ, often called Euler angles, must be calculated by converting the spherical co-ordinate system to a Cartesian co-ordinate system. The calculations of the three rotation parameters ω,

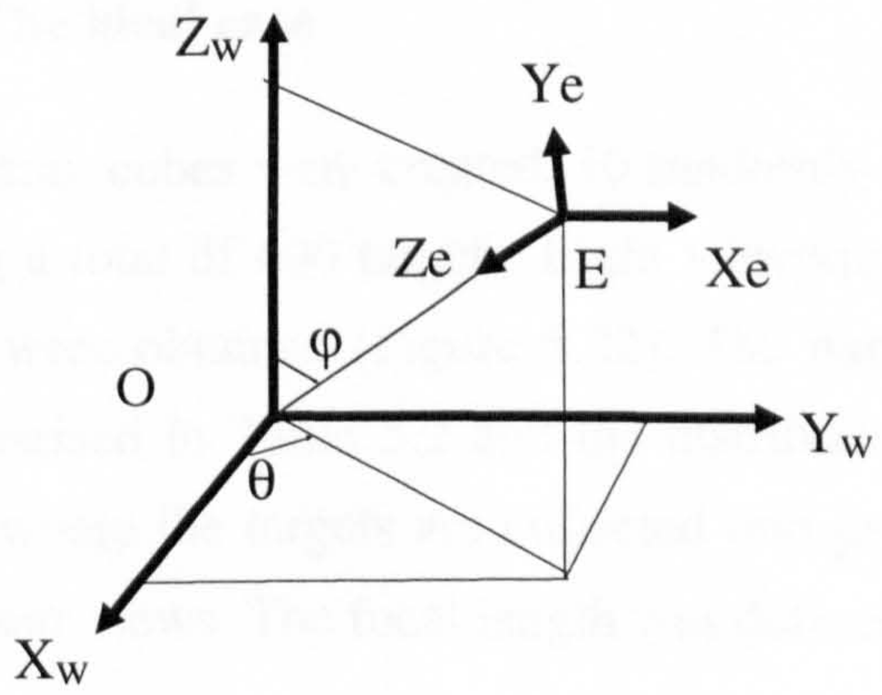

Figure 5.20 The perspective transformation in spherical co-ordinate system

φ, and κ are as follows: To complete the co-ordinate transformation of cubes and targets from the object co-ordinates system to an eye co-ordinate system (camera co-ordinate system) and then to a screen co-ordinate system (view image co-ordinate system), a viewing transformation has to be applied. The transformation is illustrated in Figure 5.20. Given the position co-ordinates $E(x_e,y_e,z_e)$, the j and q are easy to calculate. The rotation matrix is then obtained as:

$$V = \begin{bmatrix} -sin\theta & -cos\varphi\cos\theta & -sin\varphi\cos\theta \\ \cos\theta & -cos\varphi\cos\theta & -sin\varphi\sin\theta \\ 0 & \sin\varphi & -cos\varphi \end{bmatrix}$$

This rotation matrix is different from the 3 x 3 orthonormal rotation matrix in Equation 2.1 as the values of θ, φ in this matrix are different to ω, φ, κ in Equation 2.1. However, the numerical values of the nine elements are exactly the same. This means that the elements m_{11}-m_{33} in both matrixes have the same values (Methley, 1986) so that the three Euler angles ω, φ, and κ may be directly calculated. However care must be taken when judging the quadrant and the sign of the three Euler angles when the viewpoint is positioned in a new quadrant.

This matrix transformation is also useful as the transformation can be used to estimate the starting values of ω, φ, and κ for bundle adjustment iterations based on only the three position parameters. Various viewpoints can be obtained by changing the three viewpoint co-ordinates $E(x_e,y_e,z_e)$. All cubes and targets have hidden surfaces and occluded targets so that the images generated are similar to those from real camera views.

5.5.1.2. Test one: The ideal case

Ten 100x100x100 mm. cubes were created. 10 randomly distributed targets were then placed on each side giving a total of 600 targets. Eight viewpoints were defined (Table 5.1) so that eight image views were obtained (Figure 5.22). The number of available target images for each view is summarised in Table 5.2 and the distribution of the visibility of the targets is given in Table 5.3 where the targets are collected into groups with, for instance, targets that will be imaged by four views. The focal length was defined as 25mm without any distortion.

Given perfect target image co-ordinates and camera orientation parameters, the correspondence algorithm can successfully match all the targets in this experiment which have between four to eight projections with a tolerance value between 0.4mm to 7mm.

View 1

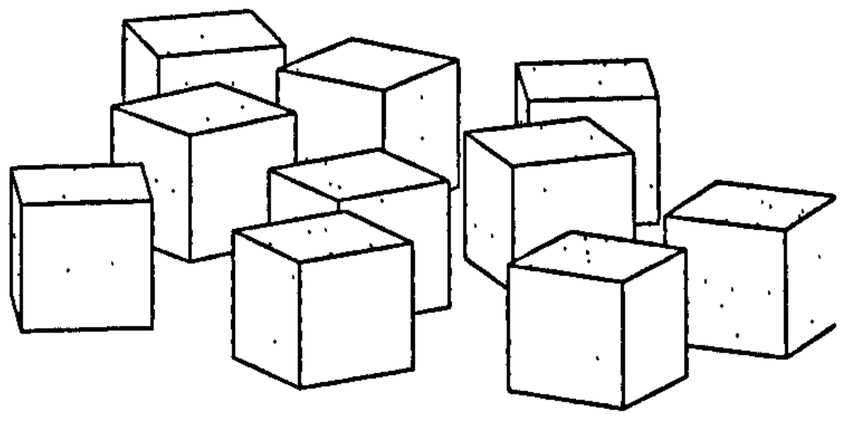

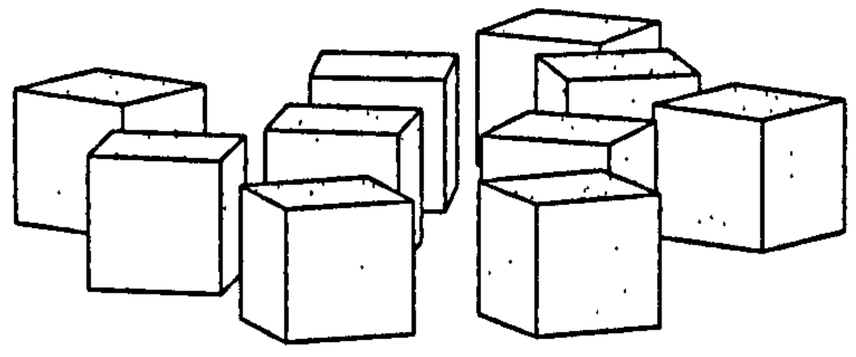

View 2

View 3

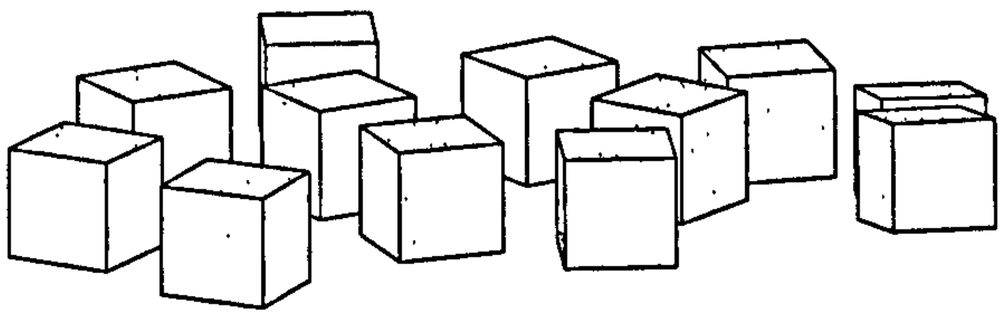

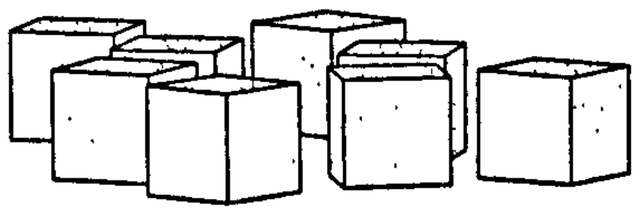

View 4

View 5

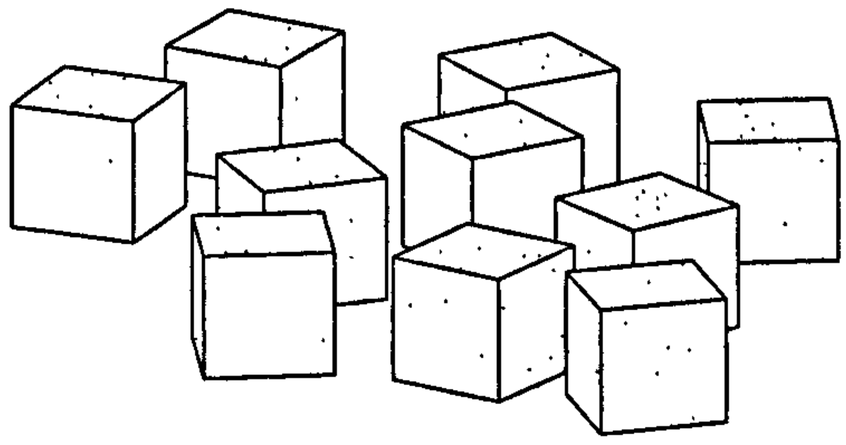

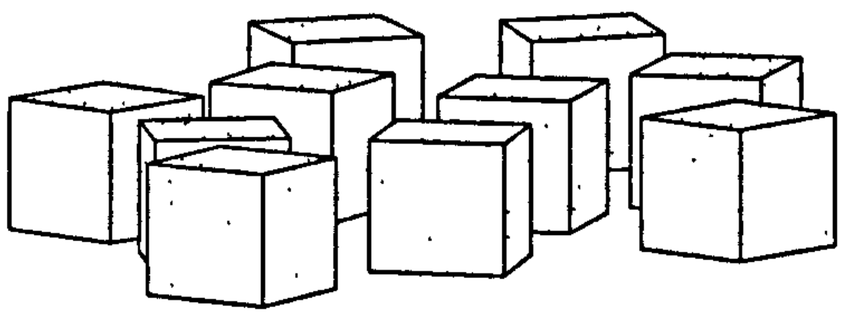

View 6

View 7

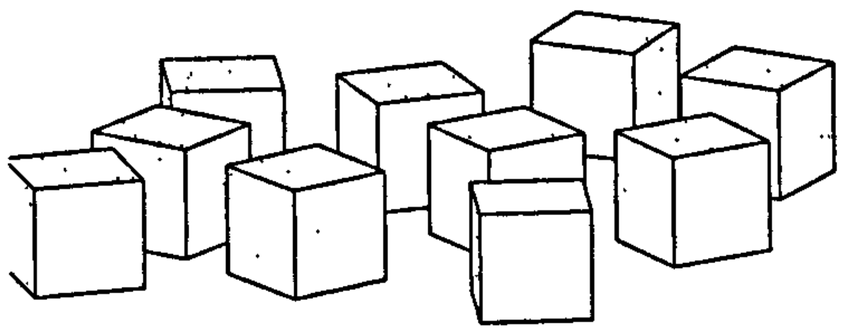

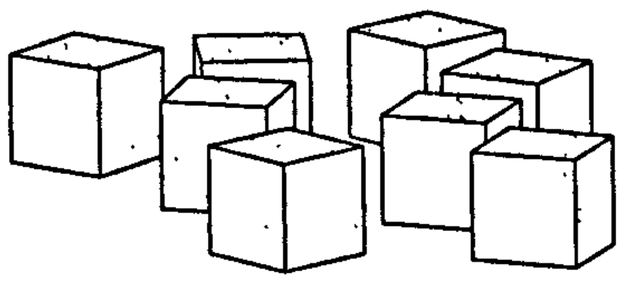

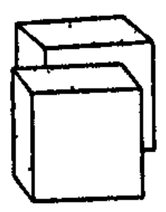

View 8

Figure 5.22 Eight views obtained from the simulation system.

View No.	Xe	Ye	Ze	w	j	k
1	2000.0	0.0	1000.0	0.0	63.43	-90.0
2	1500.0	1500.0	1000.0	-56.31	39.76	-23.09
3	0.0	2000.0	1000.0	-63.43	0.0	0.0
4	-1500.0	1500.0	1000.0	-56.31	-39.76	23.09
5	-2000.0	0.0	1000.0	0.0	-63.43	90.0
6	-1500.0	-1500.0	1000.0	56.31	-39.76	156.91
7	0.0	-2000.0	1000.0	63.43	0.0	-180.0
8	1500.0	-1500.0	1000.0	56.31	39.76	-156.91

Table 5.1 Definition of viewpoint orientation.

View number	1	2	3	4	5	6	7	8
Total number of visible target images out of 600 maximum.	233	230	232	233	219	199	217	206

Table 5.2 Number of target images visible in each view.

No. of Views of target	1	2	3	4	5	6	7	8
No. of targets viewed	5	56	146	100	5	1	9	90

Table 5.3 Table of the distribution of target visibility.

However, four of the 146 targets which are viewed by three cameras only are not matched because of ambiguities described by case three in 5.4.3. The range of the tolerance band that provides reliable results is 0.4mm-5mm in this trial. It may be concluded that given ideal conditions, target correspondences can be successfully found except in the case of ambiguities. These occur more frequently in the three viewpoint case than any other. The next step in the analysis of the matching method was to change the target image co-ordinates and viewpoint orientation parameters by adding random noise to simulate inaccuracies found in practice.

5.5.1.3. Test two: The introduction of random errors

To investigate the effect of noise on matching performance, random noise was added to various parts of the network. The data set used in the previous section was used again and random noise was added to the camera position parameters; camera rotation parameters; and measured target image co-ordinates.

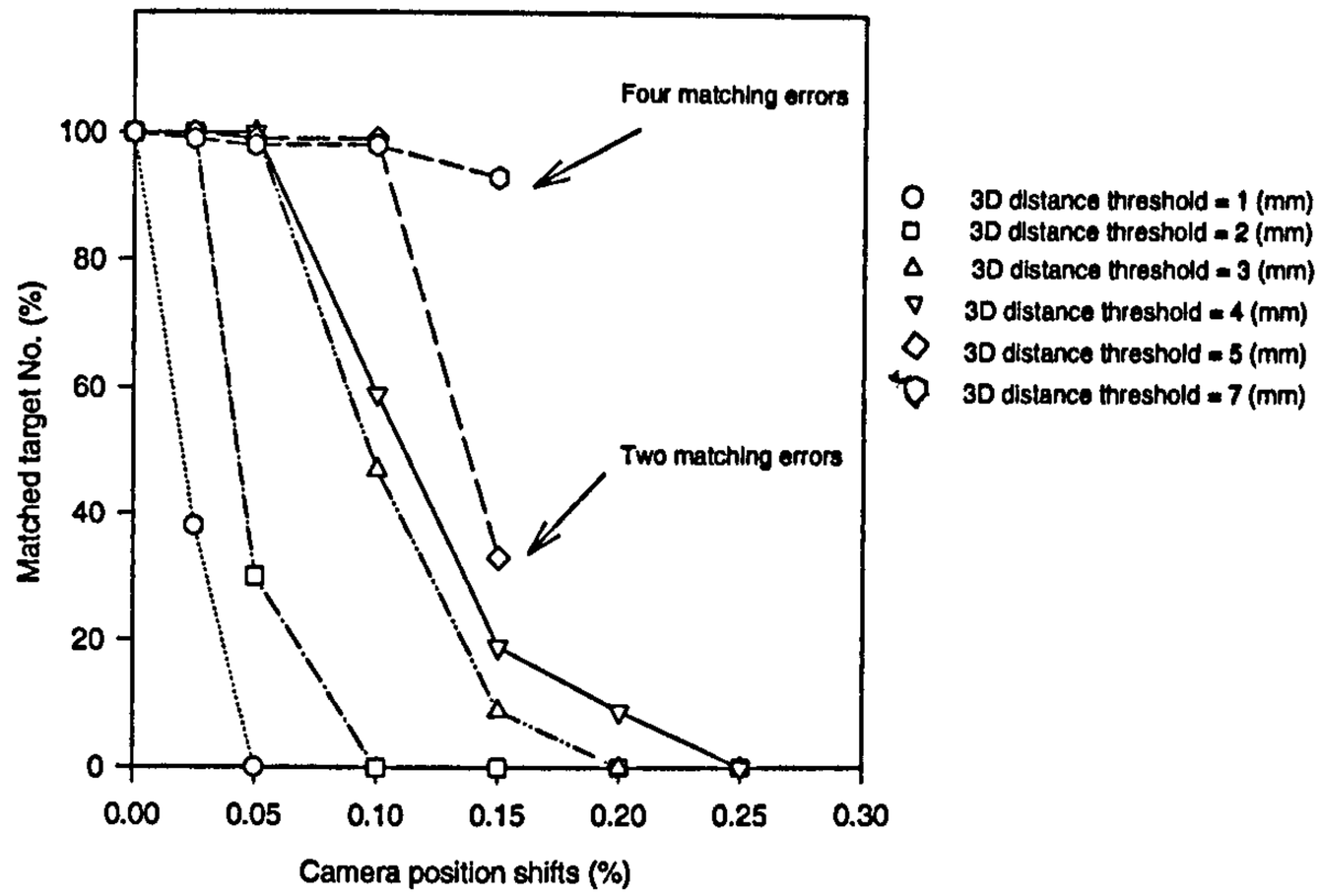

Figure 5.23 The result of random camera position parameter shifts.

Figure 5.23 shows the results of matching performance when random noise was added to the position parameters for the eight cameras. The camera rotation parameters and the target images co-ordinates were unchanged. By analysis of these results, the following effects were observed:(i) when the camera position parameters errors increase the number of target matched dramatically decreases; (ii) the number of matching targets increases as the 3-D tolerance value is increased. However, if the value is too big incorrect matching will take place; (iii). when the 3-D tolerance value changes from 5mm to 7mm the number of matched targets decreases. This is because when the tolerance value is increased beyond an appropriate

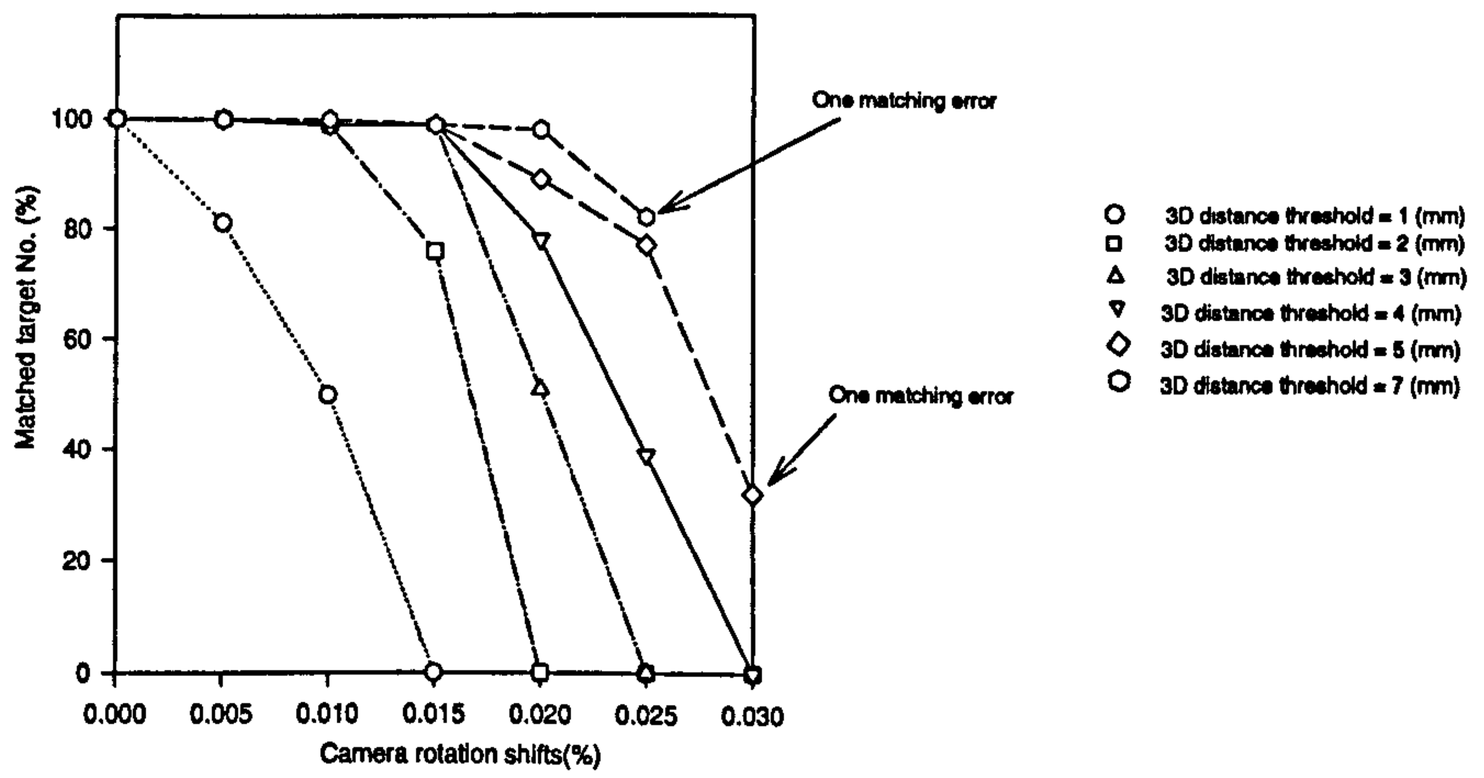

Figure 5.24 Result of camera rotation parameter shift.

value more ambiguous targets are introduced in each epipolar plane so that violations of the uniqueness constraints occur and these targets are rejected.

Figure 5.24 shows the result of the effect of matching performance when noise is introduced to the three camera rotation parameters. Comparing Figure 5.24 with Figure 5.23, both trends are similar. The number of targets matched when larger rotation errors are introduced decreases as more rays coming from target images will not lie inside the 3-D tolerance and are rejected by the algorithm.

Figure 5.25 shows the effect on matching performance when noise is added to the target

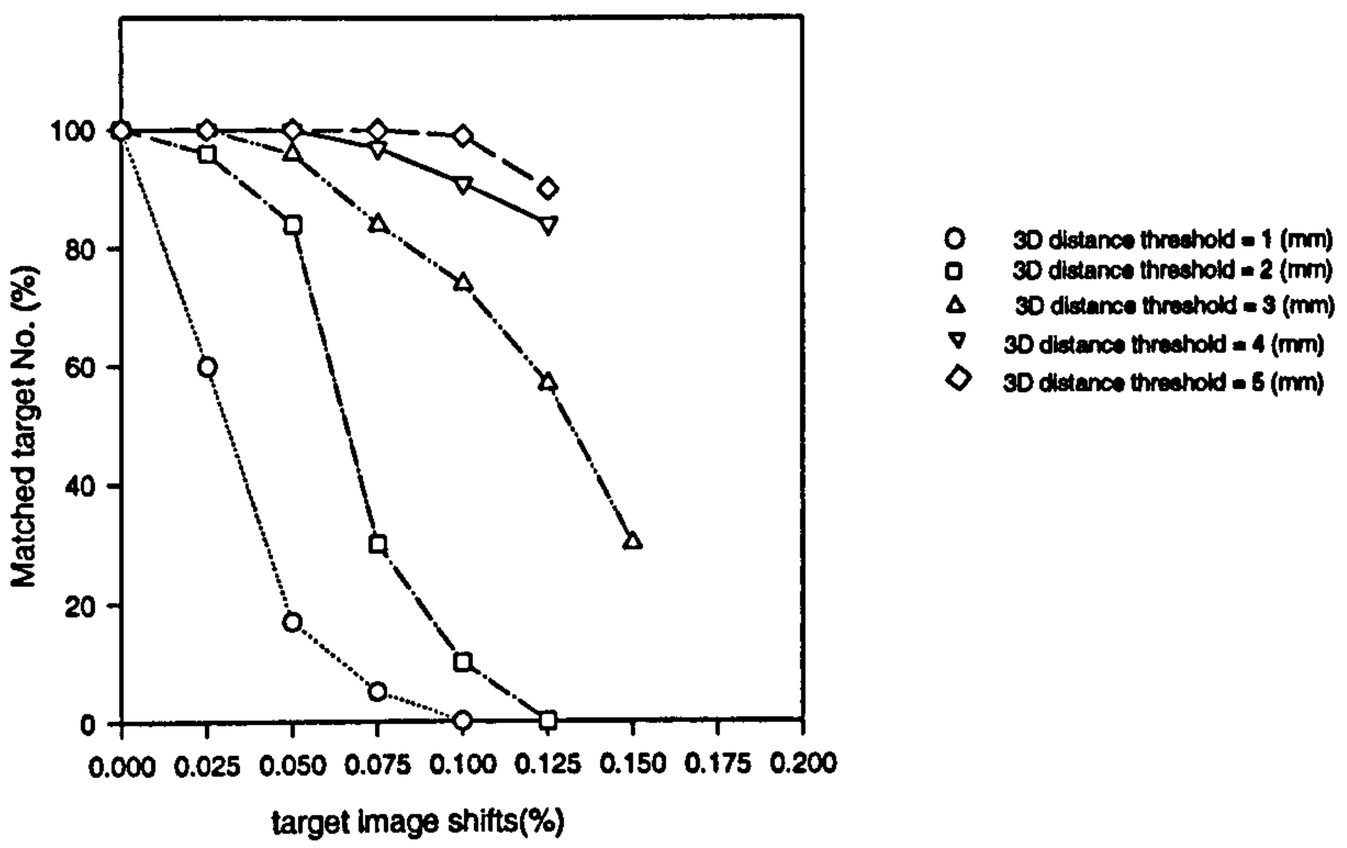

Figure 5.25 Result of target image co-ordinates x, y shifts.

image co-ordinates. This noise may be generated by various sources such as quantisation, target image location, and camera distortion as discussed in chapter three. This figure indicates that under the circumstances of ideal camera orientation parameters, the target image co-ordinates can occupy a wide of range, as much as 30 microns, and still be correctly matched. In general, the level of target image location error lies below 0.5 pixels or about 4 microns. It can be concluded from that test that given an ideal lens, the camera orientation parameters shifts have most significant effect on the matching performance.

Figure 5.26 shows the effect of combing the noise introduced to the six camera parameters at the same time. Comparing these results with Figure 5.24 and Figure 5.23 it can be seen that the effects are similar to those camera from separate location and rotation parameters.

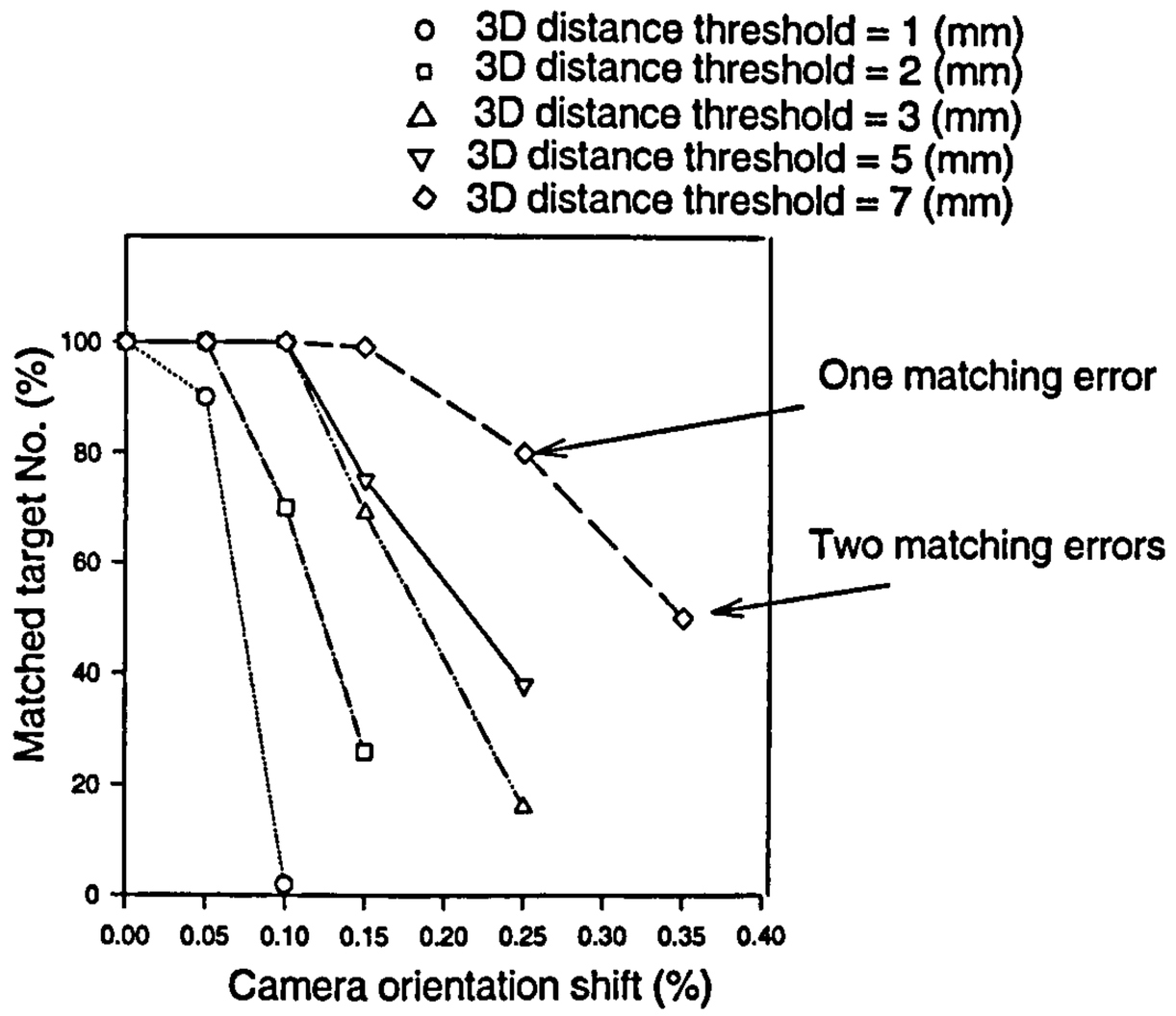

Figure 5.26 Result of camera orientation parameters shift

5.5.1.4. Test three: The influence of target density

This trial was designed to evaluate the influence of the matching algorithm for various target densities. Mass, 1992a, reported that the number of ambiguities grows approximately with the square of the number of particles. Ten cubes were randomly created and the number of randomly placed targets on each side of cubes was varied from four to sixteen in each test so that the total number of targets varied from 200 to 800. The group of dense targets are formed in each cubic as targets are gradually introduced into the cubes.

Figure 5.27 illustrates the results of target matching with differing numbers of targets introduced and various 3-D tolerance values. The number of matched targets dramatically decreased as the tolerance value increases. This is because more ambiguities are rejected with higher tolerance value. The higher the target density, the lower success matching rate. The matching error rate also increases with tolerance value and target density. This is illustrated in Figure 5.28. Figure 5.29 shows the result of using the same number of targets but all the targets are produced on a single cube. In this situation the number of correctly matched targets is much reduced and more errors are produced. This is because primarily the single cube occupies only a small region of the whole space, hence the imaged targets are very dense.

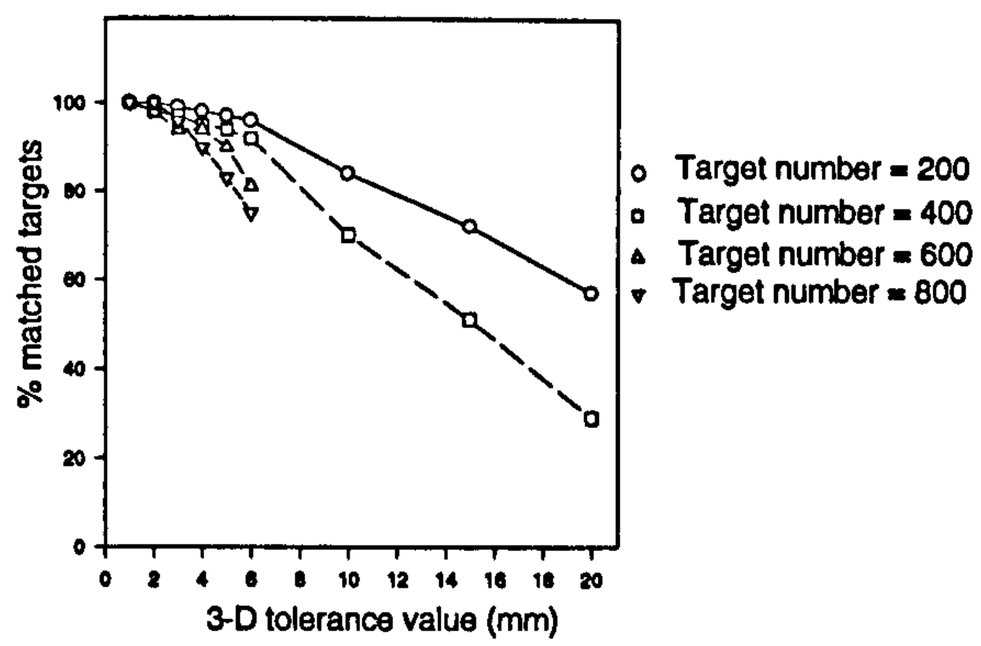

Figure 5.27 Results of matching with different target image densities

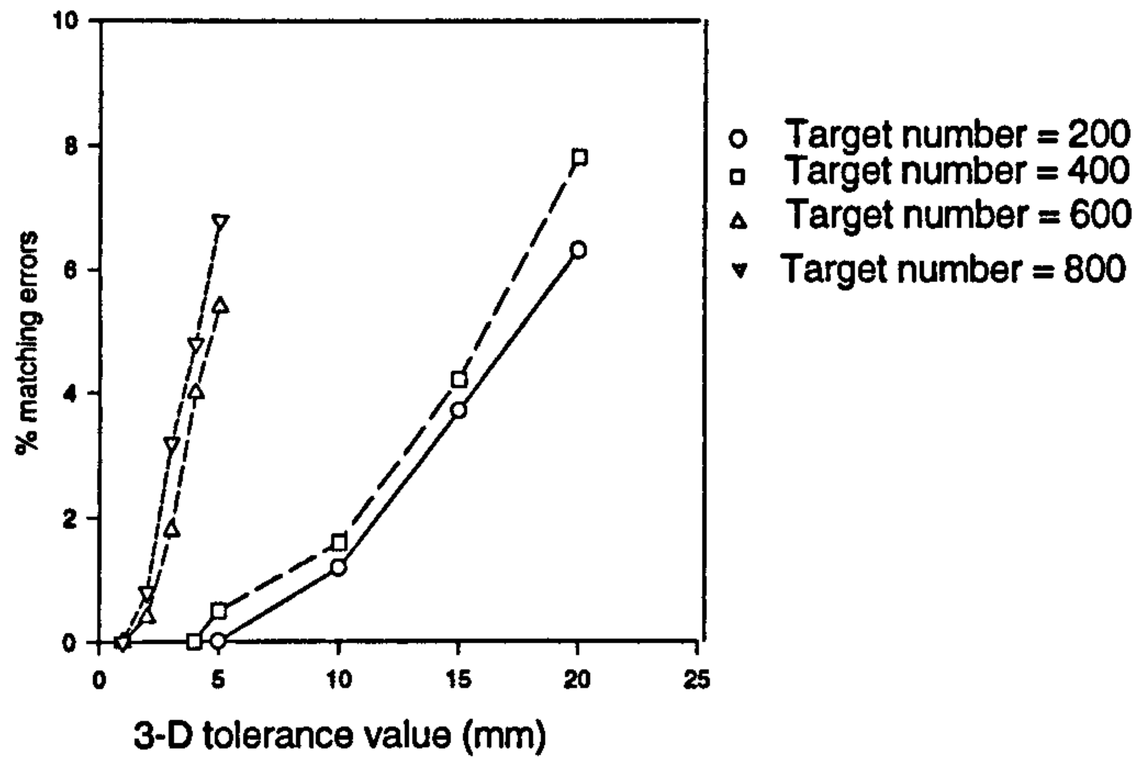

Figure 5.28 Matching errors in ten cubes

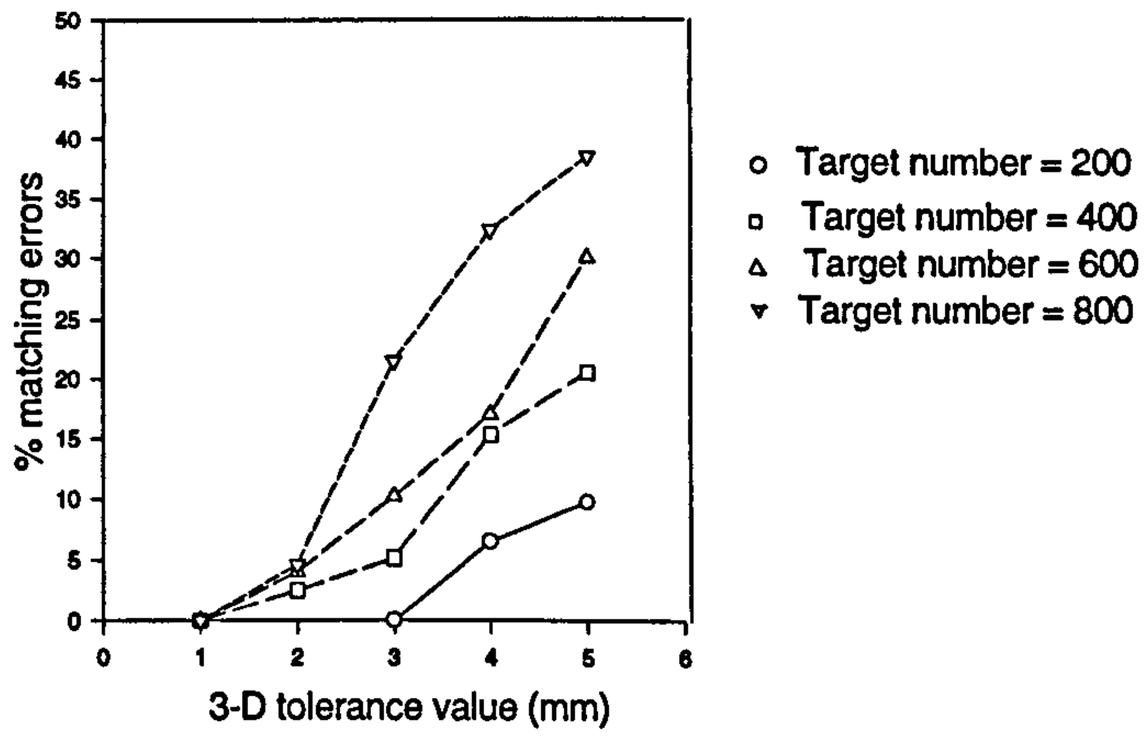

Figure 5.29 Matching errors in one cube

5.5.2. Evaluation by experiment

5.5.2.1. Experimental test using targeted brick

The characteristics of the matching method have been demonstrated by simple simulation. The current method may be sufficient to solve target ambiguities and occlusions by increasing the number of viewpoints. To test the method further a target field was constructed using a number of wooden bricks arranged on a surface in various positions. A projector was placed on front of the toy bricks. A black piece of 35mm slide film into which a number of random small holes had been made was used in the projector to produce targets on the brick surface. A cover was used to reduce ambient lighting.

Nine images were collected from viewpoints located to the left, middle and right of the test field Two of these images, one from the left and another from the right, are illustrated in Figure 5.30a) and b).

The first step in the measurement process is target segmentation. The images were segmented to give a binary image using a threshold chosen to remove the dark background illumination from the light targets. Hence, only the target outlines and other artefacts of a similar nature remain in the image. The second step consists of using the pattern recognition algorithm described in chapter two to recognise the targets and note their approximate position. The third step used a weighted centroid algorithm on the grey scale image to gain the accurate subpixel position of each target. The six steps discussed in the previous section are used to

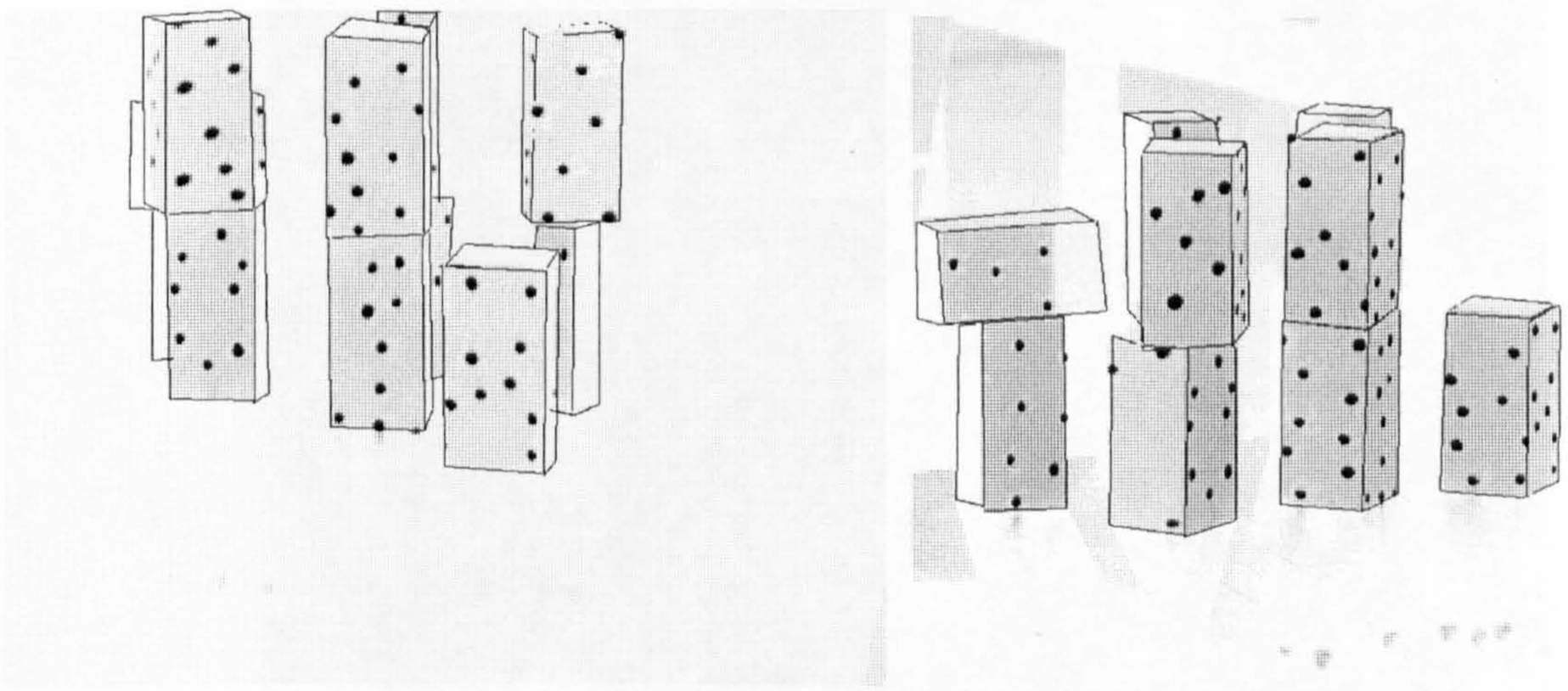

Figure 5.30 a) Image from view 1 b) Image from view 8

complete the matching procedure. The results of the target matching are given in Table 5.4. From this table, it can be seen that at the first iteration of the first stage, a significant number of targets have been matched. This is because the targets placed on the bricks are sparse enough for a small tolerance to be used. The second iteration uses the refined camera orientation parameters and can match the rest of the targets which have common projections. In stage two, a number of targets, which have less projections, are matched by reducing the matching group number. Some remained unmatched because of target images which were falsely identified as targets in some of the viewpoints, for example those at the base of viewpoint 8.

	Iteration No.	V1	V2	V3	V4	V5	V6	V7	V8	V9
Image points	-	62	65	67	102	112	111	75	87	84
Stage 1	1	51	51	51	81	81	81	56	56	56
Stage 1	2	3	3	3	8	8	8	6	6	6
Stage 2	-	6	8	8	13	23	22	8	16	16
unmatched		2	3	5	0	0	0	5	9	6

Table 5.4 Number of correct matches per viewpoint.

5.5.2.2. Experimental test using car gear box

To test the method further, a car gearbox was used as a test object and is shown in Figure 5.31. This is a significantly complex object. About 250 circular retro-reflective targets were placed on the gearbox surface. Four camera viewpoints were used, each at a distance of

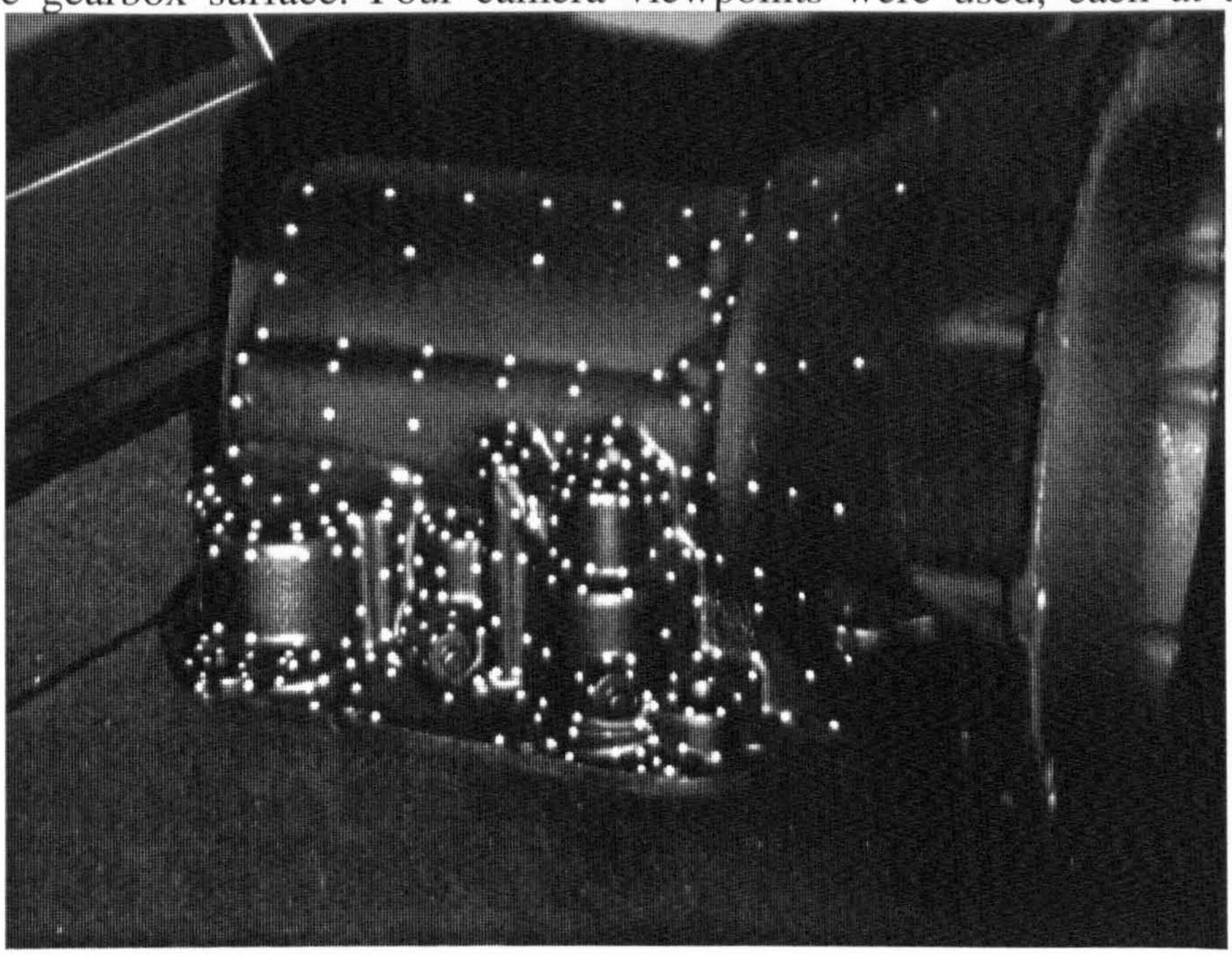

Figure 5.31 Car gearbox

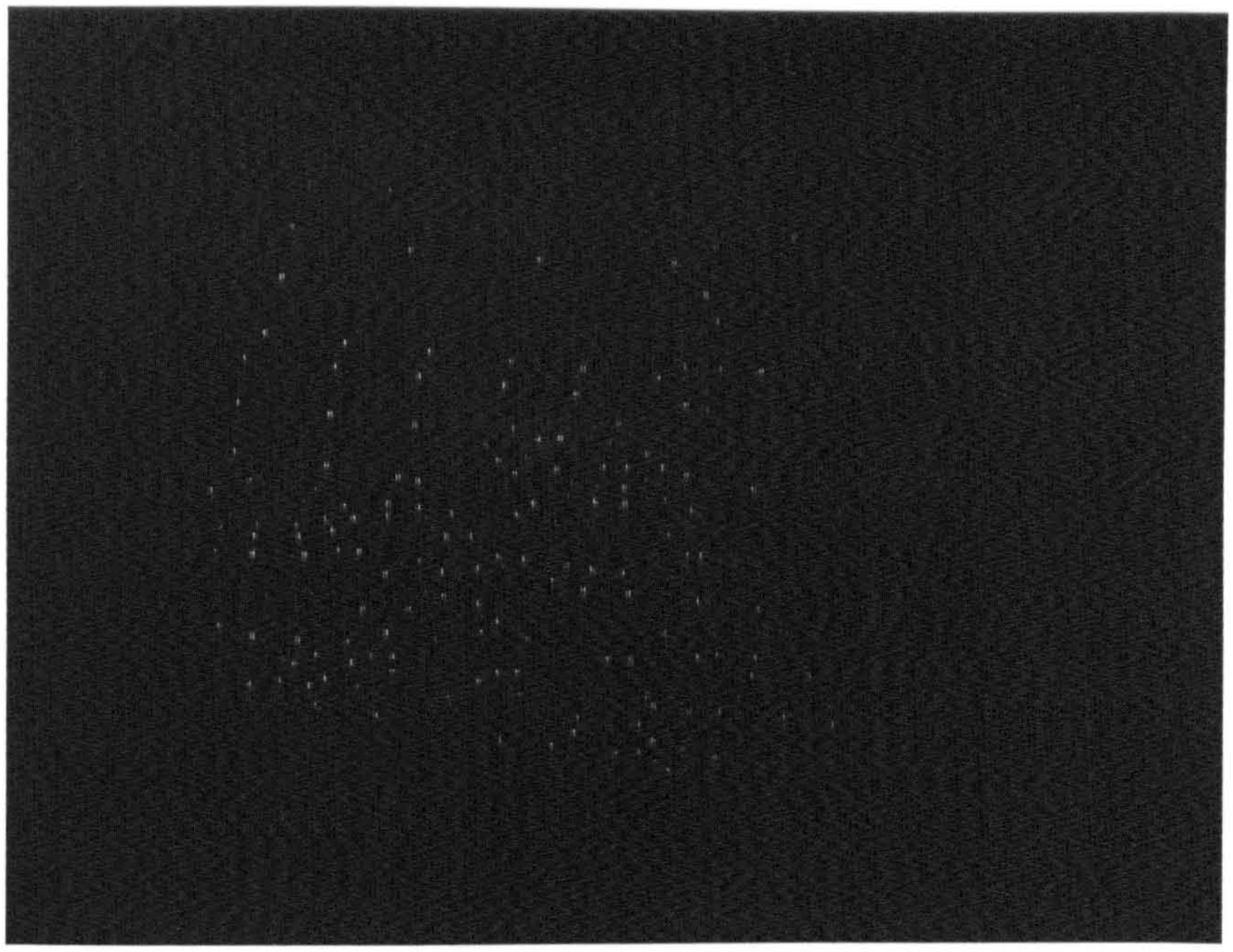

Figure 5.32 One view of the gearbox

approximately 1 metre from the gearbox. Figure 5.32 shows one of the images used for target location. The weighted centroid algorithm was again used on the grey scale image to compute the sub-pixel location of the target image. The matching method is analogous to that used in the toy brick test section. Results from the 3-D matching process, which took about 4 minutes on a 33Mhz 80486, are shown in Table 5.5. Figure 5.33 shows a primitive reconstruction produced by downloading the data into a CAD system.

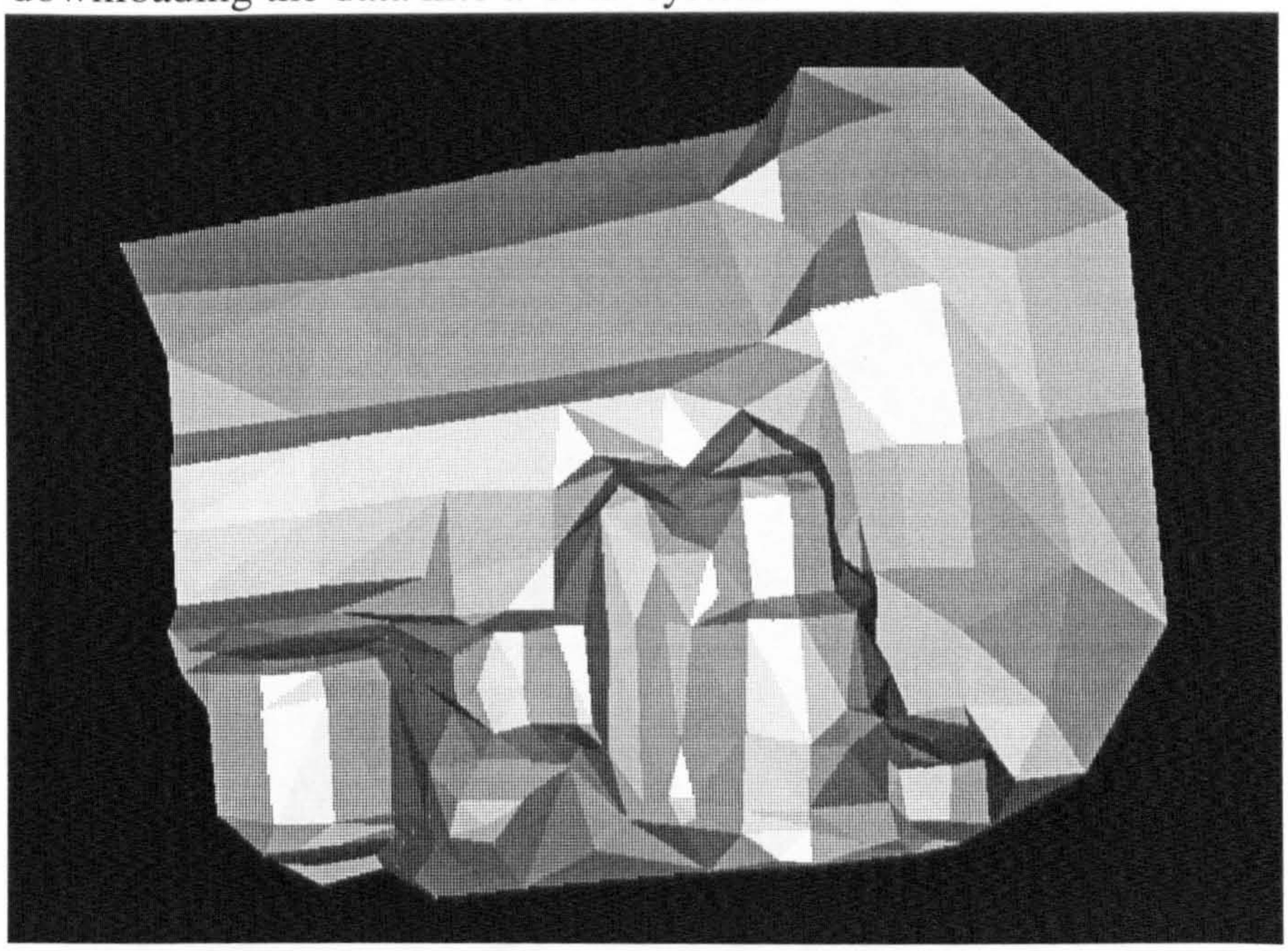

Figure 5.33 CAD reconstruction of the gearbox

	V_1	V_2	V_3	V_4
Total targets	179	221	237	220
Stage 1	42	42	42	42
Stage1	101	101	101	101
Stage 1	9	9	9	9
Stage 2	26	69	81	67
Final result	178	221	233	219

Table 5.5 Successful matches from the gearbox application

5.5.2.3. Experiment test using a plaster cast of a foot

To test the algorithm the inside of a plaster cast of a foot was selected as a test object because of it's geometry since it provided a difficult shape to measure (Figure 5.34). A number of retro-reflective targets were placed on the plaster cast at positions that were considered necessary to reconstruct the level of detail required. No consideration was given to the difficulty of viewing these targets or whether the retro-reflective targets would reflect enough light from a given viewpoint due to the angle of the target presented to the camera (Figure 5.35). Hence, a large number of targets would be expected to either be occluded or invisible from many viewpoints. Four larger targets were used for rough estimation of camera exterior parameters. A large number of views was used to attempt to get the minimum of three projections of each target (Figure 5.36). A single camera was used to grab the 25 images by using a rotation table on which the plaster cast was placed. The number of targets observed in

Figure 5.34 View of foot model

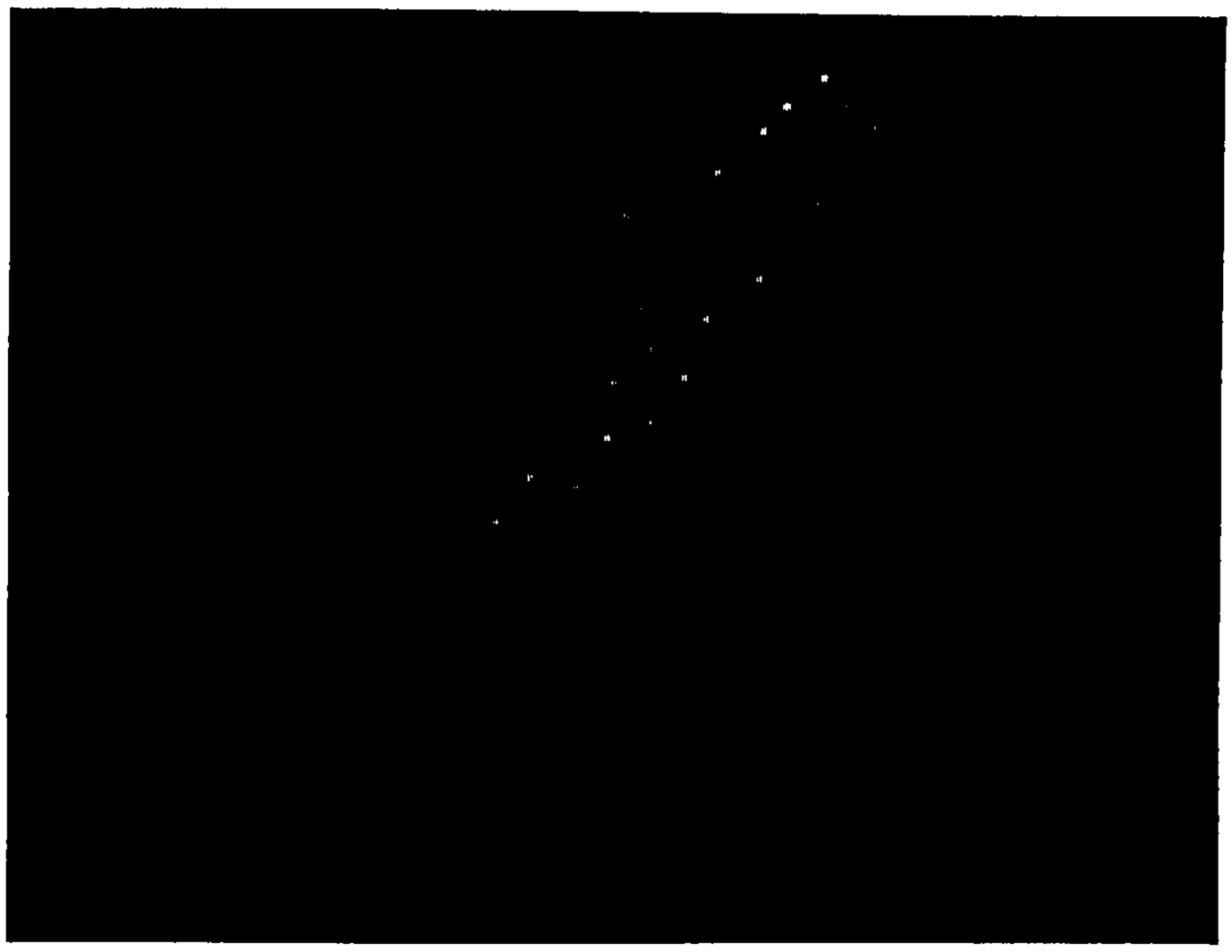

Figure 5.35 Image grabbed for target location

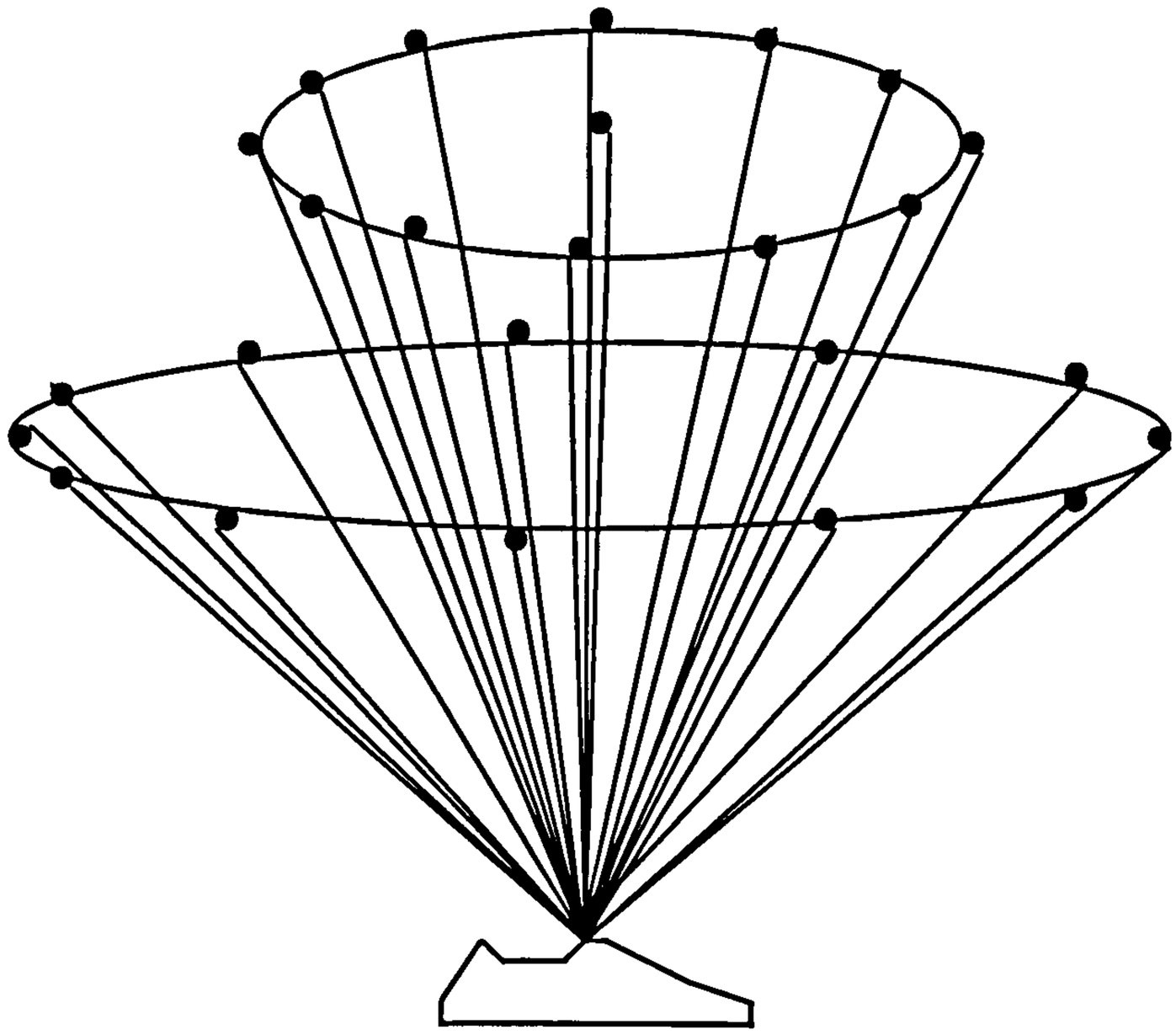

Figure 5.36 Position of the 25 camera views

Iteration No.	1	2	3	4	5	6	7
Matching group(mt)	7	4	4	3	3	3	2
Tolerance Value(mm)	5	3	2	1	1	1	0.5
No. Matched Targets	18	63	26	64	22	9	28
Total Matched Targets	18	81	107	171	193	202	230

Table 5.6 Target matches by iteration

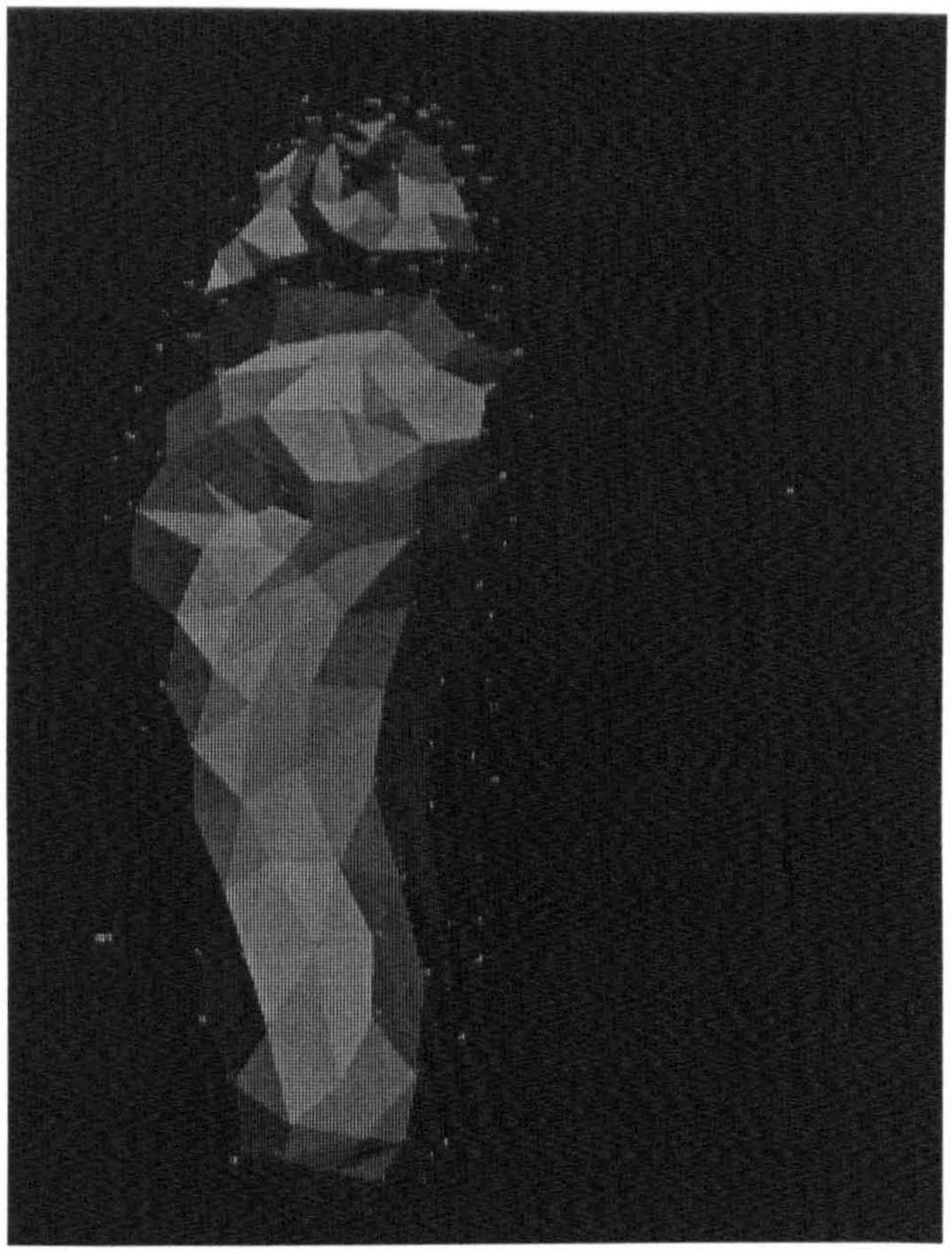

Figure 5.37 CAD reconstruction of the foot (looking up from bottom)

each view ranged from 15 - 90. It would be extremely difficult to manually solve the correspondences due to the lack of any distinguishable features on the targets. The optimised matching algorithm developed in this paper was used to match all the target images on the 25 images. The camera parameters were iteratively refined. The number of matched targets is shown in Table 5.6. Figure 5.37 shows reconstruction of the plaster cast by placing the 3-D co-ordinates into a CAD package and manually connecting the points to form a 3-D surface.

5.6 Summary

In this chapter a method of 3-D target matching using an optimised constrained search method has been discussed in detail. A tree search method has been used to minimise the computation time and when camera parameters are not accurately known targets are gradually introduced in an iterative manner. The use of multiple viewpoint constraints is used to robustify the matching process. Pseudo target images are defined in the search process to overcome occlusion problems and make the matching strategy flexible. Hypothesis-testing and heuristic processes are used to make the matching computation more efficient.

The benefits of the optimised 3-D matching method are: (i) initial camera parameter estimates are not required to a high accuracy and initial values can be improved by bundle adjustment based procedures; (ii) target matching tolerances can be changed during the bundle

adjustment process according to a statistically derived formula; (iii) targets can be progressively introduced into the measurement network to enable a more robust correspondence matching technique; (iv) target images can be arranged in an arbitrary order to build the matching tree; (v) this algorithm can be combined with bundle adjustment procedure.

In conclusion, an algorithm has been developed which is analogous to the epipolar method. This algorithm has been optimised for speed of operation. Problems due to occlusions and ambiguities have been considered and largely overcome. The method has been tested both in simulation and in practice with complex objects. The results of these tests have revealed fundamental relationships and proved the algorithm in practice.

Chapter 6 The design of an automated 3-D measuring system

6.1. Introduction

The main limitation to the common place industrial application of digital photogrammetric 3-D measurement systems has been the difficulty for non experts in using such systems and the typical time lapse between image acquisition and the availability of measurement results. Hence, two aspects must be considered: automation and real-time. The two terminologies are closely linked in photogrammetric applications. The term **automatic** often means that a process is self-running without human interruption. An automated 3-D measurement system should be a system that is capable of completing all processes from the digital image acquisition to finally obtaining 3-D information. The term **real-time** has also been used in many different ways depended on different applications. In machine vision and robot vision applications, real-time often implies operating at the standard video-rate. A more general definition of real-time is time-constrained, giving a limited time in which the task must be solved. In photogrammetric applications, El-Hakim, 1986a, gave a formal definition of real time system is as: "**a system without interruptions, or appreciable time lags, between acquiring the image and the final results which are the three-dimensional object co-ordinates.**" Hence, the goal for designing an automated 3-D measurement system is that the system is capable of automatic operation preferably in real-time. For these requirements to be met it is clear that any system will have to be carefully designed with respect to both hardware components such as: targeting; lighting; camera mounts; interfacing; and system construction, as well as software modules for operations such as: camera orientation estimation; target image location; correspondence solving; bundle adjustment; and network design for non experts.

In recent years, industrial photogrammetric 3-D measuring systems have been developed in a large number of scientific and technical environments (Gruen, 1994). The difference between them has often depended on the background of the developers and the particular application. The main characteristics of several photogrammetric systems are given in Table 6.1 based on a literature survey of photogrammetric systems since 1980.

By analysis of these systems it appears that the developing trends of digital photogrammetric measurement systems are in two directions: large multi-functional general systems, and small specialised systems. Within these two groups are high speed systems: in which most of the algorithms are realised by hardware and huge quantities of data can be stored; and flexible systems, in which all algorithms are realised by software. The question raised by those considering using digital photogrammetry are: **(i)** how to choose the appropriate system for a

Author / date	Cams	Application	Object size max/m^3	Target	Feature location	Real time	Hardware	Algorithm	Accuracy
El Hakim/1986	2	Research	0.3	Bl.on Wh.	Centroid	Y	68010	DLT	-
Haggren/1987	4	Inspection	25	Bl. on Wh.	Centroid	P	PC286 / 287	DLT	1/10000
Yamashita/1988	3	Human body	2	Laser	Peak	P	Hardware	Triangle	1/300
Jeschke/1990	2	Geology	0.3	Nat. features	LSM	N	PC / VAX 11-750	-	-
El Hakim/1990	1	Inspection	0.5	Edges/ Proj.	LSM	NA	SUN 4/160	Bundle	No report
Beyer/1992	3	Car body	5	Bl. on Wh.	LSM	N	Sparc	Bundle	1/12000
Wong/1992	3x3	Human body	2	Proj.	-	N	PC+ Station	DLT	5%
Maas/1992	4	Various	0.5	Proj.	LSM	P	-	Bundle	1/20000
Godding/1992	3+3	Metrology	2	Retro	Ellipse	P	Sparc 2	Bundle	1/40000
Aliverti/1993	4	Human body	0.6	Laser	X correl.	N	SG 4D/25	-	-
Peipe/1993	1	Conveyer	1.2	Retro	LSM	N	PC486	Bundle	1/35000
Vlugt/1994	1	Inspection	0.5	Proj.	MPGC	Y	PC	DLT	1/4000
Gruen/1994	9	General	2	Retro.	LSM	N	Sparc	Bundle	1/50000

Table 6.1 A summary of some of the 3-D measuring system (Least squares matching (LSM); Multi-photo geometrically constrained (MPGC))

particular application; and **(ii)** how to design and develop these systems to measure physical information quickly, accurately and automatically to solve the problems which human operators would find difficult or impossible.

Most of the digital photogrammetric measurement systems currently used by industry can be divided into two kinds: Unix workstation based systems; and IBM PC based systems. The Unix workstation based system has a high resolution display, high speed, and a high storage capacity, but will usually cost several times, more than an IBM PC based system. The IBM PC based frame-grabber system has the advantages of low cost, flexibility, industry standard support for its data bus, but generally has had speed and storage capacity limitations. However, with the advent of the Intel P5 chip and SCSI based disk storage for IBM PC's the difference is not so clear. IBM PC based systems are often chosen because of the lower cost of hardware, peripherals and software. In connection with this thesis the intention is to build an automated 3-D measuring system which would function under specific circumstances, the IBM PC based frame grabber is discussed and a study concerning both the hardware and software to build this system has been made.

6.2. System Hardware

The automated 3-D measuring system is systematically designed by taking account the following primary criteria:

- the capability of measuring targeted objects of 0.5m x 0.5m x 0.5m in size;
- flexible camera positioning;
- automatic camera orientation parameter estimation;
- automatic solution of the target image correspondences;
- automatic recognition and location of target images with a subpixel accuracy;
- both free bundle adjustment and space intersection algorithm methods;
- the capability of displaying generated 3-D co-ordinates by means of a CAD package;
- operation by personnel without any need of a thorough knowledge of photogrammetry;
- IBM PC based computing system for low budget.

In order to achieve these specifications, hardware components and appropriate software have been chosen, designed and developed. Figure 6.1 illustrates the overview of this prototype system and a system schematic chart is shown on Figure 6.2.

There is a direct relationship between functionality and cost for this system. The system is flexible in use and easy to master because of its simple structure, small size, and the general

Figure 6.1 Overview of the prototype system.

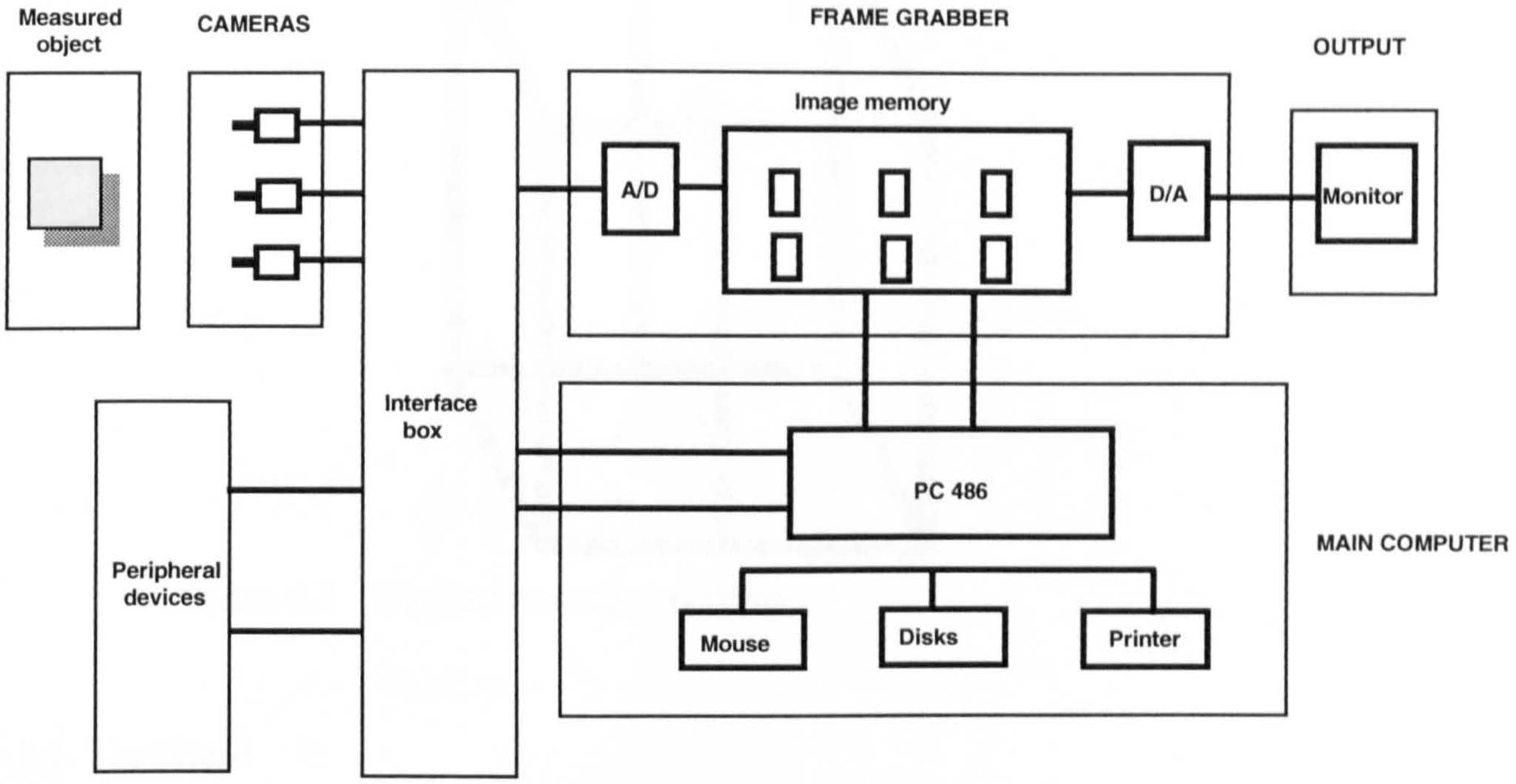

Figure 6.2 Structure of the 3-D measuring system.

availability of software libraries for almost all functions. The system is suitable for task oriented digital photogrammetric measurement.

6.2.1. Support frame

The support frame was constructed by a collection of 25mm square "speed frame" cross-section tube. These tubes were used to construct the frame on which the cameras were mounted and which supported a controlled lighting arrangement. The size of the support frame is 1.8m x 1.4m x 1.7m. A diagram of the support frame is shown in Figure 6.3. The design of the frame allowed a number of cameras to be fixed to the top surface of the frame and adjusted to view the object. An object size of 300mm x 300mm x 300mm could be used with 25mm lenses and an object size of 700mm x 700mm x 700mm with 12.5mm lenses. The frame was placed on a black carpet and could be completely covered with black or white cloth. Illumination could then be placed outside in order to produce diffuse light internally. Currently, retro-reflective target spots are illuminated by projecting a light source as near to coaxial with each camera optical axis as the physical size and location of the camera will allow.

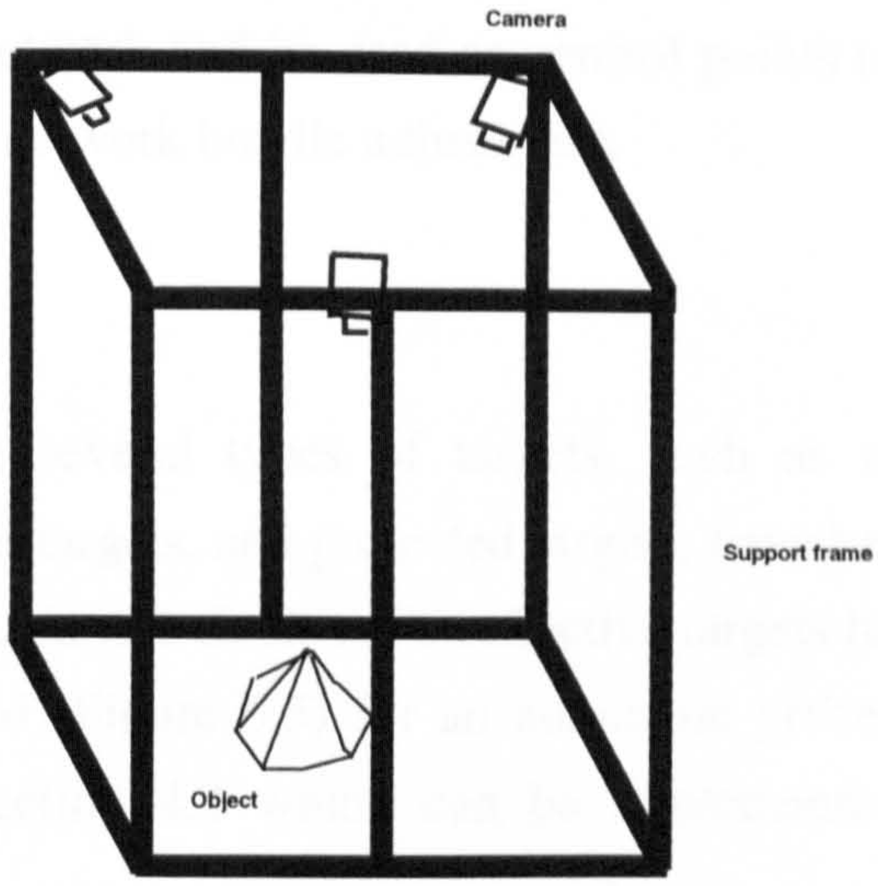

Figure 6.3 The camera support frame.

6.2.2. Test field

A testfield, consisting of a 250mm x 230mm aluminium base plane with 28 inserted rods of differing lengths was constructed (Figure 6.4). The whole assembly was painted matt black and round retro-reflective targets were placed on top of the rods. An extra 17 retro-reflective targets were placed on the base plate so that a total of 45 targets were attached to the testfield. All targets were 2mm diameter circles produced by a punch tool. Three retro-reflective lines were placed on three sides so that the automatic camera orientation estimation method described in section 4.2 could be used. These targets could be measured by an independent system to high accuracy using a co-ordinate measuring machine. These co-ordinates could

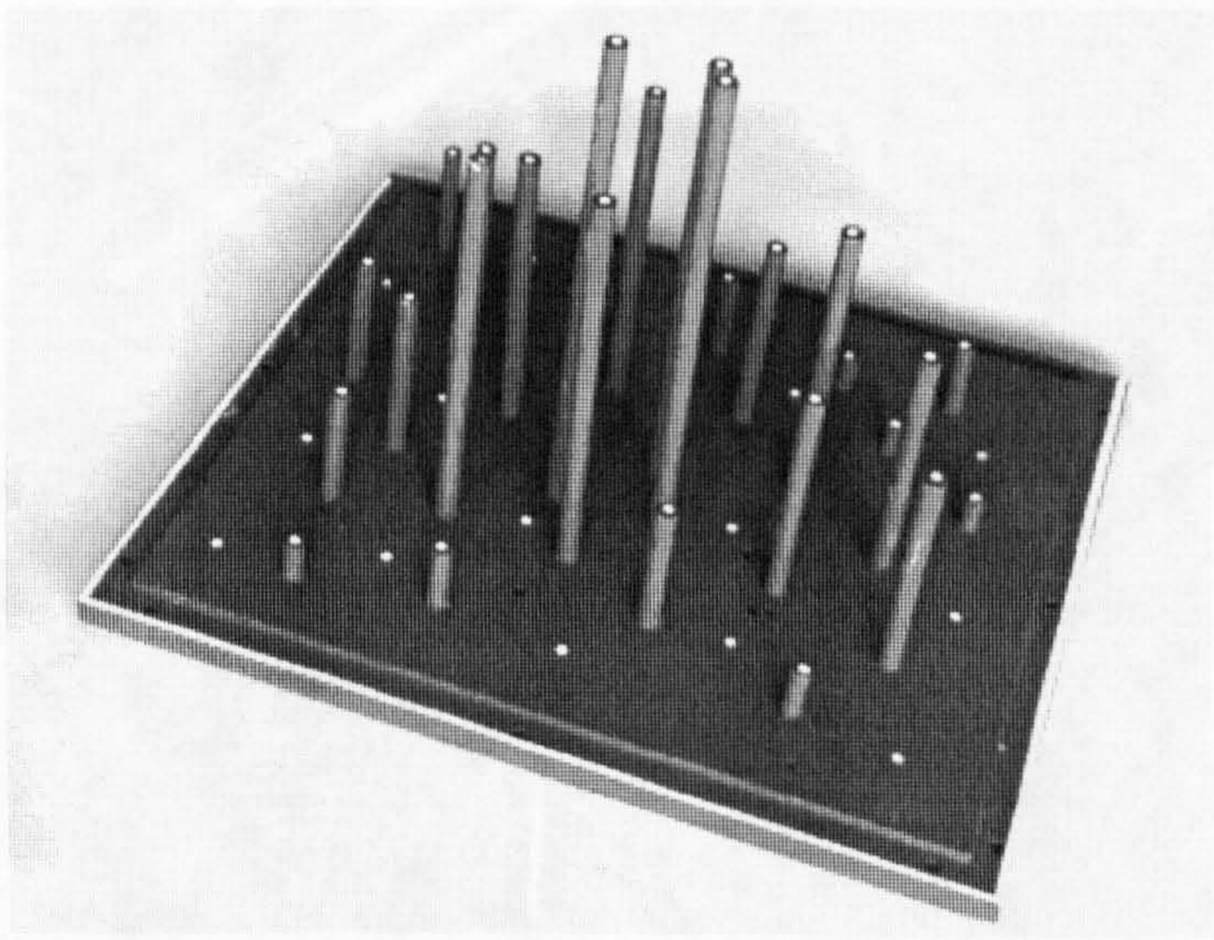

Figure 6.4 Test field for camera calibration and orientation.

then provide scale to the network and be used as control points to check on the co-ordinates derived from any later free network bundle adjustment.

6.2.3. Targeting

The characteristics of the several types of targets, such as naturally reflective targets, retro-reflective targets, laser targets, and projected targets, have been discussed in section 3.2. For most of the experiments in this thesis retro-reflective targets have been chosen. Four laser targets have also been used (Figure 6.5) for an automatic procedure of camera orientation estimation described in section 4.2 which can be implemented by using the laser spot information.

6.2.4. Translation and rotation mechanisms

The translation and rotation mechanisms consist of several parts: the laser translation mechanism; an object rotation mechanism; and a camera pan and tilt mechanism. All of these mechanisms are equipped with stepper motors and controlled by computer. This allows the maximum flexibility of the automated system.

(i) The laser holder and translation mechanism

The laser translation mechanism is shown in Figure 6.5. This mechanism is able to hold the

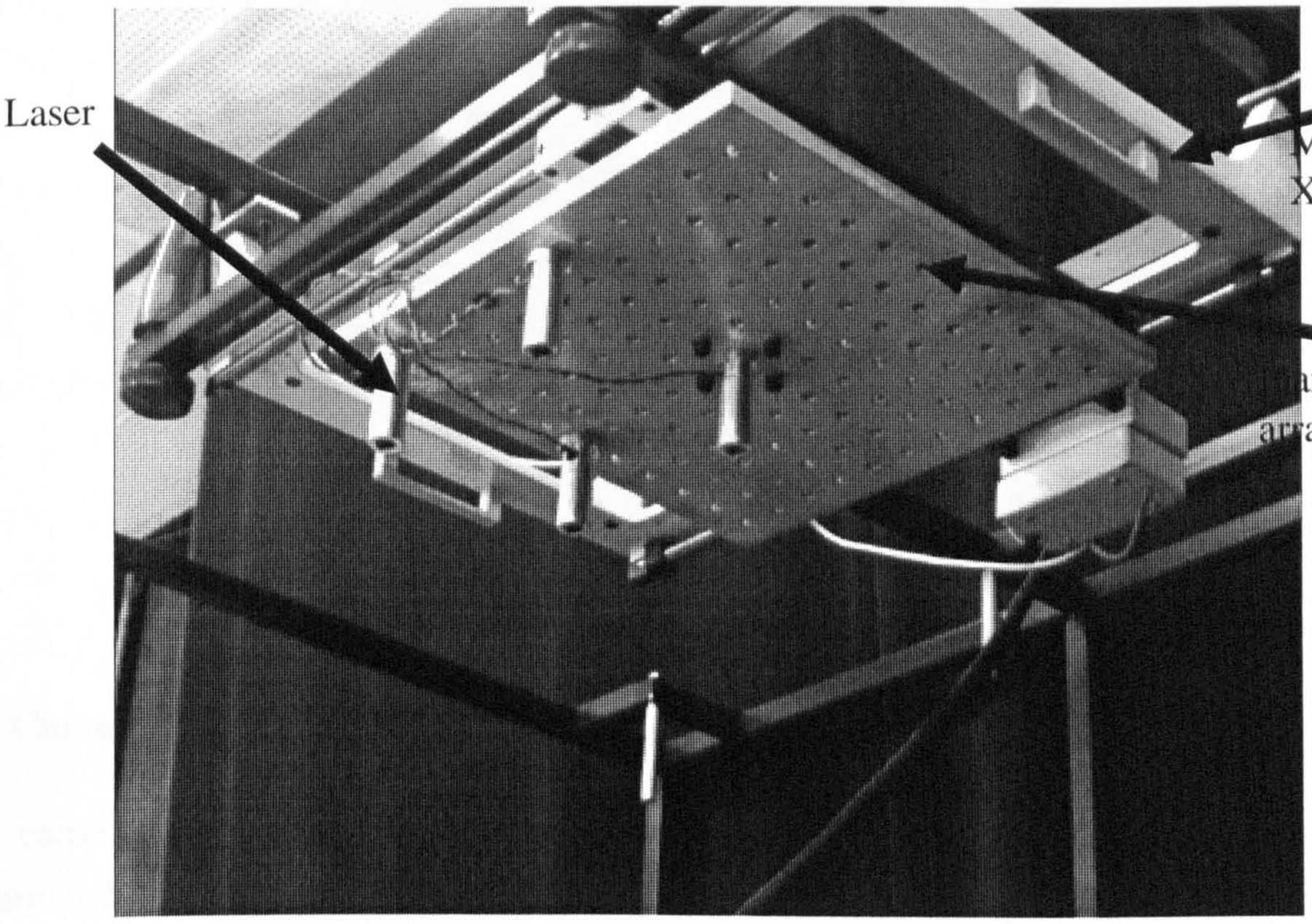

Figure 6.5 Laser target projection system.

lasers and adjust the lasers to desired positions. The laser translation mechanism is a Maxtascan X-Y table, which allows the array of lasers to move over an area of 400x230 mm. The Maxtascan X-Y table is computer controlled and can produce a movement precision at ±5 microns. All four lasers are mounted in holders which allow precise adjustment of their position. Care is required to align the lasers to ensure the laser beams are emitted parallel to each other. The laser holders can be positioned over an array of 11x11 holes which cover an area of 280x280mm, depending on the measured object size. By these means, the distances between the four lasers can be adjusted and their position controlled through the interface box which is connected to the computer via the controlling software.

(ii) The object rotation mechanism

The object rotation mechanism consists of a rotation table (Figure 6.6) upon which the measured object is placed. The rotation of the table is driven by a stepper motor which is controlled by computer so that the object can be automatically imaged from any direction by rotating the table. In this case only one camera is necessary to acquire multiple images which can be equivalent to the use of multiple cameras placed around the object.

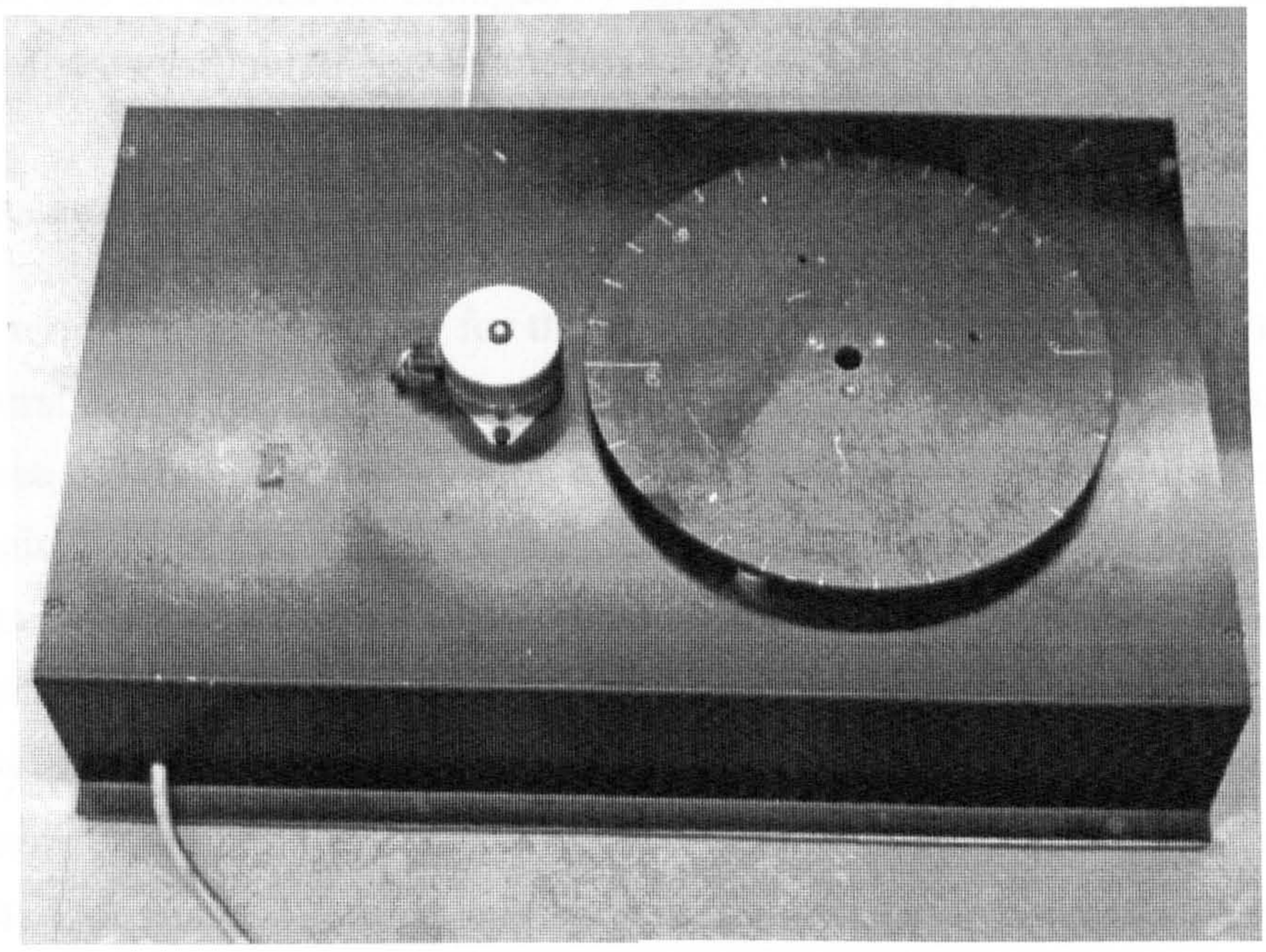

Figure 6.6 The object rotate mechanism.

(iii) Camera pan and tilt mechanism

The camera pan and tilt mechanism, which was designed by Dr T.A. Clarke, is shown in Figure 6.7. The camera is mounted in such a way that the panning and tilting axes are arranged to coincide with the front node of the lens. This mechanism allows the individual

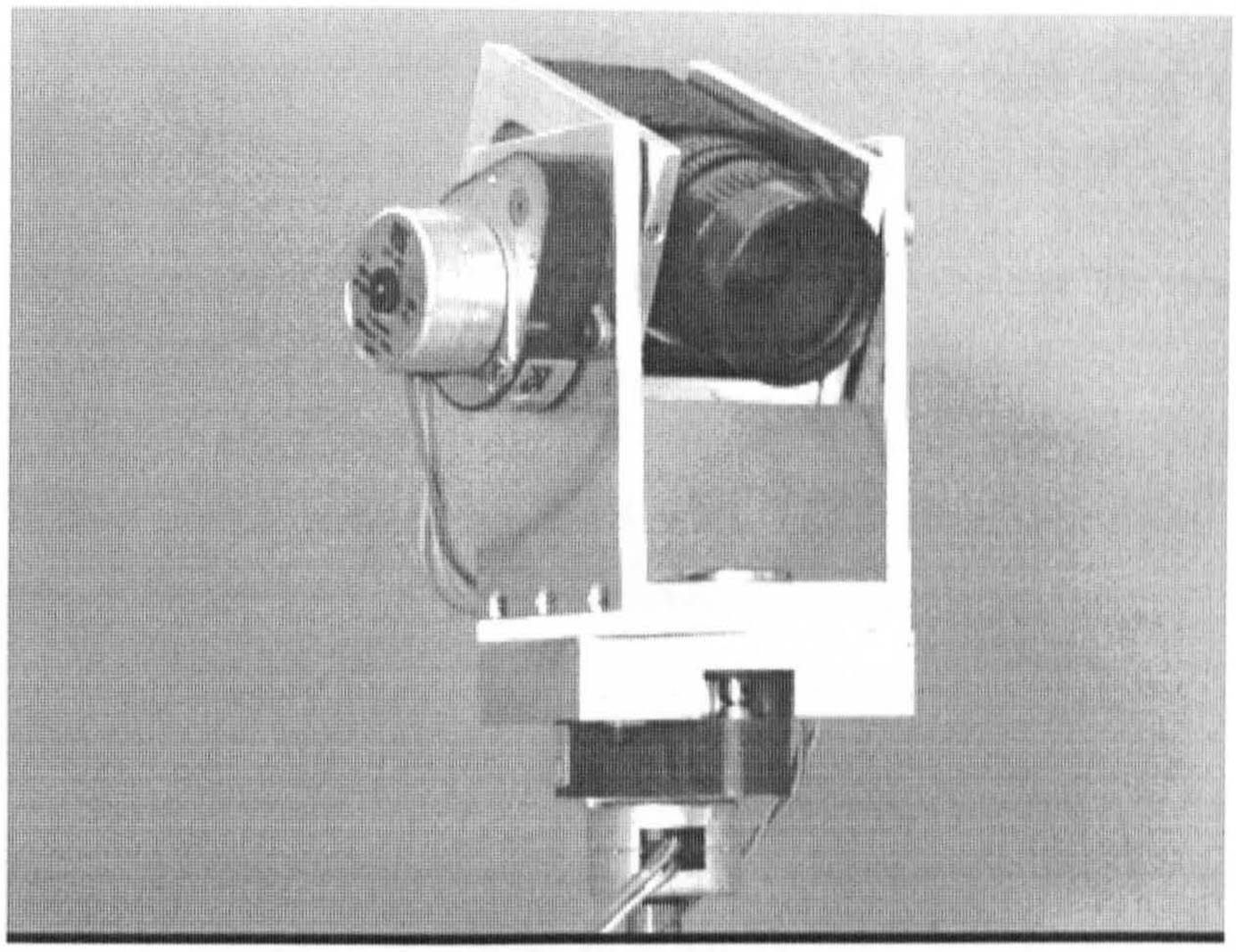

Figure 6.7 The camera pan and tilt mechanism.

orientation of the camera by panning and tilting the camera. The two degrees of freedom are sufficient to find the object to be measured anywhere inside of the measurement support frame. The pan and tilt angles are changed by separate two stepper motors, which are driven by computer software through the interface box.

6.2.5. Cameras and lens

The accuracy requirement necessary for the application of photogrammetric methods means that fully understanding the characteristics of CCD cameras is highly important. The desired camera qualities are the highest resolution consistent with geometric stability at a affordable price. The main factors that influence the performance of camera systems are: lens radial distortion; lens decentering distortion; analogue signal distortion, electronic shutter speed, and temperature affects. Some factors, such as lens distortion can be overcome by calibration. The lenses used by the system are three Fujinon (25mm, f/1.8, c-mount) and some other lenses, such as Fujinon (12.5mm, f/1.4, C-mount), Fujinon (8mm, f/1.4, C-mount), and Fujinon (6.5mm, f/1.4, C-mount). The characteristics of the 25mm lenses have been discussed in chapter three. Some factors such as the analogue signal output should be considered by choosing appropriate cameras. The requirement for pixel clock is to ensure that the analogue to digital (A-D) conversion occurs in synchronisation with camera analogue output, as opposed to using the common, but inaccurate, phase locked loop (PLL) timing method. The importance of using a pixel clock is assessed in Beyer, 1992a, but its use ensures that theoretical resolution is increased by a factor of three or more. PLL line jitter is quoted by Analogic, 1991 as 1/4 pixel to 1/8 pixel, whereas the potential subpixel accuracy of target

location with pixel clocking is 1/20 pixel and 1/50 pixel. Early tests using a plumb line have shown errors of between 1/5 pixel and 1/10 pixel without the pixel clock.

Six Pulnix TM6CN cameras (Pulnix, 1991) were selected to use for the system. A thorough analysis of the characteristics of three of the cameras, and their interaction with the frame-grabber has been presented in chapter three. These cameras offer the following features: good stability, high sensitivity, small size, CCIR standard video, pixel clock, and variable electronic shutter speed (1/60s to 1/10000s).

6.2.6. Frame grabber

A frame grabber is necessary for interfacing the computer to the cameras which have analogue output video signals. The frame grabber is usually not just a device for image acquisition, but can also include digital image data storage, image processing, and image display. The image processing capabilities of a frame grabber can vary significantly between frame grabbers, for instance, some have hardware image filtering or DSP for general purpose computing. The choice of a frame grabber depends on the requirement of a particular system. For the purpose of an automated 3-D measuring system the frame grabber must satisfy the following criteria: **(i)** multiplexed inputs to support up to 6 cameras; **(ii)** pixel clock to control the A/D converter for overcoming line jitter; **(iii)** enough memory to temporarily hold all image views coming from the multiple cameras; and **(iv)** relatively low cost. The frame grabber SVMGRB4MB (Figure 6.8) made by EPIX (EPIX, 1991) is suitable because it has six inputs, a single pixel clock input, 4Mb of image memory and an architecture easily controlled by software. This frame-grabber is made in the USA and is marketed world-wide. The cost of the frame grabber, was just over 2000 pounds.

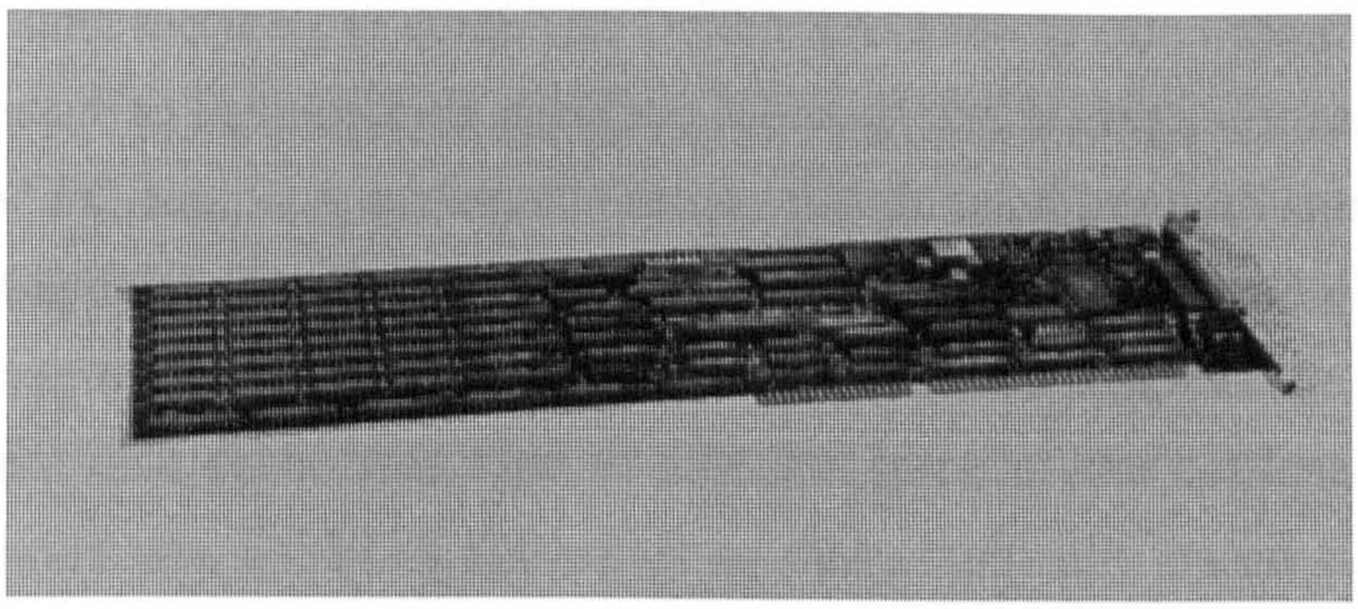

Figure 6.8 Structure of the EPIX frame grabber.

6.2.7. Interface box

In order to control the various hardware components of the system, such as the Maxtascan

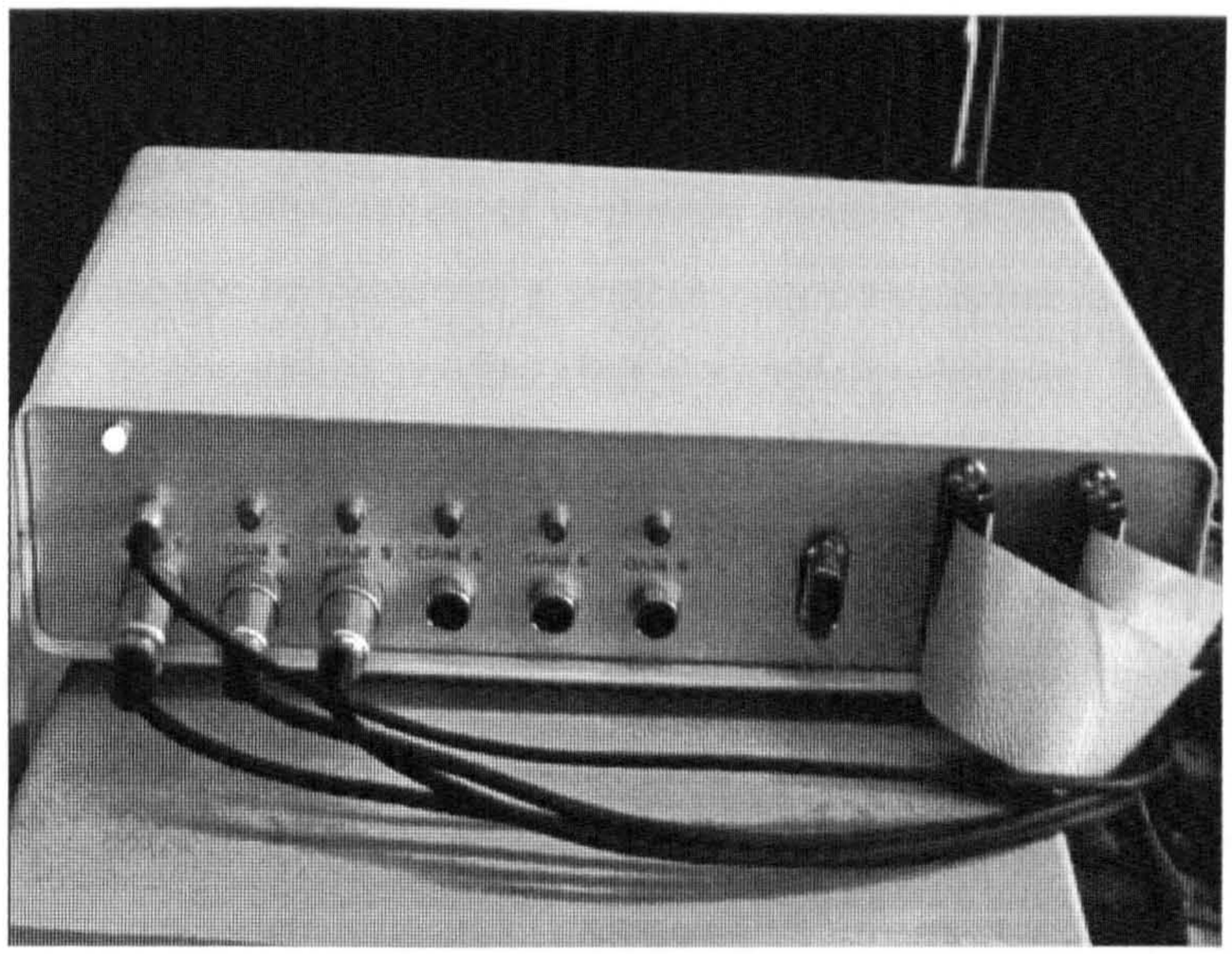

Figure 6.9 Overview of computer interface box.

X-Y table, laser translation mechanism, object rotation table, and exposure time control for each camera, an interface box (Figure 6.9), which was built by Katsimbris, 1993, is used. This interface box made use of a ninety six line parallel I/O card which connects the computer to the various periphery items. The interface box contains a 12 V power supply for the cameras and the lasers. All the periphery devices can be controlled by computer through the interface box.

6.2.8. Computer

The task of image processing, target recognition, target location, finding correspondences and free bundle adjustments generally requires a lot of processing power if the measurement process is not to take too long to complete. Double precision is often required if the derived XYZ co-ordinates are to be numerally accurate. Memory size is also a critical specification. A 80486 based IBM PC computer system can satisfy this demand but with some restrictions. In this project, for financial reasons, a 80486 motherboard with 33MHz and 4Mb memory was installed in the case of an old PC 80286 PC system. The hard disk storage was upgraded to 110Mb and a hard disk cache was used to alleviate some of the bottleneck problem. The display card selected was a SVGA(800X600) so that graphically based display algorithms could be used. The "C" language was chosen for programming for reasons of flexible syntax, structured programming, and popular use. The Microsoft C/C++ version 7.0 compiler, as well as Turbo C/C++ version 3.1 compiler were used and some interface subroutines were written in assembly language for higher efficiency.

6.3. Software system design.

In the research process the importance of software modules is often more critical than the hardware. This is because the hardware of a system may be updated and changed but the same software should provide consistent results after a simple recompile. Therefore, the software should be written in a modular manner with portability in mind.

An IBM PC based operating system has been chosen for software development. MS-DOS is not expensive and is easy to install and use. The supply of compatible software is immense. However, the 640Kbyte memory limitation is a great disadvantage for the large data structures used in image processing and photogrammetric algorithms. The 16-bit segmentation of memory also requires much extra effort when programming. Partial alleviation of these problems may be obtained by using DOS extenders which some compilers are specially designed to make use of. Another approach is to use expanded memory via standard drivers and interface routines. This supplies more RAM, but with similar segmentation problems. Another operating system is Microsoft Windows^{TM}, which is a Graphical User Interface (GUI) operating system and an extension of Microsoft DOS. The Windows environment is comparable to SUN's Open Windows, or the Motif Window manager. DOS applications can be run in a Window. MS Windows offers two advantages: the processor runs in the so called "protected mode", each application protecting from the others; and the use of a mechanism allowing access to all the available memory, swapping on to disk when necessary. Although MS Windows has the reputation of being easy for users but difficult for programmers, aspiring photogrammetric researchers, especially those considering commercial applications, are using it as the development environment of choice. Microsoft Windows was not chosen for the primary software development of this system, at the first stage, due to the lack of supporting drivers for peripheral devices such as frame grabbers and interface cards. However, by the end of the project a Microsoft Windows package was written and has proved successful. Therefore, three versions have been implemented for this system: DOS command version, DOS menu version, and Windows GUI version.

(i) DOS command version

All of the functions in the system were written in C (Microsoft C/C++ 7.00 compiler) and assembly language, so the hardware potential of the IBM PC could be fully used. The functions of the system, such as grabbing images and various image processing algorithms, were compiled into individual executive files. Under the DOS prompt, when you type in the function name and relative parameters required, the related function is executed. The DOS version is similar to the interpreters in some software packages, in which the input command

is analysed and executed. Such a method has the advantages of being simple to write, easy to modify, and quick to operate.

(ii) DOS menu version

All of the programs in this version are written in C using the Microsoft C/C++ 7.00 compiler and assembly language. A simple DOS menu interface was constructed to control the complete system (Figure 6.10). The objective was to provide a logical and easy to use system with step by step control of each element of the system to set up measurement. The operation of the system is controlled by a software-driven pop up menu. The user's interaction with the system takes place with a standard keyboard and a mouse. The 3-D measurement of an object can be completed, in a step by step manner, by choosing the appropriate function, or automatically by using a quick question and answer module.

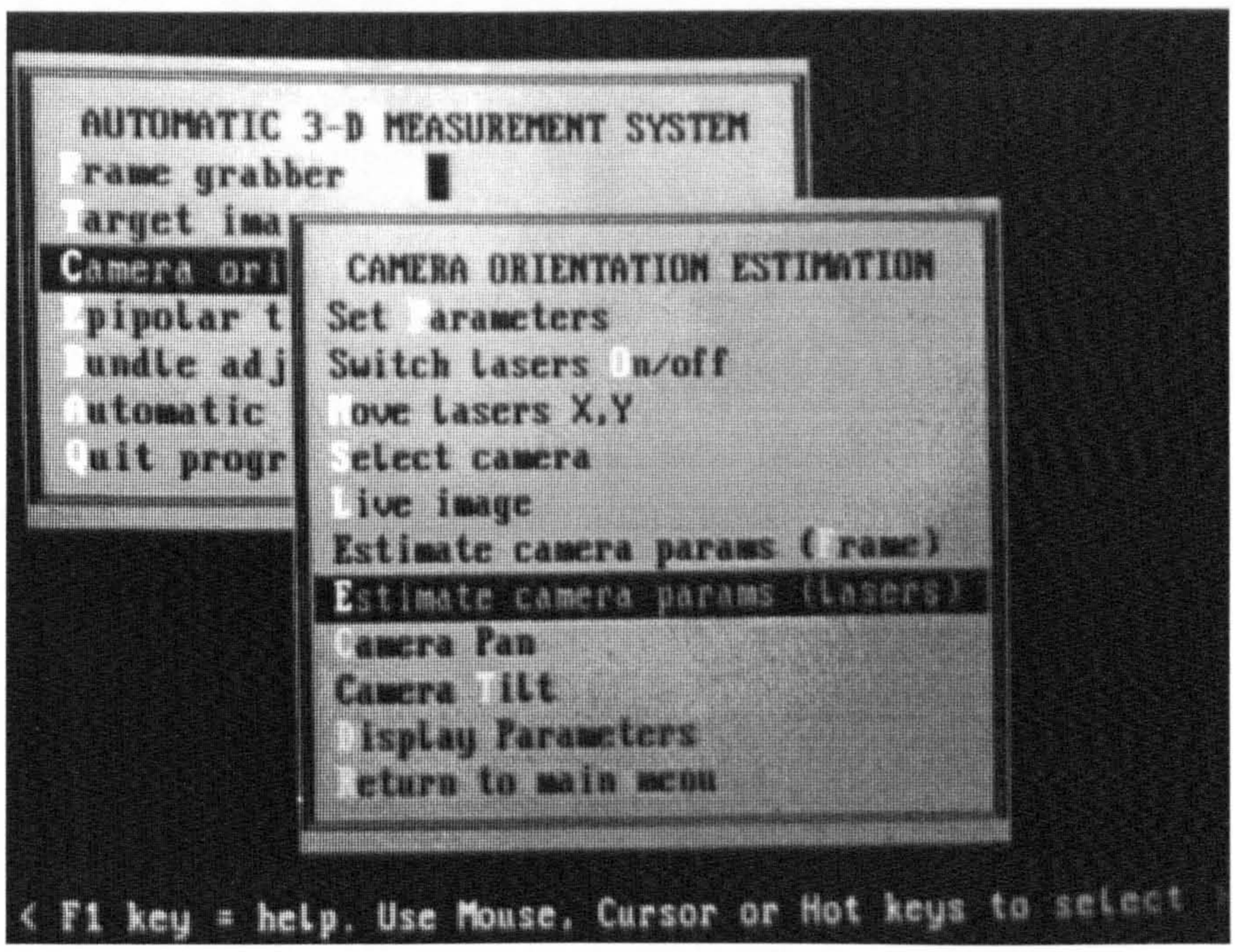

Figure 6.10 DOS version system menu.

(iii) Windows GUI version

A Windows GUI version has been developed because Windows provides considerable advantages to both users and programmers over the conventional MS-DOS environment. The benefits to users and the benefits to program developers are really quite similar because the job of a program developer is to give users what they need and want. Windows makes this possible. By using Windows, the users are no longer expected to spend long periods of time learning how to use the computer or mastering the operations. Windows helps because all

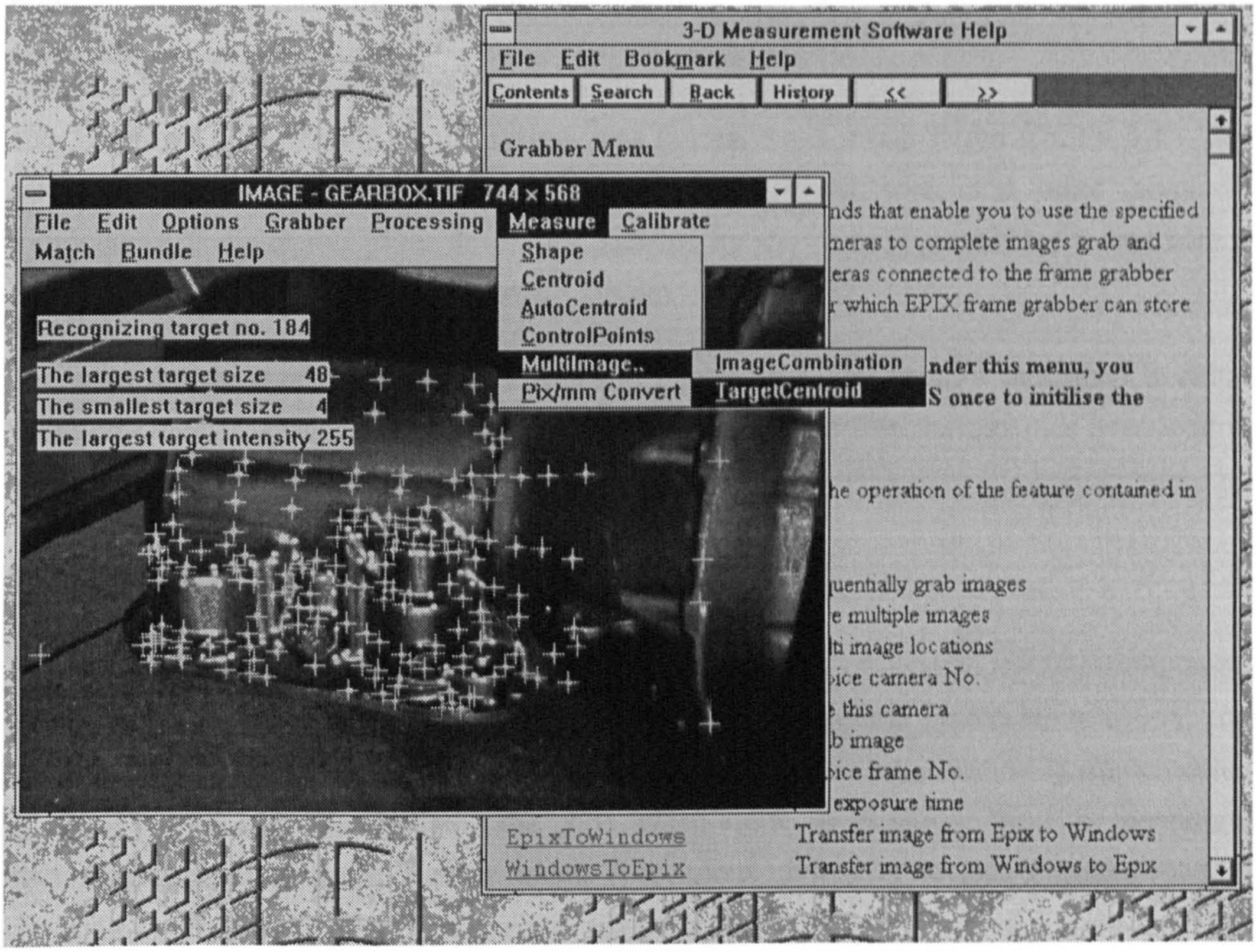

Figure 6.11 Windows version system menu

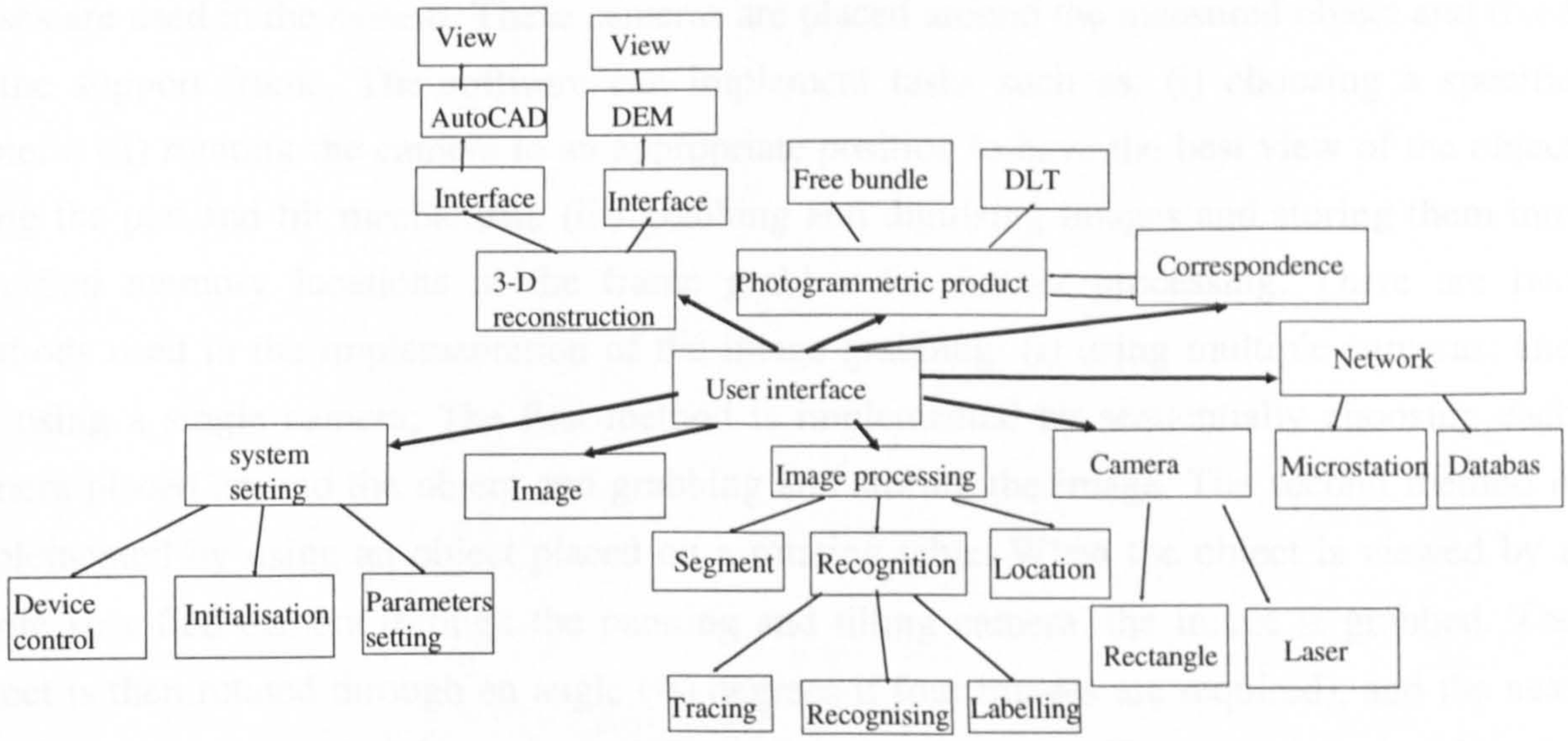

Figure 6.12 Diagram of the system software.

Windows program have the same fundamental look and feel. This is true for the system developed as part of this thesis.

The Windows GUI version of the system was implemented using Turbo C/C++ 3.1. The package allows the use of menus, dialogue boxes, scroll bars, and other graphical components. Some menus of the developed package are shown in Figure 6.11. On-line help is also developed to help users to operate this system.

The main functions of the system are shown in Figure 6.12. and are now described in detail based on DOS GUI version. The Windows GUI based version uses the modules described in this section with some minor modification.

6.3.1. The image acquisition module

The image acquisition software module includes the functions of: system initialisation; target object location; peripheral device control; camera selection; system parameter selection; and sequential image grabbing by use of multiple cameras. System initialisation is implemented by using pop up menus to initialise the ports which are to be used to control the peripheral devices and the EPIX frame grabber board. The various peripheral devices are controlled by choosing options in the menu. The camera selection has to be performed each time an image is grabbed as the EPIX A/D converter has to be synchronised to the camera video signal. The system parameters include the setting of the camera exposure time, the camera to be used, and various status flags for automatic procedures. Currently many as six cameras with various lenses are used in the system. These cameras are placed around the measured object and fixed to the support frame. The software can implement tasks such as: (i) choosing a specific camera; (ii) rotating the camera to an appropriate position to have the best view of the object using the pan and tilt mechanism; (iii) grabbing and digitising images and storing them into specified memory locations in the frame grabber for further processing. There are two methods used in the implementation of the image grabbing: (i) using multiple cameras; and (ii) using a single camera; The first method is implemented by sequentially choosing each camera placed around the object and grabbing and storing the image. The second method is implemented by using an object placed on a rotating table. When the object is viewed by a single specified camera through the panning and tilting camera, the image is grabbed. The object is then rotated through an angle (90 degrees if four images are required), and the next image is again grabbed and put into a different memory location. The second method has the advantage of reducing the number of camera interior parameters. Another advantage is that only a single camera and lighting equipment is needed. This is convenient because it is often difficult to simultaneously set up good lighting for several cameras. Figure 6.13 illustrates

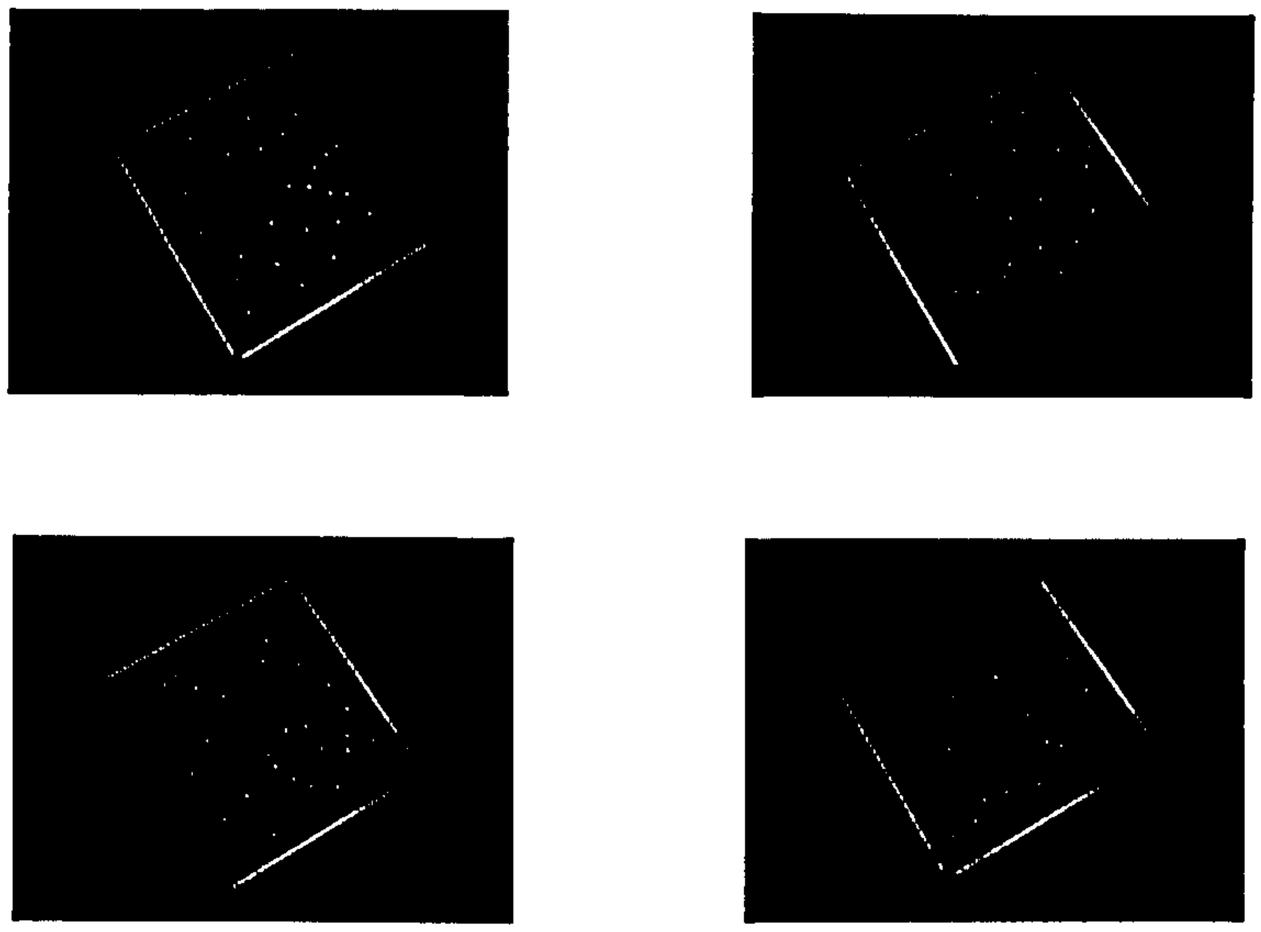

Figure 6.13 Four image views of an object grabbed by one camera and lens.

four different views of the test field object by using one camera where the object has been rotated through 90 degrees four times. The module FGRABBER performs the image acquisition operation.

6.3.2. The image processing and analysis module

The digitised images, obtained by the image acquisition module and stored in the memory of the EPIX frame grabber, consist of 744 x 568 pixels each with a grey-level value ranging from 0-255. The next step for the system is to identify the targets in each of the images. The success of this step depends mainly on factors such as the illumination of the work area and on the algorithms used for identification. In order to improve the quality of the digital images which will be used in 2-D and 3-D analysis, the system provides some basic image processing function modules. These modules are divided into several groups:

- image management, including: image read, write, clear, camera selection, frame selection, image display;
- image filtering, including: low pass filters such as median filter, smoothing, and averaging filters; and high pass filters such as Robert, Sobel, or Laplace filters;
- image algebraic operation, including: two image arithmetic operations: such as *add*, *subtract*, *multiply*, and, *divide*; and image logical operation such as the *and*, *or*, and *not*;
- image geometric operations, including: image enlarging, shrinking, or rotation;
- image edit operations, including: point, line and area editing, or extraction of regions of interest; and

• Other miscellaneous image operations such as image histogram and image profiling.

The main steps for target 2-D co-ordinate extraction often consist of three parts: (i) image segmentation; (ii) target recognition; and (iii) target subpixel location.

6.3.2.1. The image segmentation module

The module SEGMENT performs the image segmentation operation. The purpose of image segmentation is to simplify target feature detection. Normally, image segmentation is implemented by converting an image into a binary form. In this process, the choice of an appropriate threshold value for binarization of the image is very critical because all subsequent processes depend very much on this. It is generally understood that automatic binary thresholding methods based on histogram analysis are not useful for most object detection applications (Haralick, 1992). Image grey scale normalisation or heuristic segmentation processes by multithresholding are generally used for poor illumination conditions where uneven brightness distributions are encountered across the image. In the case of the experiments performed in this thesis, retro-reflective targets are used. These can provide a black background and a white target image with relatively little, if any unwanted background resulting in almost perfect contrast. Because of these properties, multiple thresholding would appear not to be necessary. Furthermore, as the binary image is only used for target recognition and a grey scale image is needed for target location, the binary segmentation process does not have to result in a stored binary image because the segmentation level can be set using the look up tables for the display. Hence a threshold value is easy to manually choose. Furthermore, a large range of values can be used without influencing recognition results. All the pixel values which are higher than the thresholding value are considered as object pixels. This method can save memory storage space because there is no need to allocate the memory to store the binary image.

6.3.2.2. The target recognition module

Target recognition is performed by module AUTOLOCA. There are several methods that are commonly used for the recognition of circular shaped targets. The first method is least squares matching. The circles are recognised by matching the shape of the segmented boundary edges with the circular shape of an ideal target. The centre location and diameter can be determined from the edge points. The advantage of the use of the boundary edge detection method is that it is computationally robust and can give high accuracy results even under bad lighting conditions. The disadvantage of the method is that a template of the ideal target must be constructed and the computation cost is large. The second recognition method in common use is edge detection and edge tracing using thinned edges (El-Hakim, 1986; Zhou, 1990; and

Trinder, 1993). This method is based on the fact that target edges in the image have a high gradient value. The intensity value surrounding the target will be composed of a few sharp changes over a small number of pixels. Edge detection is implemented by an detector such as Sobel, Robert, Laplace, or Canny edge detectors. The tracing and thinning algorithms are well documented (Pavlidis, 1982). The circular targets are then recognised by judging their shape and size as described in chapter 2.4. A further method uses a recognition algorithm consisting of object edge tracing and then object filling. In most cases the edge detection process is not necessary because the retro-reflective target contrast highly with the background. Edge tracing is implemented on a grey scale image by finding the edge of a grey scale target through judging whether its grey level value is higher than the chosen threshold value. At the same time as tracing, the co-ordinates of each edge pixel are recorded. These co-ordinates are used for calculating the shape factor. A filling algorithm is implemented based on the set of edge co-ordinates to calculate the area of the object. The object is recognised by the method described in chapter 2.4. and the approximate position of the target is also obtained.

6.3.2.3. The subpixel target location module

The module AUTOLOCA contains the automatic target location operations. It is necessary to locate the precise co-ordinates of the centre of each target image with subpixel accuracy. The subpixel precision of the location algorithm has a direct influence on the overall precision that can be achieved by the measuring system. This is because that the 2-D co-ordinates of each target image, acquired from multiple views by the subpixel location algorithm, are the only observation information used in a bundle adjustment to calculate the 3-D co-ordinates of the targets on the object. There are two main subpixel location methods in general use: (i) the least squares method; and (ii) the centroid method. The two location methods have been discussed in chapter 2.4. The centroid method is chosen for the system due to its simplicity, quick computation, and reasonable accuracy (Trinder, 1989). The most common method for finding the position of the centroid of a target image is to place a rectangular window over the target image. All pixels in this window are checked and calculated by the centroid equation 2.18 or equation 2.19. If there are any non zero background values, a global threshold is necessary to remove the background noise and all values less than the threshold value are made zero (Wong, 1986). In practice, using a rectangular window shape to calculate the location of a circle shaped target can cause problems, for instance if two targets are close together the window may contain some unwanted pixels which belong to the second target. This will result in error for the subpixel location of the first target. An alternative method for defining the centroid of a target image has been developed which avoids the unwanted intensity value problem caused by adjacent target image in a rectangular window (Clarke,

1993). An arbitrary pixel within the target image is chosen and a recursive fill algorithm (Pavlidis, 1982) is applied to all pixels within the image which have intensity levels above the threshold value.

The format of the data output by the location algorithm is a line for each target, i.e. camera number, target number (normally labelled as x if unknown), x co-ordinate (mm), y co-ordinate (mm), initial standard deviation for x (μm), and initial standard deviation for y (μm). The following is an example of the data output for two target images:

1000	x	2.3445	-0.2153	1.0	1.0
1000	x	0.8103	-1.2308	1.0	1.0

6.3.3. The camera orientation module

Within the industrial environment it is often the case that each photogrammetric measuring task may be very different, and thus it is usually necessary to individually design the photogrammetric network both to optimise the operation for ease of setting up and economy as well as to ensure that a certain level of precision of measurement will be attained. Hence, the automatic determination of camera exterior orientation is one of the first tasks that has to be solved in an automated 3-D measuring system. As the emphasis of the research has been towards a flexible system it has not been assumed that this information would be determined for a given system, rather, that the cameras may be placed at any point and orientation. Two implementations of the closed form space resection are implemented as discussed in chapter four. The first method is an automatic frame extraction method, in which a three line rectangular frame is used for an automatic and rapid extraction of the orientation parameters. The second method is an automatic laser spot target extraction method, in which four lasers are used for the automatic estimation of camera parameters.

6.3.3.1. The automatic three sided rectangle extraction module

The module RORIENT performs the automatic determination of the camera exterior orientation by extracting a three sided rectangle in the image view. This module automatically processes the image in which a three sided rectangle surrounds the measured object by completing the detection and extraction of line segments, the fitting and merging of line segments, the determination of the co-ordinates of the intersection and termination points, and finally calculation of the camera orientation parameters. The input to this module are the 3-D co-ordinates of the two termination and two corner points which have previously been measured and are not required high accuracy, and the camera focal length. The output of the

module are the 2-D co-ordinates of the four image points and their correspondences to the object points, and the exterior orientation parameters of each image viewpoint ranging (Xc, Yc, Zc, ω, φ, κ).

6.3.3.2. The automatic laser target extraction module

The module LORIENT automatically determines camera exterior orientation by extracting four laser spots in the image view. The correspondence between the laser spot in the object space and the laser target images in the image plane can be obtained by switching specified lasers on and off. The rest of the procedure for computing the camera exterior orientation estimation and the input and output data is as the same as the module RORIENT.

6.3.4. The target correspondence module

The computation of target correspondences is a critical step in the measurement of a 3-D object. A 3-D target matching algorithm has been developed which is based on a 3-D intersection and is combined with a bundle adjustment process. The theory has been discussed in chapter two and the performance has been evaluated in chapter three. The module MATCH3D is used to automatically compute the correspondence between target images. The inputs of this module are: **(i)** camera orientation parameters from the module RORIENT or LORIENT at the beginning of system operation, or from the bundle adjustment output in the form of refined parameters; **(ii)** camera interior parameters which are determinated by plumbline method or from the output of a self calibration bundle adjustment procedure; **(iii)** the minimum number of target views is allowed, and the matching 3-D tolerance value which can be manually specified or automatically decided by the RMS of targets from the output of the bundle adjustment; and **(iv)** the unlabelled target image data. All these data are accessed by the module from files rather than manually input so that automatic operation is possible. The outputs of this module are three files: **(i)** the co-ordinates of matched target images; **(ii)** the co-ordinates of the remaining unmatched target images; and **(iii)** the 3-D co-ordinates of the matched targets. The matched target images can be combined with any previous matched target images and put into the bundle network. The camera exterior and interior parameters can be further refined by the output of a new bundle adjustment. These parameters can then be fed back into the MATCH3D module to assist in matching any remaining unmatched target images. The process continues until all target images are matched or satisfactory object coverage result has been achieved. When the matching procedure is completed, the 3-D co-ordinates of the targets and the camera parameters are usually obtained to a high degree of accuracy because the free bundle adjustment procedure has been used through out the matching process.

6.3.5. Bundle adjustment module

The module SCBA (Self Calibrating Bundle Adjustment) performs the bundle adjustment operation. The SCBA module offers flexibility for the adjustment of a general photogrammetric multi-station network which can be simultaneously combined with various types of control constraints. The main features of the SCBA module are:

- multiple cameras and lenses;
- camera self calibration;
- free network adjustment;
- the use of weights to constrain some parameters;
- flexibility to fix or free any: target co-ordinates; camera interior parameters; or camera exterior parameters;
- the use of the Cholesky triangular matrix inversion;
- statistical analysis of the output;
- the dynamic allocation of memory based on data quantity;
- the use of control constraints such as the distance between: targets; camera positions; or between targets and a camera position;
- an algorithm for the minimisation of storage requirements and computing time;

This software package performs an iterative adjustment of all variables consisting of the target co-ordinates, camera exterior and interior parameters. New estimations of these parameters are produced in each iteration. These new values are used to produce new variables which are then fed back into SCBA to produce further estimations. The iterations continue until SCBA can produce a solution that is within strict convergence criteria. The inputs of the SCBA module are: the starting values of target co-ordinates from the matching module or from the SCBA output; the starting values of camera exterior orientation from the automatic orientation estimation procedure or the output of SCBA; the camera interior parameters from plumb-line estimation or the output of a self calibration bundle adjustment; and target image co-ordinates from the AUTOLOCA module. The input of SCBA can also include distance constraints (often called survey data). The distance between the targets, between the cameras, or between the targets and a camera position can be used as constraints. The output of SCBA includes the refined 3-D co-ordinates of targets, camera exterior and interior parameters and the statistics relating to these data, such as the average and maximum co-ordinates RMS of each target and the camera parameters, and the image measurement residual of each target image. The target co-ordinates RMS can be use as a tolerance for further target image matching. All of these statistical values can be used to evaluate the adjustment procedure and providing a systematic analysis which reflects the accuracy and precision of the input data and the network. The resulting 3-D co-ordinate data can be put into AutoCAD after they are

converted to a compatible format of AutoCAD.

6.3.6. Object reconstruction module

The visual presentation of results is an essential tool which can allow the verification of the measurement process. There are many commercially available graphics software packages such as AutoCAD, or Microstation. These packages need special data formats for their use. Considering the cost of these packages and the requirements of this prototype system, an AutoCAD software interface module was written to allow the creation of a simple DTM.

6.3.6.1. An AutoCAD interface module

AutoCAD has two common data formats, DXF and DXB, which consist of ASCII data and binary data respectively. The task of this module is to translate the 3-D co-ordinates of targets into one of these data formats so that AutoCAD can directly manipulate and display the 3-D information. The DXB format was chosen as it stores data more efficiently. The module DXBTA performs the automatic conversion of target 3-D co-ordinates to the AutoCAD compatible DXB format. Figure 6.14 illustrates the reconstruction of the test field by AutoCAD, in which the three sided rectangle is chosen as a base plane and rods are constructed with a line that is perpendicular to and connected to the plane.

In practice, 3-D co-ordinates are normally required to be in wire frame mesh form for hidden line removed, and rending. The task of reconstruction of a 3-D surface is not simple because

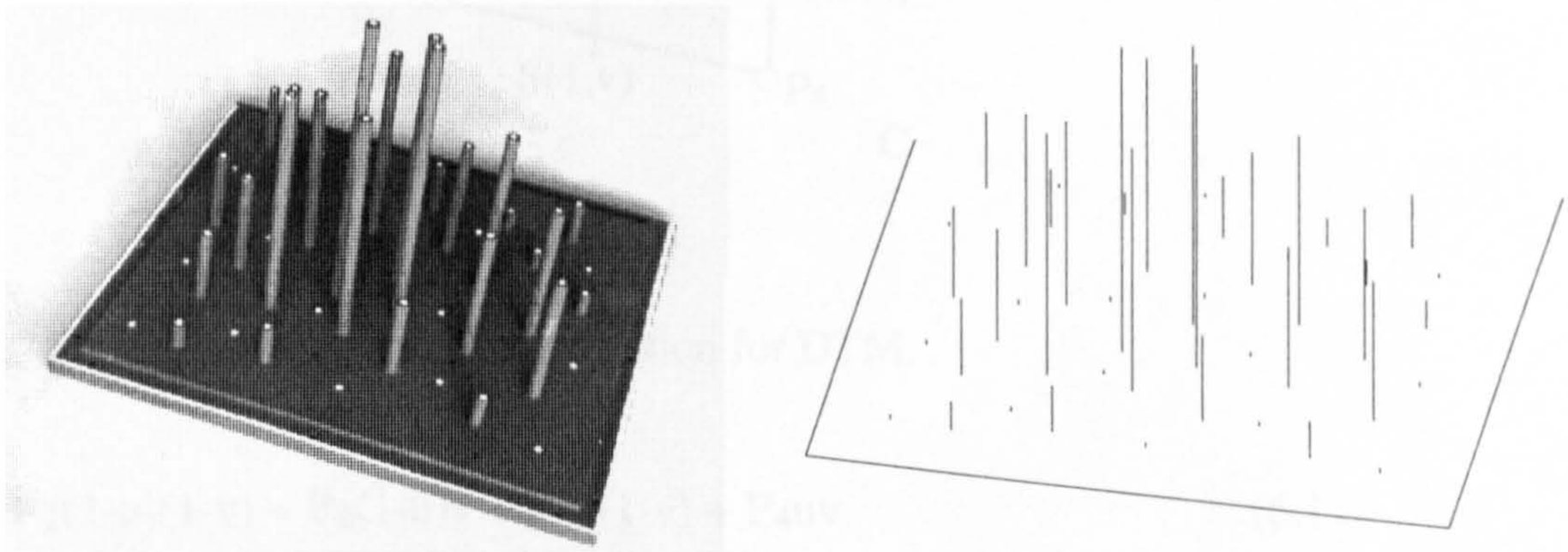

Figure 6.14 a) The testfield b) Reconstruction of the test field

the 3-D co-ordinates are often randomly distributed it is difficult to automatically make the correct connection between the targets.

6.3.6.2. The DTM module for reconstruction of 3-D surface

A digital terrain model usually consists of a regularly distributed set of connected grid points. Although in some cases, the calculated surface points are relatively sparse where the surface relief varies slowly, in other cases, the surface points are likely to be dense where the surface changes rapidly. To build a surface model with regular grid intervals from an irregularly distributed set of grid points from the output of a bundle adjustment procedure, interpolation and resampling methods may be required. The resulting surface model is a single valued function, i.e. for any (x,y) point co-ordinates, there is only one Z value. The 3-D co-ordinates of targets obtained do not usually produce a regular grid in the object space, so a regular grid has to be defined to construct the DTM data format. In this case grid point co-ordinates are computed by bilinear interpolation between neighbouring points.

(i) Bilinear interpolation of grid points

In the bilinear interpolation method (Pavlidis, 1982), a grid surface is described by the following form of vector equation (Figure 6.15):

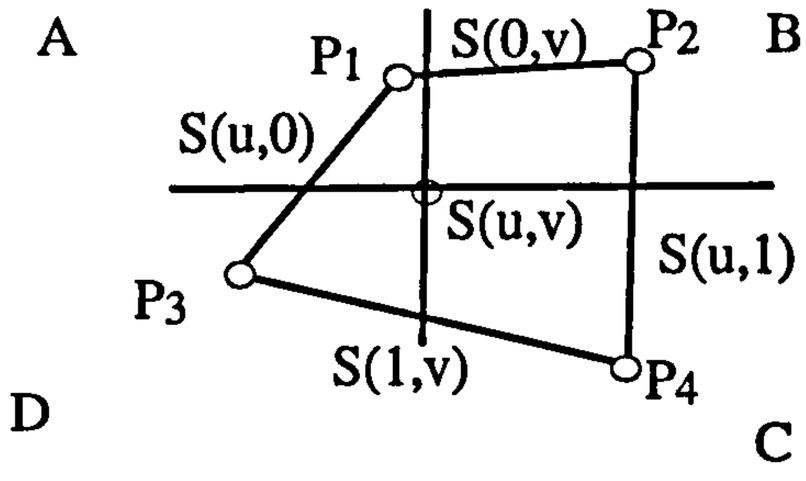

Figure 6.15 Bilinear interpolation for DTM.

$$S(u,v) = \mathbf{P_1}(1-u)(1-v) + \mathbf{P_2}(1-u)v + \mathbf{P_3}u(1-v) + \mathbf{P_4}uv \qquad (6.1)$$

where 0 â u,v â 1 and S(u,v) is the grid point and $\mathbf{P_1}$, $\mathbf{P_2}$, $\mathbf{P_3}$, $\mathbf{P_4}$ are four neighbouring points.

The task is to calculate the **u** and **v** based on the four neighbour points so that the value of the interpolated grid point can be computed. It can be seen that $S(0,0) = P_1$, $S(0,1) = P_2$, and so on. Also S(0,v) is the line segment joining P_1 and P_2, S(1,v) is the line segment joining P_3 and P_4, and so on. If the four points are coplanar, then the surface is a quadrilateral plane

otherwise the points represent a surface of the second degree. The value of the surface with respect to **u** and **v** can be found by solving the quadratic equation. Rewriting the vector equation 6.1 as:

$$x = x_1(1-u)(1-v) + x_2(1-u)v + x_3u(1-v) + x_4uv \quad (6.2a)$$

$$y = y_1(1-u)(1-v) + y_2(1-u)v + y_3u(1-v) + y_4uv \quad (6.2b)$$

$$z = z_1(1-u)(1-v) + z_2(1-u)v + z_3u(1-v) + z_4uv \quad (6.2c)$$

where **x, y, z** are the co-ordinates of the grid point and x_1~x_4, y_1~y_4, and z_1~z_4 are co-ordinates of the four neighbour points respectively. Using equation 6.2a and 6.2b, the **u** and **v** can be computed by solving the quadratic equation. The **z** value of the grid point is then computed using equation 6.2c.

(ii). Choice of the four neighbour points

The choice of the four neighbour points for bilinear interpolation is described as follows: the x,y co-ordinates of the grid points are decided within two loops so that the x,y co-ordinates of all targets are searched. On each quadrant of the surface grid point a target is used which has the shortest distance to this grid point. Four targets which are located in each of the four quadrants (A, B, C, D), are used to construct this four neighbour points. The module DTMTA performs the conversion of irregular target co-ordinates into regular DTM in grid form. The DTM data are expressed as AutoCAD DXB data format so that this package can be used to

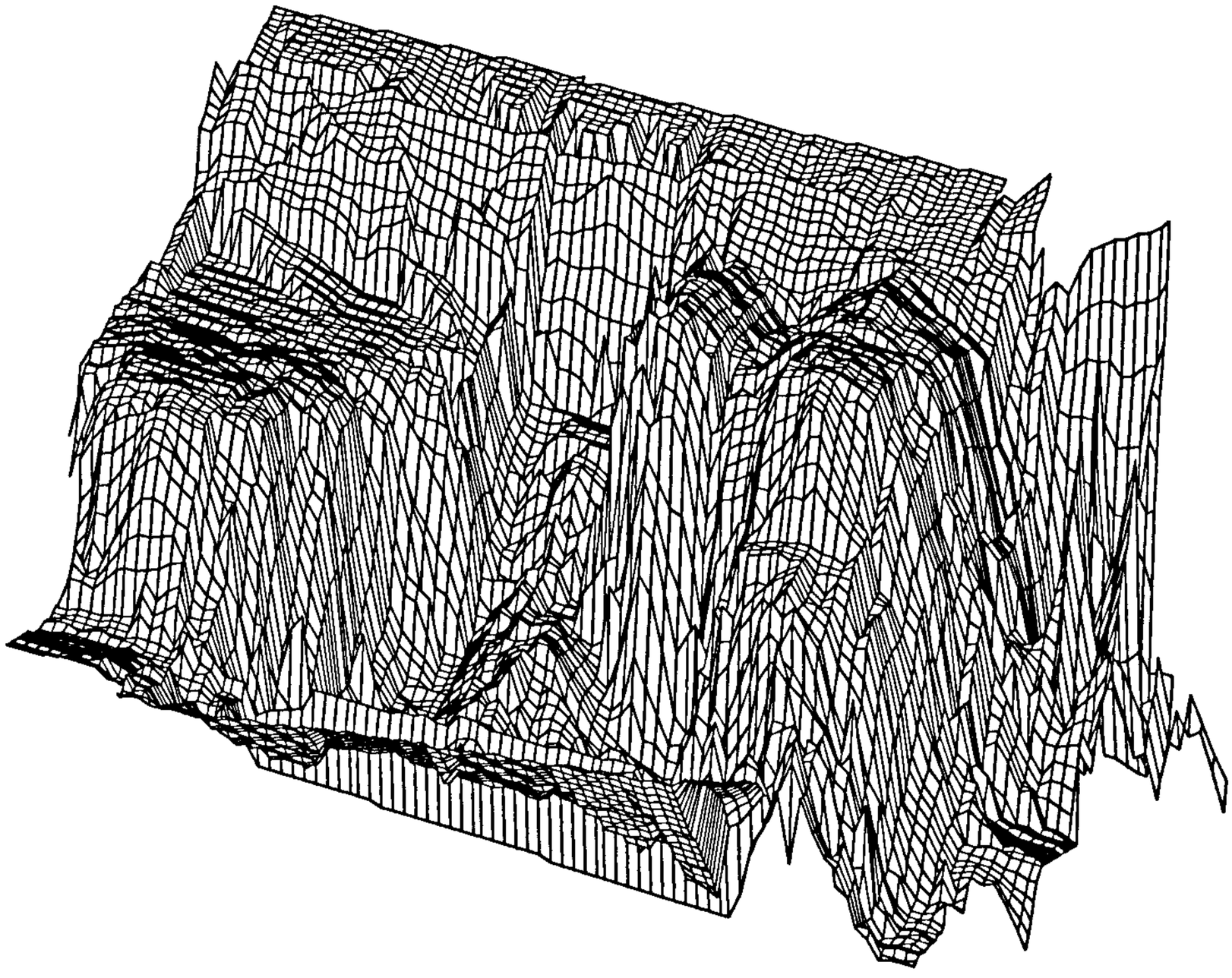

Figure 6.16 Reconstruction of a gearbox through the DTM module

display the DTM. Figure 6.16 illustrates an example of reconstruction of surface of a gearbox through the DTM by using the bilinear interpolation algorithm.

6.4. Summary

This chapter has discussed the design of an automated 3-D measuring system. The aim of the design is to an automated 3-D measurement system using photogrammetric and machine vision techniques that are robust and economic. It has been assumed that initially this system will be used in a controlled environment. At a later stage it is anticipated that further developments will allow the system to be used in an uncontrolled environment. In this chapter the hardware components and software modules have been integrated. Further systematic analysis and example applications will be discussed in the next chapter.

Chapter 7 Some system application examples

7.1 Introduction

There are a number of factors which will influence the overall performance of the measuring system. These factors originate in both hardware and software. For example: the warm-up effect causes a shift in target location centre; the characteristics of the CCD sensors and associated electronics influence both radiometric and geometric performance; the target location algorithm performance is critical for the precise target location; and the performance of the correspondence matching algorithm will influence the system reliability. The analysis of the system as a whole is of great importance in order to discover whether the care taken to minimise these factors has an impact on the ideal performance of the system.

7.2. Example applications

The performance of individual hardware components has been tested and evaluated in chapter three. This chapter concentrates on the automated system applications as a whole using several examples and assesses the influence of various factors, such as: the imaging network and alternative location algorithms. The analysis is based on two set of experiments: laboratory tests, where a number of test fields were used for performance analysis; and on site tests, where the system was used for deformation analysis of fine art wood panels.

7.2.1. Object measurement under laboratory conditions

Within the industrial environment it is often the case that one photogrammetric measuring task may be very different from the next, and thus it is usually necessary to individually design the photogrammetric network both to optimize the operation in the sense of accuracy and economy and also to ensure that a certain level of measurement precision will be attained.

7.2.1.1. Test one: Propeller

A small three bladed marine propeller (Figure 7.1), was chosen as a subject to be measured in the early stages of research and is used here as an example of the progress that was made during the investigations carried out for this thesis. A number of processes were performed manually, such as: target location; camera orientation parameter estimation; target 3-D co-ordinate starting value estimation; and finding target correspondences. The complete propeller was targeted with small circular retro-reflective targets. The target diameter was

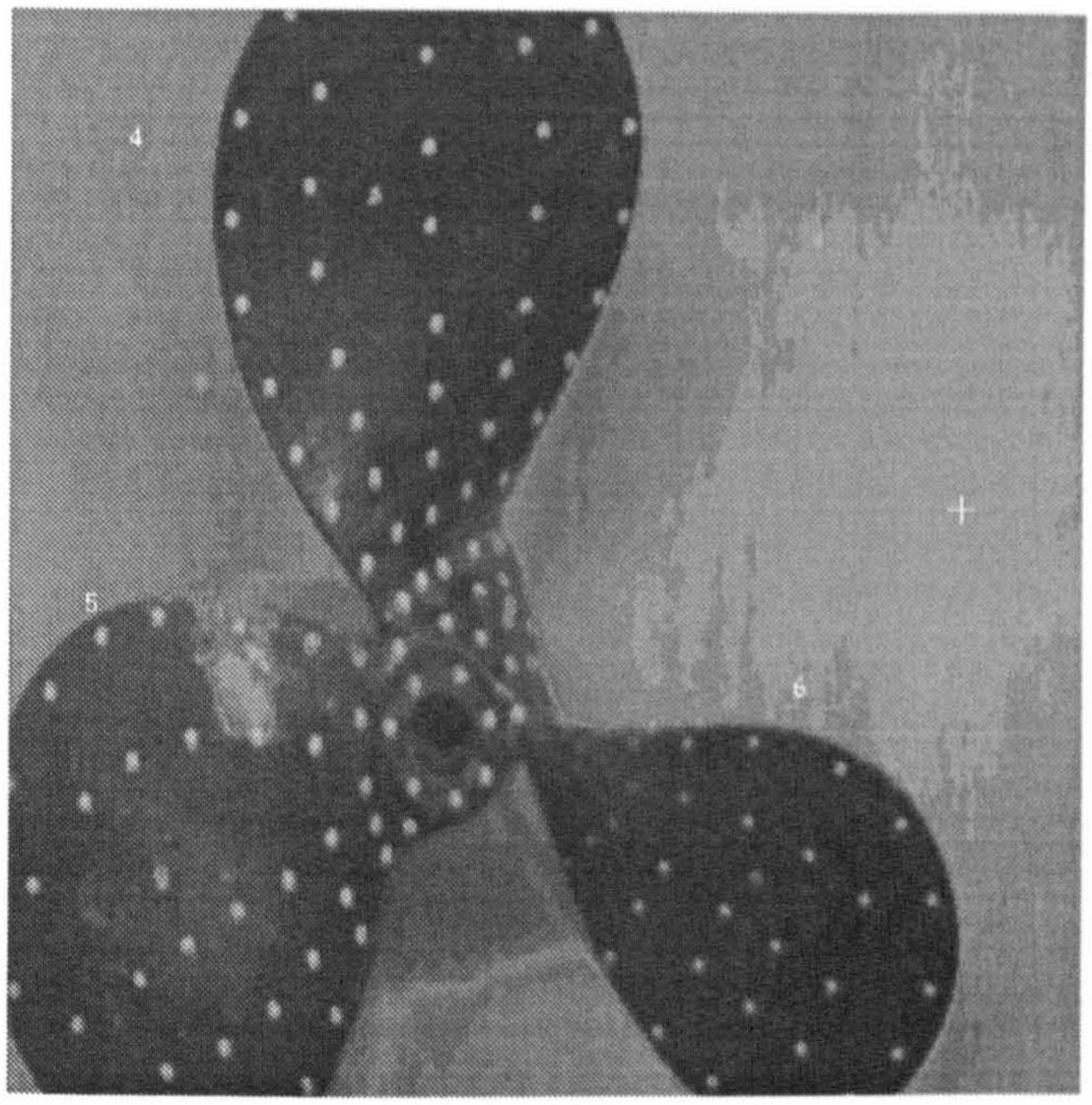

Figure 7.1 Original propeller with some targets

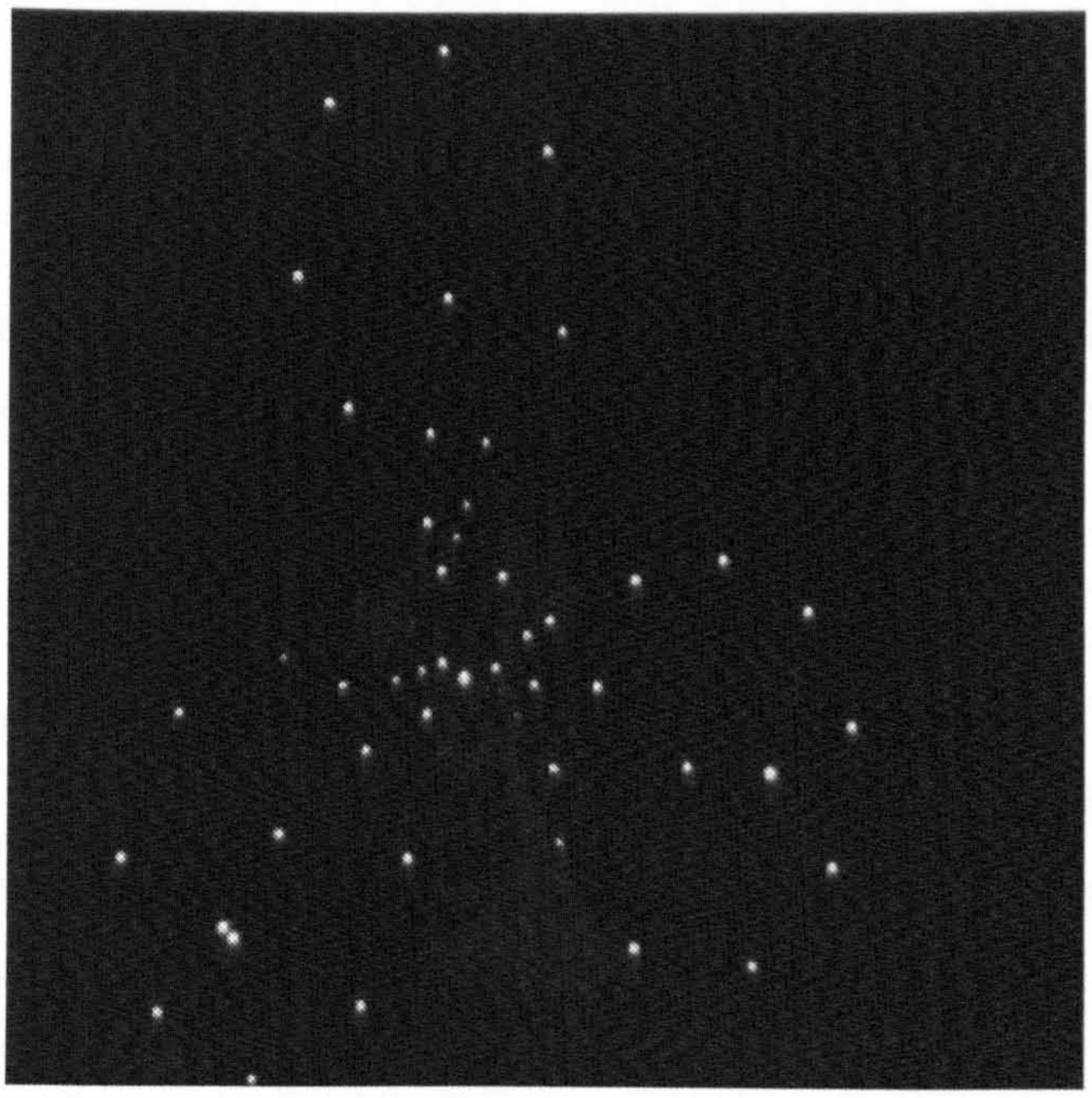

Figure 7.2 Propeller image grabbed for location

chosen to occupy an area of approximately 5x5 pixels in the image. The targets had to be distinguished from the background illumination and precisely located. Poor target image signal-to-noise ratios and uneven background illumination are known to cause poor target location, hence, the image obtained under diffuse lighting conditions (Figure 7.1) was not suitable for accurate measurement. By using retro-reflective targets and illumination which was axial to the camera the quality of the image was improved (Figure 7.2). The targets were identified using binary thresholding and shape detection based on three parameters: area,

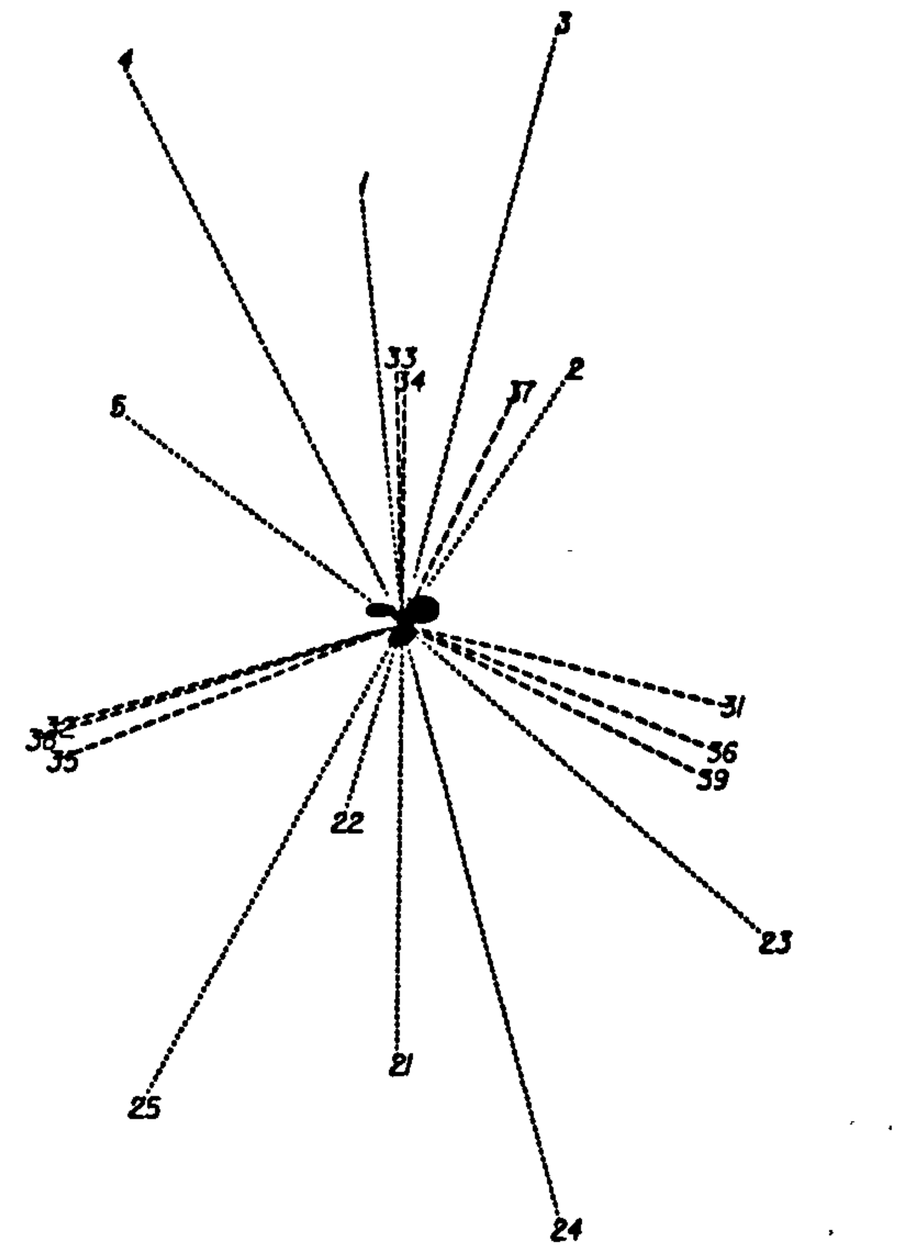

Figure 7.3 Position of the nineteen camera views

perimeter length and degree of circularity. Each target in each image, was given a label and an approximate position. The centroid of each target was then computed using the grey scale image to provide a subpixel estimation of each target location. The final image processing task gave consistent labels for each object target point in all images. Labelling was carried out manually because the automatic labelling algorithm was not available at that time.

Nineteen views were taken in an attempt to obtain a minimum of two target images of each target. The distribution of these nineteen views is shown in Figure 7.3. The dotted lines show the main positions of the cameras which viewed the propeller from the front and the back, while the dashed lines show the positions of some additional viewpoints which were used to link together the upper and lower surfaces of the propeller.

Following manual target location and labelling, all image co-ordinates were used to determine the 3-D object co-ordinates of each target using a bundle adjustment method incorporating self calibration of the camera system used. A software package called the Generalised Adjustment Program (GAP) previously developed at City University was used for the bundle adjustment calculation. As redundant measurements were available, it also provided statistics concerning the precision and accuracy of all the estimated parameters. The average RMS error in 3-D object space and the average standard deviations of target images are shown in Table 3.5. These statistics indicated that in this case a subpixel image measurement accuracy of around a tenth of a pixel was attained. Given the network geometry, this resulted in a precision of approximately 1 part of 5,000 of the object space.

	$RMS_{\sigma X}$	$RMS_{\sigma Y}$	$RMS_{\sigma Z}$
RMS of object target co-ordinates(mm)	0.0632	0.0603	0.0611

Table 7.1 Result of bundle adjustment

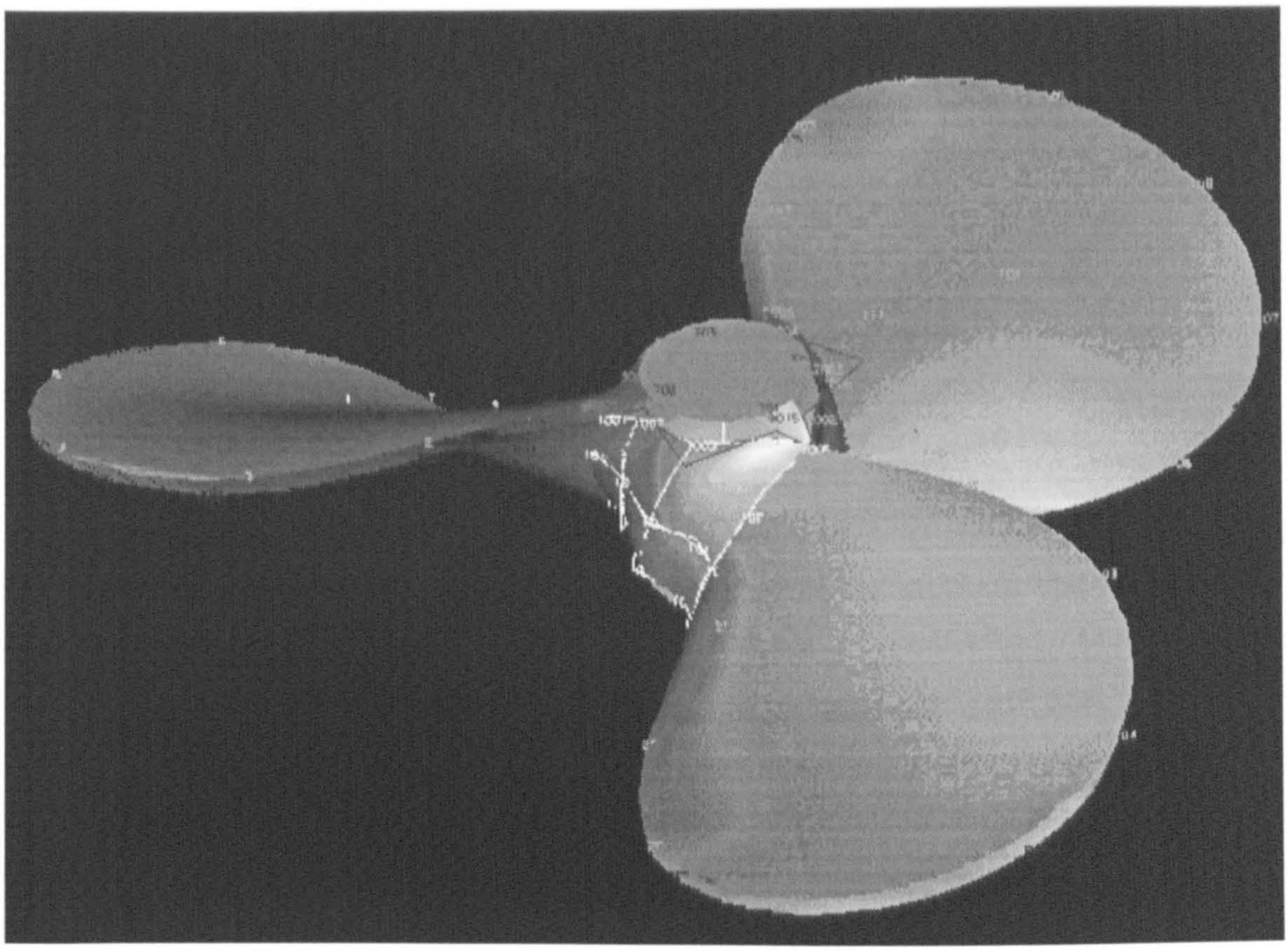

Figure 7.4 A view of the 3-D model of the marine propeller

The resulted X, Y, Z co-ordinates of the target points were downloaded into a CAD package and used to derive three dimensional B-Spline surfaces representing each of the propeller surfaces. A view of this CAD model is shown in Figure 7.4.

The initial results obtained in this initial study are due to several causes: the low resolution (512x512) of the old Pcvision frame grabber; and an old CCD camera which was poorly adjusted. Subsequent work has shown that precisions of 1 part in approximately 30,000, or better, may be obtained by careful use of modern hardware, such as using an EPIX frame grabber and Pulnix TM-6CN cameras.

One thing to be noticed here is the operation time required for processing the data. Without automatic procedures, it is difficult to determine target correspondences because all the circular retro-reflective targets have neither distinct geometric or intensity features (Figure 7.2). Another set of images, in which the background and contour of the propeller were visible (Figure 7.1) had to be grabbed and printed out. The locating and labelling of the target

images were manually carried out by carefully comparing and identifying targets between the printed image and the image grabbed for location (Figure 7.2). This procedure took a long time and was very laborious. Even with care, there were still a number of mistakes which were made in labelling. The estimation of 3-D target co-ordinate starting value and the estimation of camera orientation parameters were also carried out manually. The manual guess of these parameters often caused errors. It took more than two days to complete all the procedures of the measurement and visualisation. These problems identified the necessity for the automation of target image correspondences, the automatic estimation of camera orientation parameters, and starting values of the 3-D co-ordinates of targets.

7.2.1.2. Test two: Test field

A number of experiments were performed with the test object shown in Figure 7.5. The test field was constructed of an aluminium base into which twenty eight round rods of differing lengths had been inserted. The whole assembly was painted matt black. Round retro-reflective targets were placed both on top of the rods and on the base. Three sides of a rectangle can be seen on the edge of the base which are used to aid estimation of the orientation parameters of each view described in chapter four. Five images were collected by one camera. Four located at the corners of the test field, and one looking straight down onto the top of the test field. The distance of the test field from the camera was approximately 1.6 metres. Lighting was placed behind the cameras so that the retro-reflective targets produced a high signal to noise ratio. The experiments were designed to evaluate the performance of the automatic procedure for

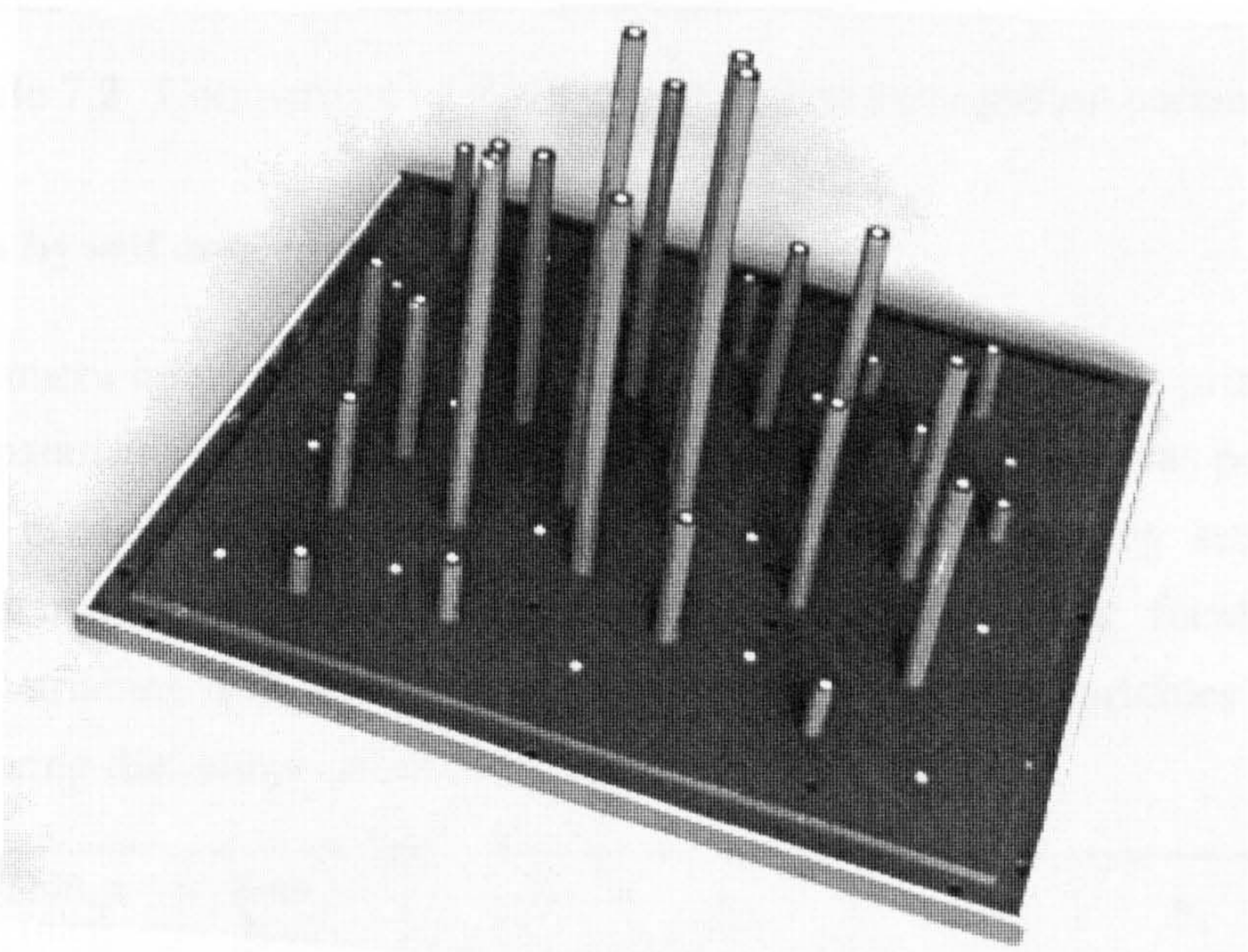

Figure 7.5 Test field

estimation of camera orientation parameters and the performance of self calibration bundle adjustment.

(i). Evaluation of the automatic three sided rectangle method

The use of the three sided rectangle method for automatic estimation of camera orientation has been discussed in chapter four. By the detection, extraction and fitting of line segments, co-ordinates of the 2 intersection and 2 termination points were computed. The camera orientation parameters were then calculated by using these 4 points in the closed form estimation procedures described in chapter four. The 3-D co-ordinates of the intersection and termination points were manually measured. The estimated camera orientation parameters were used in the 3-D matching algorithm to match the all the targets on the test field. Table 7.2 gives the average RMS errors of computed 3-D target co-ordinates. Errors in the estimation of the camera orientation parameters may come from: **(i)**. errors in estimation of the four initial 3-D co-ordinates of the four targets, which were manually measured with a ruler; and **(ii)**. the three side rectangle thinning algorithm. The latter error is because the thinning algorithm uses a binary image so that only a pixel level of accuracy can be achieved. Additionally, the density of target distribution is limited. The relationship between the target density and the estimated camera orientation parameters requires further investigation.

	$RMS_{\delta X}$(mm)	$RMS_{\delta Y}$(mm)	$RMS_{\delta Z}$(mm)
RMS error of targets for initial camera orientation	8.193	7.917	12.285
RMS error of targets for final camera orientation	0.035	0.031	0.040

Table 7.2 Comparison of RMS error in camera orientation parameters

(ii). Evaluation by self calibration.

To assess the camera interior parameters parameters, such as camera lens principal point, and lens distortion parameters described in chapter three, a self calibration was performed. A self calibration was carried out within the bundle adjustment algorithm, by setting the camera interior parameters as variables. Parameters investigated included: focal length f, two principal point variables shift_x and shift_y, three radial distortion variables K_1, K_2 and K_3, and two decentering distortion variables P_1 and P_2.

f (mm)	Shift_x (mm)	Shift_y (mm)	K_1	K_2	K_3	P_1	P_2
25.2803	-0.0548	-.1557	1.983×10^{-4}	-9.996×10^{-6}	4.145×10^{-7}	6.301×10^{-5}	-1.021×10^{-5}

Table 7.3 Results of self calibration

A self calibrating bundle adjustment, using all 5 images such that all targets which were imaged at each viewpoint, was computed. The 478 image co-ordinate measurements gave rise to 310 degrees of freedom. Some results are shown in Table 7.3. The adjustment results show good correlation with the principal point offset and radial lens distortion coefficients K_1 estimated in chapter three. The radial lens distortion coefficients K_2 and K_3, and the decentering distortion coefficients P_1 and P_2 values are significantly different. This may be caused by other factors which have not been modelled by the adjustment. However, these coefficients have less influence on the results of the bundle adjustment. The calibration demonstrates that high precision results can be obtained using the self calibration procedures.

7.2.1.3. Test three: Mirror

To evaluate the accuracy of the system targets were placed on the surface of the large convex mirror (Figure 7.6).

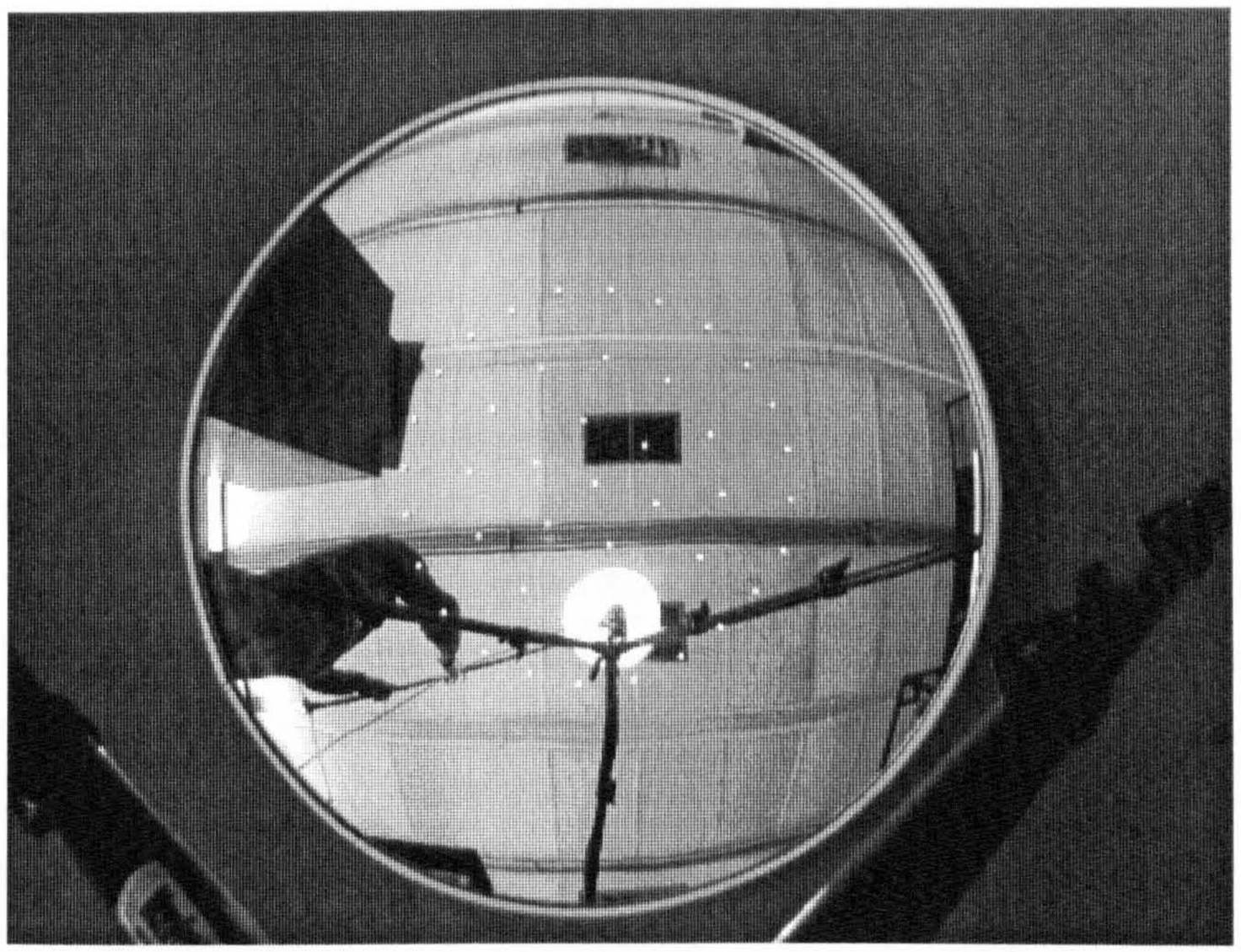

Figure 7.6 Image of targeted mirror

The mirror was measured using a single camera which was moved to view the mirror from four positions with a ninety degree roll about its axis at each position resulting in eight images. This measurement arrangement was used to strengthen the network and provide more redundant data. The forty three targets provided 514 degrees of freedom in a free bundle adjustment. The results of the adjustment are given in Table 7.4 and Table 7.5. The image co-ordinates RMS values equate to approximately 1/40th of a pixel image resolution, and the RMS co-ordinate of a target corresponds to approximately one part in 30,000 of the 280 mm. sized object. The accuracy is not so high as compared with that obtained by Beyer, 1992,

RMS image shift	sx	sy
mm	0.21	0.20
subpixel	1/40	1/43

Table 7.4 Precision of image co-ordinates

	$RMS_{\sigma X}$	$RMS_{\sigma Y}$	$RMS_{\sigma Z}$
RMS error of targets	0.008	0.008	0.011
Accuracy	1:35,000	1:35,000	1:25,500

Table 7.5 Precision of object co-ordinates

where one part in 70,000 accuracy in object space and 1/100th pixel precision in image space have been achieved. This may be due to the several factors used by his system: **(i).** the pixel clock for synchronising data sampling; **(ii).** least squares template matching for target location; and **(iii).** a stronger and more distributed network. The system described in this thesis has not attempted to achieve such high accuracy but has concentrated on automation and speed of operation.

7.2.2. The application of this system to deformation analysis of wood panels

The application of this system to deformation analysis of wood panels brings together results of recent research in art conservation and the digital photogrammetric measuring system which has been described in this thesis. A deformation analysis of movement occurring in wood panels was required by the Hamilton Kerr Institute (HKI), University of Cambridge, where a number of wood panels used for supporting fine art paintings were being tested. These panels may swell and shrink as a result of changes in the humidity or temperature of the surrounding air. Effects are amplified in the case of panels which are painted on one side only because moisture penetrates the two surfaces of the panel at different rates. To obtain the characteristics of the various panels is very important because they are widely used and few systematic studies have been carried out. Different types of wood have different characteristics. A lack of knowledge about the effect of the many different types of reinforcements applied to wood panel paintings to prevent deformation has sometimes led to increased local deformation of the surface and even splitting, cracking, and loss of paint. Therefore it is critical that a method of measurement of the panels is devised to give accurate information about in-plane and out-of-plane deformation. The task for the application here is to use the measuring system to obtain this information for quantitative analysis so that the restoration options for each panel type can be decided.

The panels to be measured were divided according to wood type: linden; oak; poplar; and

Scots pine. Each type was supported by a number of different reinforcement types to give 74 pane; reinforcement combinations.

7.2.2.1. System configuration

The photogrammetric system used for this project, although based on that described earlier in this thesis, was upgraded to enhance its data processing and measurement abilities, is consists of hardware and software:

Hardware:

- PC-486: 66MHz clock frequency, 8M byte memory, tape backup, and 500M byte disk;
- frame grabber: Epix frame grabber with 4M byte memory.
- camera: Five Pulnix TM6CN camera were used, four of which were located on the four corners and one in the centre to ensure to a minimum of three projections of each target even if the panels be same considerably bent during the experiments. Four 8.5mm lenses and one 6.5mm lens were used to achieve good fields of view from all camera location.
- interface box: DC power supply for six cameras and connection between the frame grabber and camera.
- lighting system and power box: To allow each camera to view the retro-reflective targets on the surface of each panel, each camera was equipped with a lighting system, consisting of four bulbs positioned in a ring around the lenses. A power box was designed to supply the power to these bulbs. By using these bulbs each camera was able to image the targets with zero background.
- scale bars: Four scale bars were used to provide scale in the object space. Three targets were placed on each bar and the distance between them measured using an optical bench.
- test field (Figure 7.7): A test field similar to that in Figure 7.5 but of a larger size was created for the purpose of estimating a camera interior and exterior parameter calibration.

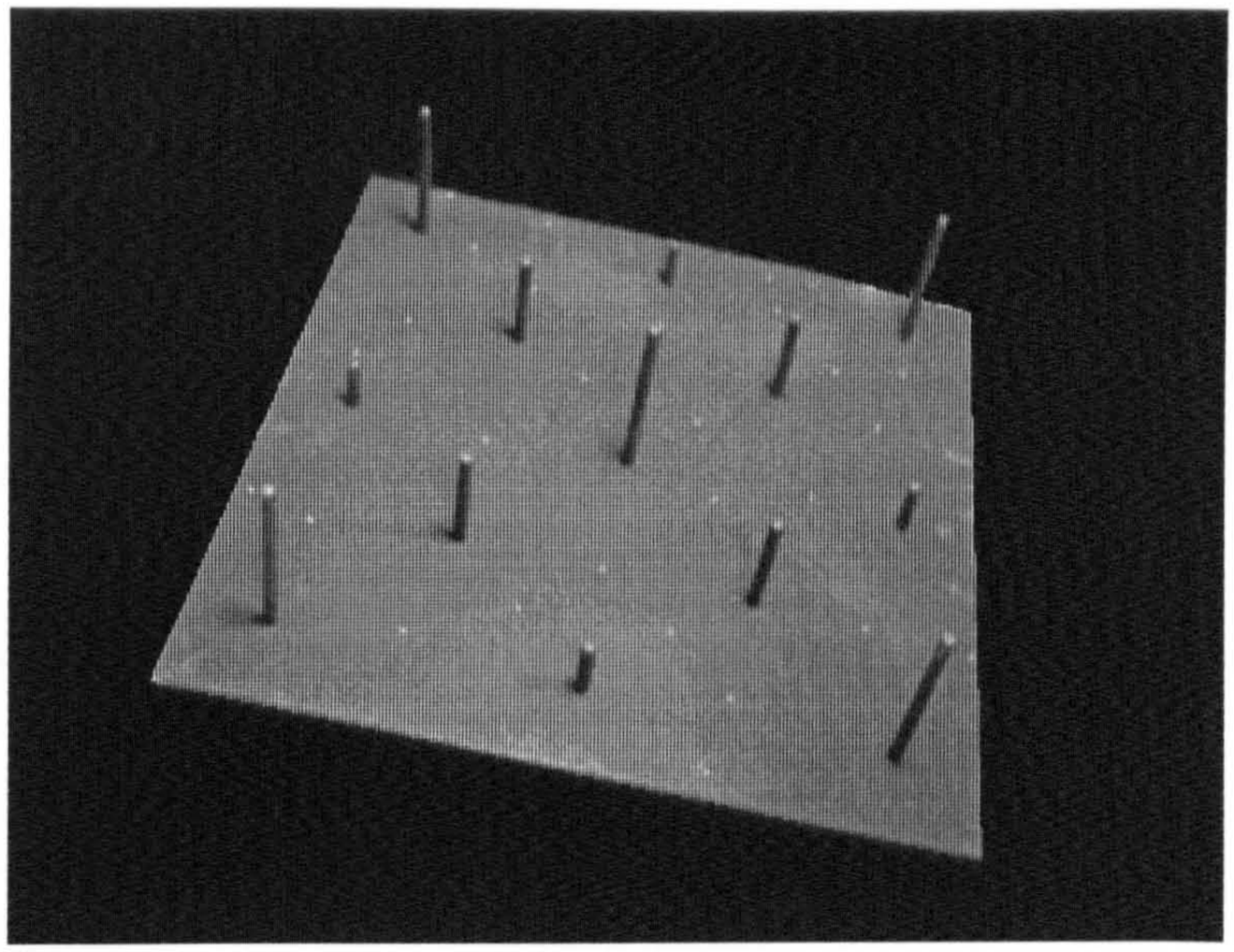

Figure 7.7 Test field

Software:

The software was written in C and implemented under the Microsoft Windows™ environment. It is operated by pull down menus. All the functions in the package are divided into several large modules: FILE, EDIT, OPTION, GRABBER, PROCESSING, MEASURE, CALIBRATE, MATCH, and BUNDLE, as described in chapter six.

7.2.2.2. System Calibration

The system calibration set out to estimate camera interior orientation parameters, camera exterior orientation parameters.

(i) Camera interior parameters calibration

Camera interior parameters calibration can be performed in two ways: Laboratory calibration and self calibration.

(A) Laboratory calibration

Laboratory calibration was used to determine each camera principal point of symmetry, radial distortion and decentering distortion parameters.

The determination of principal point of symmetry was carried by the method described in chapter three based on a method presented by Burner et al, 1990. The five Pulnix cameras were each mounted on an optical bench. A low power laser was aligned with the centre of the CCD array (with lens off) by causing the primary reflection from the surface of the sensor to

coincide with the incident beam. Coincidence was identified by symmetry with the diffraction pattern caused by the surface structure of the sensor. The lens was then fitted to the camera, with the light beam attenuated, and an image of the laser spot grabbed. An automatic location algorithm was used to locate the spot to subpixel level. Several measurements were taken after resetting each component to avoid operator bias and several images were grabbed for each measurement to minimise the noise. Table 7.6 shows the results of the principal point of symmetry for the five cameras.

Test No.	1		2		3		4		5		average	average
Co-ordinate	x	y	x	y	x	y	x	y	x	y	x	y
Camera 1	347.21	272.03	347.21	272.02	347.20	272.05	347.20	272.07	347.18	272.05	347.20	272.04
Camera 2	343.22	283.86	343.22	283.86	343.20	283.86	343.20	283.85	343.21	283.85	343.21	283.85
Camera 3	364.97	297.19	364.96	297.20	364.95	297.19	364.95	297.19	364.94	297.19	364.95	297.19
Camera 4	380.29	294.31	380.27	294.31	380.27	294.32	380.25	294.33	380.24	294.33	380.26	294.32
Camera 5	385.59	302.79	385.58	302.80	385.58	302.81	385.58	302.82	385.57	302.83	385.58	302.81

Table 7.6 Results of principal point of symmetry

	K_1	K_2	K_3	P_1	P_2
Camera 1	$3.546x10^{-03}$	$-1.943x10^{-04}$	2.187x10-06	$3.086x10^{-04}$	$-1.177x10^{-03}$
Camera 2	$1.133x10^{-03}$	7.455x10-05	$-3.675x10^{-06}$	$4.197x10^{-04}$	$2.136x10^{-04}$
Camera 3	$1.606x10^{-03}$	1.133x10-06	$-5.133x10^{-07}$	$-1.871x10^{-05}$	$1.213x10^{-04}$
Camera 4	$1.659x10^{-03}$	-5.605x10-06	$-2.680x10^{-07}$	$-2.148x10^{-04}$	$1.739x10^{-04}$
Camera 5	$1.775x10^{-03}$	-2.309x10-05	$1.889x10^{-07}$	$-2.284x10^{-04}$	$3.168x10^{-04}$

Table 7.7 Convergence value of K_1, K_2, K_3, P_1, and P_2

The distortion parameters for the four 8.5mm lenses and the single 6.5 mm lens were determined by the plumb line method, which was derived by Brown, 1971, and was extensively used in this thesis for the calibration of various camera lenses. The calibration method and procedure has been discussed in detail in chapter three. The distance between the camera and plumb line frame was adjusted to the appropriate distance. Table 7.7 summarises the K_1, K_2, K_3, P_1, and P_2 parameters of the five lenses. Figure 7.8 and Figure 7.9 illustrate the curves of radial and decentering distortion. From the figures, the following information can be obtained: the radial and decentering distortion of the five lenses was far larger than that of 25 mm lenses discussed in chapter three; the four 8.5 mm lenses have very similar radial distortion characteristics and very different decentering characteristics; the 6.5 mm lens has

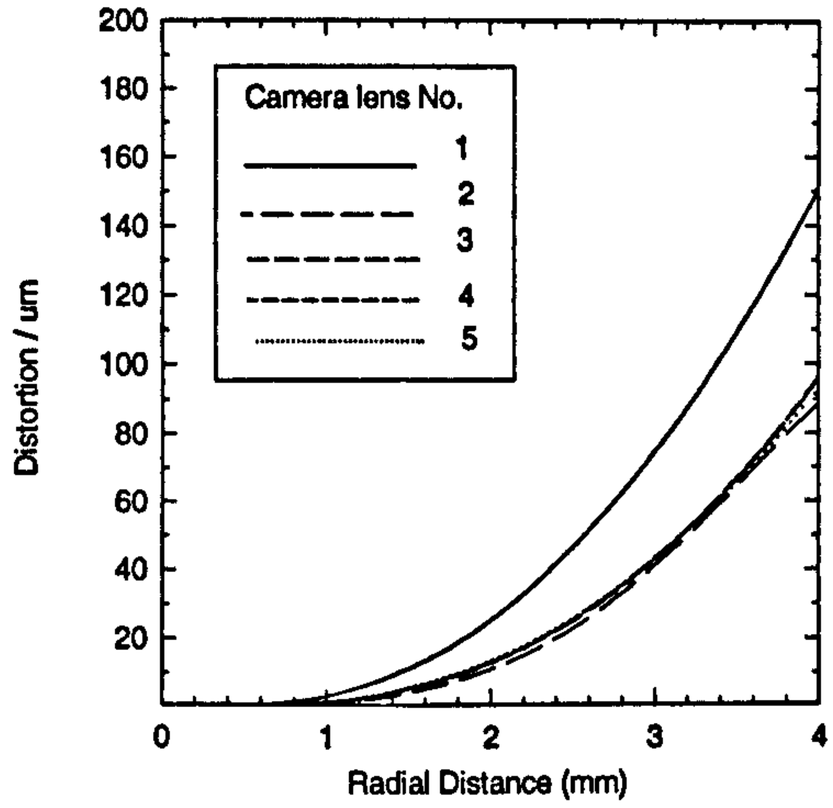

Figure 7.8 Radial distortion of the five cameras

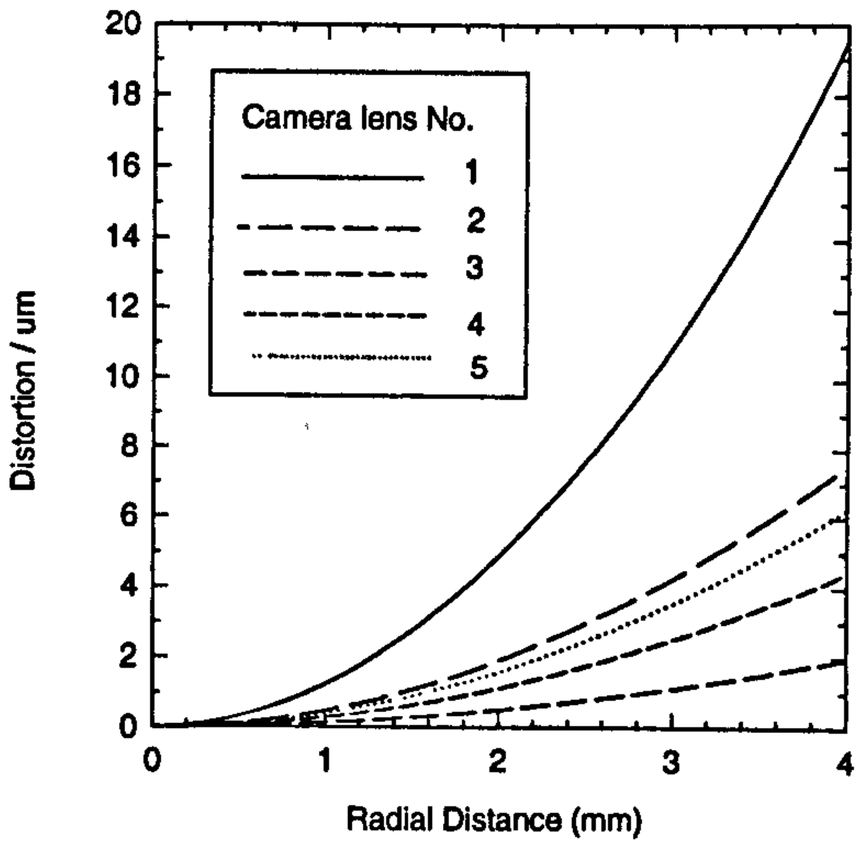

Figure 7.9 Decentering distortion of the five cameras

very large distortion, up to 17 pixels shift on the sensor edge to the extent that the distortion can easily be detected by eyes (Figure 7.10); radial distortion still dominates all distortions when compared to decentering distortion and the numerical value of radial distortion is about ten times larger than that of decentering distortion. However the decentering distortion cannot be ignored because it still represents a maximum of 2 pixel shift for the 6.5 mm lens and 1 pixel shift for two of the four 8 mm lenses.

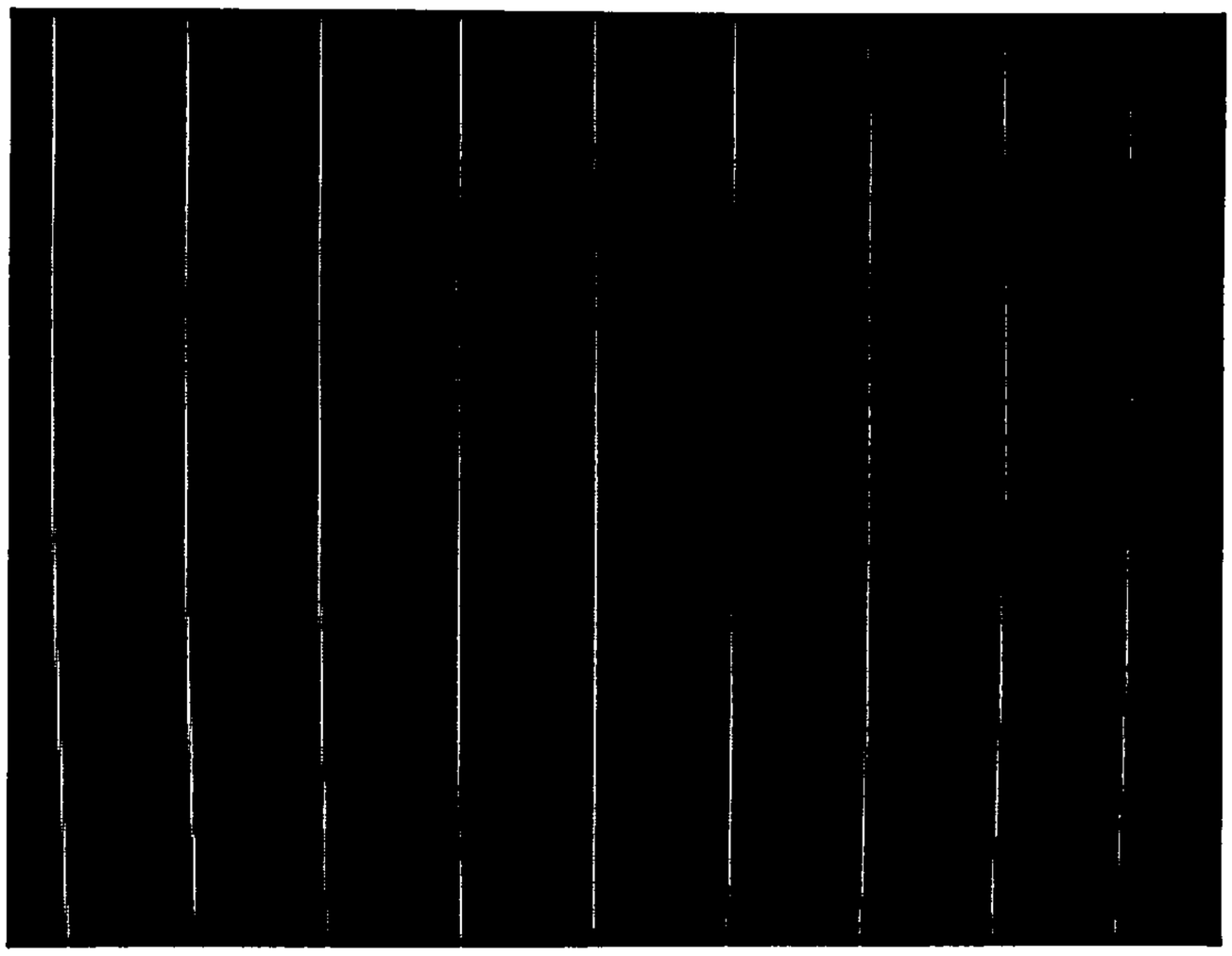

Figure 7.10 Plumb line image grabbed by the 6.5 mm lens

(B) Self calibration

A self calibration computed using the test field was used to estimate the camera lens focal length and camera orientation parameters before the panels were measured. The test field was grabbed four times by each camera. Each time the test field was rotated through 90 degrees so that a very strong geometric network was obtained. The targets on each image were automatically located by the location algorithm. Four specially coded targets, were manually identified to estimate the camera orientation parameters. Using this estimation, the 3-D matching algorithm and iterative with bundle adjustment were used to match all the targets on each of the views. The bundle adjustment was run to refine the camera orientation parameters and the 3-D co-ordinates of targets. The focal length parameter was then freed. Table 7.8 gives the final results of the focal length for each camera and Table 7.9 gives the results of each camera orientation. The focal length of each camera lens may be held fixed from this calibration. However, the camera orientation parameters shown in Table 7.9 are likely to change slightly between measurement sets and should remain free. Therefore, at the beginning and the end of each set of measurement the test field was imaged by each of the five cameras and refined camera orientation parameters computed.

Camera No.	1	2	3	4	5
Focal length	6.214	8.587	8.511	8.623	8.681

Table 7.8 Focal length calibration

Camera No./Parameters	Xc	Yc	Zc	ω	φ	κ
1	90.6787	-256.5009	1306.9459	7.7555	2.8762	179.3895
2	941.0329	857.9759	1298.3480	-29.2169	30.4502	-81.6658
3	-1119.9979	911.9229	1346.1322	-32.3744	-33.1386	69.8784
4	-1164.0772	-1100.0015	1315.8275	41.1134	-34.4922	121.1116
5	944.3382	-1158.9853	1278.2698	39.2615	28.5893	-109.7060

Table 7.9 Camera orientation calibration

7.2.2.3. Data acquisition

A double-walled portion of a workshop at the Hamilton Kerr Institute, with an approximate floor area of 2.8 m^2 was sealed with walls of thick polyethylene sheet (Figure 7.11). A rack

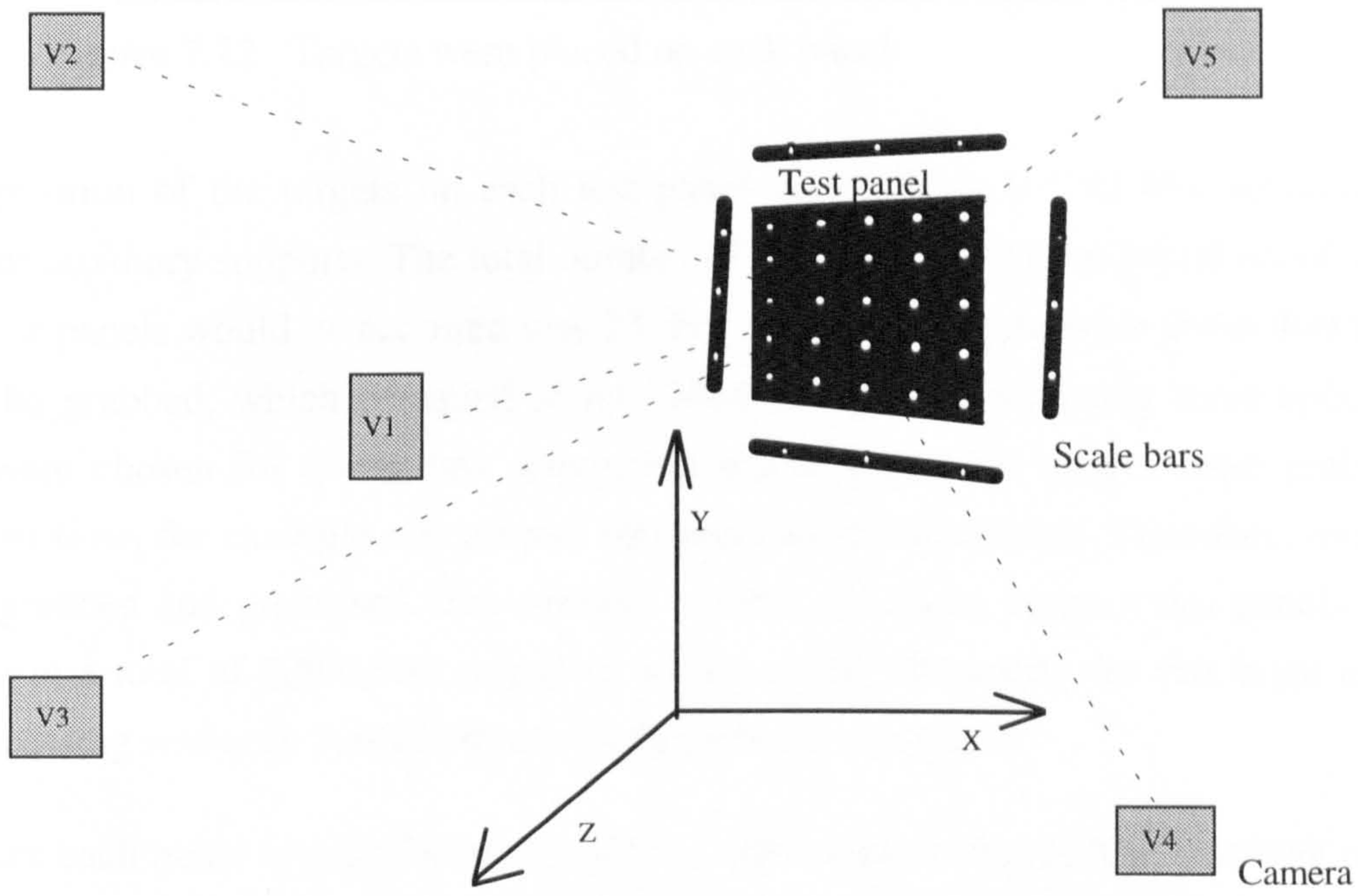

Figure 7.11 The system setting up

was constructed to hold and adjust the panels to be measured. Four scale bars were installed on the four edges of the panel for scale reference for each measurement. An air temperature of about 20°C was controlled by thermostats and electrical heaters. Relative humidity was maintained at regimes of 40% or 80%, ±5%, so that a difference of about 40% could be applied for the experiments. A humidifier and dehumidifier, stabilised to the desired level with salt solution, were used to control the humidity, A small fan maintained slow air-circulation.

An array of retro-reflective target (Figure 7.12) were placed on each test panel. The number

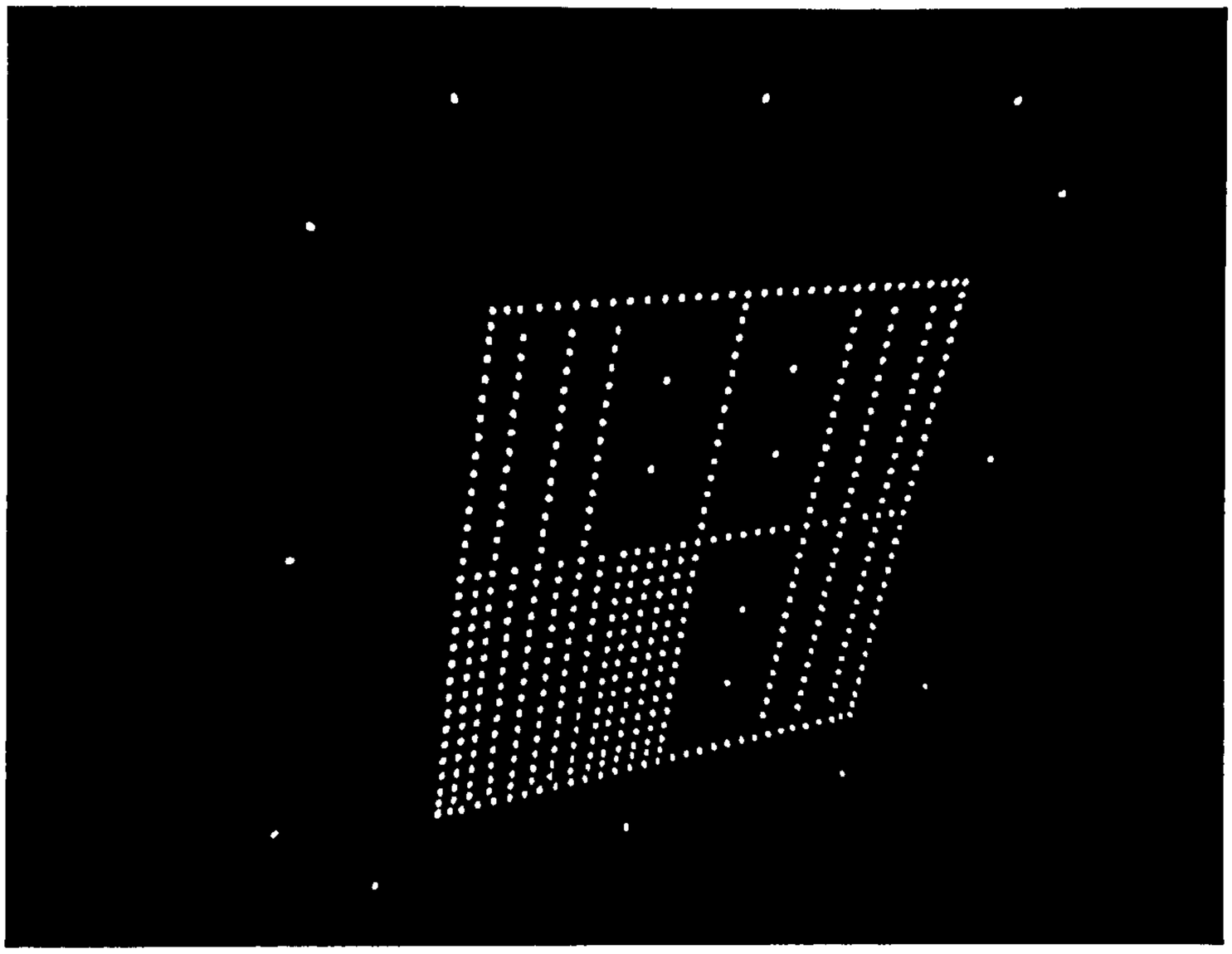

Figure 7.12 Targets were placed on each panel

and disposition of the targets on each test panel varied from 157 to 464 according to the pattern of auxiliary supports. The total number of epochs at which the initial set of images of the 74 test panels would be acquired was 25. For each epoch, there were about 400 images in total to be grabbed, which occupied about 170M storage. During every three epochs, some panels were chosen for quick data acquisition where sequential images were grabbed over very short time, for example one minute between each measurement. Therefore, over 10,000 images grabbed and processed. The average number of targets on each test panels was 250, resulting in a total of 2,500,000 targets to be processed. Obviously for this huge amount of data processing was only feasible if automatic methods were used.

In practice each panel was placed in the middle of the support frame. The grabbing of the five images could be automated for all five cameras, but the background of the panel would receive four times the illumination in this way. To avoid background illumination, five images were sequentially grabbed by manually switching on and off the lighting installed on the front of each camera (Figure 7.13a). During the period that the test panel was swapped for another, the five images grabbed were automatically saved (Figure 7.13b) and all the target images on each image were automatically located (Figure 7.14). The procedure was repeated until images of all panels were grabbed. About one and a half hours were required for each epoch. All images were then compressed and put into an archive file for future use. The 2-D co-ordinate data of each image were transferred to City University for further data processing.

In the image grabbing menu (Figure 7.13a) the camera used is indicated by a radio button, which, if OK, means that the camera has been chosen by clicking the mouse and the grabbed

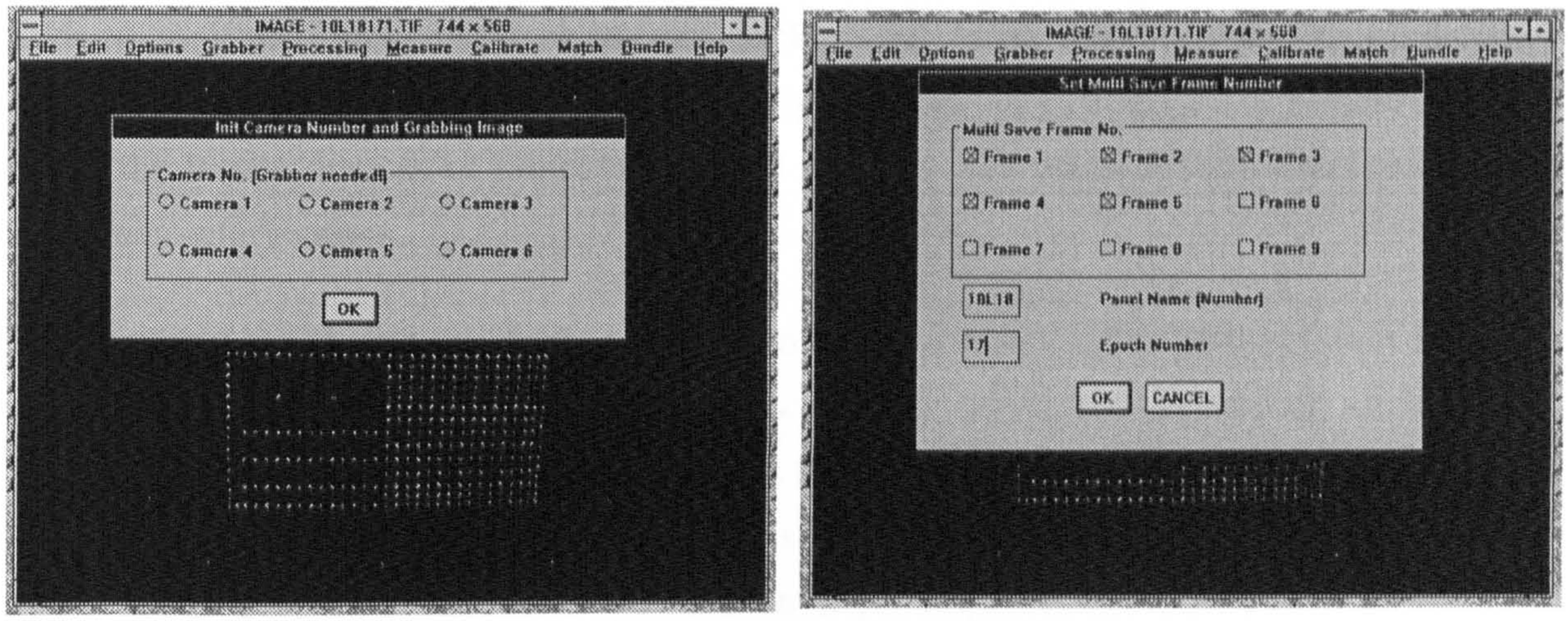

Figure 7.13 a) Image grabbing menu b) Image save menu

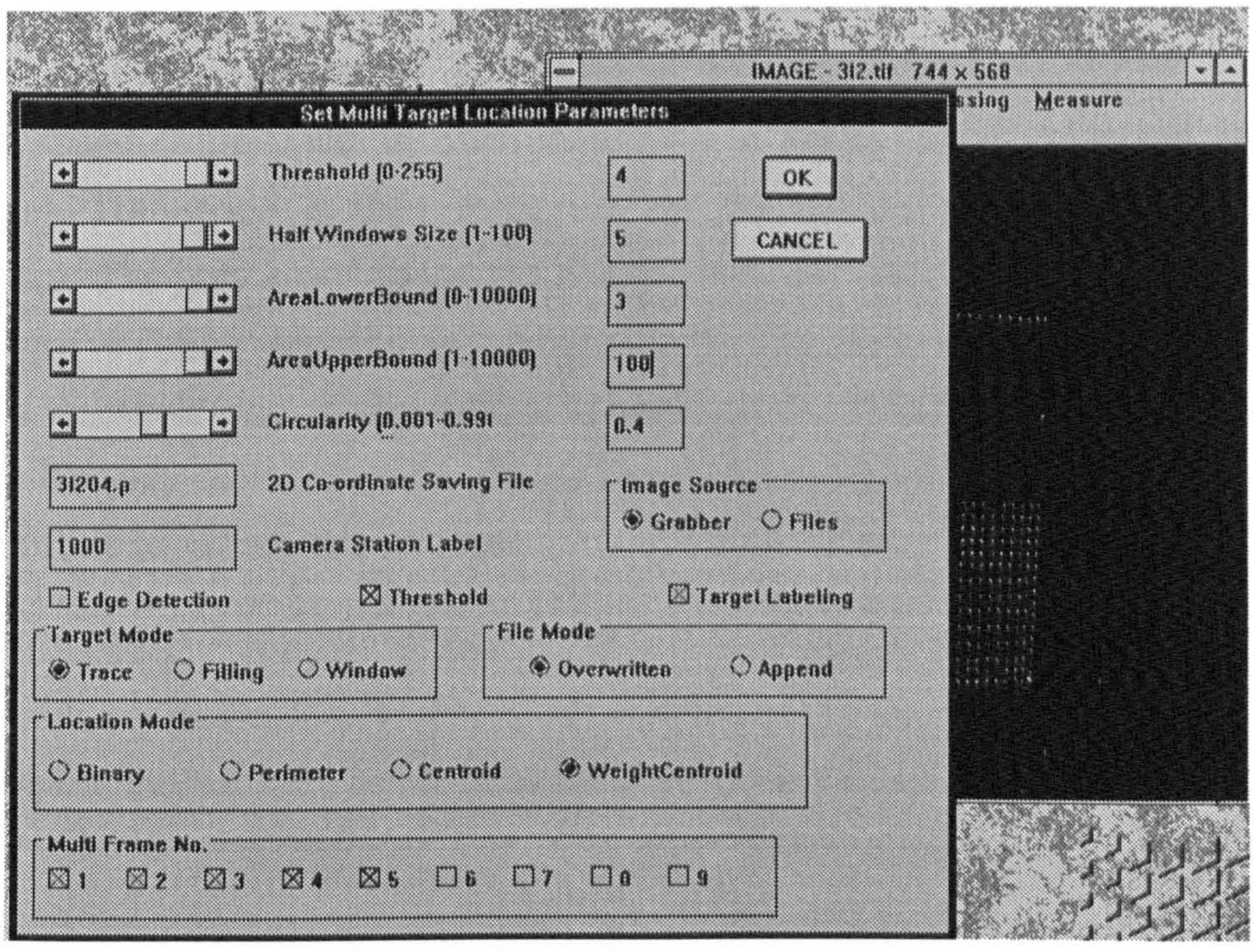

Figure 7.14 Target location menu

image stored into the frame memory of the frame grabber. Each camera must be used at least once for each test panel. In the image save menu (Figure 7.13b), the five images are grabbed and saved and the file names are based on the panel name and the epoch number. In the target location menu (Figure 7.14), a number of options can be chosen, such as the number of images to be processed and the source of images (from the grabber or files), the threshold of image segmentation, the window size for target location, the target recognition parameters (area lower bound, upper bound and circularity), the 2-D target location output file and write

mode (overwrite or append), camera view station, target location mode (trace, filling or a window), uniform background or uneven background (edge detector), and target location algorithms (binary, perimeter, centroid and weighted centroid). When these parameters were set up, the whole process of target image 2-D location was automatically executed without any human intervention.

The precision, speed, and reliability of 2-D target measurement are important issues in digital photogrammetric research because the accuracy of all subsequent processes, such as 3-D matching, and bundle adjustment, are based on the measurement of 2-D target locations. The efficiency of the image processing requires serious consideration. Normally, for circular targets, image preprocessing includes two main steps: target recognition and target location. The target recognition process is required to reject spurious targets and identify genuine targets. A target location process is then used to compute a subpixel estimation of the position of the target.

In the target recognition procedure, each object in the image is traced along its edge to obtain an outline shape. This trace is often based on a binary image obtained from image segmentation. The shape is then recognised by prior knowledge of the desired target characteristics. The grey scale image can also be used for target recognition (Clarke, 1993) where a recursive filling algorithm is used to both find the intensity values within a target that are above a threshold and at the same time compute the centre of gravity of the intensity values. Another grey scale image based target recognition algorithm (Shortis et al, 1994) uses a scan-line filling algorithm which is more efficient than the recursive filling algorithm.

In the target location procedure, a function of the pixel values forming the target image are used to obtained a measurement of sub-pixel accuracy. To compute the locations of target images, different methods can be chosen depending on the requirement of speed and accuracy of tasks. These location methods are: perimeter based; binary based; normal centroid; weighted centroid; ellipse fitting; gaussian shape fitting; and least squares template matching. These location methods have been analysed and evaluated by Shortis et al, 1994 and Clarke et al, 1993. The weighted centroid location method is mainly used in the system as a good compromise between speed and accuracy. The automatic measurement module, written as part of this thesis, combines the common two step approach into a single step. This technique is described as follows:

The image is scanned from top to bottom and left to right. When a pixel intensity value is larger than a given threshold value, decided by ***a priori*** knowledge, the object is traced beginning from this pixel using an eight-way search. The search takes place on the grey scale

image. When the search returns to the original beginning pixel, a set of all the periphery pixels of this object can be obtained. Based on this periphery data, the circularity of the object can be calculated and used for object shape recognition. A scan line filling algorithm is then used to fill the object. During this filling period, the elements required for the weighted centroid algorithm are computed to eventually provide the centroid of the x and y co-ordinates of the object. An accumulator is also used for counting the number of pixels in the object. After finishing the filling, the subpixel level position and the size of this object are also obtained. The circularity and the size of the object are used for recognition of the target. If the object is recognised as a target, the 2-D subpixel position is known. If it is not a legitimate target, then the next object is searched for and traced in the same manner. The combined method is better than the normal two step method, not only in computation efficiency, but also in removing the risk of using a window for target location which may include other inappropriate outlier pixels. If the background of this image is not uniform, an edge detector may be used during the trace procedure. The edge detector works on the image intensity gradient to provide a perimeter, therefore the effect of any uneven background will be much reduced. The Roberts edge detector was used in the method.

By use of the methods described above, 1/40th of a pixel precision of target location is routinely achieved. About 3 seconds are required for automatic target measurement under a PC-486 with 66MHz clock frequency and 8M byte memory, with a 744x576 pixel image and about 500 targets on the image.

7.2.2.4. Data process and analysis

In order to analyse the deformation of the wood panels, there are two steps are necessary after all the 2-D target images co-ordinates have been collected: the target image labelling and 3-D data analysis. Target image labelling includes target image uniqueness matching between different views in each epoch for each panel and the target image uniqueness matching between different epochs for the same panel. 3-D data analysis includes: the refinement of the 3-D co-ordinates of each target; the comprehensive statistical tests of hypotheses about the quality of the data; and an analytical and graphical display of the deformation of each panel.

The 3-D matching method has been used for uniquely matching target images between different views in each epoch for each panel. The performance of this method has been discussed in chapter five. The problem encountered in this application is the targets on the panel are very close, some targets as close to each other as 20 mm. Ambiguities were possible because the camera orientation estimation was not accurate enough and the computation cost was too high to iteratively match the all target images for the bundle adjustment (for example,

the use of 464 targets in a panel will require about half an hour for each iteration of the bundle adjustment). Therefore, an attempt has been made to try to get both camera interior and exterior parameters as accurate as possible. The five camera interior parameters were carefully calibrated by use of the plumb line method, optical bench calibration, and the use of a test field described in previous section. The camera exterior parameters were estimated by using the test field at the beginning of each measurement for each epoch.

The matching algorithm was called twice. In the first call, a group of three for the threshold of target matching was chosen because in some circumstance where the panels were extremely deformed some targets on one side of the panel edge were occluded from the two of the cameras located on the other side. A small 3-D distance tolerance value was chosen to give a strict constraint for target matching. An average of over 90% of the total targets were matching in the first matching procedure. In the second match, the 3-D tolerance value can significantly increased, because the remaining unmatched targets were reasonably sparse in their distribution. Hence, the remaining target images are expected to get matched and labelled. It is emphasised here that the series of experiments are currently ongoing so that is difficult to guess what will be achieved by the end of the project.

In order to ensure that targets have identical labelling between different epochs, the data needs to be processed after matching between the different views in the same epoch. Each target on the scale bar can be identified using the space projection method. This is because the scale bars were firmly constructed and the 3-D co-ordinates of each bar target can be precisely obtained. Each camera was also fixed in the same location such that the exterior parameters of each camera could be consistently used for each epoch. The scale bar targets could be uniquely identified by reprojection because their co-ordinates were approximately known and they were imaged in uncluttered regions of each image. The scale bar target images were used as scale constraints in the bundle adjustment procedure so that the size of each panel in each measurement could be determined. The only change between epochs was the position of the same panel in each object space because the panel had to be taken off and then put on again some object space shift of the panel position occurred.

The matching of targets between different epochs was based on the principal of similar triangles. The panel could have be expanded or contracted between measurements at each epoch and could also have a significantly different shape. This is shown in Figure 7.15. However, any local triangular relationship will still be very similar. Based on the properties of triangular similarity, the matching of targets between each epoch can be achieved. The matching procedure is described as follows. Assume there are two targets, which are physically close in both data sets. Given two targets in the first dataset, a third target, which is

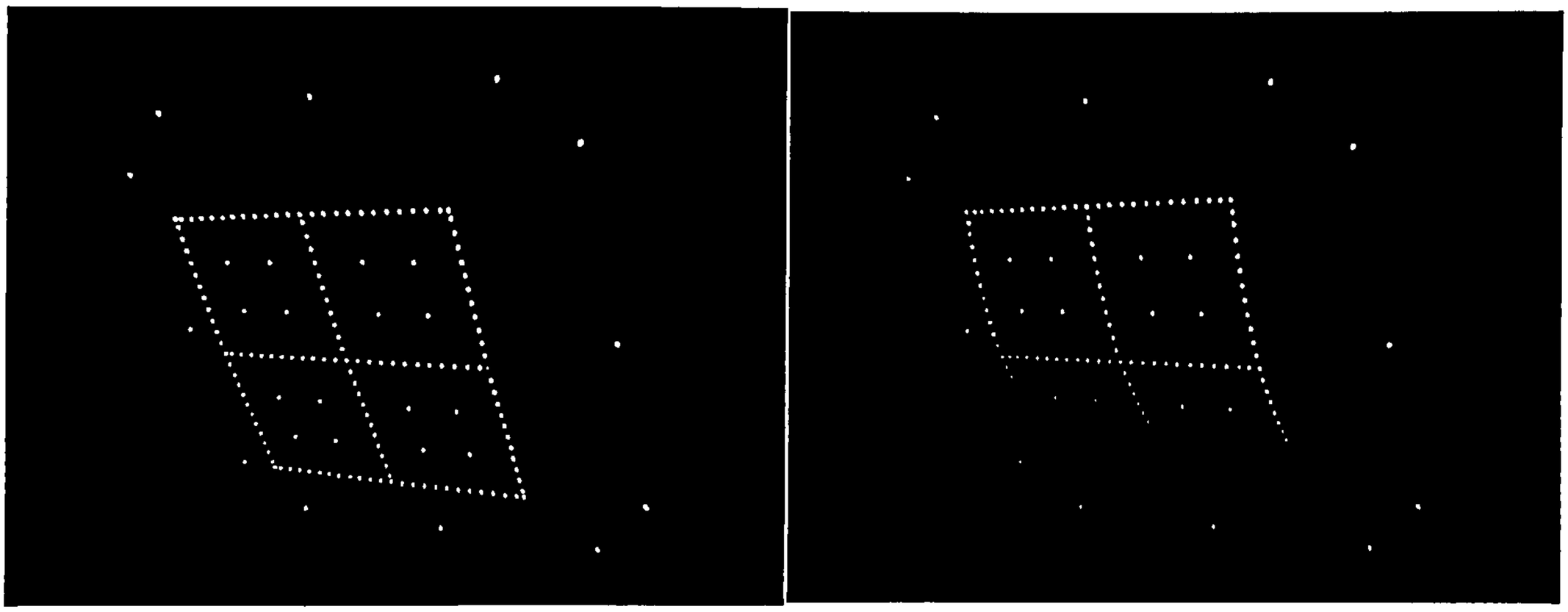

Figure 7.15 a) Previous epoch b) Current epoch

the nearest in space to the two targets, can be found. A triangle linking the three targets is constructed. In the same way, two targets in the second dataset can also used to construct a triangle by combining them with any one of the other targets. From all possible triangles, the one which most closely coincides with the triangle constructed by the first dataset is chosen as correct one. The corresponding third target in the second dataset can then be matched to that in the first dataset.

At some time, some targets may be missed in some of the epochs. To minimise the number of unmatched targets, a threshold was used by which only the target lying inside the threshold distance are considered as the matching candidates. The search is extended by selecting the

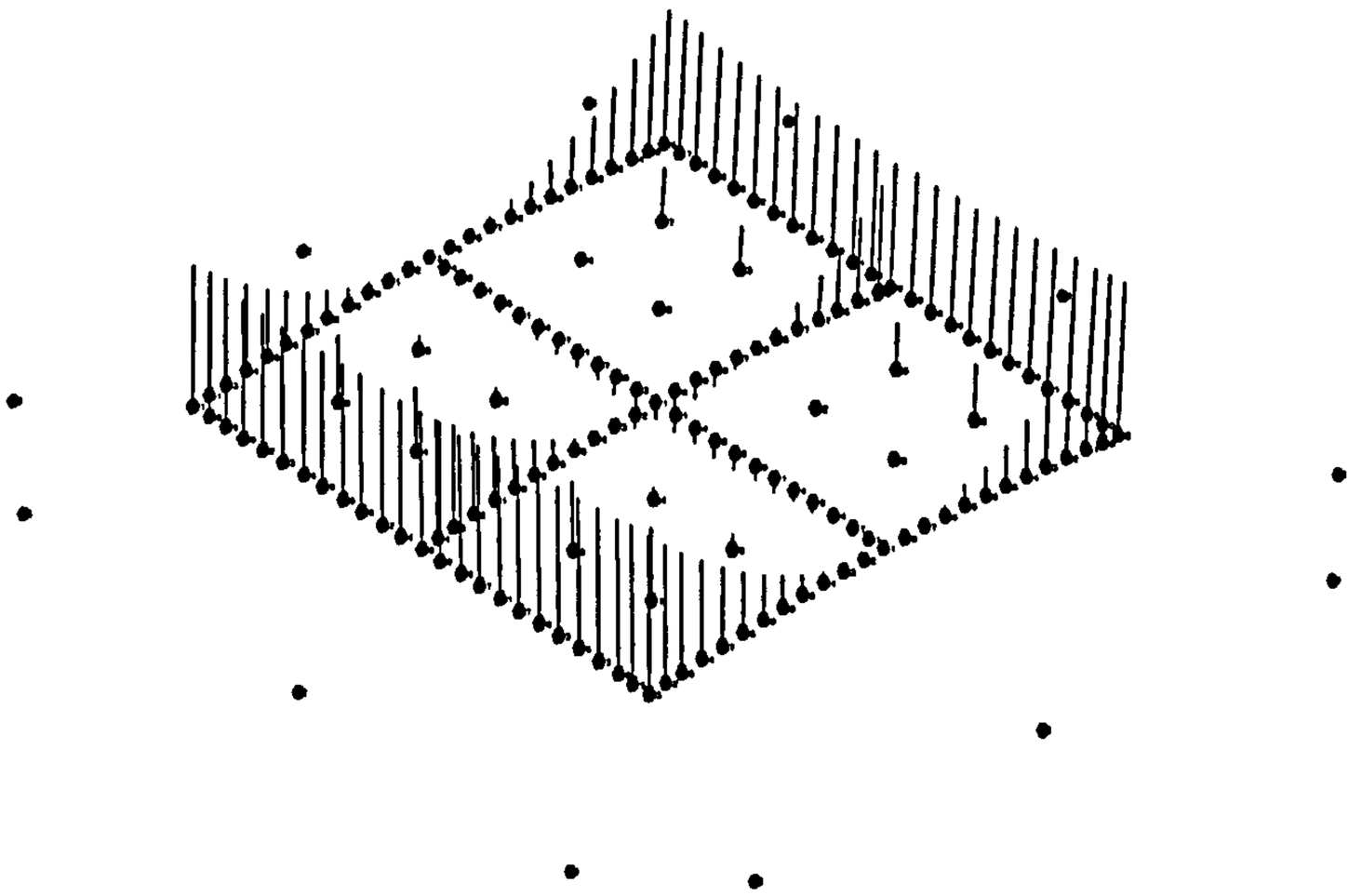

Figure 7.16 Visualisation of deformation of the panel 3O8

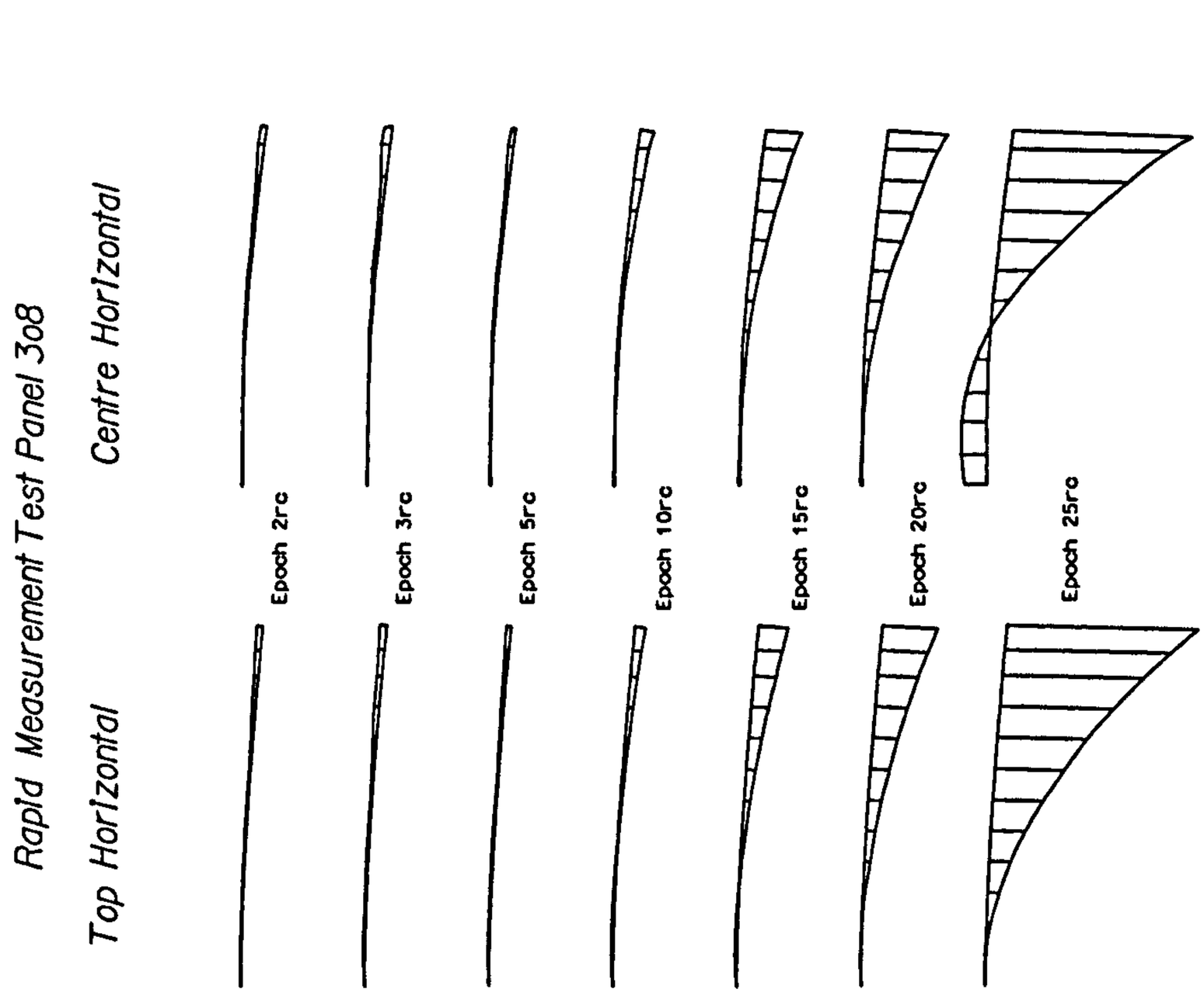

Figure 7.17 Edges for panel 3O8 rapid test (10x exaggeration)

next two closest targets in the first dataset as the basis for the next triangle.

After the targets in all epochs have been matched, the panel deformations can be analysed. These processes are still ongoing. Figure 7.16 and Figure 7.17 give two examples of deformation analysis output and visualisation. Figure 7.16 shows the deformation of the whole panel when the humidity change and Figure 7.17 demonstrates the extraction of a series of profile comparisons for panel 3O8. The deformation analysis of the panel data collected by the system is currently ongoing and the results will be supplied to art conservators for further analysis.

7.3. Summary

An automated 3-D measuring system using photogrammetric and machine vision techniques has been developed. The flexibility of the system has been evaluated by a number of example applications under both laboratory and experimental conditions. A successful application of this system to deformation analysis of wood panels as part of a research project is presented. The case studies to evaluate the system feasibility demonstrates that the developed system is capable of rapid 3-D measurement for various tasks.

Chapter 8 Conclusions and suggestions for further work

8.1 Contributions of investigations and researches

This thesis has been primarily aimed at developing an automated photogrammetric 3-D measuring system. The developed system can be used for:

- Image processing;
- Target recognition and subpixel location;
- Camera lens distortion parameter calibration;
- Camera orientation estimation;
- Target 3-D co-ordinate estimation;
- Target image matching based on any reasonable number of views and any reasonable number of target images;
- Bundle adjustment with options for free bundle adjustment, self calibration bundle adjustment, observation control point constraints and geometrical inner constraints;
- Error analysis of 3-D targets by error variance matrix output;
- Blunder detection with the standard residual based on robust testing; and
- Interface between bundle adjustment and a CAD package for visualisation, with DTM modelling based on 2-D grids.

The basic characteristics and merits of the system are:

- Integration of machine vision and photogrammetric techniques;
- Multiple camera inputs with different focal lengths.
- A number of image processing functions for various purposes, such as image editing and image enhancing;
- Reliable, high speed, high accuracy, and robust target recognition and location algorithm. The algorithm can deal with an either ideal situation with zero background, or non-uniform illumination with noise background. The window size, filling, and tracing can be chosen for target location. The rate of recognition and location of target images can be up to 150 targets / per second using a 486 IBM PC. The accuracy of location can be up to 1/30th of a pixel depending on the quality of images.
- Camera orientation parameters can be automatically estimated by a machine vision technique where a rectangle is used and processed by using various algorithms for thinning tracing, merging and line fitting of a rectangle, and a closed form using four points for the calculation of camera orientation parameters.
- Several ways to calibrate the camera radial and decentering distortion parameters by

plumbline and self calibration bundle adjustment.

- Automatically match target image in 3-D space based on 3-D intersection and epipolar plane constraints. Optimisation methods have been developed to overcome ambiguities and occlusion and to deal with any number of cameras and any number of target image projections on each camera.
- Bundle adjustment with flexible options such as: any variables of target 3-D co-ordinates, camera exterior parameters (location and rotation) and interior parameters (focal length, principal point shift, scaling, radial and decentering distortion) can be fixed or included in the adjustment, blunder detection, output of the RMS of 3-D target co-ordinates.

However, during the course of the investigations a new method of automatically solving target correspondences was developed. This method was optimised and thoroughly tested by simulation and experiment. The development of this method is the substantial contribution of this thesis.

The following conclusions can be drawn regarding specific aspects of development of this system:

Photogrammetry and machine vision have been discussed as two distinct disciplines. However, they are closely related and there is a large area of overlap between the technologies. The understanding of both photogrammetry and machine vision theory is very helpful for the development and research of 3-D measurement techniques and system developed. This thesis discusses work which combines both photogrammetry and machine vision techniques to contribute to an automated digital photogrammetric system which have provided the first steps towards a fully automated digital photogrammetric system suited to engineering measurement.

Tests to evaluate the fundamental characteristics of components for a digital photogrammetric system have been discussed. Warm-up effects were investigated, and demonstrated that the framegrabber has a large influence compared to any warm-up effects in the cameras. A shift of four pixels was found in the x image direction of the Epix framegrabber due to the mismatch of frequency between framegrabber and camera. A 0.2 pixel shift was found to occur in the Pulnix TM6CN camera during the warm-up period, possibly due to thermal expansion of the sensor. It is therefore recommend that the warm-up time for the CCD camera and the grabber is at least one hour, since after that only 0.01 pixels shift were observed.

An investigation into the location of the principal point demonstrates that there can be a significant co-ordinate difference between the principal point and the center of the chip array. Lens distortion calibration demonstrated that K_1 was the dominant factor for lens distortion in

the Fujinon 25mm lenses. Using a frame test field is a reasonable method to quickly estimate the lens distortion on line with similar accuracy to conventional off line calibration and self calibration methods.

As a result of the tests carried out in the thesis it is hoped that there is potential to increase the accuracy of the integrated digital photogrammetric system further, by reducing individual component errors, for example concentrating on the use of a pixel clock, averaging target co-ordinates, improving target locating algorithms, and improving the bundle adjustment procedure. An automated procedure could also be obtained by solving the problem of initially estimating the camera orientation and performing target image matching automatically.

Two automatic methods have been discussed for the estimation of camera orientation parameters and target matching. (1) The implementation of two methods of automatic estimation of camera orientation parameters have been discussed. In particular, the general solution of a closed form space resection was considered. A three sided rectangular frame method and a laser spot extraction method were used to develop an automatic and rapid extraction of the parameters. Implementation of the three sided rectangle method by using line thinning, line tracing, and a least square line fit was described. The laser spot method was implemented using switching and some simple logic. Experiments were described and evaluations made of the techniques. (2) Two target matching methods for multi-viewpoints were introduced, the 2-D epipolar line matching method and a new 3-D space intersection matching method. The latter method converts the traditional epipolar line matching method in 2-D to 3-D space so that several benefits can be achieved: (i) collinearity equations are used in which the camera additional parameters are included; (ii) the matching takes place in 3-D space so that the tolerance value is based on the RMS of the computed 3-D co-ordinates of object target; (iii) the estimation of co-ordinates of the 3-D object targets results directly from the matching procedure; and (iv) it can be directly combined with the iterative bundle adjustment.

Further discussions of these automatic methods have concentrated on several aspects: (i) the combination of 3-D space intersection matching with the bundle adjustment; (ii) the optimisation of this matching method for multiple viewpoints; (iii) the theoretical analysis of sources of error caused by ambiguity, occlusion, target image location, and error of viewpoint orientation estimation; (iv) the integration of image processing, target location, computing target correspondences, and the self calibrating bundle adjustment into a single software package as a step towards an automatic photogrammetric measuring system. A method of 3-D target matching using an optimised constrained search method has been discussed in detail. A tree search method is used to minimise the computation time and when camera parameters are

not accurately known targets are gradually introduced in an iterative manner. The use of multiple viewpoint constraints is used to robustify the matching process. Pseudo target images are defined in the search process to overcome occlusion problems and make the matching strategy flexible. A hypothesis-testing and heuristic process are used to make the matching computation more efficient. The benefits of the optimised 3-D matching method mean that: (i) initial camera parameter estimates are not required to a high accuracy and initial values can be improved by bundle adjustment based procedures; (ii) target matching tolerances can be changed during the bundle adjustment process according to a statistically derived formula; (iii) targets can be progressively introduced into the measurement network enabling a more robust correspondence matching technique; (iv) target images can be arranged in an arbitrary order to build the matching tree; (v) this algorithm can be combined with the bundle adjustment procedure. In conclusion, an algorithm has been developed which is analogous to the epipolar method. This algorithm has been optimised for speed of operation. Problems due to occlusions and ambiguities have been considered and largely overcome. The method has been tested both in simulation and with several complex real objects. The results of these tests have revealed fundamental relationships and have proved the algorithm in practice.

The design of an automated 3-D measuring system has been discussed. The aim of the design is an automated 3-D measurement using photogrammetric and machine vision techniques that is robust and economic. It has been assumed that initially this system will be used in a controlled environment. At a later stage it is anticipated that further developments will allow the system to be used in an uncontrolled environment. The hardware components and software modules have been integrated and the performances of these for the resulting system has been analysed.

8.2 Suggestions for further work

The state-of-the-art of automated photogrammetric 3-D engineering measurement system can be summarised as follows:

Digital photogrammetry is now fully accepted. The transition from an automated digital systems having "potential" to being used in real-world applications to their regular application in industrial settings is being achieved. Progress has been shown in measurement methodology and the characterisation of digital systems. Novel developments in hardware will occur because of consumer electronics demand: large format CCD chips; smart CCD chips with on-board and real-time A/D conversion; image enhancement; data reduction and other preprocessing functions, and at the computer industry: powerful CPUs; broad system buses; huge storage devices; integrated data processing and visualisation capabilities;

combined image analysis and image synthesis functionality. Digital close-range photogrammetry is growing and expanding as these technologies are becoming available at reasonable cost. Improved system performance is offering new capabilities and will lead to novel applications.

Researchers in the photogrammetric field are paying more attention to multiple sensor integration, the optimisation of photogrammetric bundle adjustment, and expert system technology for network design.

Today, in spite of extensive research towards automated 3-D measuring systems based on photogrammetric and machine vision techniques, some important limiting factors still remain. An fully automated, reliable, and general system, able to adapt to different applications and situations does not exist yet. Several of the most important topics which are still open and thus objectives of further research should include:

- A further integration of computer vision techniques. Computer vision is still a widely unexplored field for photogrammetrists and demands more attention.
- While common sense plays an important role in object targeting, models for standard targeting schemes should still be investigated. This may also include target densification, e.g. when the existing target field is relatively sparse or has too little extent to permit a strong self-calibration.
- Further improvements to the 3-D matching method, such as tree searching, this could be achieved by simulation.
- Investigations should be carried out to determine the functions regularly chosen by an operator so the system can learn or memorise the functions which have been used to automatically rerun them.
- Further performance analysis of this system for its precision, accuracy, reliability, and speed.

References

Abdel-Aziz, Y.A., Karara, H.M., 1971, **Direct Linear Transformation from Comparator Co-ordinates into Object Space Co-ordinates,** Symposium Close-Range Photogrammetry, American Society of Photogrammetry, Falls Church, Virginia, pp. 1-8.

Ade, F., Peter, M., Rutishauser, M., Trobina, M., and Jaaski, A.Y., 1993, **A Vision System for Deriving 3-D Gripping Information for a Robot,** Optical 3-D Measurement Techniques, Zurich, pp. 513-520.

Ailisto, H, Mitikka, R., Moring, I., Kaisto, I., 1994, **Guiding 3-D Co-ordinate Measurement with Integrated Video Camera,** SPIE Optical Tools for Manufacturing and Advanced Automation Videometrics III, SPIE Vol. 2350, pp. 100-107.

Aliverti, A., Ferrigno, G., Pedotti, A., 1993, **Surface Analysis by Laser Beam Scanning and Stereophotogrammetry,** SPIE Vol. 2067, pp. 209-219.

Alkertz, J., Koenig, G., 1984, **A Digital Stereophotogrammetric System,** International Archives of Photogrammetry and Remote Sensing, Vol. 25, A2, Commission II, Rio de Janeiro, pp. 1-7.

Alkon, S., 1988, **Measurement and Inspection Using Non-Contact Electro-Optical Systems: Non-Contact Gauging and Measurement with Laser Triangulation,** SPIE Sixth Meeting in Israel on Optical Engineering, SPIE Vol.1038, pp. 28-35.

American Society for Photogrammetry and Remote Sensing, 1989, **Non-Topographic Photogrammetry,** Second Edition, 435 pages.

Ammeraal, L., 1992, **Programming Principles in Computer Graphics,** Published by John Wiley & Sons Limited.

Analogic, 1991, **High Performance PC/AT Data Acquisition Products,** Analogic Ltd., 360 Audubon Road, Wakefield, MA 01880, USA, Vol. 1, 64 pages.

Anderson, H., Stevens, D., 1984, **'Mono-photographic Tunnel Profiling.', Close-Range Photogrammetry & Surveying State of the Art,** American Society of Photogrammetry, USA, pp. 863-869.

Andrew,W.D., 1993, **Digital Imaging & Audio Meet on Your Desk: DSPs and Multimedia,** Advanced Imaging, April, pp. 24-30.

Axelsson, P., 1992, **Real-Time Photogrammetric Systems-Who Are the Developers,** Int. Archives of Photogrammetry and Remote Sensing, Vol.29(5), pp. 674-682.

Ayache, N., 1991, **Artificial Vision for Mobile Robots: Stereo Vision and Multisensory**

Perception, Massachusetts Institute of Technology, The MIT Press, 342 pages.

Ayache, N., Lustman,F., 1991, **Trinocular Stereo Vision for Robotics**, IEEE Transactions on PAMI, Vol.13, No.1, pp. 73-85.

Ayache, N., Faugeras, O.D., 1987, **Building a Consistent 3D Representation of a Mobile Robot Environment by Combining Multiple Stereo Views**, In Proc. International Joint Conference on Artificial Intelligence, August, Milano, Italy.

Ayache, N., Faugeras, O.D., 1989, **Maintaining Representation of the Environment of a Mobile Robot**, IEEE Transactions on Robotics and Automation, 5(6), December.

Ballard, D.H., Brown, C.M., 1982, **Computer Vision**, Prentice Hall, Englewood Cliffs, NJ.

Baltsavias, E.P., Stallmann, D., 1990. **Trinocular Vision for Automatic and Robust s-D Determination of the trajectories of Moving Objects**, Int. Archives of Photogrammetry and Remote Sensing, Vol.28(5/1), pp. 620-629.

Baltsavias, E.P., 1991, **Multiphoto Geometrically Constrained Matching**, Dissertation, ETH Nr.49. 221 pages.

Bammeke, A.A, Baldwin, R.A., 1992, **Designing and Planning of Close-Range Photogrammetric Networks: Is An Expert System Approach Feasible?** Int. Archives of Photogrammetry and Remote Sensing, Vol.29(5), pp. 454-460.

Beni, G., Hackwood, S., 1985, **Recent Advances in Robotics**, A Wiley-Interscience Publication, 426 pages.

Beyer, H.A., 1987, **Some Aspects of the Geometric Calibration of CCD-Cameras.** ISPRS intercommission Conference on Fast Processing of Photogrammetric Data, pp. 68-81.

Beyer, H.A., 1989, **Calibration of CCD-Cameras for Machine Vision and Robotics**, Automated Inspection and High-Speed Vision Architectures III, SPIE Vol.1197, pp. 88-98.

Beyer, H.A., 1990, **Linejitter and Geometric Calibration of CCD- Cameras.** Photogrammetric Engineering and Remote Sensing, vol.45. pp. 17-32.

Beyer, H.A., 1992a, **Advances in Characterisation and Calibration of Digital Imaging Systems.** International Archives of Photogrammetry and Remote Sensing. Vol.29(5) pp. 545-555.

Beyer, H.A., 1992b, **Automated Dimensional Inspection with Real-Time Photogrammetry**, Int. Archives of Photogrammetry and Remote Sensing, Vol.29(5), pp. 722-727.

Beyer, H.A., 1992c, **Geometric and Radiometric Analysis of a CCD- Camera Based Photogrammetric Close-Range Systems.** Dissertation, ETH Nr.9701. 185 pages.

Blake, A., McCowen, D., Lo., H.R., Konash, D., 1990, **Epipolar Geometry for Trinocular Active Range-sensors**, British Machine Vision Conference, BMVC90, pp. 19-24.

Brooks, R., 1985, **Visual Map Making for a Mobile Robot,** In Proc. International Conference on Robotics and Automation, IEEE, Saint-Louis, USA, pp. 824-829.

Brown, D.C., 1958, **A Solution to the General Problem of Multiple Station Analytical Stereo-Triangulation,** RCS TR43, Patrick Airforce Base FLORIDA.

Brown, D.C., 1971, **Close-Range Camera Calibration,** Photogrammetric Engineering, pp. 855-866.

Brown, D.C., 1982, **Advances in Computer Vision,** Lawrence Erlbaum Associates Publishers, Volume 2, 186 pages.

Burner, A.W., Snow, W.L., Goad, W.K., 1985, **Close-Range Photogrammetry with Video Cameras,** Technical Papers of 51st Annual Meeting ASP, Vol.1, pp. 717-724.

Burner, A.W., Snow, W.L., Shortis, M.R., Goad, W.K., 1990, **Laboratory Calibration and Characterisation of Video Cameras,** Close-Range Photogrammetry Meets Machine Vision, SPIE Vol.1395, pp. 664-671.

Canny, J., 1986, **A Computational Approach to Edge Detection,** IEEE Trans. PAMI., Vol. 78, No.6, pp. 255-274.

Case, J.B., 1982, **The Digital Stereo Comparator/Compiler (DSCC).** International Archives of Photogrammetry, Vol. 24-II, pp.23-29.

Chang, Y.L., Lebegue, X., Aggarwal, J.K., 1993, **Calibrating A Mobile Camera's Parameters,** Pattern Recognition, Vol.26, No.1, pp. 75-88.

Charles R. S., Johan, J.K., 1994, **Blunder Detection and Data Snooping in LS and Robust Adjustments,** Journal of Surveying Engineering, Vol.119, No.4, pp.127-136.

Chen, J., Clarke, T.A., 1992. **The Automatic Recognition, Location and Labelling of Targets in Digital Photogrammetric Engineering measurement,** Int. Archives of Photogrammetry and Remote Sensing, Vol.29(5), pp. 587-693.

Chen, J., Clarke, T.A., Robson, S., 1993, **An Alternative to the Epipolar Line Method for Automatic Target Matching in Multiple Images for 3-D Measurement,** Optical 3-D Measurement Techniques, Zurich, pp. 197-204

Chen. J., Clarke, T.A., Robson, S., Grattan, K.T.V., 1994, **An Optimised Target Matching Based on a 3-D Space Intersection and a Constrained Search for Multiple Camera Views,** SPIE Optical Tools for Manufacturing and Advanced Automation Videometrics III, SPIE Vol. 2350, pp. 324-335.

Clarke, T.A., Robson, S., and Chen, J., 1993, **A Comparison of Three Techniques for the 3-D Measurement of Turbine Blades,** International Symposium on Measurement Technology and Intelligent Instruments, SPIE Vol. 2101, pp1-12.

Clarke, T.A., Cooper, M., Fryer, J., 1993, **An Estimator for the Random Error in Subpixel Target Location and its Use in the Bundle Adjustment.** Optical 3-D

Measurement Techniques, Zurich.

Clarke, T.A., Robson, S., 1993, **Building a Digital Close Range Three Dimensional Measuring System for Less Than £5000**, Photogrammetric Record, Vol.14(82), Oct, pp. 675-680.

Clarke, T.A., Katsimbris, A., 1994, **The Use of Diode Laser Collimator for Targeting 3-D Objects**, ISPRS Commission V, Intercongress Symposium, Melbourne.

Clarke, T.A., 1994, **An Analysis of the Properties of Targets Uses in Digital Close Range Photogrammetric Measurement**, Videometrics III. SPIE Vol. 2350. pp. 251-262.

Clarke, T.A., Cooper, M.A.R., Chen, J., Robson, S., 1995, **Automated 3-D Measurement Using Multiple CCD Camera Views**, Photogrammetric Record, In press.

Cooper, M.A.R., Clark, J.S., 1984, **Final Report on a Feasibility Study of the Use of Photogrammetry for Health Monitoring of Bridges**, Transport and Road Research Laboratory Research Contract TRR/842/392, 75 pages.

Cooper, M.A.R., 1979, Analytical Photogrammetry in Engineering: Three Feasibility Studies, Photogrammetric Record, Vol.9(53), pp. 601-617.

Cooper, M.A.R., Cross, P.A., 1988, **Statistical Concepts and Their Application in Photogrammetry and Surveying**, Photogrammetric Record, Vol.12(71), April, pp. 637-663.

Cooper, M.A.R., Cross, P.A., 1991, **Statistical Concepts and Their Application in Photogrammetry and Surveying (Continued)**, Photogrammetric Record, Vol.13, April, pp. 645-678.

Crippa, B., Mussio, L., Maas, H.G., 1992, **Spatial Analysis of Turbulent Flows by Deterministic and Stochastic Approaches**, Int. Archives of Photogrammetry and Remote Sensing, Vol.29(5), pp. 380-389.

Dahler, J., 1987, **Problems in Digital Image Acquisition with CCD Cameras**. ISPRS intercommission Conference on Fast Processing of Photogrammetric Data, pp. 48-59.

Davies, E.R., 1990, **Machine Vision: Theory, Algorithms, Practicalities**. Published by Harcourt Brace Jovanovich, 547 pages.

Dickmanns, 1987, 4D-Dynamic **Scene Analysis with Integral Spatio-Temporal Models**, In ISSP, Santar-Cruz, USA.

Dold, J., 1994, **A strategy for Photogrammetric Multiple Camera Calibration without Additional Object Information**, ISPRS Commission V Symposium: Close-Range Techniques with Machine Vision, Vol.30(5), pp. 61-70.

Dowman, I.J., Ebner,H., and Heipke,C., 1992, **Overview of European Developments in Digital Photogrammetric Workstations**. Photogrammetric Engineering and Remote Sensing, vol.58, No.1, pp. 51-56.

El-Hakim S.F., 1985a, **A Photogrammetric Vision System for Robots,** Photogrammetric Engineering and Remote Sensing, Vol.51, No.5, pp. 545-552.

El-Hakim S.F., 1985b, **Photogrammetric Measurement of Microwave Antennae,** Photogrammetric Engineering and Remote Sensing, Vol.51, No.10, pp. 1577-1581.

El-Hakim S.F., 1986a, **Real-Time Image Metrology with CCD Cameras,** Photogrammetric Engineering and Remote Sensing, Vol.52, No.11, pp. 1757-1766.

El-Hakim S.F., 1986b, **The Detection of Gross and Systematic Errors in the Combined Adjustment of Terrestrial and Photogrammetric Data,** Photogrammetric Engineering and Remote Sensing, Vol.52, No.1, pp. 59-66.

El-Hakim, S.F., 1989, **A Hierarchical Approach to Stereo Vision.** Photogrammetric Engineering and Remote Sensing, vol.55, No.4, pp. 443-448.

El-Hakim, S.F., 1990, **Some Solution to Vision Dimensional Metrology Problems,** SPIE, Vol. 1395, pp. 480-487.

Ellis, T.J., Rosin, P.L., 1991, **Model-Based Vision for Automatic Alarm Interpretation,** IEEE AES Systems Magazine, pp. 14-19.

EPIX, 1991. **Silicon Video MUX Users Manual** V.2.4. 62 pages.

Faugeras, O.D., Ayache, N., Faverjon, B., 1986, **Building Visual Maps by Combining Noisy Stereo Measurements,** In Proc. International Conference on Robotics and Automation, April, San Francisco, USA, pp. 1433-1438.

Fischler, M.A., Bolles, R.C., 1980, **Random Sample Consensus: A Paradigm for Model Fitting with Applications to Image Analysis and Automated Cartography,** Communications of the ACM, Vol.24, No.6, pp. 381- 395.

Fraser, C.S., 1982, **Optimization of Precision in Close-Range Photogrammetry,** Photogrammetric Engineering and Remote Sensing, Vol.48, No.4, pp. 561-570.

Fraser, C.S., 1984, **Network Design Consideration for Non-Topographic Photogrammetry,** Photogrammetric Engineering and Remote Sensing, Vol.50, No.8, pp. 1115-1126.

Fraser, C.S., 1985, **Photogrammetric Measurement of Thermal Deformation of a Large Process Compressor,** Photogrammetric Engineering and Remote Sensing, Vol.51, No.10, pp. 1569-1575.

Fraser, C.S., and Browm, D.C., 1986, **Industrial Photogrammetry: New Developments and Recent Applications,** Photogrammetric Record, Vol.68, No.12, pp. 197-217.

Fraser, C.S., 1986, **Microwave Antenna Measurement,** Photogrammetric Engineering and Remote Sensing, Vol.52, No.10, pp. 1627-1635.

Fraser, C.S., 1988a, **State of The Art in Industrial Photogrammetry,** Int. Archives of Photogrammetry and Remote Sensing, Vol.27(5), pp. 166-181.

Fraser, C.S., 1988b, **Periodic Inspection of Industrial Tooling by Photogrammetry,** Photogrammetric Engineering and Remote Sensing, Vol.54, No.2, pp. 211-216.

Fraser, C.S., 1992, **Photogrammetric Measurement to One Part in a Million,** Photogrammetric Engineering and Remote Sensing, Vol.58, No.3, pp. 305-310.

Fraser, C.S., Legac, A, 1994, **Industrial Applications of Single-Sensor Vision Metrology,** ISPRS Commission V Symposium: Close-Range Techniques with Machine Vision, Vol.30(5), pp. 82-91.

Frobin, W., Hierholzer, E., 1982, **Calibration and Model Reconstruction in Analytical Close-Range Stereophotogrammetry.** Photogrammetric Engineering and Remote Sensing, Vol.48. No.1, pp. 67-72.

Fryer, J.G., and Fraser, C.S., 1986, **On the Calibration of Underwater Cameras.** Photogrammetric Record, Vol.67, No.12, pp. 73- 85.

Fryer, J.G., and Mason, S.O., 1989, **Rapid Lens Calibration of a Video Camera,** Photogrammetric Engineering and Remote Sensing, Vol.55, No.4, pp. 437-442.

Fryer, J., 1987, **Lens Distortion: The Forgotten Component of Digital Photogrammetry,** Symposium on the Applications of Close Range Photogrammetry, pp. 117-129.

Fryer, J., Clarke, T.A., Chen, J., 1994, **Lens Distortion for Simple C-Mount Lenses,** ISPRS Commission V Symposium: Close-Range Techniques with Machine Vision, Vol.30(5), pp. 97-101.

Gao, Y., Krakiwsky, E.J., Czompo, J., 1992, **Robust Testing Procedure for Detection of Multiple Blunders,** Journal of Surveying Engineering, Vol.118, No.1, pp.11-23.

Godding, R., Luhmann, T., 1992, **Calibration and assessment of a Multi-Sensor On-line Photogrammetric System.** International Archive of Photogrammetry and Remote Sensing, XXIX(5), pp. 24-29.

Godding, R., Luhmann. T., 1994, **Calibration and Accuracy Assessment of A Multi-Sensor Online-Photogrammetric System,** ISPRS Commission V Symposium: Close-Range Photogrammetry with Machine Vision, pp. 24-29.

Grafarend, E., 1974, **Optimisation of Geodetic Networks,** Bollettino di Geodesia a Scienze Affini, 33(4), pp. 351-406.

Granshaw, S.I., 1980, **Bundle Adjustment Methods in Engineering Photogrammetry,** Photogrammetric Record, Vol.10, Oct, pp. 181-207.

Grimson, W.E.L., 1990, **Object Recognition by Computer: The Role of Geometric Constraints.** Published by The MIT Press, 512 pages.

Gruen, A.W., 1982. **The Accuracy Potential of the Modern Bundle Block Adjustment in Aerial Photogrammetry,** Photogrammetric Engineering & Remote Sensing, Vol.48, No.1, pp. 45-54.

Gruen, A.W., 1985. **Algorithmic Aspects in On-Line Triangulation,** Photogrammetric Engineering & Remote Sensing, Vol.51, No.4, pp. 419-436.

Gruen, A.W., 1988. **Geometrically Constrained Multiphoto Matching,** Photogrammetric Engineering & Remote Sensing, Vol.54, No.5, pp. 633- 641.

Gruen, A.W., 1989. **Digital Photogrammetric Processing Systems: Current Status and Prospects,** Photogrammetric Engineering & Remote Sensing, Vol.55, No.5, pp.581-586

Gruen, A.W., Kersten, T., 1992, **Sequential Estimation in Robot Vision**, Int. Archives of Photogrammetry and Remote Sensing, Vol.29(5), pp. 923-931.

Gruen, A.W., 1994, **Digital Close-Range Photogrammetry - Progress Through Automation,** ISPRS Commission V Symposium: Close-Range Techniques with Machine Vision, Vol.30(5), pp. 122-135.

Haggren H., Leikas, E., 1987, **Mapvision: The Photogrammetric Machine Vision System,** Photogrammetric Engineering & Remote Sensing, Vol.53, No.8, pp. 1103-1108.

Hahn, M., 1994, **Corner Detection in Range Images,** ISPRS Commission V Symposium: Close-Range Techniques with Machine Vision, Vol.30(5), pp. 136-143.

Haralick, R.M., 1980, **Using Perspective Transformation in Scene Analysis,** Computer Graphics and Image Processing, Vol.13, pp. 191-221.

Haralick, R.M., 1989, **Determining Camera Parameters from the Perspective Projection of a Rectangle,** Pattern Recognition, Vol.22, No.3, pp. 225-230.

Haralick, R.M., 1993, **Computer and Robot Vision,** Volume II, Published by Addison-Wesley Publishing Company, 630 pages.

Heipke, C., 1992. **A Global Approach for least-Squares Image Matching and Surface Recognition in Object Space,** Photogrammetric Engineering & Remote Sensing, Vol.58, No.3, pp. 317-323.

Hinsken, L., 1988, **A Singularity Free Algorithm for Spatial Orientation of Bundle,** XVI Cong. of ISPRS, Kyoto.

Isaguirre, A., Pu, P., Summers, J., 1985, **A New Development in Camera Calibration: Calibrating a Pair of Mobile Cameras,** In Proc. International Conference of Robotics and Automation, pp. 74-79.

Jansa, J., Trinder, J.C., **A Knowledge Based System for Close Range Digital Photogrammetry,** Int. Archives of Photogrammetry and Remote Sensing, Vol.29(5), pp. 461-463.

Jeschke, W., 1990, **Digital Close-Range Photogrammetry for Surface Measurement.** SPIE VOl. 1395, pp. 1058-1065.

Karara, H.M., 1985, **Close-Range Photogrammetry: Where Are We and Where Are We**

Heading? Photogrammetric Engineering & Remote Sensing, Vol.51, No.5, pp. 537-544.

Karras, G.E., Pesta, E., 1993, **DEM Matching and Detection of Deformation in Close-Range Photogrammetry without Control**, Photogrammetric Engineering and Remote Sensing, Vol.54, No.9, pp. 1419-1424.

Katsimbris, A., 1993, **The Use of Laser Diode Collimators to Provide Targets and Scaling in an Automated 3-D Measurement System**, Dissertation of Master of Science, City University, 101 pages.

Karara, H.M., 1979, **Handbook of Non-Topographic Photogrammetry**, American Society for Photogrammetry and Remote Sensing, First Edition, 206 pages.

Karara, H.M., 1989, **Non-Topographic Photogrammetry,** American Society for Photogrammetry and Remote Sensing, Second Edition, 445 pages.

Kearney, J.K., 1991, **Trinocular Correspondence for Particles and Streaks**, Dept. of Computer Science, The University of Iowa, Technical Report 91-01.

Kenefick, J,F, 1977, **Applications of Photogrammetry in shipbuilding**, Photogrammetric Engineering and Remote Sensing, Vol. 43, No.9, pp. 1169-1175.

Konecny, G., 1985, **The International Society for Photogrammetry and Remote Sensing - 75 years Old, or 75 years Young,** Photogrammetric Engineering and Remote Sensing, Vol. 57, No.7, pp. 921-925.

Kennie., T.J.M., Petrie, G., 1990, **Engineering Surveying Technology**, Published by Blackie and Son Ltd, 485 pages.

Koo, T.K., Aw, Y.B., 1991, **A Three-Dimensional Visualization Approach to Traffic Accident Mapping**, Photogrammetric Engineering and Remote Sensing, Vol. 51, No.7, pp. 919-933.

Kubik, K., Weng, W., 1985, **Oh, Grosserrors!** Austrian Journal of Geod. Photo. Survey, No.42, pp. 1-18.

Kubik, K., Merchant, D., Schenk, T., 1987, **Robust Estimation in Photogrammetry**, Photogrammetric Engineering and Remote Sensing, Vol.53, No.2, pp. 167-169.

Kubik, K., Lyons, K., Merchant, D., 1988, **Photogrammetric Work Without Blunders**, Photogrammetric Engineering and Remote Sensing, vol.54, No.1, pp. 51-54.

Lenz, R., **Image Data Acquisition with CCD Cameras,**

Lenz, R., Fritsch, D., 1988, **On the Accuracy of Videometry**, Int. Archives of Photogrammetry and Remote Sensing, Vol.27(5), pp. 335-345.

Li, M.X., 1991, **Hierarchical Multipoint Matching**. Photogrammetric Engineering and Remote Sensing, vol.57, No.8, pp. 1039-1047.

Low, A., 1991, **Introductory Computer Vision and Image Processing**, Published by

McGRAW-HILL Book Company (UK) Limited, 244 pages.

Luh, J.Y., Klaasen, J.A., 1985, **A Three-Dimensional Vision by Off-Shelf System with Multi-cameras**, IEEE Transaction Pattern Analysis and Machine Intelligence, Vol. PAMI-7, pp. 35-45.

Lunetta, R.S., Congalton, R.G., Fenstermaker, L.K., Jensen, J.R., McGwire, K.C., Tinney, L.R., 1991, **Remote Sensing and Geographic Information System Data Integration: Error Sources and Research Issues**, Photogrammetric Engineering and Remote Sensing, Vol.57, No.6, pp. 677-687.

Marr, D., 1982, **Vision - A Computational Investigation into the Human Representation and Processing of Visual Information**, Freeman, 397 pages.

Maas, H.G., 1991, **Digital Photogrammetry for Determination of Tracer Particle Coordinates in Turbulent Flow Research**, Photogrammetric Engineering and Remote Sensing, vol.57, No.12, pp. 1593-1597.

Maas, H.G., 1992a. **Complexity Analysis for the Establishment of Image Correspondences of Dense Spatial Target Fields**, Int. Archives of Photogrammetry and Remote Sensing, Vol.29(5), pp. 102-107

Maas, H.G., 1992b. **Robust Automatic Surface Reconstruction with Structured Light**, Int. Archives of Photogrammetry and Remote Sensing, Vol.29(5), pp. 709-713

Maas, H.G., 1992c. **High-Speed Solid State Camera Systems for Digital Photogrammetry**, Int. Archives of Photogrammetry and Remote Sensing, Vol.29(5), pp. 482-485.

Mason, S., Kepuska, V., 1992, **On the Presentation of Close-Range Network Design Knowledge**, Int. Archives of Photogrammetry and Remote Sensing, Vol.29(5).

Mason, S., 1994, **Conceptual Model of the Sensors Station Placement Task in COnfiguring Multi-Station Convergent Networks**, ISPRS Commission V Symposium: Close-Range Techniques with Machine Vision, Vol.30(5), pp. 256-264.

Matthies, L., Kanade, T., 1987, **Using Uncertainty Models in Visual Motion and Depth Estimation, In International Symposium on Robotics Research**, August, Santa-Cruz, USA.

Meissel, P., 1974, **The Strength of Continental Terrestrial Networks**, The Canadian Surveyor, 28(5), pp.582-589.

Melen, T., 1993, **Extracting Physical Camera Parameters from the 3 by 3 Direct Linear Transformation Matrix**, Optical 3-D Measurement Techniques II, pp. 355-365.

Methley, B.D.F., 1986, **Computational Models in Surveying and Photogrammetry**, Thomson Press Limited, 346 pages.

Muller, J.P., 1988, **Computing issues in Digital Image Processing in Remote Sensing**,

Digital Image Processing in Remote Sensing, London.

Naidu, D.K., Fisher, R.B., 1991, **A Comparative Analysis of Algorithms for Determining the Peak Position of a Stripe to Sub-pixel Accuracy,** Processing of the British Machine Vision Conference, pp. 217-225.

Nasrabadi, N.M., Liu, Y., 1989, **Stereo Vision Correspondence Using a Multichannel Graph Matching Technique,** Image and Vision Computing, Vol.7, No.4, pp. 237-245.

Nasrabadi, N.M., 1992, **A Stereo Vision Technique Using Curve-Segments and Relaxation Matching,** IEEE, Transactions on PAMI, Vol.14, No.5, pp. 566-572.

Nolette, C., Gagnon, P.A., Agnard, J.P., 1992, **The DVP: Design, Operation, and Performance,** Photogrammetric Engineering and Remote Sensing, Vol.58, No.1, pp. 65-69.

Nomura, Y., Sagara, M., Naruse, H., and Ide, A., 1989, **High Accuracy Camera Calibration for 3-D Computer Vision.** IEEE, CH2795-3, pp. 480-485

Oldfield, S., 1986, **Photogrammetry Plate Measuring facilities at NPL,** International Archive of Photogrammetry, Vol. 26(5), pp. 541-545.

Okamoto, A., 1981, **Orientation and Construction of Models,** Photogrammetric Engineering and Remote Sensing, Vol.47, No.10, pp. 1437-1454.

Overington, I., Greenway, P., 1987, **Practical First-Difference Edge Detection with Subpixel Accuracy,** Image and Vision Computing, Vol.5, No.3, pp. 217-224.

Papo, H.B., 1985, **Deformation Analysis by Close-Range Photogrammetry,** Photogrammetric Engineering and Remote Sensing, Vol.51, No.10, pp. 1561-1567.

Paquette, L., Stampfler, R., Davis, W.A., Caelli, T.M., 1990, **A New Camera Calibration Method for Robotic Vision,** Close-Range Photogrammetry Meets Machine Vision, SPIE Vol.1395, pp. 656-663.

Pavlidis, T., 1982, **Algorithms for Graphics and Image Processing,** Published by Springer-Verlag, Berlin, 416 pages.

Peipe, J., Schneider, C.T., Sinnreich, K., 1993, **Digital Photogrammetric Station DPA -A Measurement System for Close Range Photogrammetry.** Proc Optical 3-D Measurement Techniques III, pp. 292-300.

Pollard, S.B., Porrill,J ., Maynew, J.E.W., Frisby,J.P., 1987, **Matching Geometrical Descriptions in Three-Space,** Image and Vision Computing, Vol.5, No.2, pp.73-78.

Pomaska, G., 1992, **Software Development for Close-Range Applications Under Consideration of Present Standards,** Int. Archives of Photogrammetry and Remote Sensing, Vol.29(5), pp. 50-55.

Powell, G.E., 1984, **Industrial Photogrammetry at McDonnell Aircraft Company,** Proceedings, Close-Range Photogrammetry and Surveying: State-of-the-art, American

Society of Photogrammetry, pp.. 750-753.

PULNIX, 1991, **Operation and Maintenance Manual for the TM6CN camera.** PULNiX House Hampshire. RG24 0PL. 27 pages.

Raynor, J.M. and Seitz, P., 1991, **The Technology and Practical Problems of Pixel-Synchronous CCD Data Acquisition for Optical Metrology Application,** Close-range Photogrammetry Meets Machine Vision, SPIE. Vol. 1395, pp. 96-103.

Riechman, W., 1990, **The Reseau-Scanning Camera; Concept and First Measurement Results,** International Archives for Photogrammetry and Remote Sensing (28) 5/2, pp.1117-1125.

Robson, S., 1991, **Some Influences of the Photographic Process on the Accuracy of Close Range Photogrammetry with a Non-metric Camera.** PhD thesis, 300 pages.

Robson, S., Brewer, A., Cooper, M.A.R., Clarke, T.A., Chen, J., Setan, H.B., Short, T., 1995, **Seeing the Wood from the Trees - An Examples of Optimised Digital Photogrammetric Deformation Detection,** ISPRS Intercommission Workshop: From Pixels to Sequences - Sensors, Algorithms and Systems.

Robson, S., Clarke, T.A., and Chen, J., 1993, **The Suitability of the Pulnix TM6CN CCD Camera for Photogrammetric Measurement,** SPIE Optical tools for manufacturing and advanced automation Videometrics II, SPIE Vol.2067, pp. 66-77

Rosenholm, D., 1987, **Multi-Point Matching Using the least-Squares Technique for Evaluation of Three-Dimensional Models,** Photogrammetric Engineering and Remote Sensing, Vol.53, No.6, pp. 621-626.

Schwarz, C.R., Kok, J., 1992, **Blunder Detection and Data Snooping in LS and Robust Adjustments,** Journal of Surveying Engineering, Vol.119, No.4, pp. 127-136.

Schowengerdt, R.A., Wang, H.L., 1989, **A General Purpose Expert System for Image Processing,** Photogrammetric Engineering and Remote Sensing, vol.55, No.9, pp. 1227-1284.

Shih, T.Y., Faig, W., 1988, **A Solution for Space Resection in Closed Form,** Int. Archives of Photogrammetry and Remote Sensing, Vol.27(5), pp. 547-556.

Shortis, M.R., 1988, **Precision Evaluations of Digital Imagery for Close-Range Photogrammetric Applications,** Photogrammetric Engineering and Remote Sensing, Vol.54, No.10, pp. 1395-1401.

Shortis, M.R., Thompson, M.W., Hall, C.J., 1994, **An Applications of Digital Close Range Photogrammetry to the Monitoring of Large Scale Engineering Structure,** ISPRS Commission V Symposium: Close-Range Techniques with Machine Vision, Vol.30(5), pp.365-373.

Shortis, M.R., Clarke, T.A., Short, T., 1994, **A Comparison of Some Technique for the**

Subpixel Location of Discrete Target Images, SPIE Optical tools for manufacturing and advanced automation Videometrics III, SPIE Vol. 2350, pp. 239-250.

Slama, C.C., 1980, **Manual of Photogrammetry,** Fourth edition, American Society of Photogrammetry, pp. 1056.

Story, M., Congalton, R.G., 1986, **Accuracy Assessment: A User's Perspective,** Photogrammetric Engineering and Remote Sensing, Vol.52, No.3, pp. 397-399.

Teskey, W.F., Bayly, D.A., Martell, H.E., 1993, **Use of Laser Targeting in Precise Machinery Surveys,** Journal of Surveying Engineering, Vol.119, No.2, pp. 59-70.

Sun, L.X., 1992, **A Microcomputer-Based Election Microscope Digital Image 3D Processing System,** Int. Archives of Photogrammetry and Remote Sensing, Vol.29(5), pp. 475-481.

Sun, L.X., Zhang, Y.M., 1994, **The Possibility of Designing PC Based Digital Close-Range Photogrammetric System(DCRPS),** ISPRS Commission V Symposium: Close-Range Techniques with Machine Vision, Vol.30(5), pp. 61-70.

Taura, H., 1988, **Determination of Pavement Cracks from Photo Imagery,** Int. Archives of Photogrammetry and Remote Sensing, Vol.27(5), pp. 578-584.

Thacker, N.A., Mayhew, J.E.W., 1991, **Optimal Combination of Stereo Camera Calibration from Arbitrary Stereo Images,** Image and Vision Computing, Vol.9, No.1, pp. 27-32.

Thompson, E.H., 1959, **Method for the Construction of Orthogonal Matrics,** Photogrammetric Record.

Torlegård, A.K.I., 1986, **Some Photogrammetric Experiments with Digital Image Processing,** Photogrammetric Record, Vol.68, No.12, pp. 175-196.

Trinder, J.C., 1984, **Pointing Precisions on Aerial Photography,** Photogrammetric Engineering and Remote Sensing, vol.50, No.10, pp. 1449-1462.

Trinder, J.C., 1987, **Measurements on Digitized Hardcopy Images,** Photogrammetric Engineering and Remote Sensing, vol.53, No.3, pp. 315-321.

Trinder, J.C., 1987, **Assessment of SIR-B for Topographic Mapping,** Photogrammetric Engineering and Remote Sensing, vol.53, No.11, pp. 1539-1544.

Trinder, J.C., 1989, **Precision of Digital Target Location,** Photogrammetric Engineering and Remote Sensing, vol.55, No.6, pp. 883-886.

Trinder, T.C., 1990, **A Close Range Digital Photogrammetry System,** Close-Range Photogrammetry Meets Machine Vision, SPIE Vol.1395, pp. 440-447.

Trinder, T.C., Huang, Y., 1993, **Edge Detection with Sub-pixel Accuracy for a Flexible Manufacturing System,** Videometrics II, SPIE, Vol. 2067.

Tsai, R.Y., 1986, **An Efficient and Accurate Camera Calibration Technique for 3D**

Machine Vision, Processing of IEEE Conference On Computer Vision and Pattern Recognition, pp. 364-374.

Tsai, R.Y., 1987, **A Versatile Camera Calibration Technique for High-Accuracy 3D Machine Vision Metrology Using Off-the-Shelf TV Cameras and Lenses**, IEEE Journal of robotics and automation, Vol. RA-3, No.4, August, pp. 323-344.

Turner, H., 1988, **Photogrammetry and Real-Time Graphics in Engineering Applications**, Photogrammetric Engineering and Remote Sensing, Vol.54, No.9, pp. 1313-1317.

Veress, S.A., Huang, Y.C., 1987, **Application of Robust Estimation in Close-Range Photogrammetry**, Photogrammetric Engineering and Remote Sensing, Vol.53, No.2, pp. 171-175.

Veress, S.A., Huang, Y.C., 1987, **A Method for Improving the Efficiency of the Sequential Estimation Processing in Photogrammetry**, Photogrammetric Engineering and Remote Sensing, Vol.53, No.6, pp. 613-616.

Vernon, D., 1992, **Machine Vision: Automated Visual Inspection and Robot Vision**, Prentice Hall, 260 pages.

Vlugt, G.V.D., 1994, **The Development of An Automated Surface Measurement System**, ISPRS Commission V Symposium: Close-Range Photogrammetry with Machine Vision, pp. 414-419.

Waldhausl, P., Mann, H., **The New Rall and Clearance Measuring Draisine of the Austrian Federal Railways**, Int. Archives of Photogrammetry and Remote Sensing, Vol.27(5), pp. 600-609.

Wang, Y.M., 1992, **A Rigorous Photogrammetric Adjustment Algorithm Based on Co-Angularity Condition**, Int. Archives of Photogrammetry and Remote Sensing, Vol.29(5), pp. 195-202.

West, G.A.W., Clarke, T.A., 1990, **A Survey and Examination of Subpixel Measurement Techniques**, Close-Range Photogrammetry Meets Machine Vision, SPIE Vol.1395, pp. 456-463.

Winston, P.H., Shellard, S.A., 1990, **Artificial Intelligence at MIT: Expanding Frontiers**, Published by The MIT Press.

Wong, K.W., 1975, **Mathematical Formulation and Digital Analysis in Close-Range Photogrammetry**, Photogrammetric Engineering and Remote Sensing, Vol.41, pp. 1355-1373.

Wong, K.W., 1986, **Close-Range Mapping with a Solid State Camera**, Photogrammetric Engineering and Remote Sensing, Vol.52, No.1, pp. 67-74.

Wong, K.W., 1992a, **A Computer Vision System for Mapping Human Bodies**, Int.

Archives of Photogrammetry and Remote Sensing, Vol.29(5), pp. 850-855.

Wong, K.W., 1992b, **Machine vision, Robot Vision, Computer Vision, and Close-Range Photogrammetry**, Photogrammetric Engineering and Remote Sensing, vol.58, No.8, pp. 1197-1198.

Wu, J., Chang, J.H., 1990, **An Algorithm for Point Positioning on Digital Images and in Object Space**, Close-Range Photogrammetry Meets Machine Vision, SPIE Vol.1395, pp. 1196-1202.

Xu, P.L., 1989, **Statistical Criteria for Robust Methods**, ITC Journal, pp. 37-40.

Yamashita, Y., Saeki, N., 1988, **Automated Three-Dimensional Measurement Using Multiple One-Dimensional Solid-State Image Sensors and Laser Spot Scanners**, Int. Archives of Photogrammetry and Remote Sensing, Vol.27(5), pp. 665-674.

Zeng, Z., Wang, X., 1992, **A General Solution of a Closed-Form Space Resection**, Photogrammetric Engineering and Remote Sensing, vol.58, No.3, pp. 327-338.

Zheng, Y.J., 1993, **Digital Photogrammetric Inversion: Theory and Application to Surface Reconstruction**, Photogrammetric Engineering and Remote Sensing, Vol.59, No.4, pp. 489-498.

Zhou, H.B., 1990, **Object Points Detection in a Photogrammetric Test Field**, Close-Range Photogrammetry Meets Machine Vision, SPIE Vol.1395, pp. 1227-1233.

Zhu, J.J., 1991, **Robust Estimate with Minimum Mean Squared Error**, The Australian Surveyor, Vol.36, No.2, pp. 111-115.